Department of Civil Engineering

Study on the effect of Sodium Sulphate

On the Shear Strength properties of bentonite clay

Samira Nazem

This thesis is presented for the Degree of

Master of Philosophy

Of

Curtin University

September 2015

DECLARATION

To the best of my knowledge and belief this thesis contains no material previously published by any other person except where due acknowledgment has been made.

This thesis contains no material which has been accepted for the award of any other degree or diploma in any university.

Signature: 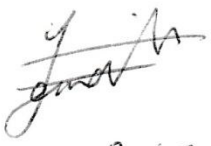

Date: 21/09/2015

Abstract

Sulphate minerals are broadly present in soils, and the sulphate anion ($SO4^{2-}$) is a typical constituent of unpolluted water. Sulphte salts can dissociate into their ions when they dissolve in water, and exchange their cations with clay particles. In Geotechnical engineering field, the research on the influence of sulphates on some geotechnical properties of soil such as swelling has been investigated considerably on the soils treated with some calcium-based stabilisers. However, more studies are required on the effect of these salts individually on the strength properties of soils particularly clays. The main reason for this lack can be expressed as the complexity of chemical reactions that occur between clay materials, and chemicals present in pore fluid in clays. Hence, the current examines the influence of Sodium Sulphate (Na_2SO_4) on the strength characteristics of a commercial bentonite (Trubond MW). A series of direct shear tests were implemented on the specimens prepared with various contents of this salt (3%, 6% and 9% by the dry weight of soil). Also, for investigating the effect of curing time all samples were cured for different periods of curing for seven days to 90 days. Some samples were cured for up to 365 days.

The numerical simulations were also employed to predict the behaviour of pure bentonite and bentonite mixed with sulphate in two typical geotechnical problems. For this purpose, the results from direct shear tests were used in the finite element software, Plaxis.

ACKNOWLEDGEMENTS

This thesis would not have been possible without the encouragement and enthusiasm

Of my supervisor, Professor Hamid Nikraz and my co-supervisor, Dr Amin Chegenizadeh, I would like to express gratitude for their continues support, patience, understanding, and encouragement added considerably to my graduate experience. I appreciate their knowledge and skills in many areas that assisted me in writing this thesis. I must thank for their positive attitudes that always convinced me in all the steps of this study. I am exceedingly thankful for having such a supervisor who is not only very supportive in the field of research but also very friendly and helpful in the case of personal difficulties.

I also would like to special thank Mark Withtaker whom without his support I was not able to overcome the difficulties involved in the laboratory. I greatly appreciate his great attentions to the laboratory responsibilities and his friendly attitude for technical support in Curtin Geotechnical Lab.

I must also thank my husband, Tom Wyard who not only has been very patient during this research but also always been very supportive and encouraging.

Finally express my great indebtedness to Curtin University for providing me this opportunity to achieve this goal at this stage of my life.

DEDICATION

To my parents

Paria and Morteza

The shining star of my life

The reason for my existence

To my Dearest Aunt and Uncle

Mahnaz and Shahram

To their endless love and support

To my Dear sisters

The flowers of my life

Samaneh, Asal and Niloofar

To my Grandmother

The Symbol of Love, Patience and Encouragement

Sedigheh

Table of Contents

Chapter 1

Introduction

1. Introduction

1.1. Background

The chemical changes in the soil's environment can influence on the geotechnical and engineering behaviour of soils. Soft soils such as bentonite or other clays are more sensitive to the chemical elements due to their high cation exchange capacity (CEC) and weaker bonds between their particles. Most of the chemical salts can dissociate into their ions when they dissolve in water, and exchange their cations with clay particles. These cation exchange reactions can change the bonding forces between clay particles leading to the changes in soil's behaviour. Most of the chemicals are usually present in the nature, and some others are as a result of human activities. Three common chemical components in nature are briefly explained below:

1.1.1 Oxides/Hydroxides

Iron and magnesium oxides/hydroxides, which are comparatively the most common components of soil, are created during the pedogenic process or from weathering of other primary minerals. The involvement of divalent or trivalent cations of Mn^{2+} and Fe^{3+} in the cation exchange reactions leads to the high sorption capacity of these oxide metals in soils.

1.1.2 Carbonates /Chlorides

Carbonates are one of the most widley distributed salts in nature. The main forms of carbonate in nature are calcite [$CaCo_3$] and dolomite [$Ca(MgCO_3)_2$]. Chlorides are the most commonly

formed soluble salts in arid or semiarid conditions. Sea water also contains 1.94% chloride. Sodium chloride (halite or NaCl), potassium chloride (sylvite or KCl), and magnesium chloride (bischofite or hydrated $MgCl_2$) are the most common salts in this group. Sodium, calcium and magnesium sulphates are products of weathering that normally form under arid to subhumid conditions (Kabata-Pendias, 2010).

1.1.3 Sulphates

Similar to Carbonates, Sulphates are broadly present in the environment. Sodium sulphates form during evaporation at the top of the soil contour. The dominant minerals in this category are gypsum [$CaSO_4.2H_2O$], anhydrite [$CaSO_4$], mirabilite [$Na_2SO_4.10H_2O$], epsomite [$MgSO_4.7H_2O$] and thenardite [Na_2SO_4]. These salts are willingly soluble, and consequently they are extremely involved in soil equilibrium mechanisms (Kabata-Pendias, 2010; Sposito, 2008). The ulphates present in pore fluid can become involved in cation exchange reactions with charged clay particles by removing the higher valence ions from the ion exchange system, resulting in the formation of insoluble salts.

Over the past twenty years, the presence of sulphate in soils treated with calcium-based stabilisers, particularly clays, resulted in damaged road surfaces. This phenomenon occurs when the calcium constituents of stabilisers react with soluble sulphates and free alumina, leading to the formation of a mineral known as ettringite (Hunter, 1988). Ettringite is a weak sulphate component that causes serious heaving when exposed to hydration. It has been shown that the presence of sulphate reduces the shear strength of soils treated with lime, particularly after long periods of curing (Sivapullaiah et al., 2000). Hence, in recent years, many studies

have been conducted on the use of chemical additives and various methods of improving soil properties to address the heave induced by sulphates in calcium-based stabilised soils.

Although most of the literature is focused on the level of application and the efficiency of chemical additives on soils with the presence of sulphate , there is still limited knowledge on the effect of these methods on the strength properties of these soil composits. Also, the effect of sulphate individually on the geotechnical and strength characteristics of soils is not currently well understood, and further research is required.

1.2 Aims and Objectives

This study examines the shear strength properties of bentonite clay under the influence of sodium sulphates. To achieve this aim, a comprehensive series of direct shear tests were carried out on bentonite specimens mixed with various percentages of sulphate and cured for different periods of time. Scanning electron microscope (SEM) observation will also be employed to gain a better understanding of the interaction between the salt and soil particles. In addition, this research undertakes a novel approach by investigating the behaviour of a sulphate-attacked clay employing the numerical modelling program, Plaxis code.

The more specific goals are summarised as follows:

- Conducting a series of experimental tests (compaction and direct shear tests) on pure bentonite clay and sulphate-attacked bentonite clay.
- Analysing the effect of various contents of sodium sulphate (Na_2SO_4) on the compaction and strength characteristics of soil after different curing times of up to 365 days.
- Studying the effect of time along with the percentage of contaminants on the strength characteristics of soil. In this stage, the impact of curing periods of 7, 14, 28, 90 and 365 (the maximum) days were investigated.
- Monitoring the soil microstructure and the reactions between sulphate salt and soil particles. In this stage, scanning electron microscopy (SEM) and energy dispersive spectroscopy (EDS) were carried out.
- Simulating the behaviour of pure and sulphate-attacked bentonite clay in two geotechnical models by Plaxis finite element program. Numerical software modelling will be involved in the final stage.

1.3 Significance

The presence of chemical contaminants in soil promotes ion exchange among clay minerals that affect the engineering properties of soil. Some chemicals can reduce the shear strength and consequently the bearing capacity of soils and the stability of slopes. Slope instability can lead to significant costs and even the loss of lives (Fell, 1994).

Chapter 1 – Introduction

Sulphates present in soils treated with calcium-based stabilisers can induce significant damage to road surfaces. In 1985, the total cost of the rehabilitation of subsoil subjected to sulphate heave in the United States was more than the original cost of improvement (Hunter, 1988).

Therefore, governments and private agencies have increasingly conducted projects relating to methods of soil improvement. Recently, deep mixing has been recognised by many countries as a method of improving the strength properties, workability and permeability of soils (Costas & Maria, 2008).

However, despite the large quantity of research in the field of chemical additives, there is little documented literature on the effect of chemicals on the shear strength of soils. Most of the literature has concentrated on the application of chemical stabilisers, while investigations on the influence of other chemicals is very rare. Hence, this study involves comprehensive research into the effect of sodium sulphate (Na_2SO_4) on the shear strength properties of clay soil over time. This novel masters project will provide worthwhile information on the behaviour of soil in the presence of sulphate ions.

Moreover, Scanning electron microscopy (SEM) will be used to observe the interaction between additives and soil particles in the samples. Furthermore, Numerical modelling was used to apply the results obtained from the experiments with the model developed to predict the behaviour of sulphate-attacked bentonite in larger scales such as two common geotechnical problems.

1.4 Research Methods

The primary aim of the study will be to investigate the effect of various contents of sodium sulphate on the shear strength properties of bentonite after different curing times. The next step will be to simulate the behaviour of sulphate-attacked bentonite in order to predict settlement under various loading conditions in two geotechnical models, using Plaxis code.

These aims will be achieved by following the steps explained below.

1.4.1 Experimental Tests

1.4.1.1 Compaction test (Index test)

For determining the maximum dry density (MDD) and the optimum moisture content (OMC) of bentonite mixtures with and without sulphate salts, the suggested compaction test method in AS1289.5.5.1 will be used. The moisture-dry density curves will be obtained for each sample and illustrated in Chapter 3.

1.4.1.2 Small direct shear test (Major test)

The small direct shear test outlined in AS1289.6.2.2 will be implemented to determine the shear strength of sulphate-bentonite mixtures with various levels of sulphate over different periods of curing. The shear stress-horizontal displacement, as well as other parameters associated with the shear strength of soil such as cohesion and friction angle, will be described in Chapter 3.

1.4.1.3 Micro-analytical Observation (SEM) / (EDS)

The effect of the additives on the interaction between soil particles will be observed by the investigation of scanning electron microscope (SEM) and energy dispersive spectroscopy (EDS). SEM will be performed on platinum coated samples to investigate the external morphology (texture), microstructure and orientation of materials making up the soil combination.

1.4.2 Numerical modelling

The results obtained from the laboratory tests on the soil samples will be transferred to Plaxis code in order to simulate the behaviour of bentonite with or without the presence of sulphate in two geotechnical models. One is the settlement of a footing under various loads, and the other is the seismic response of a retaining wall under earthquake loads.

1.4 2.1 Footing Model

The settlement of a a concrete footing under a static load and a dynamic load will be modelled by finite element Plaxis code. A vibration source such as a generator will be used to produce a uniform harmonic load. The Mohr-Coulomb model will be employed to predict the behaviour of bentonite soil in the presence and absence of sulphate.

1.4.2.2 Retaining wall model

The second model will investigate the behaviour of bentonite clay at the bottom of and behind a retaining wall under seismic loads. A large earthquake with a moment magnitude of 8.8 (Ms=8.8) wich took place off the coast of central Chile on February 27, 2010 will be applied for the seismic oscillations. Once more, the Mohr-Coulomb model will be employed to predict the behaviour of bentonite in the presence and absence of sulphate.

1.5 Review of the Thesis in Chapters

The rest of the thesis is presented into the following chapters:

Chapter (2) is devoted to the detailed review of litratures about the previous experimental, theoretical and numerical studies on the effect of chemical additives on soils, particularly the clays.

Chapter (3) outlines the primary objective of this proposal, as well as the details of the materials used and their relevant parameters. This section also contains all of the experimental tests, including the primary compaction test, comprehensive series of small direct shear tests and scanning electron microscopy (SEM) and energy dispersive spectroscopy (EDS). These tests are conducted to evaluate the effect of sodium sulphate on the geotechnical properties of bentointe clay such as shear strength, cohesion and angle of friction , and to monitor the changes in the microstructure and orientation of materials making up the bentointe soil combination.

Chapter (4) presents the Plaxis code as a numerical modelling program for simulating the behaviour of a sulphate- attacked bentonite clay in the larger scales. In this section two common geotechnical problems including settlement of a footing under various condition of loads (static and dynamic) and a retaining wall under earthquake loads will be modelled. The exprimental results obtained from Chapter 3 will be applied as the properties of soil clusters. So, the behaviour of pure bentointe and bentonite with sulphate in these models will be predicted. Finlay, the results of both problems with or without sulphate will be evaluated and compared to each other.

Chapter (5) Summarizes and concludes the contributions of the current work , along with some recommendations for further work.

Figure 1.0 shows the general procedure that will be applied in this research. The details of each part will be thoroughly described in the relevant sections.

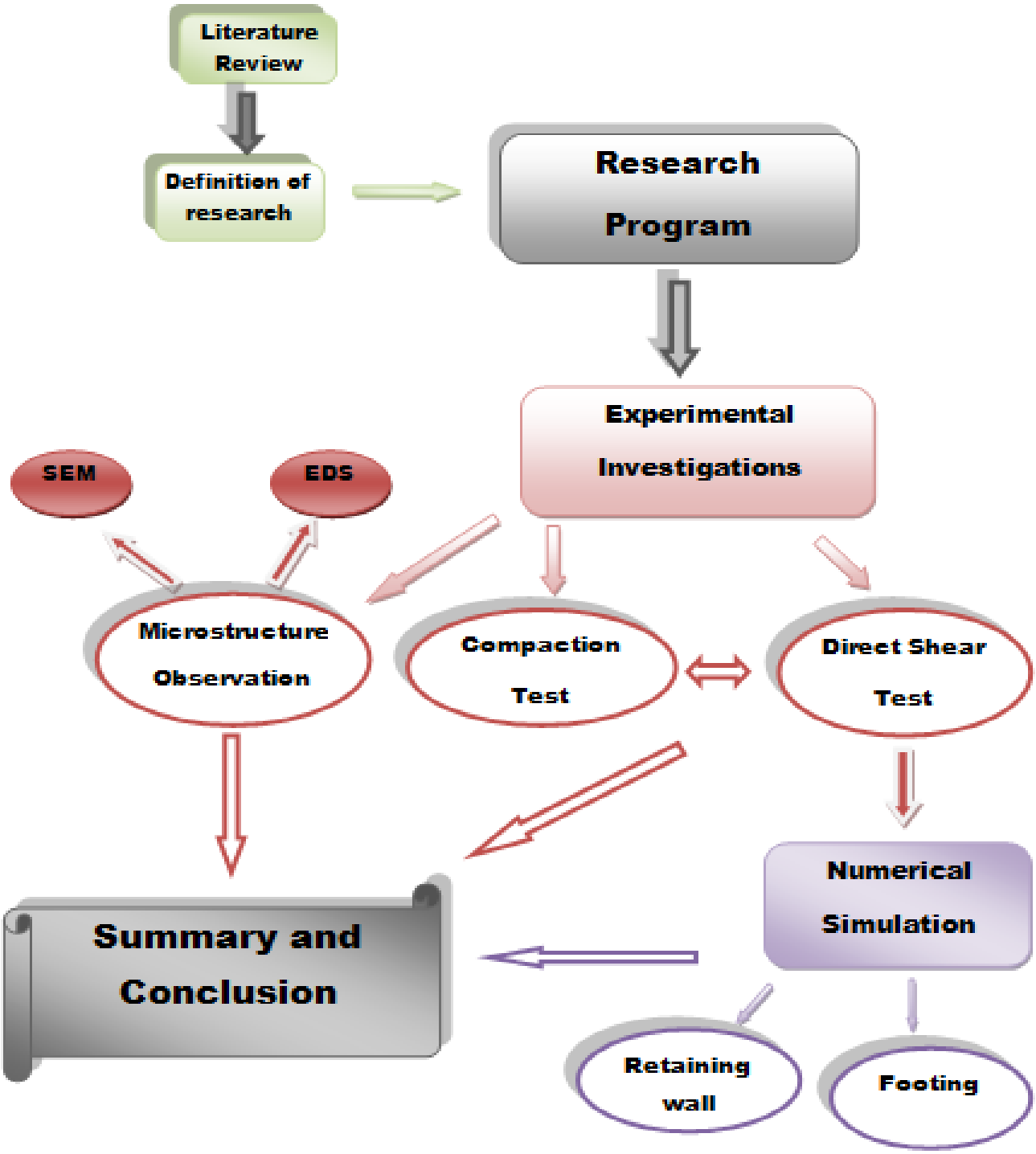

Figure 1.0: Thesis Overview

Chapter 2

Literature Review

2. Literature Review

2.1 Introduction

This chapter reviews the effect of some chemicals on physical and geotechnical properties of various soils. To demonstrate a better review, these studies were separated in different categories in this chapter as outlined in Figure 2.0

2.2 Background

Many studies have been conducted to investigate the effect of chemical additives on physical and geotechnical properties of various soils. Of all the soils, much attention has been devoted to clay due to its specific mineralogy and significant volume change. The most important parameters influencing the volume change behaviour of clays are pore water composition, cation exchange capacity (CEC), history of stress, temperature and weathering (Delage, 2007; Gens & Alonso, 1992; Komine, 2008).

Of all clay minerals, several studies have focused in particular on bentonite, mostly composed of montmorillonite, due to its extensive use for geosynthetic clay liners (GCLs) in sanitary landfills. The shrink-swell cycle, as well as the freeze-thaw cycle, can cause considerable physicochemical changes in smectite clays that lead to serious problems in such landfills.

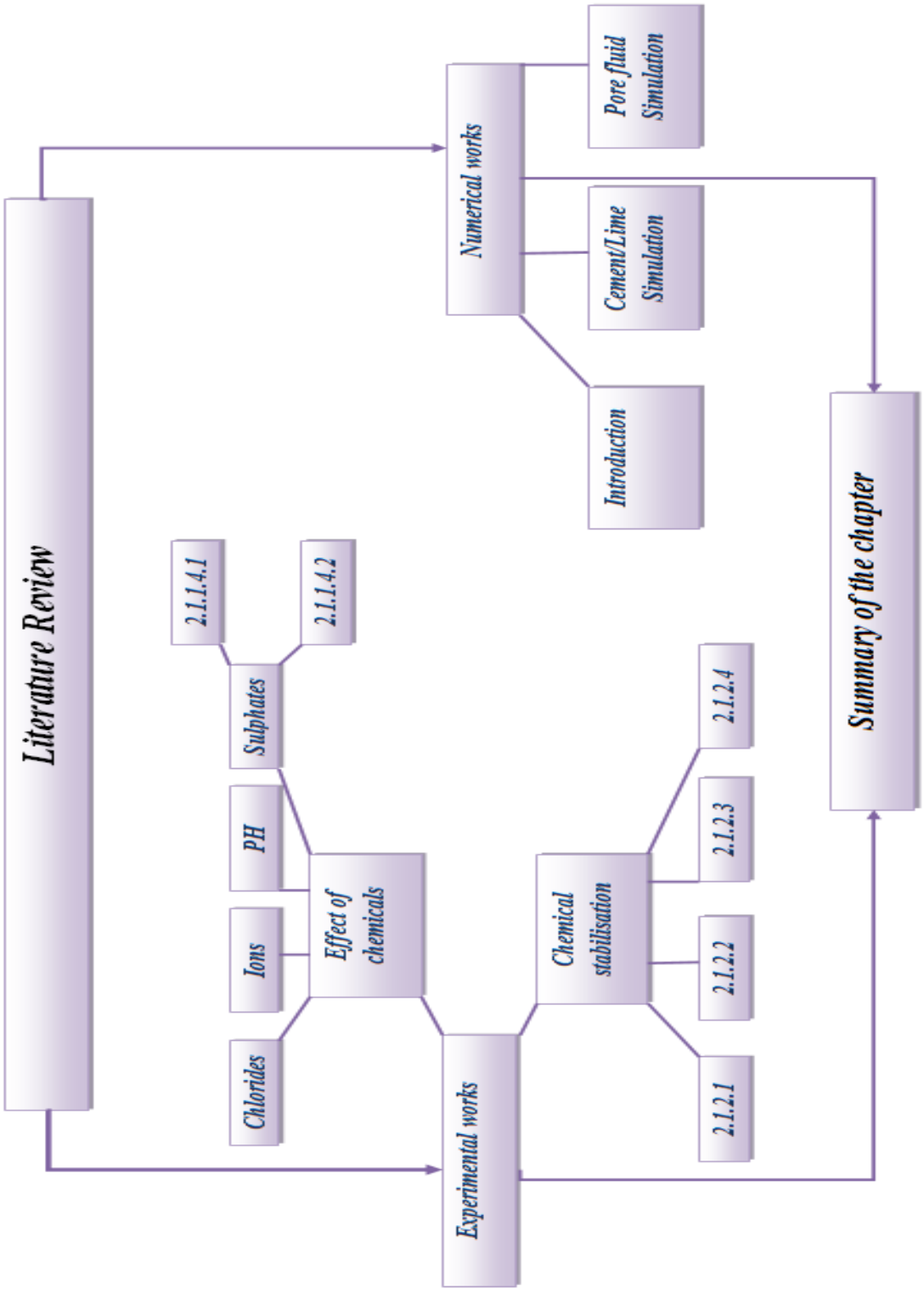

Figure 2.0 Literature review structure

2.3 Experimental works on the effect of chemicals on soil behaviour

The pore water chemistry has a crucial role in the behaviour of clay. Accordingly, there have been some studies into the effect of chemicals on clay minerals. These studies can be classified into two main categories. In the first category, researchers have investigated the impact of some chemicals on the properties of clay. These materials can have a positive or negative influence on soil behaviour. The former can lead to the discovery of new stabilisers, while the latter reveals the need for more studies to find a way to eliminate or minimise the effect of materials with a negative effect. In the second category, researchers have examined the use of particular chemical admixtures for enhancing the properties of clay. Even though the efficiency of some chemicals in soil mixtures has been validated by previous research, most of these investigations have been conducted with the aim of improving the method of application.

2.3.1. Investigations into the effect of some chemicals on soil properties

Many studies have been carried out on the impact of chemicals and pore fluid composition on the physical and geotechnical behaviour of soils. Most of this research has focussed on chemicals that are naturally distributed in soil or water. Chlorides are broadly distributed in nature. Normally, some small amounts of chloride, in the form of calcium, potassium and sodium salts ($CaCl_2$, KCl and NaCl) can be found in many soil minerals. Sulphates are common components of filtered water, and two oxidants of iron (Fe^{2+} and Fe^{3+}) exist in the marine environment. These studies have significantly enhanced knowledge about the mechanism of the

reactions between mineral compositions of clay or the diffuse double layer of clay and the pore fluid chemicals.

2.3.1.1. Effect of chlorides

Di Maio and Fenelli (1994) investigated the effect of sodium chloride solution on the residual strength of kaolin and bentonite. Firstly, they examined both distilled water- saturated clays and then replaced the distilled water with sodium chloride solutions (NaCl). They reported that this solution did not have any impact on kaolin, but it significantly increased the residual shear strength of bentonite. However, these changes were not stable, and the samples returned to their previous values when the soil was re-exposed to distilled water. Di Maio (1996) has also examined the residual strength of bentonite when exposed to NaCl and two other electrolytes, KCl and $CaCl_2$, and then re-exposed to distilled water. He noticed that all of the salt solutions increased the residual strength and decreased the liquid limit significantly. However, exposure of bentonite to KCl and $CaCl_2$ generated almost permanent changes, while the changes caused by the NaCl solutions were reversible. So, he suggested that re-exposure of clay to distilled water after exposure to salt solutions can only reverse the effect of the salt if the cation of the salt (such as Na in NaCl) that diffuses into the pore fluid is the same as its counter ion in the clay (such as Na in Na-montmorillonite).

Similar studies were carried out by Calvello et al. (2005) on the liquid limit, compressibility and residual shear strength of two bentonite clays and a natural clay under the effect of different salt solutions and organic fluids. Abood et al. (2007) conducted a series of tests to investigate the impact of some salts, including NaCl, $MgCl_2$ and $CaCl_2$, on the physical and

geotechnical behaviour of high plasticity clay. They concluded that the dry density as well as the unconfined compressive strength of the soil increased with the incremental addition of chlorides from 0% to 8%, while the Atterberg limits decreased.

A series of tests were conducted by Studds et al. (1998) on a bentonite-sand mixture and a sodium bentonite to compare the effects of sodium, potassium, caesium, magnesium, calcium and aluminium chloride salt solutions at different concentrations on the swelling behaviour and hydraulic conductivity in both soils. Their results revealed that the effect of chlorides was less noticeable under vertical stresses of greater than 200 kPa. However, at vertical stresses lower than 200 kPa, the void ratio of the bentonite powder decreased with increased salt solution concentrations. Also, the hydraulic conductivity of bentonite at a given void ratio increased with increased molarities of chloride salt solutions. Refer to Figures 2.1 and 2.2 for more information. Furthermore, among the bentonite-sand mixtures, those mixtures with a higher proportion of bentonite showed behaviour similar to that of the bentonite specimen.

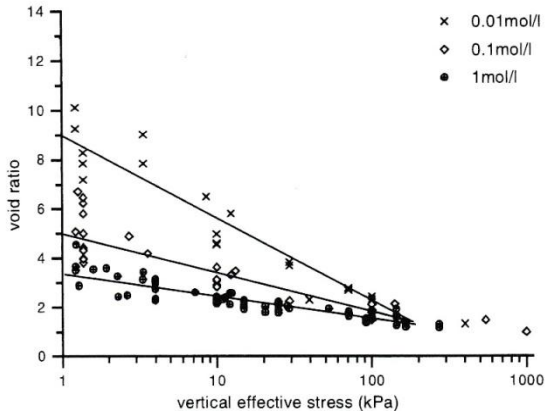

Figure 2.1: Swelling of the bentonite powder with different content of chloride salt solutions (Studds et al., 1998)

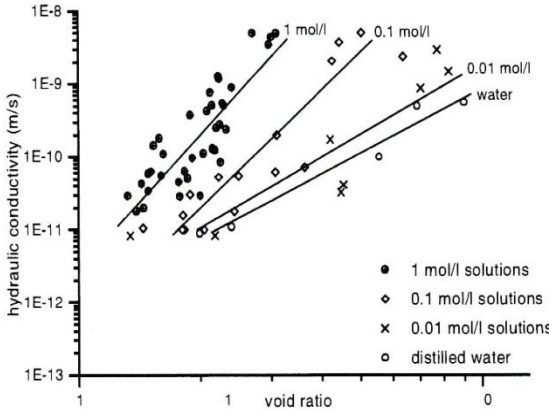

Figure 2.2: Hydraulic conductivity of bentonite with distilled water and different content of chloride salt solutions (Studds et al., 1998)

Similar tests were carried out by Shariatmadari et al. (2010) on two types of clay-bentonite mixtures (with two proportions of bentonite, 10% and 20%, in the mix), in order to review the effect of sodium chloride (NaCl), magnesium chloride ($MgCl_2$) and calcium chloride ($CaCl_2$) on the geotechnical properties of these soil mixtures. They found out that subjecting both mixtures to these chlorides increased the maximum dry density and hydraulic conductivity. They also found that the optimum moisture content, swelling volume, liquid limit and compression index (C_c) decreased with the addition of the salts to both mixtures. Moreover, they noted that salts with a higher cation valence, at a higher concentration, had more impact on the optimum moisture content, swelling volume, liquid limit and hydraulic conductivity. Nonetheless, the effects of salt concentration on dry density and cation valence on compressibility were not pronounced.

Di Maio et al. (2004) obtained a decrease in compressibility and an increase in swelling and the coefficient of consolidation by increasing the concentration of NaCl solutions in clay soils. They also demonstrated that the influence of salt on the soil depends on the stress level.

A complete series of tests were performed by Turkoz et al. (2014) to determine the engineering properties of natural clay under the influence of different percentages of magnesium chloride ($MgCl_2$) up to 13%. They demonstrated that the Atterberg limits, as well as the swelling percentage of this soil, decreased with the addition of any percentage of $MgCl_2$. Figures 2.3 and 2.4 illustrate these variations. They also noted that the optimal percentage of this salt was 7%, at which the compaction characteristics improved, the angle of friction decreased and the cohesion increased. Beyond this percentage, the effect on these properties of clay was reversed.

In addition, they showed that the shear strength of specimens treated with 7% magnesium chloride rose with increasing the time of curing. Figures 2.5 and 2.6 show the compaction curves and the failure envelope of the soil with various contents of $MgCl_2$.

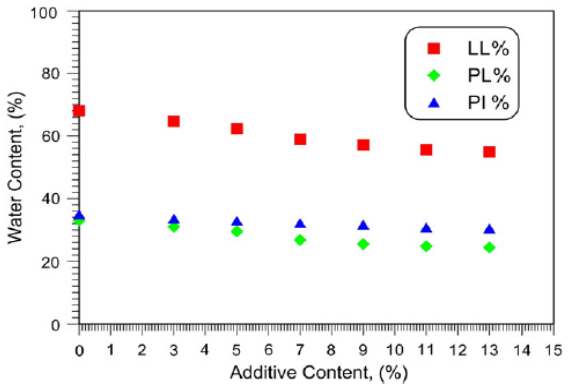

Figure 2.3: Variation of Atterberg limits with $MgCl_2$ solution contents (Turkoz et al., 2014)

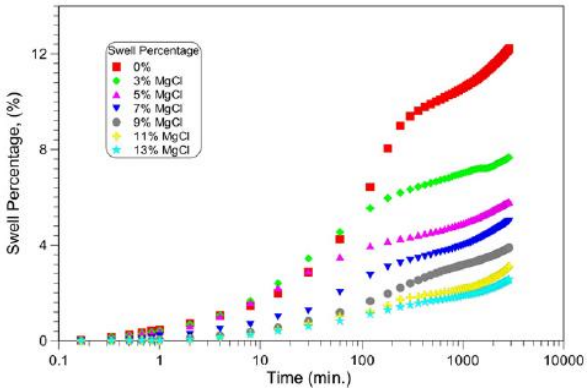

Figure 2.4: Swell percentage versus time plots for samples with different $MgCl_2$ solution contents (Turkoz et al., 2014)

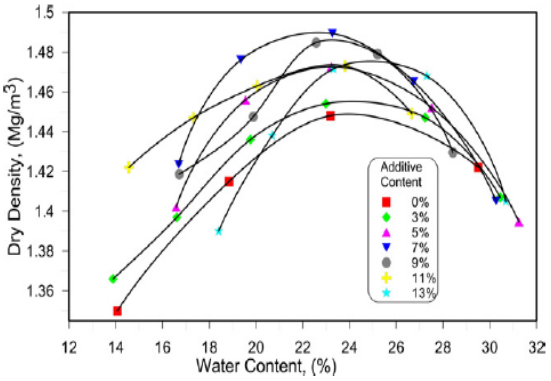

Figure 2.5: Compaction curves of samples with various content of $MgCl_2$ solution (Turkoz et al., 2014)

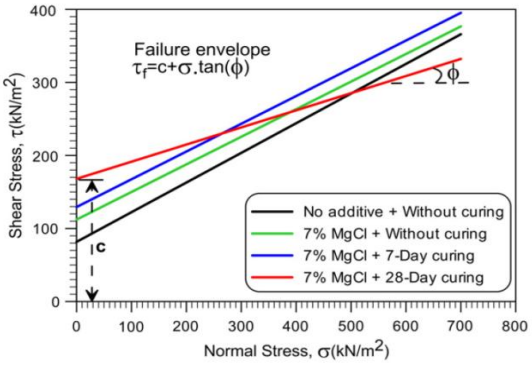

Figure 2.6: Effect of curing on the UU test results of samples with 7% $MgCl_2$ (Turkoz et al., 2014)

Zhang et al. (2014) conducted a series of unconfined compression strength (UCS) tests to evaluate the effect of the concentration of sodium chloride (NaCl) on marine clay stabilised

with different percentages of ordinary Portland cement type I. They noted a reduction in the strength of soil with an increased salt concentration. These results were compatible with those obtained by Sinat (2006), but did not agree with the results presented by Miura et al. (1988), Onitsuka et al. (2004) and Nor (2007), who reported an increase in strength with an increase in the salt content in cement-stabilised clay. Zhang et al. (2014) argued that high humic acid content had a dominant influence on the strength of cement or lime treated clay in the aforementioned studies. Furthermore, they showed that increasing the cement content decreased the disturbing effect of salt and consequently increased the strength of salt-clay mixtures. Figure 2.7 shows the variation in UCS with the addition of different quantities of salt and cement.

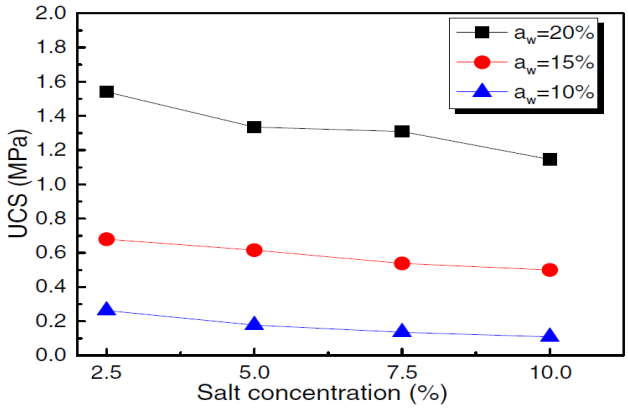

Figure 2.7: Variation of UCS versus salt concentration and cement content (a_w) (Zhang et al., 2014)

2.3.1.2. Effect of Some Metal cations and Sulphate and Chloride anions

Xing et al. (2008) examined the effect of different concentrations of Mg^{2+}, Cl^- and SO_4^{2-} on salt-rich soil treated with cement at curing times of 7 days, 28 days and 90 days. They reported that the presence of these ions along with cement had an adverse impact on the unconfined compressive strength of this soil. Among these ions, chlorine ions (Cl^-) had the most negative influence on the strength of the soil while sulphate ions (SO_4^{2-}) had the least effect on this soil.

Ajalloeian et al. (2013) investigated the effect of saline water mostly containing Ca^{2+}, Mg^{2+}, Na^+ and K^+ ions on the geotechnical behaviour of a fine-grained soil containing 28% clay. Their results revealed a decrease in Atterberg limits, compression index, swelling index, the coefficient of volume compressibility (m_v) and coefficient of compressibility (A_v). Additionally, there was an increase in the coefficient of consolidation and shear strength with an increased quantity of saline water in the mixtures.

2.3.1.3. Effect of Acidic and Alkaline agents

Gratchev and Sassa (2009) conducted a series of tests to explore the impact of different pH levels on various clays under cyclic loading. They used two low plasticity clays, kaolin and illite-sand mixtures, and medium plasticity clay, a bentonite-sand mixture. Sulphuric acid (H_2SO_4) was used as an acidic agent and sodium hydroxide (NaOH) was used as an alkaline agent. They reported that there was a decline in the liquid limit of the illite-sand mixture in the acidic environment. By contrast, in the kaolin-sand mixture the liquid limit and consequently the liquefaction increased slightly in the acidic environment (see Figures 2.8 and 2.9). Also, the

cyclic shear resistance, as well as the liquid limit, decreased in the bentonite-sand mixture under the effect of both intermediate acidic and alkaline agents (see Figure 2.10). . Generally speaking, they concluded that the mineralogy of clay soils has the main role in determining the effect of pH on their liquefaction resistance and liquid limit. Based on previous studies conducted by many researchers in relation to the influence of chemicals on the diffuse double layer in clays, including D'Appolonia (1980), Ruhl and Daniel (1997) and Kashir and Yanful (2001), they hypothesised that an intermediate acidic environment in bentonite-sand mixtures will increase the number of H^+ ions, which can weaken the interparticle forces of the diffuse double layer. This condition can lead to a decrease in the liquid limit and consequently a decline in the liquefaction resistance of bentonite. In the intermediate alkaline environment, the large numbers of Na+ ions of bentonite are responsible for aggregation and accordingly a reduction in the liquefaction resistance and liquid limit.

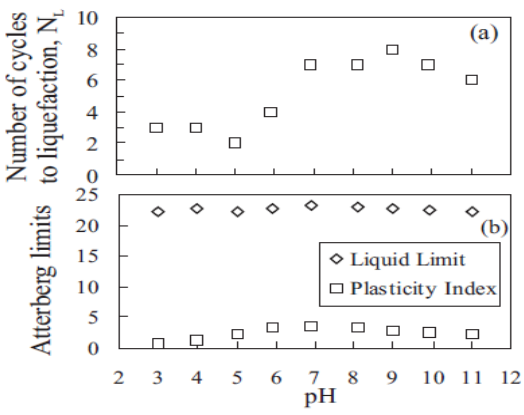

Figure 2.8: The PH levels vs the number of cycles to liquefaction (a) and Atterberg limits (b) for Illite-sand mixture (Gratchev & Sassa, 2008)

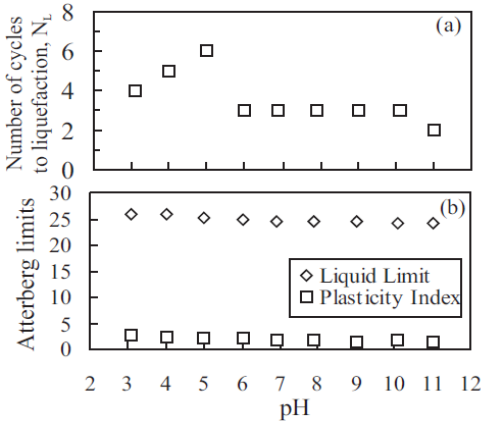

Figure 2.9: The PH levels vs the number of cycles to liquefaction (a) and Atterberg limits (b) for Kaolin-sand mixture (Gratchev &Sassa, 2008)

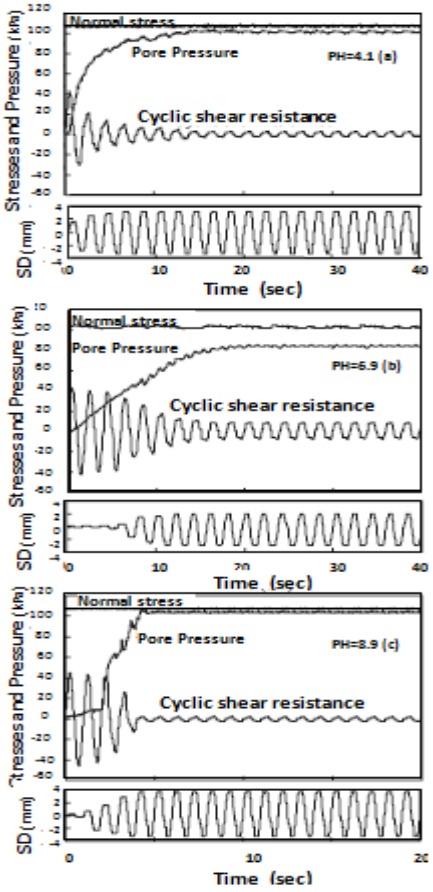

Figure 2.10: Undrained cyclic shear vs time results at PH=4.1 (a); PH=6.9 (b) and PH=8.9 (c) on bentonite – sand mixture. (SD is shear displacements) (Gratchev & Sassa, 2008)

In 2013, Gratchev and Towhata performed similar tests on montmorillonite and kaolin clays to investigate the effect of pH level on the shear strength and stress-strain curves of these clay minerals. Based on previous research by Meegoda and Ratnaweera (1994), Sridharan and Prakash (1999), D'Appolonia (1980), Kashir and Yanful (2001), Gajo and Maines (2007) and Gratchev and Sassa (2009), they demonstrated that clay mineralogy is the primary factor in the influence of an acidic environment on clay minerals. Their results showed that the shear strength of both montmorillonite and kaolin increased slightly with a decrease in pH level to 6.

However, further reduction to a pH level of 4 had a remarkably negative impact on kaolin and decreased its shear strength significantly. Figures 2.11 and 2.12 show the stress-strain curves for both soils with acidic fluid.

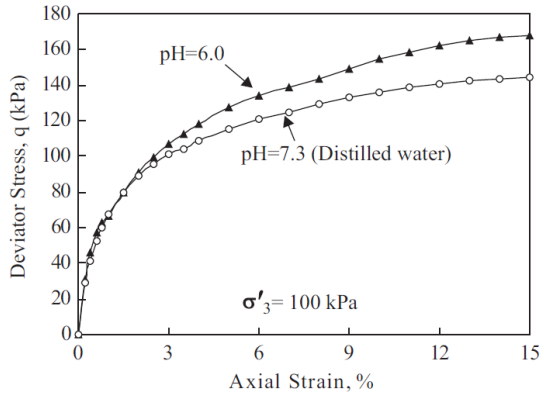

Figure 2.11: Axial Strain-Deviator Stress curves at different PH level for the soil containing montmorillonite leached with acidic fluid(σ_3' is effective confining stress) (Gratchev & Towhata, 2013)

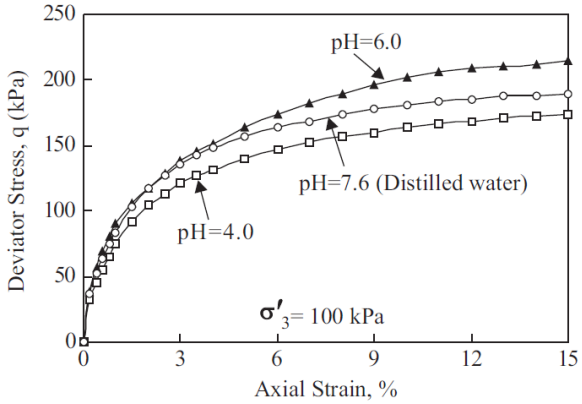

Figure 2.12: : Axial Strain-Deviator Stress curves at different PH level for the soil containing kaolin leached with acidic fluid. (Gratchev & Towhata, 2013)

Umesha et al. (2012) conducted a comprehensive series of experimental tests in order to review the geotechnical properties of a soil mostly containing clay exposed to hydrochloric, phosphoric and sulphuric acids at different concentrations from 1.25% to 15%. They reported a decrease in the values for liquid limit, maximum dry density and, more remarkably, in the shear strength of the soils with an increase in the concentration of any of the three acids. The plastic limit and optimum moisture content also had a tendency to increase with an acid concentration of up to 5%, and then decreased with an acid concentration of up to 15% for all of the acids. Moreover, comparing the results for all of the acids showed that at any given acid

concentration, the hydrochloric acid caused the highest liquid limit and the lowest optimum moisture content. In addition, the specimens subjected to phosphoric acid showed the minimum value of dry density at any percentage of acid concentration.

Slaty et al. (2013) performed a series of tests to study the unconfined compressive strength of a kaolinite clay activated by different levels of sodium hydroxide (NaOH) as the alkali solution and silica sand as the filler, at curing times varying from six to 72 hours, and temperatures varying from 50°C to 80°C. Their results showed that using a mixture of NaOH and silicate sand increased the shear strength and workability of kaolinite. The highest shear strength was achieved for the samples with a silica sand/kaolinite ratio of one and 16 parts of NaOH, over a curing time of 24 hours at a temperature of 80°C. Increasing the temperature of curing also led to a significant increase in the shear strength of the soil.

2.3.1.4. Effect of Sulphates

Sulphate salts play a crucial role in the geotechnical properties of soils. Calcium, magnesium and sodium sulphates are the products of weathering in arid to subhumid climates. The most common sulphate salts present in the soil are gypsum ($CaSO_4.2H_2O$), anhydrite ($CaSO_4$), epsomite ($MgSO4.7H_2O$), thenardite (Na_2SO_4) and mirabilite ($Na_2SO_4.10H_2O$). The sodium sulphates usually form at the surface of the soil through the evaporation of the soil profile (Sposito, 2008).

2.3.1.4.1. Effect of sulphates individually or with another salt

Although many studies have been conducted on the impact of chemicals on soil properties, few have been done in relation to the influence of individual sulphate contaminants on soil. Much has been published about the effect of sulphates in combination with other chemicals on the properties of clay soils, in particular, chemical stabilisers such as lime, cement and fly ash.

Ayininuola et al. (2009) reported an initial increase and a subsequent decrease in the shear strength, cohesion and angle of friction of subsoil clay subjected to calcium sulphate ($CaSO_4$). They stated that the initial increase in the strength properties of soil was due to unstable strong bonds generated by exchangeable cations (Ca^{+}) with the negatively charged particles in the clay at the beginning of the tests.However, this increase was not durable and would dissipate over time. Therefore, they concluded that even though the shear strength of soil decreased over time after an initial increase, the presence of calcium sulphate was not harmful to soil. In addition, the cation exchange capacity (CEC) and the level of Ca^{2+} and SO^{4-} ions were the main factors in the high tendency of the soil to regain its cohesion and angle of friction.

Zhang et al. (2011) evaluated the effect of different concentrations of a solution of sodium sulphate (Na_2SO_4) with sodium chloride (NaCl) (NaCl:Na_2SO_4 = 2:1 by mass) on bentonite mixed with different ratios of sand. As seen from Figures 2.13(a), (b) and (c), the liquid limit and plasticity index were reduced substantialy, and a slight increase in the plastic limit of bentonite in the presence of NaCl–Na_2SO_4 solution.These changes were aggravated by increasing the amount of this solution as seen in Figures 2.13(a) and (c), which show that the

reduction in liquid limit and plasticity index was most visible with the addition of salt solution up to 2g/L, moderate at 2–4g/L and almost negligible beyond 4g/L of this solution.

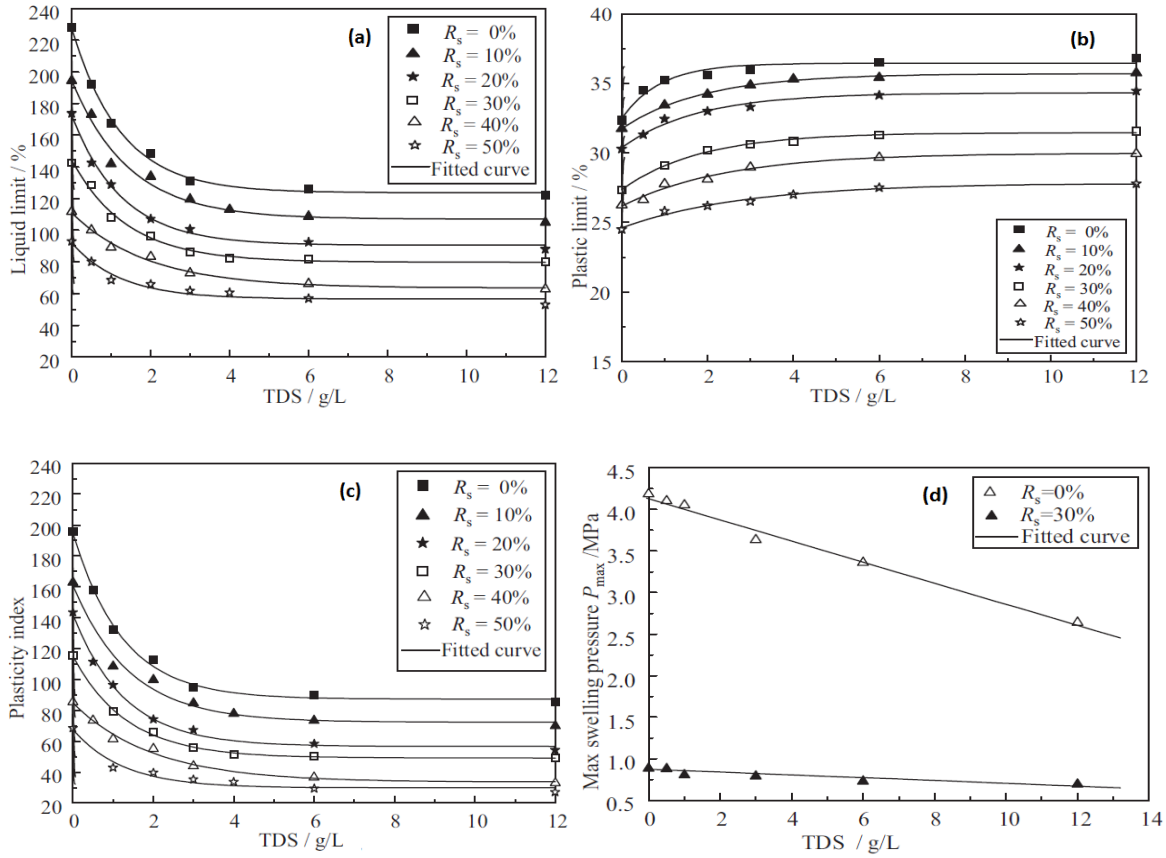

Figure 2.13: Liquid limit (a); Plastic limit (b); Plasticity index and maximum swelling pressure (d) vs. total dissolved solids (TDS) for bentonite-sand mixtures (Zhang et al., 2012)

They also observed a linear reduction in the maximum swelling pressure of bentonite at a given ratio of sand and with an incremental addition of solution. However, this reduction was much more noticeable in pure bentonite without any added sand .Therefore, Zhang et al. (2011) concluded that pure bentonite was more sensitive to chemical attacks than bentonite mixed with sand (see Figure 2.13(d) for more information).

2.3.1.4.2. Effect of sulphate with calcium-based stabilisers

Lime and cement are the stabilisers most commonly used to improve the strength and other engineering properties of soil. The improvement in the deformability and geotechnical behaviour of soil is due to pozzolanic reactions. During these reactions, the monovalent cations of clay, such as sodium or potassium, are replaced with the divalent calcium ions from lime or cement. These reactions make the clay particles clump together and create larger particles (Das, 2012). According to Hunter (1988, P. 163), these reactions can be written as below:

$$6Ca^{2+} + 2Al(OH)_4^- + 4OH^- + 3(SO_4)^{2-} + 26H_2O$$

$$= Ca_6[Al(OH)_6]_2 \bullet (SO_4)_3 \bullet 26H_2O$$

$$Ca_6[Al(OH)_6]_2 \bullet (SO_4)_3 \bullet 26H_2O + 2H_2SiO_4^{2-} + 2CO_3^{2-} + O_2 = Ca_6[Si(OH)_6]_2 \bullet (SO_4)_2 \bullet (CO_3)_2 \bullet 24H_2O + 2Al(OH)_4^- + SO_2^- + 4OH^- + 2H_2O$$

In recent years, a great deal of attention has been given to ettringite-induced heave in soil by many researchers including Braga Reis (1981), Hunter (1988), Little et al. (2009), Mitchell and Dermatas (1992), Puppala et al. (2005), Sherwood (1962) and Sridharan et al. (1995) .

Ramesh et al. (2013) studied the impact of sodium sulphate (Na_2SO_4) along with curing time on the Atterberg limits and compaction characteristics of a soil known as shedi soil (SS), containing 31% clay and 87% silt stabilised with Neyveli fly ash (NFA). They applied 1% of the salt to the optimised fly ash-soil mixture (soil + 20% NFA + 1% Na_2SO_4). Their results showed that adding 1% of sodium sulphate to the mixture increased the maximum dry density and optimum moisture content of the soil. There was also an increase in the liquid limit and a

decrease in the shrinkage limit at the beginning of the test, however these changes remained almost negligible after a curing time of seven days. Figures 2.14(a) and (b) show the variation in the liquid limit and shrinkage limit of an SS-NFA mixture treated with 1% sodium sulphate.

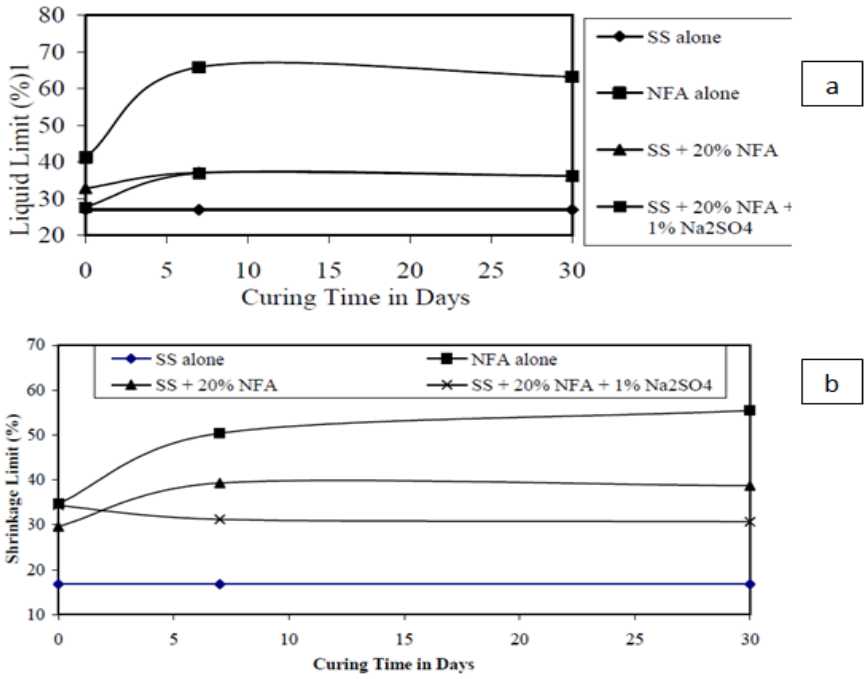

Figure 2.14: Variation of liquid limit (a); and shrinkage limit (b) of shedi soil (SS)-NFA (Neyveli fly ash) mixture treated with 1% sodium sulphate (Ramesh et al., 2013)

Kinuthia et al. (1999) studied the influence of cation valence in sulphate salts on the compaction and Atterberg limits of a kaolinite soil stabilised by 6% wt lime. They proved that the type of cations in sulphates played a crucial role in the effect of these salts on the properties of clay soil. They used two sulphate salts with monovalent cations, including sodium sulphate (Na_2SO_4) and potassium sulphate (K_2SO_4), and two sulphates with divalent cations, including magnesium sulphate ($MgSO_4$) and calcium sulphate dehydrate ($CaSO_4.2H_2O$). The results

illustrated that all of the sulphates reduced the liquid limit of clay. However, those sulphates with monovalent cations caused a greater reduction in the liquid limit. The plastic limit increased with the divalent cations but decreased with the monovalent cations. Overall, there was a decline in the plasticity index which was more noticeable at higher salt concentrations and under the effect of the divalent cations. Figures 2.15(a), (b) and (c) demonstrate the Atterberg limits moisture contents against sulphate content for 6% wt lime-mixed kaolinite.

In addition, both monovalent and divalent sulphates reduced the soil's maximum dry density (MDD) and increased its optimum moisture content (OMC). Overall, the divalent cations were more effective in reducing or raising the compaction factors and sodium sulphate had the least influence. Refer to Figures 2.16(a) and (b) for more information.

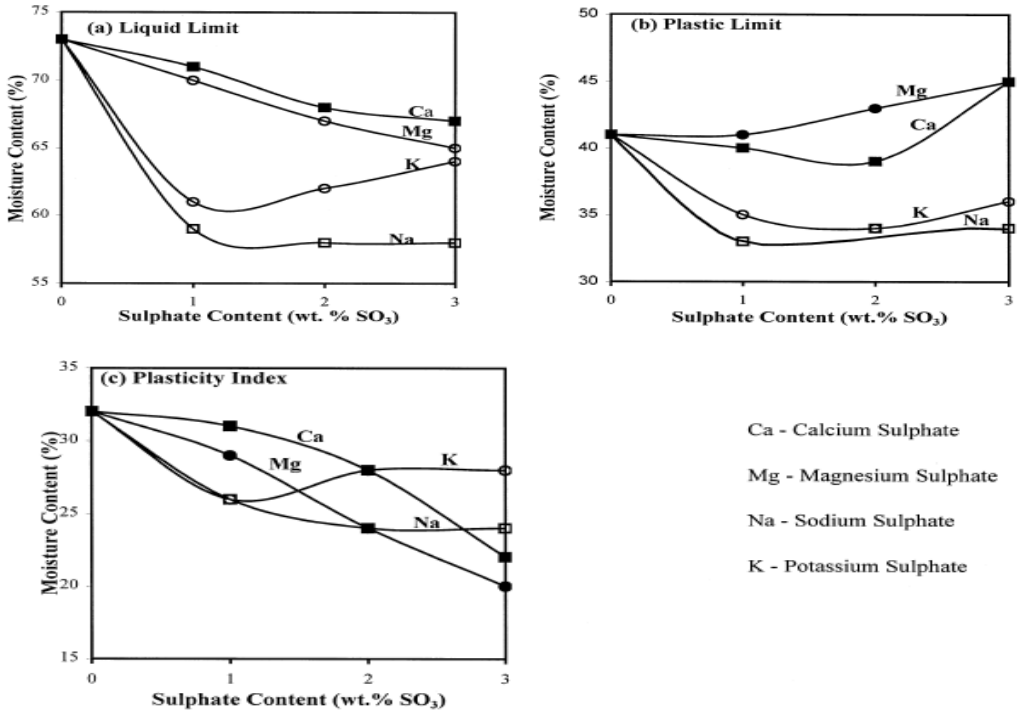

Figure 2.15: Atterberg limits vs. sulphate content for 6% wt lime-mixed kaolinite (Kinuthia et al., 1999)

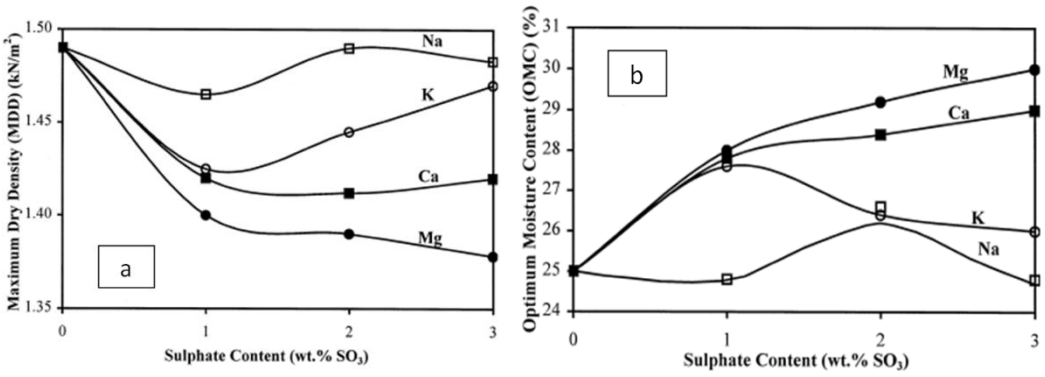

Figure 2.16: (a) (MDD); and (b) (OMC) vs. sulphate content for 6% wt lime-mixed kaolinite (Kinuthia et al., 1999)

Sivapullaiah et al. (2000) studied the effect of different levels of sodium and calcium sulphate on the strength characteristics of a natural montmorillonite stabilised with 6% wt of lime after a long curing time (up to 365 days) by implementing a series of conventional triaxial tests under CU conditions. They observed that sulphate had a minimal influence on the stress-strain curves of lime-treated soil over short curing periods, but its influence was very noticeable over longer curing periods (up to 365 days). The peak shear stress had its lowest value after 365 days curing for samples with 1% wt of Na_2SO_4 and $CaSO_4$. Figure 2.17 illustrates the impact of sodium sulphate and calcium sulphate content on stress-strain curves for lime-treated black cotton (BC) soil after 365 days of curing.

Based on previous literature, Sivapullaiah et al. (2000) concluded that a reduction in the effective cohesion of soil (c') was the main reason for the decrease in the soil strength over long curing periods. The reduction in the effective cohesion of soil (c') was due to the formation of ettringite during longer curing times, which would prevent the cementation of clay particles.

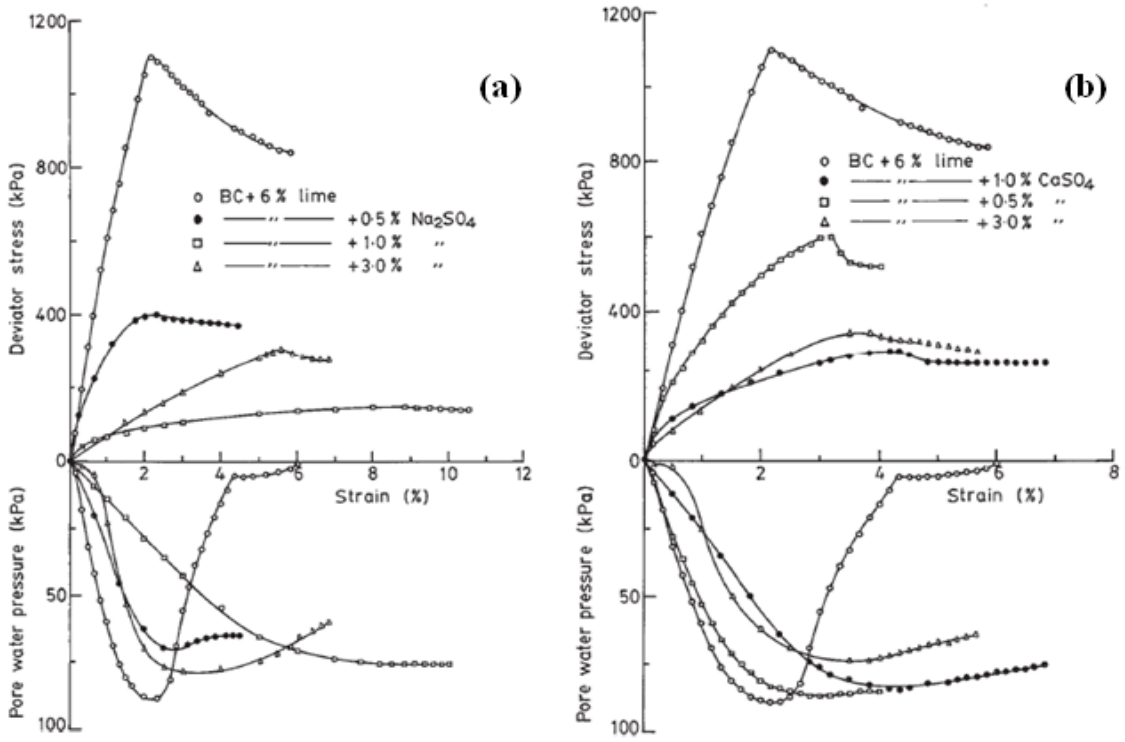

Figure 2.17:The impact of of the amount of Na_2SO_4 (a); and (b) $CaSO_4$ on the stress vs deviator stress and pore water pressure curves of lime-treated black cotton (BC) soil at a cell pressure of 100 kPa and after 365 days of curing (Sivapullaiah et al., 2000)

Puppala et al. (2005) simulated the chemical conditions of soil treated with lime or cement stabilisers using sodium sulphate (Na_2SO_4), sodium alumina oxide ($Al_2O_3Na_2O$) and quicklime (CaO) to synthesise ettringite in the laboratory. They note that adding synthesised ettringite to the soil not only did not induce heave in compacted kaolinite, but also decreased the swelling, possibly due to reinforcement of the soil particles by fibrous and needle-shaped ettringite which increased the interlocking attractions between clay particles. Refer to Figure 2.18 for more information.

However, in the presence of sodium sulphates and sodium aluminates, the lime-treated specimens produced ettringite inside the soil pores, resulting in an increase in the one-dimensional swelling test. The researchers concluded that the presence of low concentrations of sulphate along with any percentage of lime resulted in minimal heave, while increasing the quantity of lime led to increased swelling and noticeable heaving. The changes in free vertical swell for kaolinite with soluble sulphate and lime are demonstrated in Figures 2.19 and 2.20.

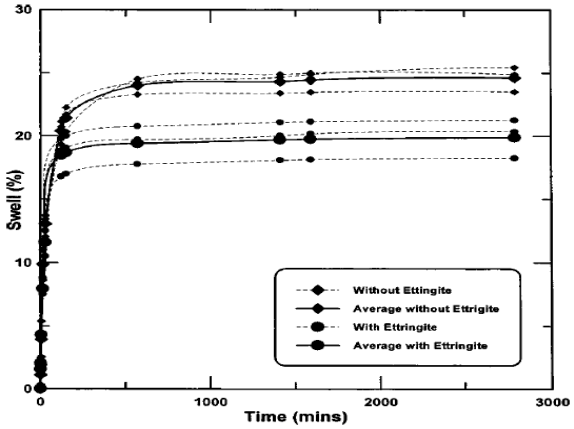

Figure 2.18: The results obtained from kaolinite clay with 8% of synthesised ettringite plotted as swell vs time (Puppala et al., 2005)

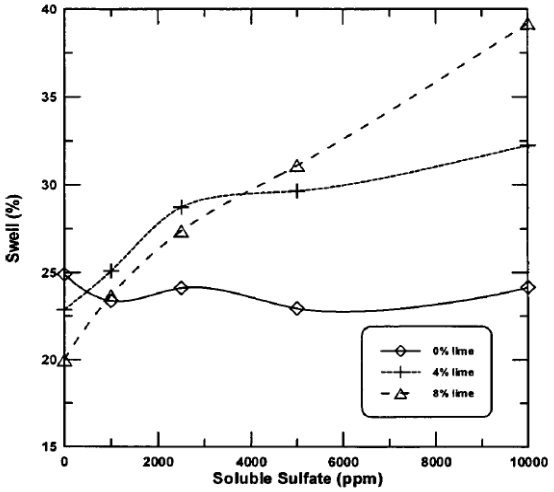

Figure 2.19: The results obtained from kaolinite clay plotted as soluble sulphates contents vs free vertical swell with different percentages of lime (Puppala et al., 2005)

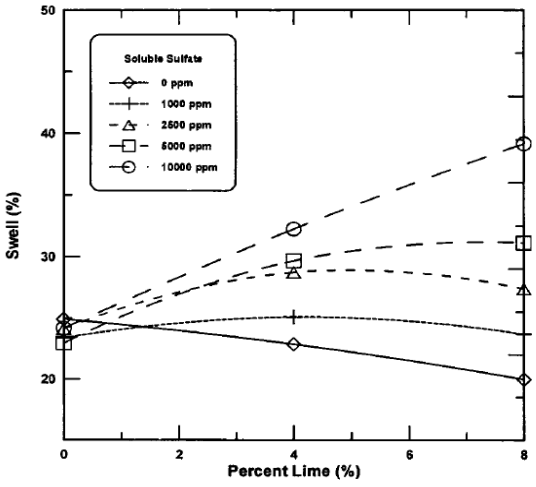

Figure 2.20: The results obtained from kaolinite clay plotted as lime contents vs free vertical swell with different contents of soluble sulphates (Puppala et al., 2005)

Little and Nair (2009) proved that reactive clay particles are responsible for the formation of ettringite.They conducted differential scanning calorimeter (DSC) tests on five soils with distinct mineralogical characteristics and treated with calcium-based stabilisers, but they did not detect any connection between the clay content and the quantity of ettringite. They also observed that increasing the time of curing up to 56 days was effective in increasing the growth of ettringite in all soil specimens.

2.3.2. The use of chemicals for stabilisation

In recent years, soil stabilisation has become a common means of improving the strength, durability and engineering properties of soil. Problems related to compaction, plasticity and shrink-swell potentials can be resolved by adding chemicals to in situ or borrowed clays (Das, 2012). The admixtures most used for soil stabilisation are usually cement, lime, fly ash and bituminous material. The most frequently used chemicals are sodium silicate, acrylamide, N-methylolacrylamide, polyurethane epoxy resins, aminoplasts, phenoplasts and lignosulfonates, to name a few (Kazemian et al., 2010).

When lime ($Ca(OH)_2$) is added to water, the lime molecules dissolve to form Ca^{2+} and OH^- ions in the water. A cation exchange occurs between the divalent calcium cations and the cations from clay, leading to modification of the diffuse double layer in clay and altering the electricity charges around the clay particles. These changes create attraction forces among clay particles and result in flocculation, which leads to stronger forces developing between clay layers and a large number of them packing together (Grim, 1962). These changes in the interparticle

reactions in clay cause the formation of thicker clay particles, leading to an increase in the strength and a decrease in the plasticity of the soil (Basma & Tuncer, 1991; Khattab, 2002 (as cited in Al-Mukhtar et al., 2012)). Whereas, Mohd Yunus et al. (2011) proved that increasing the lime content beyond 5% in the mix with humid acid content up to 3% decreased the shear strength moderately.

Many researchers have studied the efficiency of stabilisers, either separately or mixed with other stabilisers, on various types of soil. Others have focused on the problematic effects of reactions between those stabilisers and other chemicals on soil properties, particularly clay minerals, an example being sulphate-induced heave in soils treated with lime.

2.3.2.1. Effect of calcium based stabilisers

Al-Mukhtar et al. (2012) conducted a series of tests to study the geotechnical and microstructural properties of lime-treated natural clay with more than 80% smectite/kaolinite. They realised that 4% wt of lime is the optimal level at which the plasticity index and swelling pressure decreased, and unconfined compression strength (UCS) and permeability increased significantly. In contrast, Mohd Yunus et al. (2011) reported that increasing the lime content beyond 5% with the humid acid content up to 3% decreased the shear strength moderately. Al-Mukhtar et al. (2012) also proved that the addition of lime beyond 4% wt had negligible influence on the swelling pressure and UCS results, however, it caused a reduction in the permeability of the soil. The limited changes were also observed with lower lime content and increase curing time. These researchers also observed remarkable changes in the texture and

morphology of clay particles with added lime by scanning electron microscopy (SEM), as illustrated in Figure 2.21.

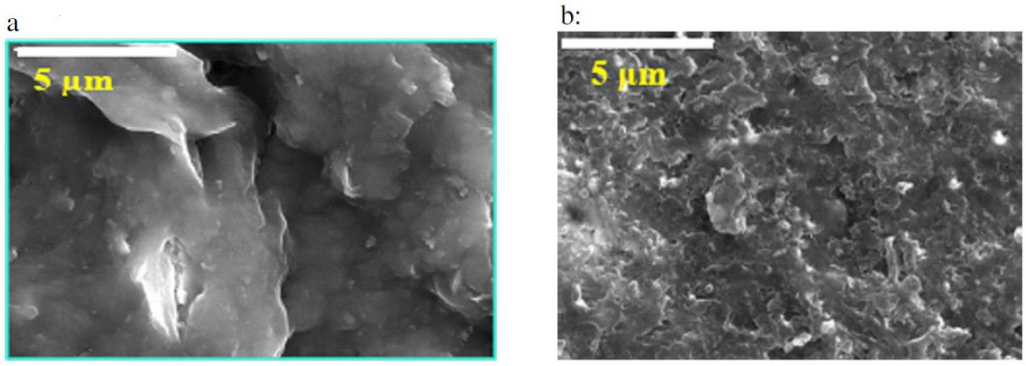

Figure 2.21: SEM images of untreated (a); and 10% lime treated (b) FoCa clay (Al-Mukhtar et al., 2012)

Bulbul Ahmed et al. (2013) studied the influence of lime and cement admixtures on the compressive strength of a local soil with a very low bearing capacity. They conducted a series of tests on untreated soil and soil treated with various quantities of lime admixture and cement admixture after curing times of three and seven days. The results demonstrated that cement admixtures had a greater impact on increasing the shear strength of soil than lime admixtures at any percentage. Furthermore, increasing the time of curing and the quantity of admixtures resulted in a further increase in the shear strength values for both admixtures. The strength of this soil is compared with various levels of cement and lime content in Figure 2.22.

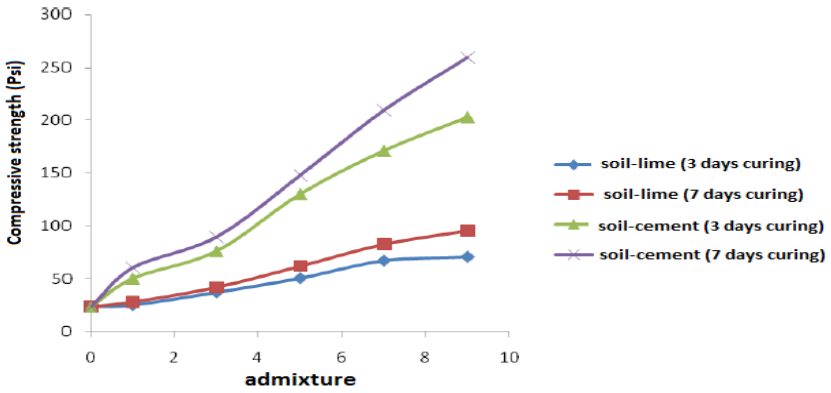

Figure 2.22: Comparison of strength vs. content (%) of admixture for stabilised soil (Ahmed et al., 2013)

Khemissa and Mahamedi (2014) evaluated the efficiency of cement and lime mixtures at various quantities on the engineering properties of an over-consolidated clay with high plasticity. Their results illustrated that the use of cement and lime in the mixture decreased the liquid limit plasticity index, swelling potential, swelling pressure and corresponding free swelling. The addition of cement and lime mixture to soil also increased the shear strength of the soil. Based on their results, they recommended that a mixture of 8% cement with 4% lime was the most efficient for improving the durability, stability and resistance of clay.

Nalbantoğlu (2004) emphasised that fly ash mainly has the role of reducing the swelling potential of soil, which prevents the problems caused by the shrink-swell of an expansive soil. The results of this study revealed that fly ash was more effective in the reduction of the plasticity index of clay with a high plasticity rather than a low plasticity, however it was effective in improving the plasticity of both soils. Also, cation exchange capacity (CEC) values revealed that the mineralogy of clays was altered by fly ash treatment due to new pozzolanic

reactions. These changes led to a more granular structure in the soil, resulting in less water absorption by clay particles.

Prabakar et al. (2004) reported a reduction in the maximum dry density and swelling of three soils classified as CL, OL and HL clays treated with fly ash. They also observed an increase in the cohesion of CL and OL soils and the shear strength of all soils. Moreover, increasing the fly ash content caused a further increase in the shear strength and cohesion values, and more reduction in the swelling.

2.3.2.2. Effect of silicate as a stabiliser

Moayedi et al. (2012) investigated the effect of sodium silicate (Na_2SiO_3) as a stabiliser in a composition with two activators including calcium chloride ($CaCl_2$) and aluminium sulphate ($Al_2[SO_4]_3$) on the unconfined compressive strength (UCS) of an organic soil containing kaolinite. Their results showed that the shear strength of untreated soil was increased by adding Na_2SiO_3. Increasing the Na_2SiO_3 content also raised the shear strength value significantly by up to 220% for 3% Na_2SiO_3. This increase was strengthened to 270% by the addition of $CaCl_2$ and/or $Al_2(SO_4)_3$ in the mixture. Moreover, the researchers realised that even though the sodium silicate grout in higher concentrations was more effective in improving the strength of the soil, it had a greater influence in the mixture with lower concentrations of activator agents ($Al_2(SO_4)_3$ and $CaCl_2$).

2.3.2.3. Effect of calcium based stabilisers mixed with other salts

The impact of different concentrations of lime, cement and NaCl salt and their combinations on the swelling properties of three soils including bentonite was evaluated by Gueddouda et al. (2011). Their results revealed that the addition of lime had the same influence as the addition of cement, leading to a decrease in the liquid limit, plasticity index and swelling potential of all soils. Also, they realised that a combination of salt with lime was more effective than using it alone or in combination with cement. A composition of 1.5 mol/L salt with 6% wt of lime was the most effective, resulting in an 80% reduction in the free swell test and more than 90% in the swelling pressure test.

Aldaood et al. (2014) implemented a comprehensive series of tests to study the effect of gypsum ($CaSO_4.2H_2O$) on the geotechnical behaviour of low plasticity clay (CL) treated with lime. They compared the results for natural clay and gypseous clay with different percentages of gypsum both treated with lime. They also considered the effect of curing time and temperature on the soil specimens. The results illustrated that increasing the gypsum content led to a decrease in the maximum dry density of lime-treated soil and an increase in optimum moisture. This was explained by the fact that the absorption of water by lime for its hydration as well as initial reactions, such as the cation exchange reaction, flocculation/aggregation and carbonation, are responsible for this soil behaviour. There was also an increase in the unconfined compressive strength of soil (UCS) with up to 5% gypsum content, and an increase beyond this content. This increase was explained as being the result of suffusing the soil pores with gypsum particles and consequently reducing the void ratio of the soil. Moreover, the strength of soil with or without gypsum was increased by increasing the time and temperature

of curing. The unconfined compressive strength variation versus curing time and gypsum content for untreated and treated soil with 3% lime are illustrated in Figures 2.23(a) and (b).

It was also noted that the free swelling potential of gypseous clay increased at some times decreased at others. This complicated swelling potential behaviour was interpreted as being due to the formation of ettringite, particularly over longer curing times. The free swell potential versus curing time and gypsum content for untreated and treated soils with 3% lime is presented in Figures 2.24(a) and (b).

The researchers also observed the formation of calcium silicate hydrate (CSH) and calcium aluminates hydrate (CAH), which operate as cementation agents and improve the shear strength of soil, and also ettringite by means of porosimetry, XRD and SEM which showed higher intensities at 40°C rather than 20°C.

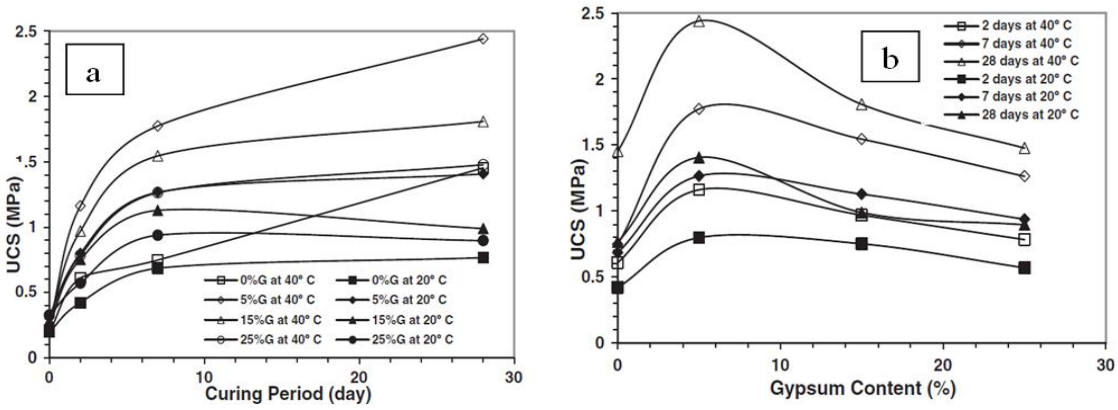

Figure 2.23: Unconfined compressive strength vs curing time (a); and Gypsum content (b) with various contents of gypsum and different temperatures for untreated and treated soil with 3% lime (Aldaood et al., 2014)

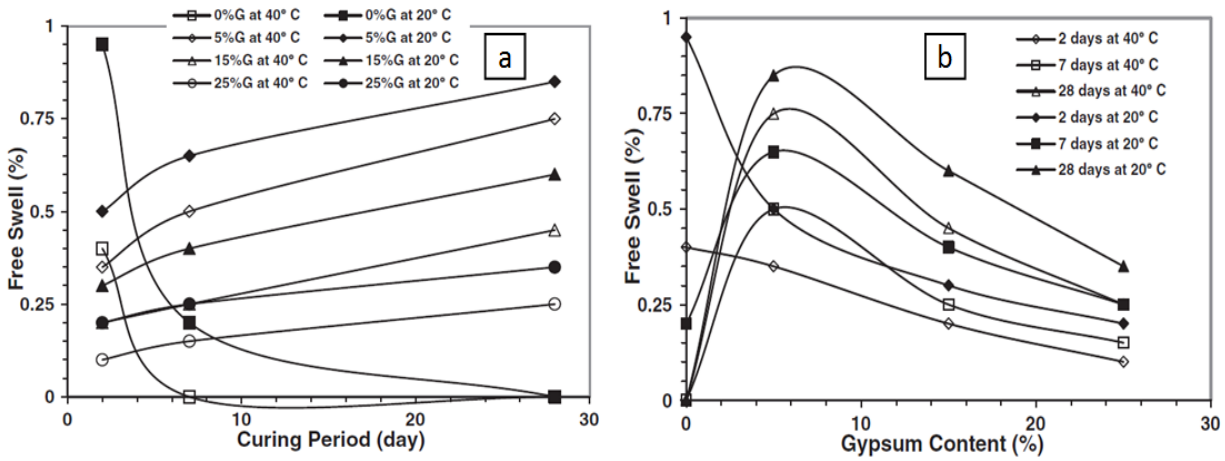

Figure 2.24: Free swell vs curing time (a); and Gypsum content (b) with various contents of gypsum and different temperatures for untreated and treated soil with 3% lime (Aldaood et al., 2014)

2.3.2.4 Effect of calcium-based stabilisers with an organic matter

Mohd Yunus et al. (2011) studied the effect of various levels of humic acid on the engineering and physical properties of artificial organic clay stabilised with lime. Their results demonstrated that increasing the humic acid content in untreated clay had a destructive impact on the unconfined compressive strength (UCS) and compaction of organic clay. The addition of lime up to 5% improved the undrained shear strength of soil remarkably. However, increasing the lime content beyond 5% as well as the humid acid content up to 3% decreased the shear strength moderately. The researchers also investigated the influence of curing time on the lime-treated organic clay in the presence of humic acid, and concluded that longer curing times of up to 90 days decreased the strength of soil, and increasing the humic acid content and the time of curing increased the rate of this decline. So they concluded that, even though organic clay containing humic acid could be stabilised by the addition of lime in the beginning, this method

was not very efficient for longer curing times and at higher percentages of humic acid. Moreover, they observed more cracks in the clay plates in the untreated samples with a higher concentration of humic acid using SEM imaging. With the addition of lime, the clay particles exhibited a well aggregated structure and the cracks disappeared. However after 28 days of curing the lime-treated samples with a higher percentage of humic acid demonstrated larger pore spaces, which explained the inefficiency of the lime over longer curing periods.

2.4 Numerical modelling on the effect of chemicals on soil behaviour

2.4.1 Introduction

In recent years, several studies have been carried out using numerical analysis to simulate soil behaviour in typical geotechnical problems such as footing, tunnelling, excavation, soil structure and soil retaining wall interactions (Athanasopoulos-Zekkos et al., 2012; Mun et al., 2012; Tiznado & Rodriguez-Roa, 2011; etc). Some others have focused on a combination of laboratory experiments and finite element simulation using empirical equations in recommended constitutive models to compare the results obtained with both methods. The primary aim of these studies is to suggest more efficient methods for geotechnical investigations in order to reduce the costs, effort and errors involved in experimental tests (Cuisinier et al., 2012; El-Zein & Balaam, 2006; Kimoto et al., 2007; Seetharam et al., 2006; Villar et al., 2008). However, studies using computer simulation to investigate the effect of chemicals on soil are very scarce.

2.4.2 Numerical simulation of the effect of cement or lime on soil

Horpibulsuk et al. (2009) simulated the behaviour of cement-treated clay with different cement contents under various values of confining stresses. They used a structured cam clay (SCC) model to consider the elastic and virgin failure behaviour of cemented clay.

They modified the mean effective stress parameter (P') by capturing the effect of cementation (C) and the slope of the Mohr failure envelope (M) in cement-treated clays (Gens & Nova, 1993; Horpibulsuk, 2001; Kasama et al., 2000). The new mean effective stress was described as below:

$$\bar{p}' = p' + C/M, \qquad \text{Eq. 2.1}$$

Two series of analyses were conducted. Firstly, the behaviour of Hong Kong's Ariake clay treated with 9% (Aw=9%) cement was simulated using the parameters obtained from laboratory tests and the results of the simulation were compared with the experimental results. Secondly, the behaviour of this soil treated with different quantities of cement was predicted using the parameters estimated from the equations recommended by Horpibulsuk (2001), Huang (1994), Kasama et al. (2000), Liu and Carter (2000, 2002 & 2003) and Nagaraj et al. (1998). The stress-strain curves for the cemented Ariake clay using the SCC model were verified by comparing these results with previous results obtained from conventional tests by Horpibulsuk et al. (2004). Refer to Figure 2.25 for more information.

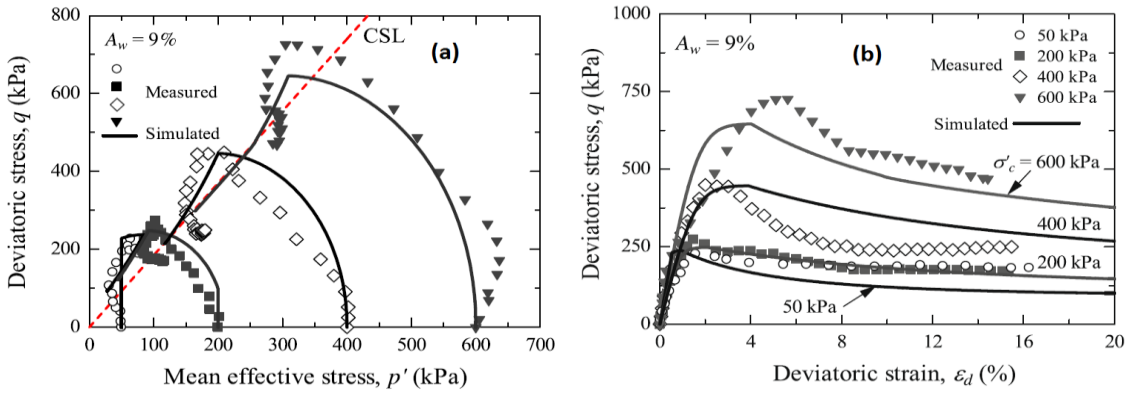

Figure 2.25: The effective stress paths (a) ; and deviatoric stress vs deviatoric strain curves for the cemented Ariake clay with Aw = 9% (Horpibulsuk et al., 2004, as cited in Horpibulsuk et al., 2009)

The simulated results from the second sets of calculations related to Ariake clay treated with various quantities of cement have been validated by some researchers. Lee and Lee (2002) confirmed their analysis with measured η _ εd and Δu _ εd and q _ εd and εv _ εd with 2% and 5% cement content. Yin and Lai (1998) and Sariosseiri and Muhunthan (2009) confirmed their findings with the evaluated q _ εd and Δu _ εd relationships for cemented Hong Kong clay and cemented Aberdeen silt with 5% cement content. Horpibulsuk et al. (2009) employed effective stress paths and stress and strain relationships with 6% and 12% cement content to validate their calculations.

Therefore, Horpibulsuk et al. (2009) concluded that the SCC model is a useful tool for anticipating the behaviour of cemented clay with different levels of cement by using the proposed experimental equations. Some parameters such as undrained shear behaviour can be predicted. However, some other parameters which depend on the amount of cement still need to be identified by experimental tests.

Azadegan et al. (2013) used the results obtained from unconfined compressive strength tests on various mixtures of two granular cement-treated soils (see Table 2.1) in the Plaxis finite element code. The aim was to evaluate the behaviour of these mixtures as base layers on soft clay as the subgrade soil in unpaved roads under a particular load. The cohesion and friction angle were calculated from the shear strength parameters obtained from the UCS for each mixture.

Table 2.1: The cement, lime and water proportions of different soil mixtures (Azadegan et al., 2013)

Mixture Type	Cement Ratio (%)	Lime Ratio (%)	Moisture Content (%)
S-1	4	6	10.4
S-2	5	5	9.5
S-3	6	4	9.1
G-1	4.5	6.8	9.4
G-2	4.5	5.6	8.9
G-3	4.5	4.5	8.2
G-4	5.6	6.8	9.6
G-5	5.6	4.5	8.9

The results from the Plaxis simulation illustrated that those mixtures with higher elasticity modulus values resulted in lower vertical displacements under the same conditions of loading. On the other hand, they exhibited lower bearing capacity unexpectedly. The maximum vertical deformation, collapse load and modulus of elasticity for each mixture are presented in Figure 2.28.

The researchers stated that if the difference in the elasticity modulus between soft clay (subgrade) and cement treated mixtures (base layer) is very high it leads to the non-uniform distribution of load between two layers and consequently a decrease in the bearing capacity of

the base layer regardless of its high stiffness due to cement treatment. They concluded that, not only should the elasticity modulus of mixtures be high enough in the cement treated layer, but it should also not be very different to that in the subgrade soil.

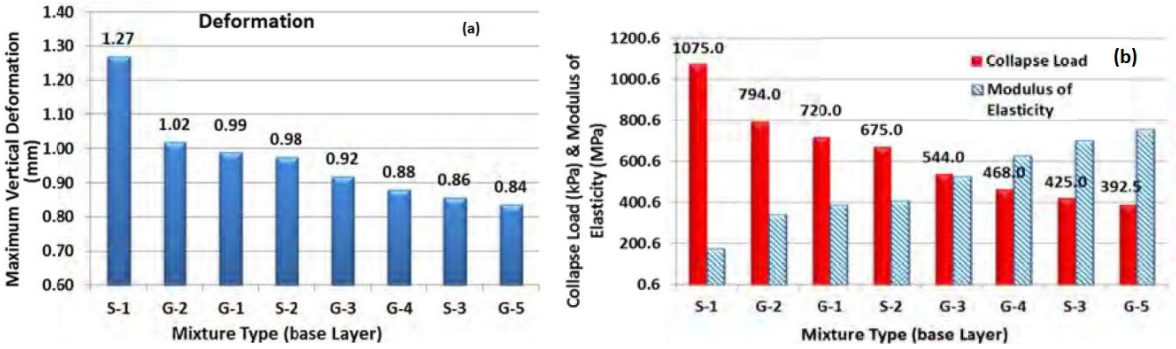

Figure 2.28: (a) Maximum vertical deformation; and (b) collapse load and modulus of elasticity vs. the mixture type (sorted with the increment of E from left to right) (Azadegan et al., 2013)

2.4.3 Numerical simulation of the effect of pore fluid on soil

Bayesteh and Mirghasemi (2012) simulated the effect of different salt concentrations, cation types and dielectric constants on the microscopic behaviour of double diffuse layer (DDL) in montmorillonite using the discrete element method (DEM). They explained that even though many researchers (Baille et al., 2010; Bolt, 1956; Delage, 2007; Di Maio, 2004; Gens & Alonso, 1992; Komine, 2008; Mesri & Olson, 1971) had conducted a large number of studies on the effect of pore fluid chemistry on the volume change behaviour in clays, these studies were still not adequate. These studies have limitations in controlling two important factors, pore fluid characteristics and the initial particle structure prior to experimental research. Hence, like other authors including Iordanoff et al. (2005), Zhang and Li (2006), Anandarajah (1994 and 2003), Yao (2001), and Katti et al. (2009), they suggested the use of DEM in their studies for a

better understanding of the behaviour of clay at the microscopic level. However, they enhanced the method for calculating repulsive forces based on the Gouy-Chapman theory presented by Van Olphen (1991). According to this theory, the double layer repulsive forces between parallelly oriented clay particles was estimated using Langmuir's Equation as presented in Equation 2.2.

$$P = 2nkT[\cosh(u) - 1] \quad \text{Eq. 2.2}$$

$$u = \frac{ve\phi}{kT} \quad \text{Eq. 2.3}$$

$$z = \frac{ve\phi_0}{kT} \quad \text{Eq. 2.4}$$

$$K = \sqrt{\frac{8\pi n v^2 e^2}{\varepsilon kT}} \quad \text{Eq. 2.5}$$

Where:

u = the potential between two aligned particles as calculated in Equation 2.3.

z = the potential on the surface of clay

k= Boltzmann's factor (=1.38 × 10^{23} J/K)

ϕ = the electrical potential at a given distance from the surface of clay

ϕ_0 = the electrical potential at the surface of clay

e = the electrical charge considered for an electron (=4.8 ×10^{-10} esu).

Bayesteh and Mirghasemi (2012) explained that the equations above and other equations suggested by Anandarajah (1994), Lu and Anandarajah (1992), Mitchell (1993) and Van

Olphen (1991) are not accurate for montmorillonite with randomly oriented particles, high surface potential value and small Kd values. Instead, they used the equation suggested by Lu and Anandarajah (1992), however they improved the equation for calculating the repulsive interparticle forces and electrical potential in montmorillonite. Equations 2.6 and 2.7 and Figure 2.29 show the compatibility of their equations with the experimental results.

$$\int_z^u \sqrt{(2\cosh y - 2\cosh u)}\,dy = -Kd \qquad \text{Eq. 2. 6}$$

$$e^{v/2} = \frac{(e^{z/2}+1)+(e^{z/2}+1)e^{-Kd}}{(e^{z/2}+1)-(e^{z/2}+1)e^{-Kd}} \qquad \text{Eq. 2.7}$$

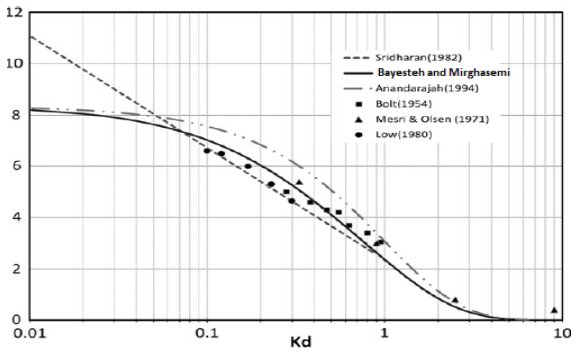

Figure 2.29: Comparison of the theoretical and experimental data for u–Kd relationship (Bayesteh & Mirghasemi, 2012)

They used the salt solutions most commonly used in previous studies, NaCl and $CaCl_2$, at concentrations ranging from 0.001 M to 0.1 M. Their results illustrated that increasing the salt concentrations and cation valence reduced the thickness of DDL and resulted in a decrease in the repulsive forces at the same void ratio. They therefore concluded that using the suggested equations in a DEM simulation proved the dependency of the thickness of DDL on the pore

fluid chemistry. Their results were also were verified by the available experimental and theoretical data. Refer to Figure 2.30 for more information.

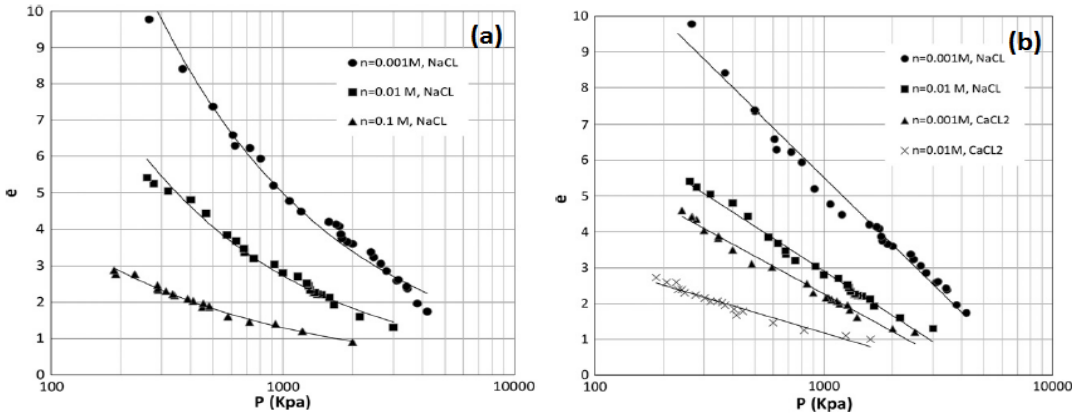

Figure 2.30: The results of e vs log p for montmorillonite saturated in (a) NaCl; and (b) NaCl and $CaCl_2$ solutions at different concentrations (Bayesteh and Mirghasemi, 2012)

2.5 A Summary of the reviewed literatures

The summary of the above literature reveals that, among all of the natural salts, much attention has been given to the effect of chloride salts on the properties of clay, while the influence of other naturally distributed salts such as sulphates and carbonates has not yet been considered adequately. Most of the researchers have focused mainly on the effect of these salts on the Atterberg limits and swelling parameters of clay due to their dominant role in the behaviour of clays. Hence, less attention has been given to the other important characteristics of clay such as the shear strength parameters. Moreover, even though the effect of sodium sulphate with calcium-based stabilisers has been investigated by many researchers due to the formation of problematic minerals, namely ettringite, studies on the influence of these salts individually are very scarce.

Further more, although there are many studies on the influence of chemicals on soils in the experimental field a few researchers have expanded these empirical studies to numerical simulations.

This research, therefore, will investigate the effect of sodium sulphate on the shear strength properties of bentonite clay, taking into account the effect of salt concentration and curing time. In order to observe the impact of this salt on a larger scale, in the next step two geotechnical problems including a footing and a retaining wall laid on a bentonite layer will be simulated using Plaxis finite element code. The data from laboratory tests on this soil will be transferred to the Plaxis simulations, and the behaviour of sulphate-attacked bentonite will be investigated under various conditions of loading.

Chapter 3

Materials and Methodology

3. Materials and Methodology

3.1 Introduction:

This chapter was separated in different phases as outlined in Figure 3.0:

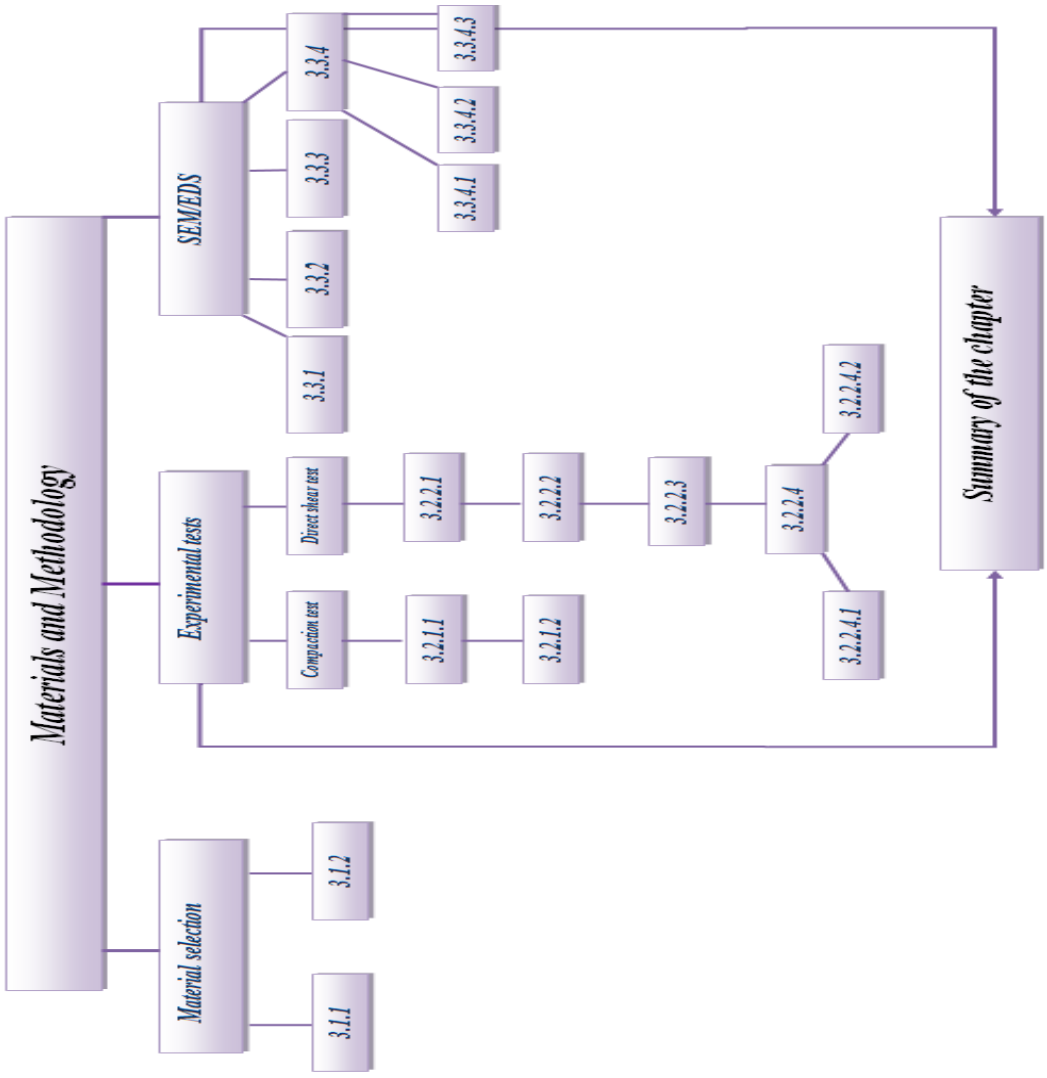

Figure 3.0: The outline of Material and Methodology chapter

3.2 Material selection

Three factors were considered in choosing the materials employed in this research, including: economic impact, the abundance of materials and the ease of supply in the Western Australian construction industry, as well as the ease of use in the laboratory, for example with relation to having stable physical and chemical properties in different weather conditions. All of the materials selected were accessible in Western Australia, and were already extensively used in various industries including the glass industry, as well as in road and construction projects.

These materials are presented in the following sections.

3.2.1 Sodium bentonite clay

Bentonite, a clay mineral, has recently become the most important clay in civil and geotechnical engineering projects due to its unique rheological and absorbent properties. There are numerous deposits of bentonite in Europe, North America, New Zealand and Australia. Australia is an abundant source of this soil and supplies low to very high quality clays for local and global markets. Australian deposits of this soil are mainly located in the eastern states, particularly in Queensland and New South Wales (NSW department of Primary Industries)

Of the bentonites, sodium bentonite is most prevalent in construction projects. It can push itself into cracks and voids due to its high swelling capacity, and forms gel-like masses when mixed with water. Premium grade sodium bentonite was chosen for this research due to its superior properties. This soil is collected and refined near Miles in Queensland and is manufactured by Sibelco, under the commercial name Trubond MW. Trubond MW contains a high proportion of

the active smectite mineral component montmorillonite. It has unique physical and chemical properties as well as absorbent properties. Trubond MW also displays considerably high thermal endurance. The following typical properties make this soil suitable for applying the fundamental tests and determining the factors essential for the preliminary steps. Table 3.1 lists the chemical, analytical and physical properties.

Table 3.1: Chemical, Analytical and physical properties of Trubond MW bentonite (Sibelco Australia)

Chemical Properties	
Chemical Formula	**Mean value by Weight (%)**
(SiO_2)	63.2
(Al_2O_3)	13.3
(TiO_2)	0.3
(Fe_2O_3)	2.6
(CaO)	0.3
(Na_2O)	1.9
(MgO)	2.2
(K_2O)	0.2
Physical Characteristics	
Water Absorption (ml/2g)	750
Suspension Characteristics	
Yield point ($N/100m^2$)	47.8
Plastic Viscosity (cP)	5
Apparent Viscosity (cP)	6
PH	9.5
API Filtrate (mls)	14
Analytical Characteristics	
Cation Exchange Capacity(CEC) (meq/100ml)	82
Bulk Density (kN/m^3)	9
Wet Screen (Retained on the75 microns sieve)%	1
Dry Screen (Passing through the 75 microns sieve)%	77
Water Content (%)	11

3.2.2 Sodium sulphate

Sodium sulphate is one of the most common salts in nature. Sodium and sulphate ions can be found in abundance in most waters such as saline lakes or playas. The sodium sulphate used in this research is a white crystalline salt with the formula Na_2SO_4, which is known as thenardite. Sodium sulphate can be completely dissolved in water into sodium and sulphate ions. These ions cannot hydrolyse. Sulphate is not a reactive ion, so it is suitable for keeping at room temperature, which is also an appropriate temperature for curing the soil mixture.

Even though sodium sulphate can be soluable in water, the behaviour of pure sodium sulphate is slightly complicated due to its sensitivity to temperature when dissolved in water.

Some researchers have examined the solubility of this salt at various temperatures. Garret (2001) has gathered data from the work of other researchers including Seidell (1965), Strakhov (1970) and Dyson (1961). Appendix 1 lists the solubility of sodium sulphate at temperatures from -1.25°C to 382°C from the information provided by Garret (2001).

The results about the solubility of sodium sulphate from the various researchers are rather variable, however there is reasonable agreement regarding temperatures from 20°C to 25°C. The amount of salt dissolved in water at these temperatures is higher than for very high temperatures. Refer to Appendix 2 for more information.

Consequently, indications are that room temperature is suitable for dissolving sodium sulphate

in water for use in making the soil mixtures in the experimental tests. These tests are presented in the following sections.

3.3 Experimental Tests

The soil tests consisted of two parts: the primary compaction tests and the comprehensive small direct shear tests. All tests were carried out under the same conditions and a number of factors such as curing time, duration and amount of loading pressure was regularly monitored for both untreated and salt-treated samples in order to achieve the proposed objectives.

3.3.1 Compaction test

Compaction is an essential procedure in construction fills and embankments to improve the engineering behaviour of soil. It enhances the shear strength of soil leading to the settlement of the ground, helping to prevent unnecessary maintenance costs or structural failure. The strength of a soil is one of the most important qualities that needs to be assessed before undertaking any construction. In this process, the compactive effort, the energy supplied by the compaction hammer, is responsible for driving the air out by packing the soil particles closer together and increasing the dry density of the soil. (See Figure 3.1)

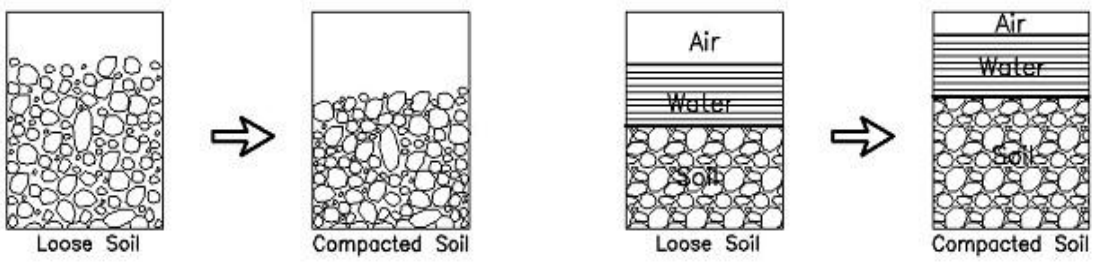

Figure 3.1: The soil body before and after compaction

3.3.1.1 Effect of some factors on the compaction of soil

The dry density obtained from a compaction test relays upon a few parameters including the moisture content of the soil, the type of soil and the compactive effort (compaction energy).

- **The effect of moisture content**

Moisture content can be considered the most important factor in the determination of the maximum dry density of soil. During the compaction process at a moisture content equal to zero (w = 0%), the unit weight of soil is equal to its dry unit weight.

$$\gamma = \gamma_{d\,(w=0)} = \gamma_1 \qquad \text{Eq. 3.1}$$

With constant compactive efforts, increasing the moisture content will lead to an increase in the solid parts of soil per unit volume. In moisture content ($w = w_1$) the unit weight of soil is equal to:

$$\gamma = \gamma_2 \qquad \text{Eq. 3.2}$$

In this condition the dry unit weight can be considered as follows:

$$\gamma_{d\,(w = w1)} = \gamma_{d(w = 0)} + \Delta\gamma_d \qquad \text{Eq. 3.3}$$

After $w = w_1$, as presented in Figure 3.2, further increasing the moisture content will lead to a decrease in the dry density of the soil. The reason is that water will occupy the holes in the soil,

and this will prevent soil particles from filling these holes. Optimum moisture content (OMC) is the limit beyond which increasing the moisture content decreases the dry unit weight of soil.

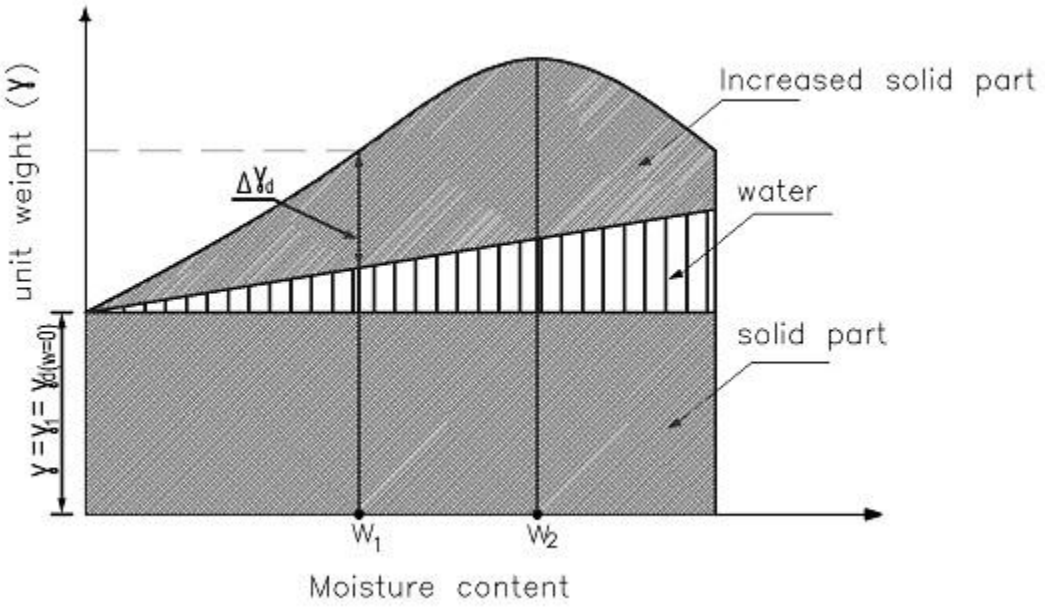

Figure 3.2: Maximum dry density (MDD) in optimum moisture content (OMC) (Das, 2008)

- ***The effect of soil type***

Each soil type has unique properties and shows different behaviour under laboratory compaction tests. Consequently, a distinctive MDD and OMC will be attained for each type of soil. The grading curve of the soil, the shape of the soil particles, the specific weight of the soil (Gs) and the type and quantity of clay particles existing in soil all have a significant impact on soil MDD and OMC. The MDD in sandy soils first decreases and then increases with the addition of water (see Figure 3.3).

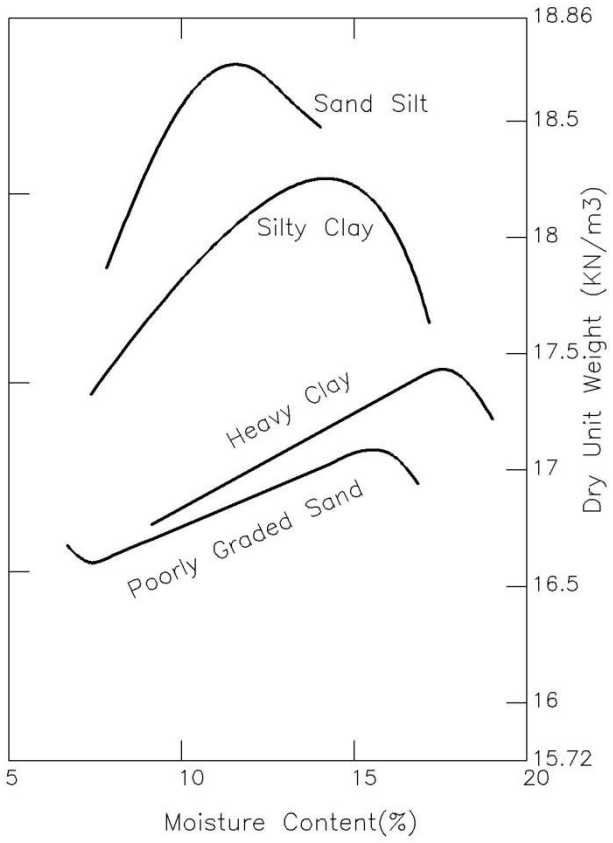

Figure 3.3: The compaction curves for four different soils (Das, 2008)

- ***The effect of compaction energy***

According to (Das, 2008), the energy of compaction obtained from the standard Proctor test can be described as follows:

$$E = \frac{\text{Number of blows For each layer} \times \text{number of layers} \times \text{weight of hammer} \times \text{height of the drop of hammer}}{\text{Volume of mould}} \quad \text{Eq. 3.4}$$

If the compaction energy per unit volume of soil changes, it will change the compaction curve (dry unit weight vs moisture content). Figure 3.4 shows typical compaction curves for sandy clay with four different compaction efforts using standard Proctor equipment. For all of the compaction tests, the soil was compacted in three equal layers, but the number of blows for each layer differed from 20 to 50. Table 3.1 shows the relationship between the number of layers and the compaction energy delivered for the three layers for the compaction curves presented in Figure 3.4.

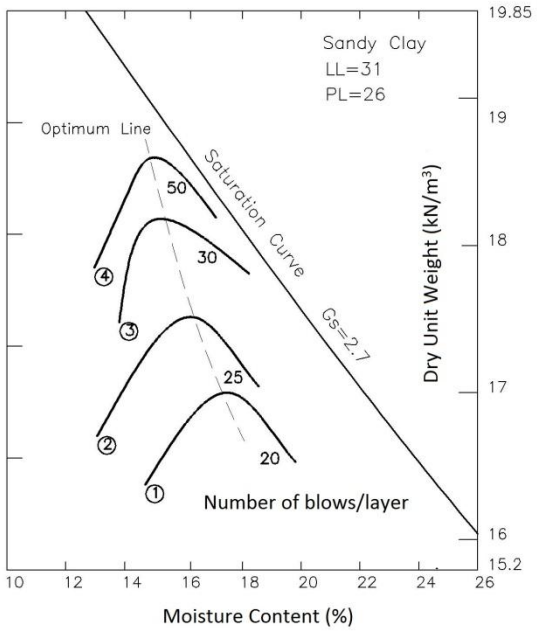

Figure 3.4: The compaction curves for four different soils (Das, 2008)

Table 3.2: The relationship between the numbers of layers and the compaction energy delivered for three layers for the compaction curves in Figure 3.4 (Das,1999)

Number of Curve in Figure 3.4	Number of Blows for Each Layer	Compaction Energy (kJ/m^3)
1	20	474
2	25	593
3	30	711
4	50	1185

3.3.1.2 Compaction test program

A series of compaction tests were performed on both pure bentonite and bentonite mixed with various percentages of sodium sulphate. Four quantities of this salt were added to bentonite (0.5%, 1%, 1.5% and 3% by dry weight of soil) to investigate the compaction properties of the mixtures. The results of the tests are presented and discussed in this chapter.

3.3.1.2.1 Compaction test method

The Proctor standard compaction test (Proctor 1933), the most commonly used laboratory test, was used to determine the (OMC) and (MDD) of the soil. In this method, the soil was compacted in three identical layers in a cylindrical mould using a 2.5 kg rammer with a drop height of 30 cm as illustrated in Figure 3.5.

3.3.1.2.2 Test requirements

- A cylindrical steel mould matched with a portable collar assembly and base plate as shown in Figure 3.5.
- A metal rammer weighing 2.5 kg and specially designed to drop 30 cm onto the mould as shown in Figure 3.5.

- A knife made of hard material.
- A sample extruder.
- A steel straight edge.
- A graduated ruler.
- A straight edge.
- Sealable bags.
- Drying oven.

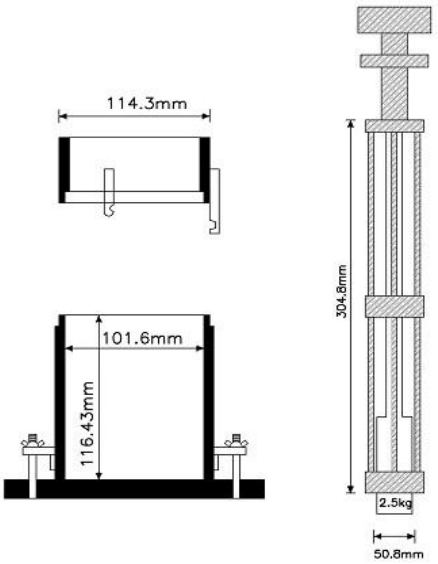

Figure 3.5: Mould and rammer for Proctor standard compaction test

3.3.1.2.3 Test methodology and procedure

- Based on AS1289. 5. 1. 1- 2003, about 3 kg of bentonite clay was thoroughly mixed and uniformly distributed with 18% of its weight in water and placed in sealed plastic bags. The storage of mixed soil in zip lock bags prevents water evaporation and loss of moisture content.

- The soil mixture was kept at room temperature (23±2ºC) for 24 hours. This time is adequate to allow the mixture to become more uniformly distributed before compaction.
- The measurement was taken of the mass of the mould and the base plate (m_1, gr).
- The assembly of the base plate, collar and mould was done and placed on a flat surface.
- The soil was compacted by 25 even blows in three layers in the mould. The height of each layer was measured with a graduated ruler to be approximately 38 mm to 43 mm.
- The final layer was added just as the compacted soil was just above the edge of the mould.
- The collar was detached carefully, and the surface of the compacted soil was trimmed with a straight edge while the mould was still fitted to the base plate.
- The measurement was taken of the mass of the mould with the base plate plus wet soil (m_2, gr).
- A heat-resistant, corrosion-resistant container was prepared and its weight was determined (m_a, gr).
- The soil specimen was removed promptly, was broken up to aid drying and transferred to the container for determination of the moisture content (w).
- The measurement was taken of the mass of the container plus wet soil (m_b).
- The container with soil was placed in the oven at 105ºC for 16 hours. After the soil had been dried adequately, the vessel was removed, and the mass of the container along with the dry soil was measured. This step was repeated for another hour and a successive drying achieved after the second hour, so 18 hours was determined to be a sufficient drying time.

- The mass of the container along with the dry soil was recorded for the last time (m_c).
- The test was repeated for soils with other moisture contents (22%, 30%, 40% and 45 % by dry weight of soil), at least two of which were dryer and one wetter than the OMC. These moisture contents were used as the best guess after conducting some primary compaction test with various moisture contents.
- The dry density against the water content curve was drawn by interpolating the achieved points , and the MDD and the OMC for each specimen were approximated on the graph.
- Compaction tests were repeated with the same moisture contents (18%, 22%, 30%, 40% and 45%) but mixed with various percentages of sodium sulphate. The sodium sulphate contents were used0.5%, 1%, 1.5% and 3% by dry weight of soil. These values were chosen close to the sulphate contents in the similar study previousley presneted by Sivapullaiah et al. (2000). The results and discussion are presented in this chapter.

3.3.1.2.4 Results and discussion

The tests were performed methodically in order to investigate the effect of sodium sulphate on the compaction properties of bentonite. Figures 3.6 to 3.10 show the compaction curves for pure bentonite (PB) and bentonite mixed with each percentages of sodium sulphate (SS), (0.5%, 1%, 1.5% and 3% of dry weight of soil) individually. Each curve is obtained from at least four different moisture contents which are presented in detail in Appendices 2 to 6. The air-void curves for different degree of saturation are plotted next to each curve considering

(Gs= 2.7). All the compaction curves are also illustrated in one graph in Figure 3.11 for a better comparison. The values of Maximum Dry Density and Optimum Moisture Content for each curve are also presented in Table 3.3 subsequently. This table shows that the OMC and MDD of the soil were affected by the addition of different percentages of the salt (SS).

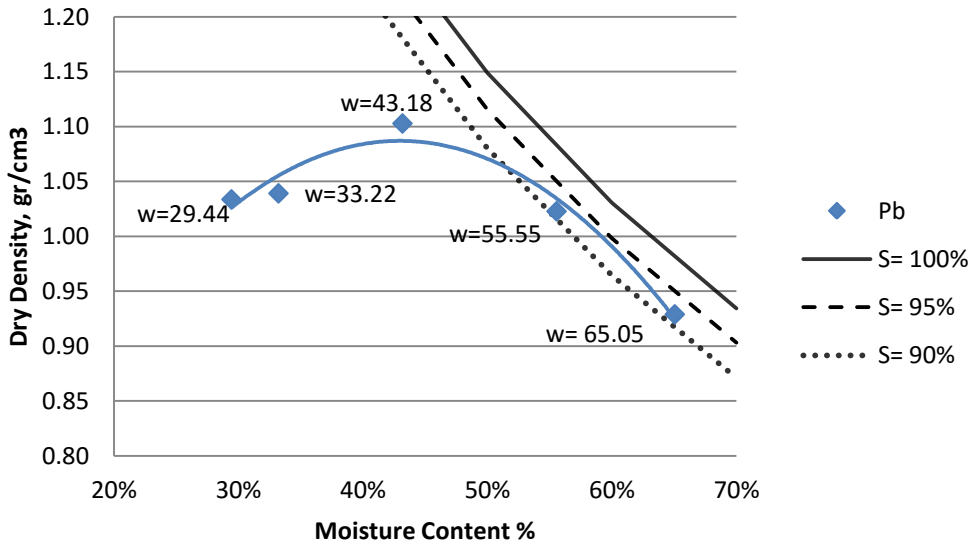

Figure 3.6: Compaction curves for pure bentonite (Pb) with various S (degree of saturation) values

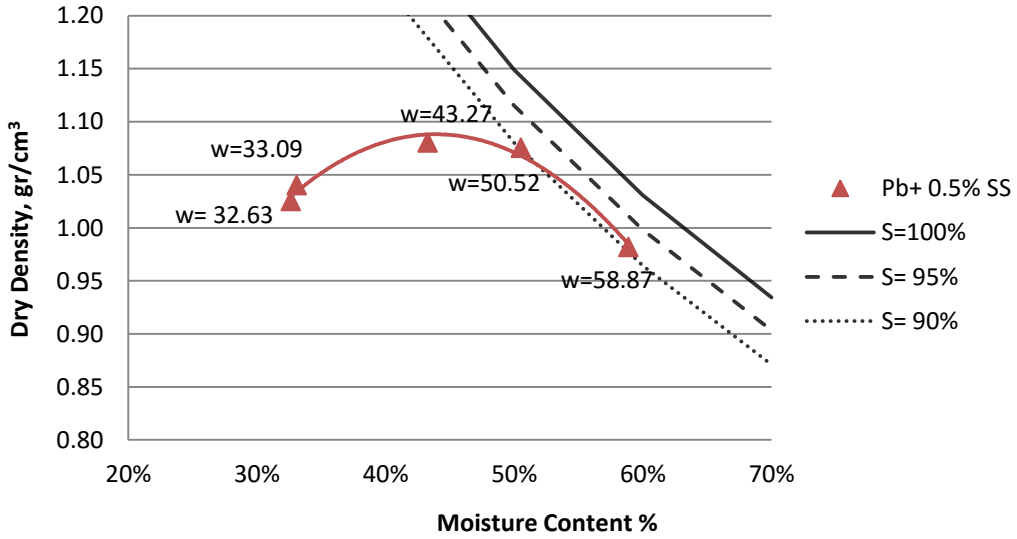

Figure 3.7: Compaction curves for pure bentonite (Pb) with 0.5% sodium sulphate with various S (degree of saturation) values

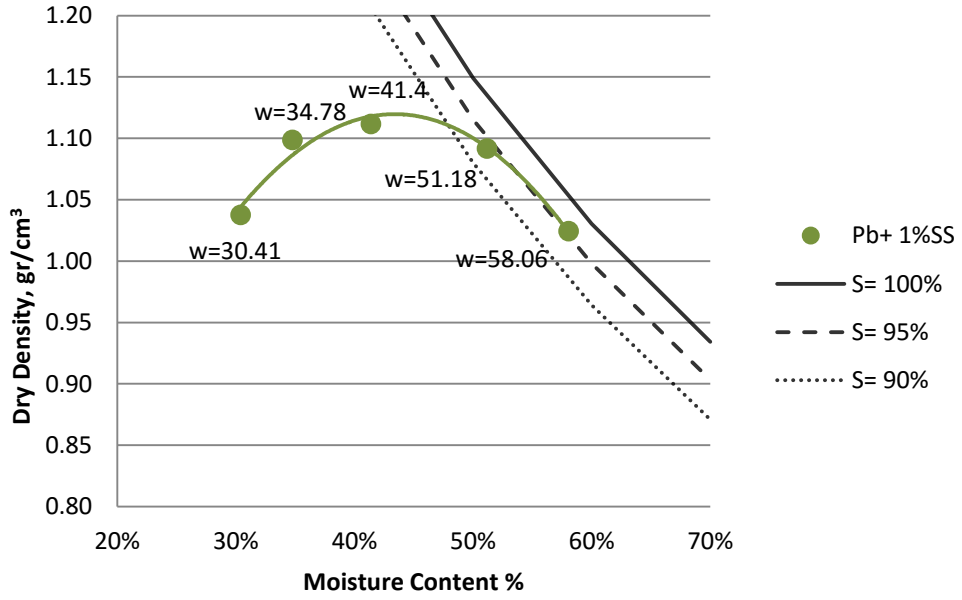

Figure 3.8: Compaction curves for pure bentonite (Pb) with 1% sodium sulphate with various S (degree of saturation) values

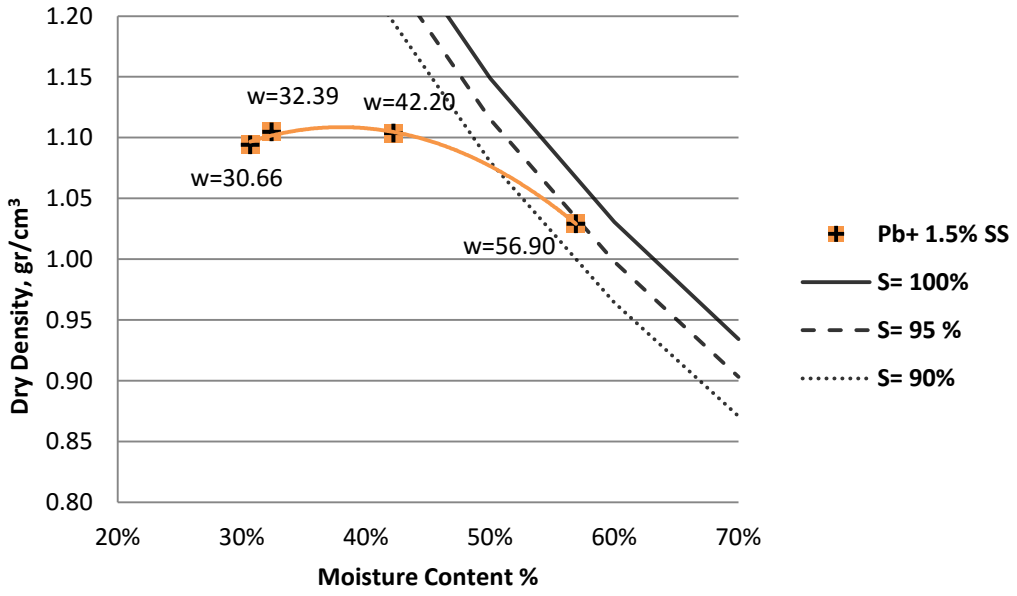

Figure 3.9: Compaction curves for pure bentonite (Pb) with 1.5% sodium sulphate with various S (degree of saturation) values

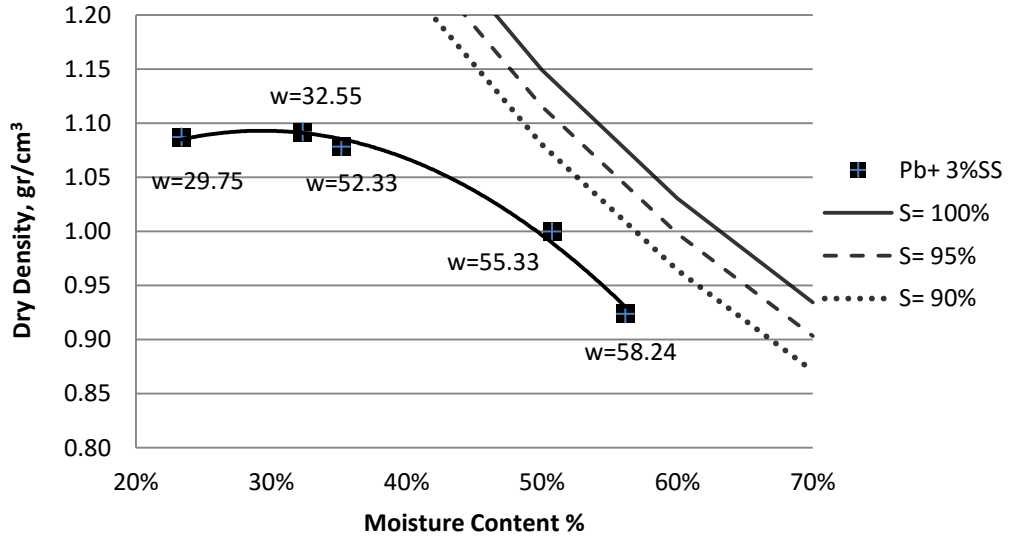

Figure 3.10: Compaction curves for pure bentonite (Pb) with 3% sodium sulphate with various S (degree of saturation) values

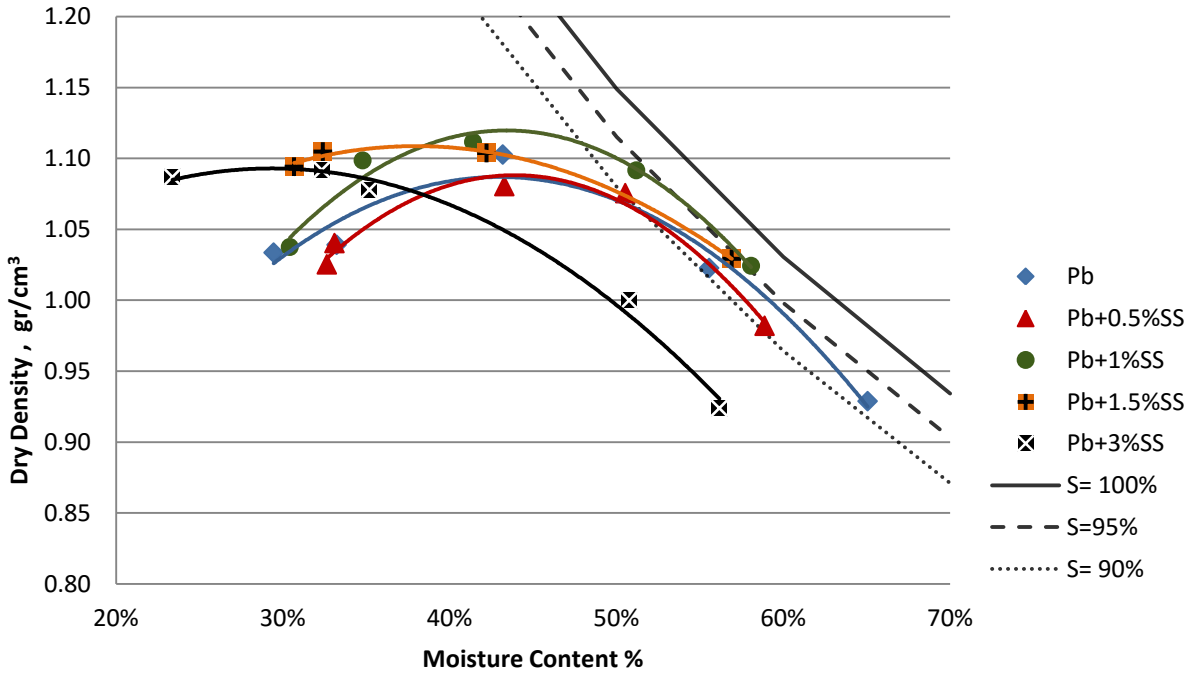

Figure 3.11: Compaction curves for pure bentonite (Pb) and bentonite mixed with different percentages of sodium sulphate (SS)

Table 3.3: Laboratory compaction test results

Soil Mixture	***Maximum Dry Density (MDD) gr/cm³***	***Optimum Moisture Content (OMC) %***
Pure Bentonite	1.087	42.94
Bentonite+0.5% SS	1.088	43.89
Bentonite+1% SS	1.119	43.40
Bentonite+1.5% SS	1.108	37.98
Bentonite+3% SS	1.093	29.33

- ***Effect of sodium sulphate (SS) on maximum dry density of bentonite clay***

As shown in Figure 3.11 and Table 3.3, that the addition of various percentages of sodium sulphate to bentonite led to a slightly upward shift of the maximum point in each curve. There was an overall increase in the values of MDD in sulphate-treated samples compared to the

untreated sample. The maximum dry density of each curve is demonstrated in a separate graph (MDD) in Figure 3.12. This chart demonstrate that the addition of 0.5% sodium sulphate to bentonite did not alter the value of MDD, while addition of 1% of this salt led to an increase in the value of MDD. Then, the incremental addition of salt to up to 3% caused a drop in MDD compare to its previous value with 1% of salt. As seen from this figure, therefore, the highest value of MDD was obtained for the mixture with 1% sodium sulphate (SS). Based on the previously reviewed literature including Gratchev and Sassa (2009), Ruhl and Daniel (1997), D'Appolonia (1980) and Kashir and Yanf (2001), one hypothesis is that increasing the concentration of Na2SO4 from 0.5% to 1% results in an increase in the amount of Na+ cations. These cations participate in cation exchange with clay particles leading to a reduction in the thickness of the diffuse double layer in bentonite clay. This results in the aggregation of clay particles and consequently a more open clay structure leading to a better compaction, and an increase in the value of MDD. However the further increase in the amount of Na+ from 1% to 3% causes the changes in the environment of deposition, and alters the way the clay particles are arranged. The changes in the orientation and arrangement of clay particles can hinder the compaction leading to a lower value of MDD.

- ***Effect of sodium sulphate (SS) on optimum moisture content of bentonite clay***

  Figure 3.11 and Table 3.3 reveal that the addition of various percentages of sodium sulphate to bentonite clay altered the moisture content. With the addition of sodium sulphate up to 1%, the optimum moisture content increased marginally by less than 1% of

its previous value. Afterwards it decreased considerably with the continued addition of salt beyond 1% to reach its minimum value in the mixtures with 3% (SS). Figure 3.12 shows the variations in OMC and MDD of bentonite soil with different quantities of sodium sulphate (SS).

- ***Effect of sodium sulphate (SS) on the nature of compaction curves***

As illustrated in Figures 3.11, the incremental addition of soil to up to 1% did not affect on the nature of compaction curves. In other words, even though the values of MDD and OMC differed slightly in the mixtures with 0.5% and 1% sodium sulphate (SS) the compaction curves of these mixture exhibit similar shapes to those of pure bentonite. Also, the air-void curves show that the degree of saturation at the points of (MDD and OMC) almost remained in the same range in these mixtures. On the other hand, the compaction curves in the mixtures with 1.5% and 3% sodium sulphate (SS) appeared with flatter shapes, and the points of (MDD and OMC) were obtained at lower degrees of saturation. This confirms that the presence of sodium sulphate in bentonite beyond 1% can cause a problematic compaction, and a proper compaction is more likely to be achieved with the absence or lower percentages of this salt.

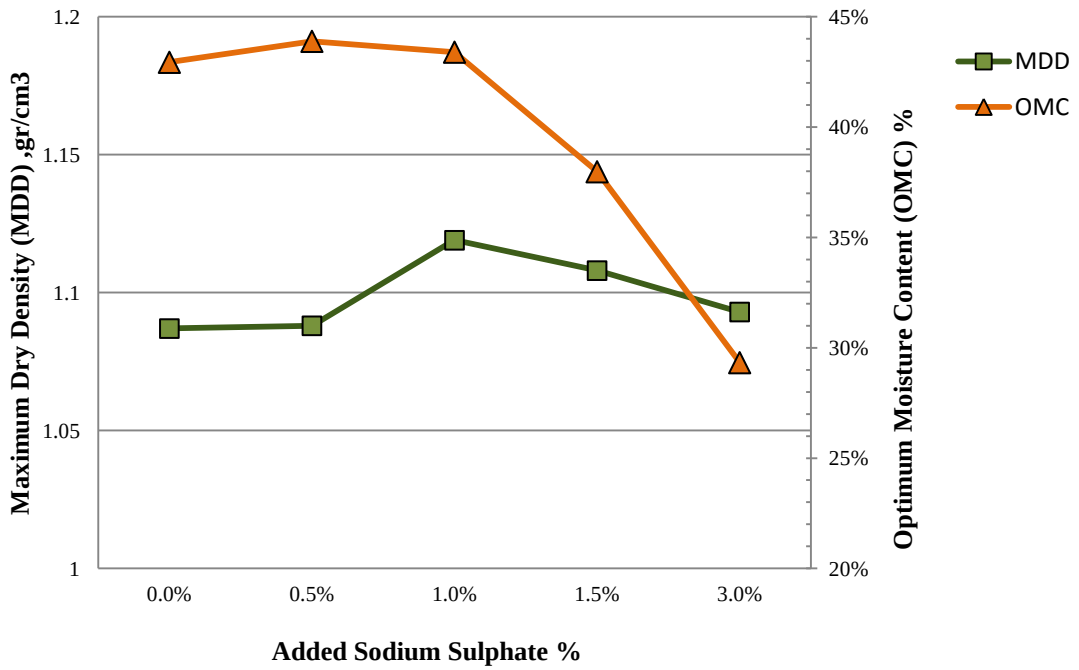

Figure 3.12: MDD (left) and OMC (right) vs different contents of SS for bentonite soil

3.3.2 Small Direct Shear test

The greatest part of the experimental tests was dedicated to the direct shear tests using the small direct shear test apparatus. A comprehensive series of test were conducted on the specimens with various percentages of sodium sulphate with different periods of curing. This part of the study mainly focused on the effect of sodium sulphate on the strength properties of bentonite clay including the peak shear strength, cohesion and angle of friction.

3.3.2.1 Introduction

The shear strength of soil is of particular interest to geotechnical engineers. This soil characteristic is the maximum resistance of the internal friction of soil to the shear forces that are associated with the nature of soils. It is necessary to determine the shear strength in order to estimate the bearing capacity of soils, the stability of slopes and the lateral pressure on retaining walls. Based on the Mohr-Coulomb theory (Coulomb, 1776; Mohr, 1900), the shear strength of soil is a function of normal stress affecting the failure surface. The two relevant parameters for determination of the shear strength of soils, C and Φ, are often determined using Mohr-Coulomb failure criteria. These parameters are generally obtained from laboratory examination of representative specimens.

The direct shear test developed by Coulomb is the oldest and simplest standard method employed on the civil engineering projects. The test is based on using a box made of two halves that are incrementally deformed by applying shear stresses (τ) (the lateral force divided by the cross section area of the box), or horizontal displacements (δ). During the test, a constant normal stress (σ, the normal force divided by the cross section area of the box) is applied to the top half of the box. The shear failure will take place along a plane between the upper and lower parts of the box as shown in Figure 3.13.

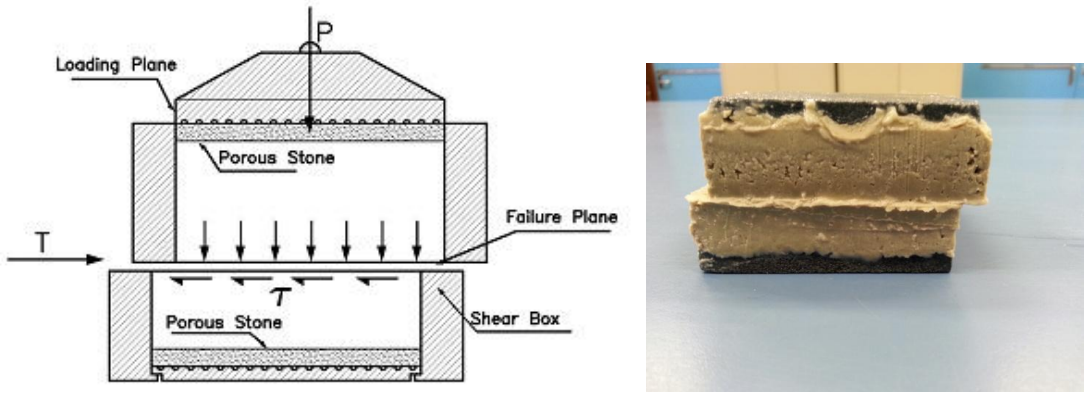

Figure 3.13: The shear failure in the middle of the box

In this research, which aimed to determine the strength characteristics of soil samples, the displacement-controlled method was employed using a digital direct shear apparatus.

3.3.2.2 Shear stress-shear displacement curve

For each sample placed under imposed vertical stress (σ), the resistance shear stresses (τ) corresponding with shear displacements were measured, and at the end of the test the shear stress versus shear displacement was plotted.

For each test the normal stress (σ) was calculated as follows:

$$\sigma = \frac{P}{A} \qquad \text{Eq. 3.5}$$

Where:

σ = the vertical stress (kN/m^2)

P = the applied vertical load (kN)

A = the horizontal cross section area of the box (mm^2)

For each test the resistance shear stress (τ) was calculated as follows:

$$\tau = \frac{T}{A} \qquad \text{Eq. 3.6}$$

Where:

τ = the shear stress (kN/m^2)

P = the shear force (kN)

A = the horizontal cross section area of the box (mm^2)

For each graph, the maximum point is known as the peak shear resistance (τ_f), which can be used to determine the strength characteristics of soil samples. Figure 3.14(a) shows the typical shear stress-shear displacement curves for two types of soil, Type I and Type II. Type I mostly includes loose sands and normally consolidated clays. Type II mainly includes dense sands and over-consolidated clays.

The vertical displacement versus horizontal displacement for these two soils are also plotted in Figure 3.14(b).This figure shows that the Type I soils incrementally compress with continued shearing, while Type II soils compress initially and then expand until they reach the critical state. In this state, no further volume changes occur under constant shearing.

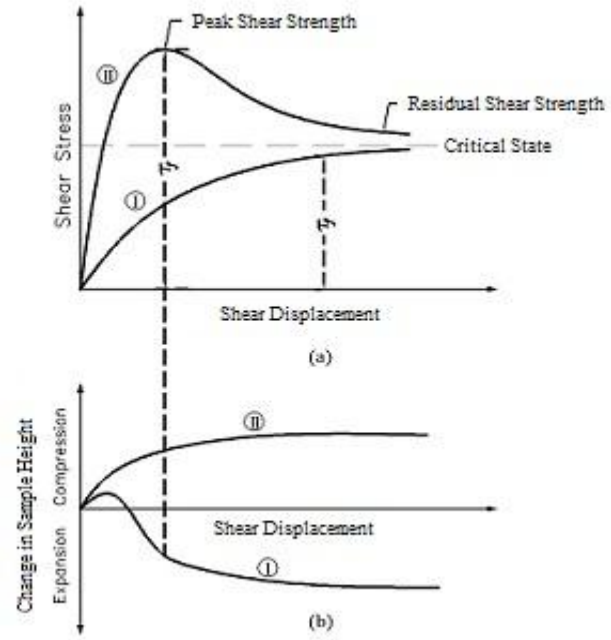

Figure 3.14: Shear strength (a) and change in the height (b) for soil type I and II vs shear displacement (Das, 2012)

3.3.2.2.1 Effect of Normal stress on shear stress-shear displacement curve

In this research, the shear strength of soil was tested under incremental normal stresses of 50, 100 and 200 kPa. The shear strength of each soil sample was determined using the results obtained from each test under imposed normal loads. For the investigation of the shear strength characteristics of soil, each sample needs to be tested under at least three incremental normal loads.

Figure 3.15 shows that the increment in normal stress will raise the magnitude of the shear resistance of the soil. For soil type II, with an increment in applied normal load the peak shear

stress tends to dissipate, while for soil type I the critical state of the shear stress will increase ("Shear Strength of Soils," 2011, p. 265).

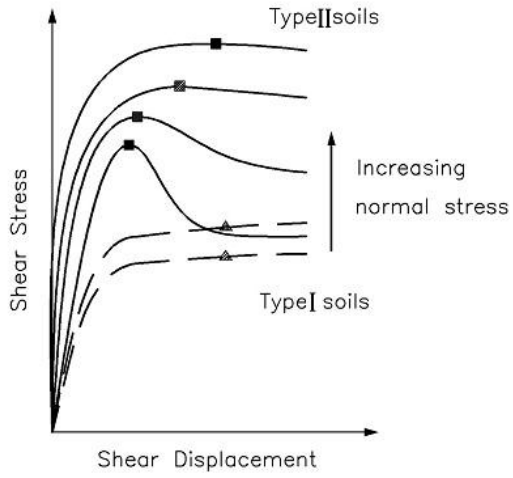

Figure 3.15: Shear stress vs shear displacement for soil types (I) and (II) under various normal stresses ("Shear Strength of Soils," 2011, p. 265)

3.3.2.2.2 Effect of consolidation on the peak shear stress

The consolidation which is the first step before running the shear test plays a significant role in the response of soil to the shearing forces. For two homogenous soil samples with the same mineralogical content but with different consolidation conditions, the soil with the greater over consolidation ratio (OCR) demonstrates a higher peak shear stress and greater volume expansion. Figure 3.16 demonstrates the effect of OCR on peak shear strength and volume expansion.

In order to remove the effect of this factor on the shear strength of soil, the same time was considered for the consolidation phase for all the soil samples.

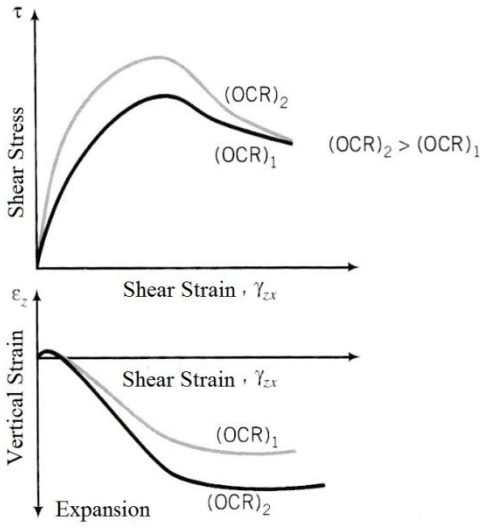

Figure 3.16: Effect of OCR on peak shear strength and volume expansion ("Shear Strength of Soils," 2011, p. 266)

3.3.2.2.3 Effect of drainage conditions on direct shear test

Drainage conditions are important while running the direct shear test. A drained condition is in effect when water can be drained during the test. In this state, the excess pore water pressure generated by a change of stresses in soil disperses, and all the stress applied to the soil is carried by the soil structure ($\Delta\sigma'$). An undrained condition happens when the water cannot be drained, or the rate of disappearance of the excess pore water is much lower than the rate of loading on the soil. Under this condition, the stress applied to the soil is taken by both the pore water and the soil structure (Δu and $\Delta\sigma'$). The relationship between the stresses and the pore water is written as follows:

$$\Delta\sigma = \Delta\sigma' + \Delta u \qquad \text{Eq. 3.7}$$

The results obtained from direct shear tests on different soils showed that under drained conditions, there will be an increase in excess pore water pressure on the soil (for example, Type I soil), with the tendency to compress. Under undrained conditions, there will be a decrease in effective stress for a soil (for example Type II soil), with the trend being towards expansion.

In this research, all of the tests were carried out under the same drainage conditions, that is, consolidated drained (CD) conditions.

3.3.2.3 Theory and background of the test

In addition to the factors mentioned above, some other factors involved in the shear strength of soil (τ_f) are due to the nature of the soil. The apparent cohesion of soil (c) is influenced by intermolecular forces, the tension between water and soil, adhesion, and the strength of the bonds among soil particles.

In this research, the direct shear test was performed using different normal loads and the shear stress-shear displacement curves were plotted for each test. The maximum shear stress (shear strength (τ_f)) obtained from each curve was plotted versus the corresponding normal stresses (σ_n) for each test. Figure 3.17 illustrates the results obtained from six tests on an over-consolidated clay (line 1) and a normally consolidated clay (line 2). These figures show the

linear relationship between the shear strength of soil (τf) and normal stress (σ_n) based on Coulombs' theory.

In this research, the soil was tested under normally consolidated conditions, so the results obtained from the tests are similar to those in to line 2 in Figure 3.17. The friction angle and cohesion of the soil, which have a critical role in civil engineering design and construction, have been obtained from these graphs, and are illustrated thoroughly in Figures 3.51 to 3.56 in this chapter.

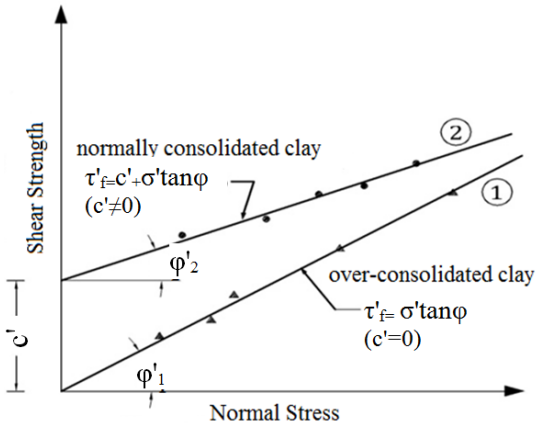

Figure 3.17: Shear strength vs normal stress for over-consolidated clay (1) and normally consolidated clay (2) (Bjerrum & Simons, 1960)

Based on Coulomb's theory, when the failure occurs the shear strength of soil in the form of effective (τ'_f) is a linear function of effective normal stress (σ'_n).

$$\tau'_f = c' + \sigma'_n \tan \varphi' \qquad \text{Eq. 3.8}$$

The cohesion of soil (c) is entirely related to the nature of the soil. It relies on the intermolecular forces between soil particles, the surface tension of water on the soil particles and the chemical bonding between soil particles. Figure 3.17 shows a clear definition of σ_n and ϕ. In this picture, τ_f is illustrated as the resistance stress between soil particles on the slip plane and ϕ is the angle between the normal stress (σ_n) and the y axis.

When considering the pore water pressure, the equation above is also written in the form of effective stresses as follows:

$$\tau'_f = c' + \sigma'_n \tan \varphi' \qquad \text{Eq. 3.9}$$

3.3.2.4 Test phases

In soils with a high coefficient of permeability such as sand, the excess pore pressure caused by vertical and horizontal loads dissipates rapidly. By contrast, in soils with a low coefficient of permeability such as clays, a longer period of time is needed for dissipation of the whole excess pore water pressure. The rate of shearing also needs to be to be very low.

For this reason, all of the tests were conducted in two phases: the consolidation phase and the direct shear phase as outlined below.

3.3.2.4.1 Consolidation phase

When a layer of cohesive soil is affected by incrementally applied loads, the soil undergoes an elastic settlement that is caused by a reduction in the void ratio. This phase of settlement is known as primary consolidation. The consolidation settlement or secondary consolidation occurs after the primary settlement. This settlement happens when the pore water pressure disperses. Due to the low permeability of clays, the whole of the excess pore water pressure will disappear over an extended time. For these soils, the consolidation settlement is several times greater than the primary settlement.

In this research, each test was conducted under one-dimensional consolidation conditions, and a vertical load was applied to the specimen. This step was carried out in the automatic direct shear device before the shear phase. Before starting the shear test the required time for consolidation, and the rate of shearing needed to be determined. The calculations about theses parameters are presented in Sections 3.2.2.4.1.1 and 3.2.2.4.1.1.

3.3.2.4.1.1 Required time for consolidation

Based on AS1289.6.2.2-1998, 90% of the consolidation needs to be complete before starting the shear test. The consolidation curve was used for estimating the required time for consolidation and the rate of shearing in the shearing phase. Two methods are introduced in AS1289.6.6.1-1998 for calculating the times needed for different percentages of consolidation. These methods are known as the log/time method and the square root/time method. The square

root/time method was used to calculate the time required to achieve 90% of primary consolidation as outlined below.

- ***Square root/time method***

Once the consolidation phase was finalised, the results from this phase were tabulated to Excel to plot the deformation versus the square root of time in minutes for each applied normal load. Figure 3.18 demonstrates a typical plot of the deformation gauge reading vs the square root of time in minutes for a particular vertical load.

- ***Calculations***

From this curve, the time required to achieve 90% primary consolidation was obtained using the following steps:

- A tangent line was plotted on the beginning part of the curves and continued to cross the Y axis at point A. This point shows the deformation at t=0 or 0% primary consolidation.
- The second line was plotted through point A and a point at which the horizontal distance from X axis was 1.15 times the x cordinate of the tangent line on the beginning part of the curves.

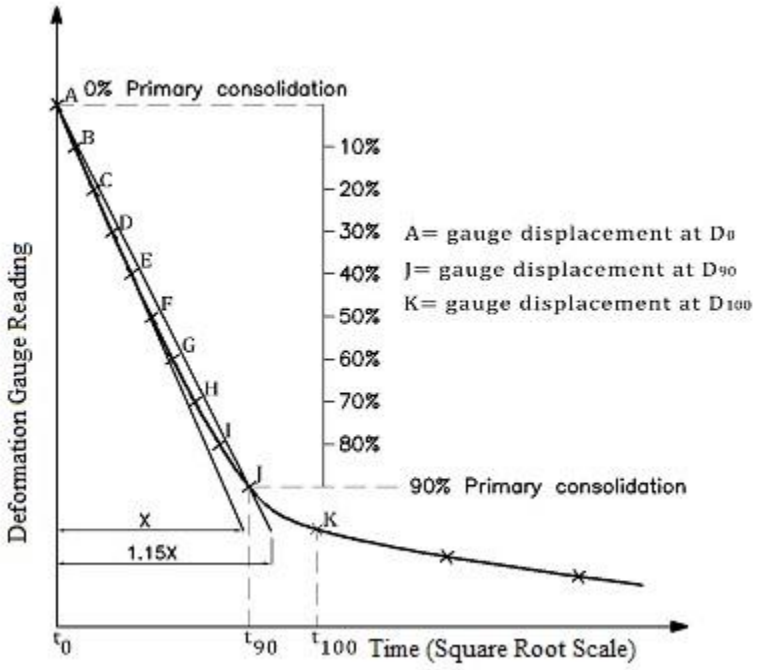

Figure 3.18: Typical compression vs time (square root scale) (AS1289.6.6.1-1998)

- The new line crossed the deformation/square root of time curve at point J; this point represents 90% of primary consolidation.
- The displacement for 100% primary consolidation was determined from the difference in displacements between 0 and 90% consolidation. This deformation is a point (K) on the curve at which the deformation is one-ninth more than this difference.

3.3.2.4.1.2 Rate of shearing

According to AS1289.6.2.2-1998, in cohesive soils such as clays, the rate of shearing on the specimen needs to be very slow in order to allow the excess pore water pressure to dissipate in

an adequate time. It is necessary to determine the rate of shearing before starting the shear phase. Based on this standard, the rate of shearing was calculated as follows:

$$R = \frac{dp}{tf} \qquad \text{Eq. 3.10}$$

Where:

t_f = 50 t50

R = the required shearing rate, in millimetres per minute

dp = the shear displacement at which the peak shear will occur, in millimetres.

t_f = the time at which the failure occurs, in minutes

t50 = the time at which the 50% consolidation is completed, in minutes

In order to determine the time required to achieve 50% primary consolidation (t_{50}), the log/time method was employed based on AS1289.6.6.1, as follows:

- ***Log/time method***

After completion of the consolidation phase, the results were tabulated in Excel once more to plot the deformation versus the logarithm of time in minutes for each applied normal load. Figure 3.19 shows a typical plot of the deformation gauge reading vs the logarithm of time in minutes for a particular vertical load.

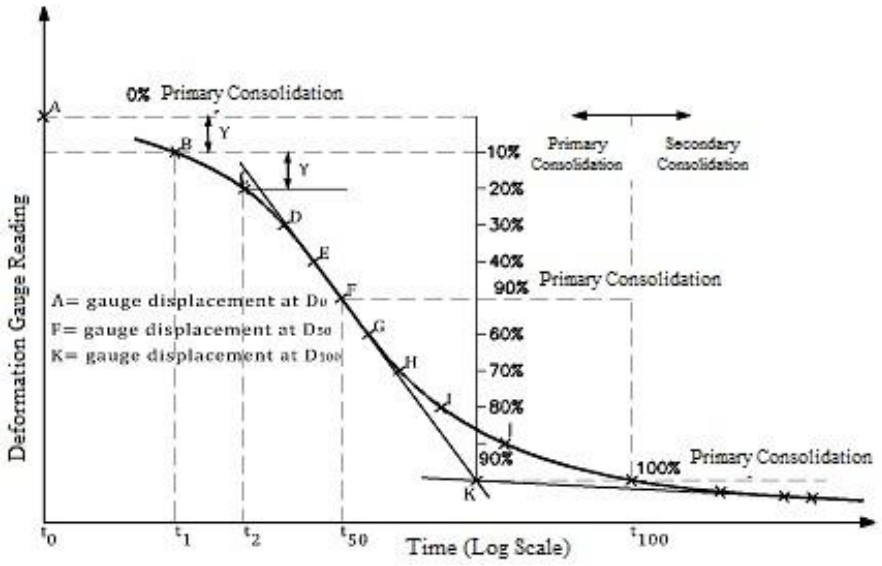

Figure 3.19: Typical compression vs time (log time scale) (AS1289.6.6.1-1998)

- ***Calculations***

From Figure 3.19, the time required to achieve 50% primary consolidation was obtained following the steps set out below:

- A tangent line was plotted along the points at the end of the curve.
- The second tangent line was plotted to the sharp slope of the curve.
- These two lines were continued to intersect each other at point K. This point describes 100% primary consolidation.
- Two times, t_1 and t_2, were chosen in the early part of the curve so that t_2 was four times t_1. The deformations associated to these times should vary less than 50% of the whole deformation from t_0 to t_{100}. The deformation related to t_0 is calculated from the

difference between the deformations at t_1 and t_2, shown on the curve as Y. So, the deformation for 0% consolidation is the deformation at t_1 less Y.

- The average of the displacement corresponding to the 0 and 100% consolidation was considered to be the deformation corresponding to the 50% consolidation (point F). The required time for 50% primary consolidation was found graphically from the deformation/log time curve (t_{50}).

3.3.2.4.1.3 Sample preparation

In order to determine the required time to achieve 90% percent primary consolidation for all of the soil mixtures, the soil was examined under three different load increments (50, 100 and 200 N). For this purpose, three specimens of bentonite clay were prepared consecutively (pure composite). The optimum moisture content was considered to be 43% of the dry weight of the soil based on the compaction test results discussed earlier in this chapter. Soil specimens were kept in the laboratory room at 23ºC for a curing time of 24 hours.

In the next step, soil samples were put in the direct shear device one after another and the consolidation phase was conducted for 24 hours on each sample.

3.3.2.4.1.4 Results and discussion

Figures 3.20 to 3.22 show the deformation/square root of time curves for three different normal loads applied to three specimens obtained from the consolidation phase. The original plots were drawn for a consolidation time from 0 to 24 hours, but only the first parts of the graphs are

shown below in order to obtain better magnification. More detailed graphs are presented in Appendices 7 to 9.

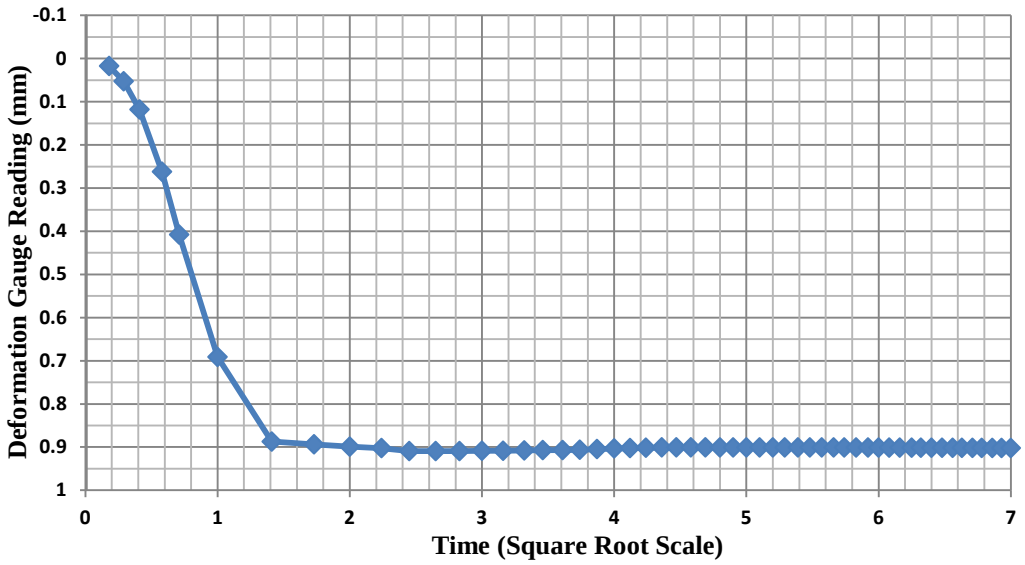

Figure 3.20: Compression vs time (square root scale) for the specimen consolidated under 50 kPa vertical load

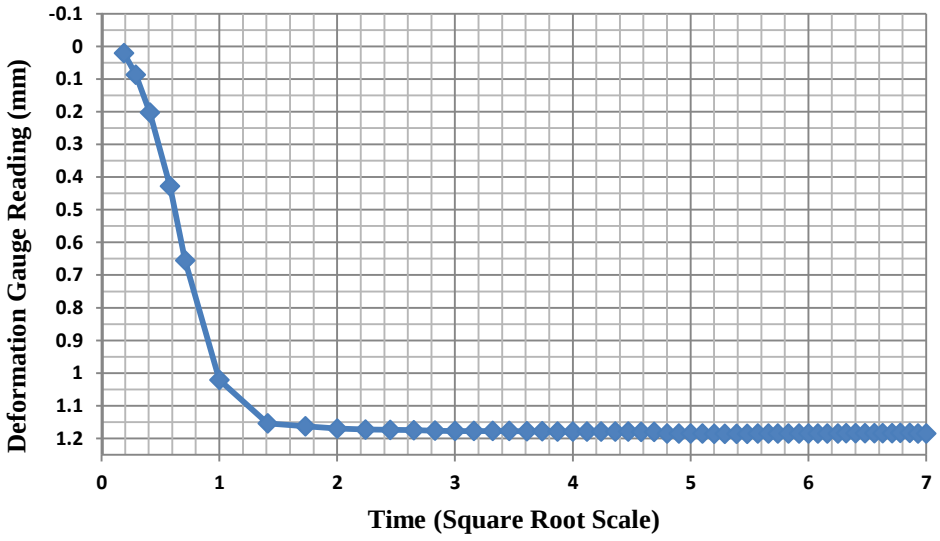

Figure 3.21: Compression vs time (square root scale) for the specimen consolidated under 100 kPa vertical load

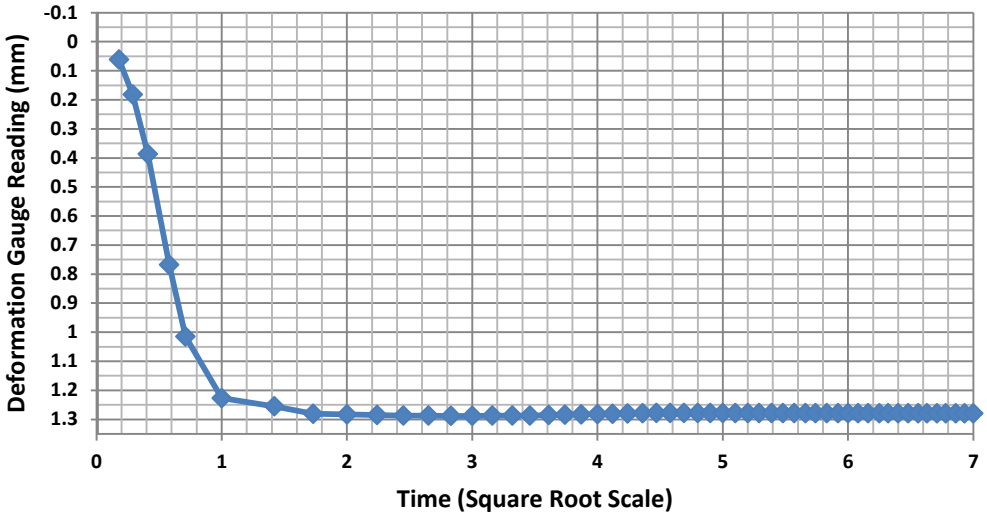

Figure 3.22: Compression vs time (square root scale) for the specimen consolidated under 200 kPa vertical load

Table 3.3 shows the following results:

Table 3.4: Required times for 90% and 100% of consolidation for normal stresses of 50–200 kPa

Normal Stress (kPa)	**Required Time for 90% Consolidation (min)**	**Required Time for 100% Consolidation (min)**
50	1.83	2.025
100	1.39	1.55
200	0.77	0.86

Figures 3.23 to 3.25 show the deformation/log time curves for the same specimens obtained from the consolidation phase. More detailed versions of these graphs are presented in Appendices 7 to 9.

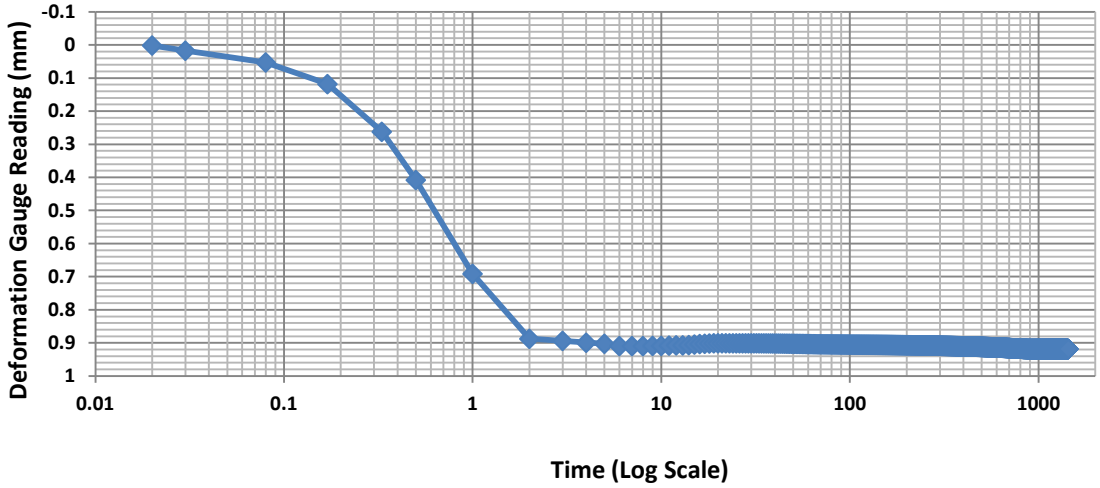

Figure 3.23: Compression vs time (log scale) for the specimen consolidated under 50 kPa vertical load

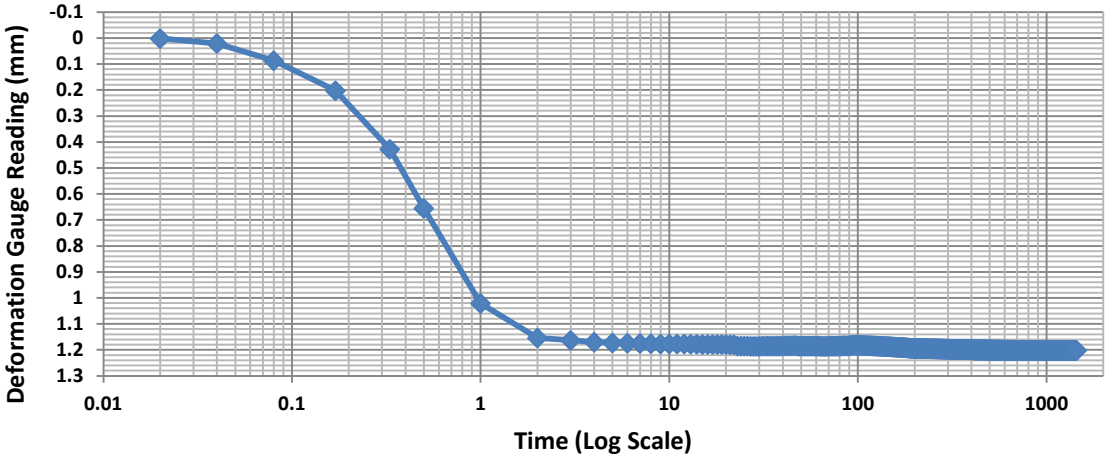

Figure 3.24: Compression vs time (log scale) for the specimen consolidated under 100 kPa vertical load

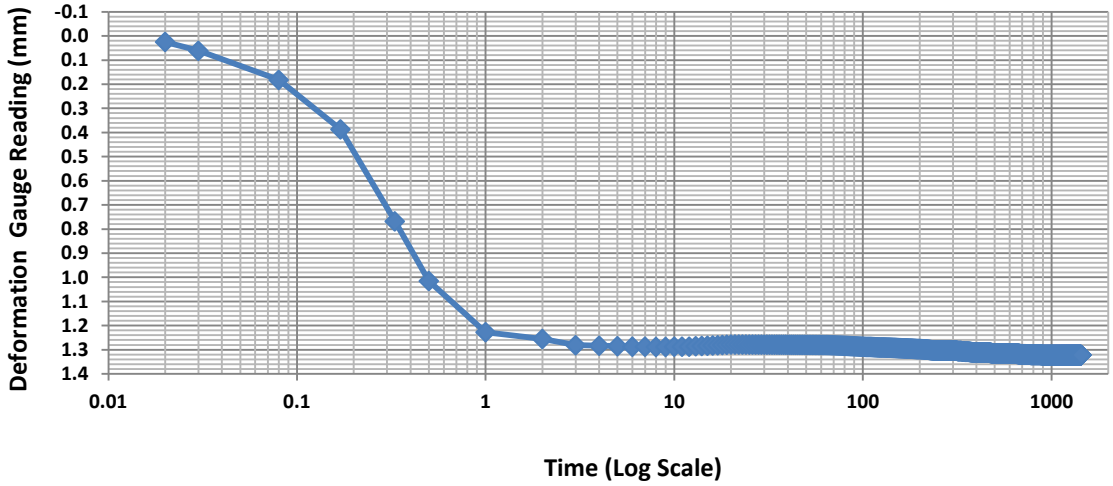

Figure 3.25: Compression vs time (log scale) for the specimen consolidated under 200 kPa vertical load

The times required to achieve 50% primary consolidation (t_{50}) for three vertical loads were obtained from the above curves as discussed in the log time method. From t_{50} the required shearing rates for reaching the failure at 2–5 mm were also calculated for each load increment. Table 3.5 shows these results:

Table 3.5: Required time for 50% of consolidation and shearing rate for normal stresses of 50–200 kPa

Normal Stress (kPa)	Required Time for 50% Consolidation (min)	Required Shearing Rate (mm/min)
50	0.5	0.08–0.2
100	0.36	0.11–0.27
200	0.25	0.16–0.4

Based on the results obtained from the preliminary consolidation tests on the pure bentonite mixture under three different load increments, the following outcomes have been extracted:

1. In all three specimens, 90% primary consolidation was completed in less than two minutes. Therefore, the condition mentioned in AS1289.6.2.2-1998 regarding the achievement of 90% consolidation before starting the shear phase was satisfied.
2. Secondary consolidation occurred after primary consolidation with a very slow rate of compression. The reduction in the volume of each sample was continued until no further change occurred and the volume remained almost constant. In all three samples, this condition occurred approximately from the 900th minute onward. Consequently, 15 hours for the consolidation phase was adequate in most cases.
3. The required rate of shearing differed slightly for each specimen. The rate of shearing was from the minimum average rate, 0.14 mm/min for the specimen under a 50 kPa load, to the maximum average rate, 0.28 mm/min for the sample under 200 kPa. Therefore, considering a shearing rate of 0.1 mm/min is slow enough to allow the excess pore water pressure to dissipate in most of the cases. It also makes it possible to apply similar conditions to all of the soil tests.

3.3.2.4.2 Direct shear phase/program

A series of direct shear tests were performed on pure bentonite and bentonite mixed with 3%, 6% and 9% sodium sulphate for periods varying from seven to 28 days. Some specimens were also tested for longer curing periods of 90 days and up to 365 days. The effect of different percentages of sodium sulphate on the strength properties of bentonite clay after different times of curing was investigated. The shear strength of the soil, as well as the internal friction angle and cohesion, were calculated for each soil sample. These results are presented and discussed thoroughly in this chapter.

3.3.2.4.2 .1. Test methodology

The methods for implementing direct shear tests have been well established in practical applications. These methods can be found in various testing soil standards for engineering purposes including the Australian Standards. In this research, AS289.6.2.2-1998: “Soil strength and consolidation tests–Determination of the shear strength of a soil–Direct shear test using a shear box” was used. The soil was examined under consolidated drained conditions using the small shear box.

Tests were performed on bentonite mixed with different percentages of sodium sulphate (0%, 3%, 6% and 9%) and cured for various periods (7, 14, 28, 90 and up to 365 days). The results obtained from the tests are described accurately, and the shear strength characteristics of the soil, such as the internal friction angle and cohesion, were calculated for each soil sample.

The tests focused mainly on the following objectives:

In order to minimise the impact of other factors, tests were conducted under identical conditions as follows:

- ✓ The same consolidation time was applied for all soil samples;
- ✓ The tests were performed in a monitored temperature room;
- ✓ The tests were run with the same weight of soil and compaction effort;
- ✓ The tests were conducted under the same applied normal stresses and shearing rate.

3.3.2.4.2 .2 Test requirements

The following items were needed in order to carry out the shear tests.

- Automatic direct shear test machine;
- Specimen preparation equipment;
- A cube made of hard plastic;
- A balance.

An automatic direct shear apparatus was used in this research. Normal load and horizontal load were applied by the use of two loading mechanisms and the magnitude of the loads and displacement in both directions were measured with two sensors. The results were transferred to Excel comfortably without any user intervention. The device is illustrated in Figure 3.26.

Figure 3.26: Shear Trac II apparatus

3.3.2.4.2.3 Sample preparations

The following steps were taken to prepare the samples for each test:

1. The soil was oven-dried at 105ºC for 24 hours. Then it was removed from the oven and allowed to cool for a few minutes as illustrated in Figure 3.27.

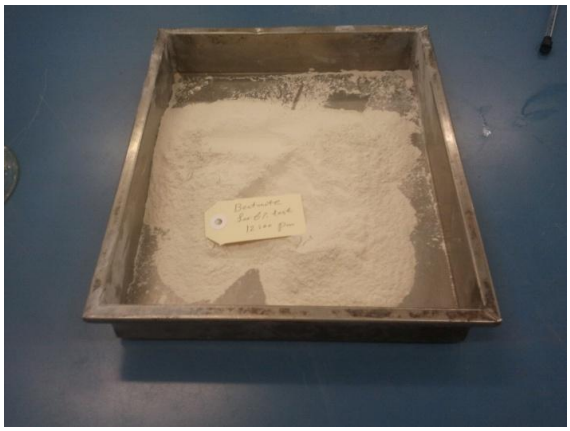

Figure 3.27: The bentonite soil after being dried in the oven for 24 hours

2. The cooled soil was transferred to a zip-lock plastic bag and weighed.
3. Sodium sulphate at different proportions (3%, 6% and 9% by dry weight of soil) was prepared based on each test's inquiry as shown in Figure 3.28(a).
4. The salt was dissolved in 23±2 ºC water at 1% greater than the optimum moisture content to take into account evaporation during the sample preparation as demonstrated in Figure 3.28(b).

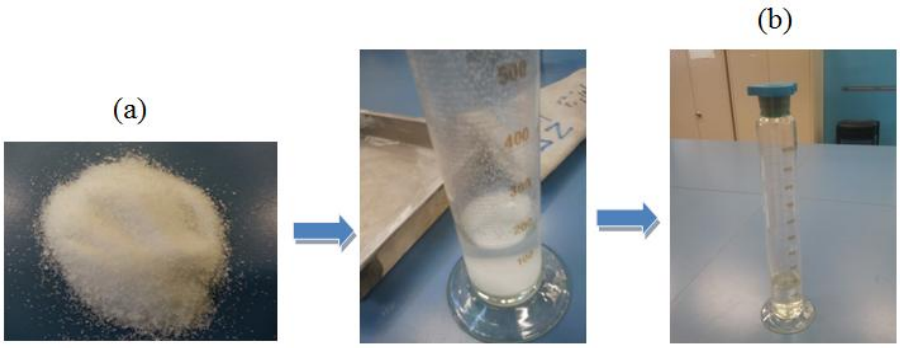

Figure 3.28: Pure sodium sulphate (a); and the sodium sulphate dissolved in water (b)

5. The salt solution was added to the pure bentonite and was mixed properly in a zip-lock plastic bag until a homogenous texture was obtained, as shown in Figure 3.29.

Figure 3.29: Bentonite mixed with sodium sulphate

6. The plastic bag was sealed, and the mixture was kept at a constant temperature of 23±2ºC for different curing times as shown in Figure 3.30.

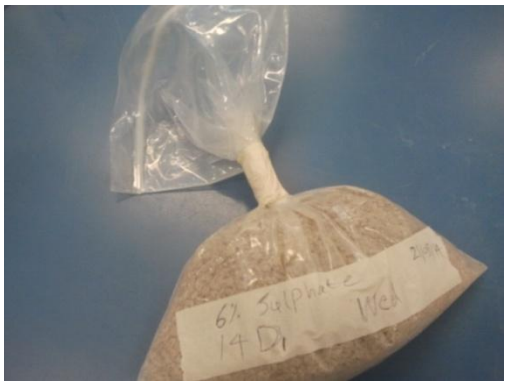

Figure 3.30: The sulphate-treated bentonite kept in sealed plastic bags

7. The same steps were taken for the preparation of all samples, excluding the addition of salt to the water for the untreated (pure bentonite) samples.

In total, more than 100 mixtures were prepared for this project in order to investigate the effect of curing time, various percentages of sodium sulphate and different normal stresses. To avoid the possibility of errors all the tests were repeated on at least three identical samples under normal stresses of 50–200 kPa.

3.3.2.4.2.4 Test procedures

1. The prepared soil sample was put into the assembled shear box (36mm×36mm×24mm) with a porous stone and a grid plate at the bottom to allow drainage to occur. A plastic cube was used for compaction to protect the alignment screws as displayed in Figure 3.31.

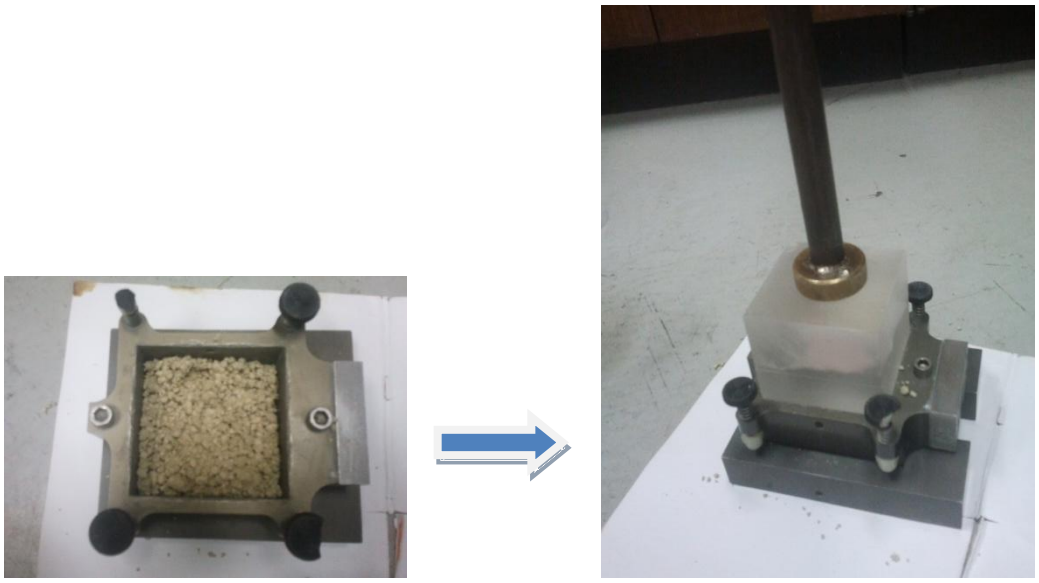

Figure 3.31: The shear box and the plastic cube used for compaction

2. The soil was compacted in the shear box in three layers by the delivery of 25 uniform blows with a hammer. In the last layer, the top edge of the upper porous stone was levelled with the top part of the shear box using a straightedge as seen in Figure 3.32.

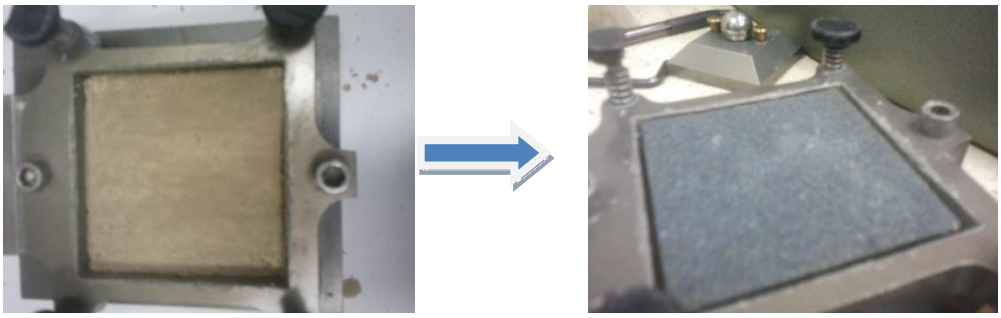

Figure 3.32: The compacted soil sample in the shear box

3. The shear box was fitted with the direct shear device.

4. The data relating to each specimen was entered into the shear software. Normal stress was applied depending on the test requirements (50 kPa, 100 kPa or 200 kPa), transferred from the loading hanger to the load plate.
5. The rate of shearing was set to 0.1 mm/min as discussed in the consolidation phase. Refer to section 3.2.2.4.1.4 for more information.
6. The required time for consolidation was set to a minimum of 15 hours and the data acquisition system was run.
7. Once the consolidation phase was finished, the alignment screws were removed and the shearing phase was started.
8. The shear stress-displacement curve was plotted to investigate the strength behaviour of soil.

3.3.2.4.2.5 Results and discussion

The main focus of this study was to examine the impact of the amount of sulphate and curing time on the strength properties of bentonite samples. So, to gain a better interpretation, these results are presented based on these two factors as follows:

- ***Effect of sodium sulphate along with curing time on shear stress-horizontal displacement curves***

To investigate the effect of curing time, soil samples were tested for different periods from seven to up to 365 days. However, the 365 day samples were only tested under a normal stress

of 100 kPa. Also, only those samples mixed with 9% sulphate were cured for 90 days due to the large number of tests and the shortage of time.

The values of normal stress (σ_n) and the peak shear stress (τ) for each percentage of sulphate after different curing times and under different normal loads are presented in Tables 3.6 to 3.8. These values can help to understand the effect of each dosage of sulphate along with the curing times under different normal stresses on the shear strength of bentonite.

Figures 3.33 to 3.35 c illustrate the shear stress-horizontal displacement curves for pure bentonite (PB) after one day of mellowing time and samples mixed with various percentages of sodium sulphate (SS) after various curing times at different constant normal stresses from 50 to 200 kPa. These figures present the effect of different curing times on samples with the same percentage of sulphate and normal pressure.

Table 3.6: The values of peak shear stress for bentonite mixed with 3% sodium sulphate at normal stresses of 50–200 kPa after various Curing Times(days)

Normal Stress (kPa)	**50**	**100**	**200**
Curing Time (days)	**Sulphate Percentage**		
	3%		
	Peak Shear Stress (kPa)		
7	64.74	88.09	117.9
14	59.74	86.01	114.5
28	57.83	83.74	114.8
365	-	72.37	-

Table 3.7: The values of peak shear stress for bentonite mixed with 6% sodium sulphate at normal stresses of 50–200 kPa after various Curing Times(days)

Normal Stress (kPa)	**50**	**100**	**200**
Curing Time (days)	**Sulphate Percentage**		
	6%		
	Peak Shear Stress (kPa)		
7	60.16	83.03	109.5
14	57.5	83.86	109.5
28	54.5	81.48	104.1
365	-	77.19	-

Table 3.8: The values of peak shear stress for bentonite mixed with 9% sodium sulphate at normal stresses of 50–200 kPa after various Curing Times(days)

Normal Stress (kPa)	**50**	**100**	**200**
Curing Time(days)	**Sulphate Percentage**		
	9%		
	Peak Shear Stress (kPa)		
7	50.57	78.62	103.5
14	43.72	67.18	102.4
28	44.37	72.07	105.8
90	44.67	67.48	87.91
365	-	69.45	-

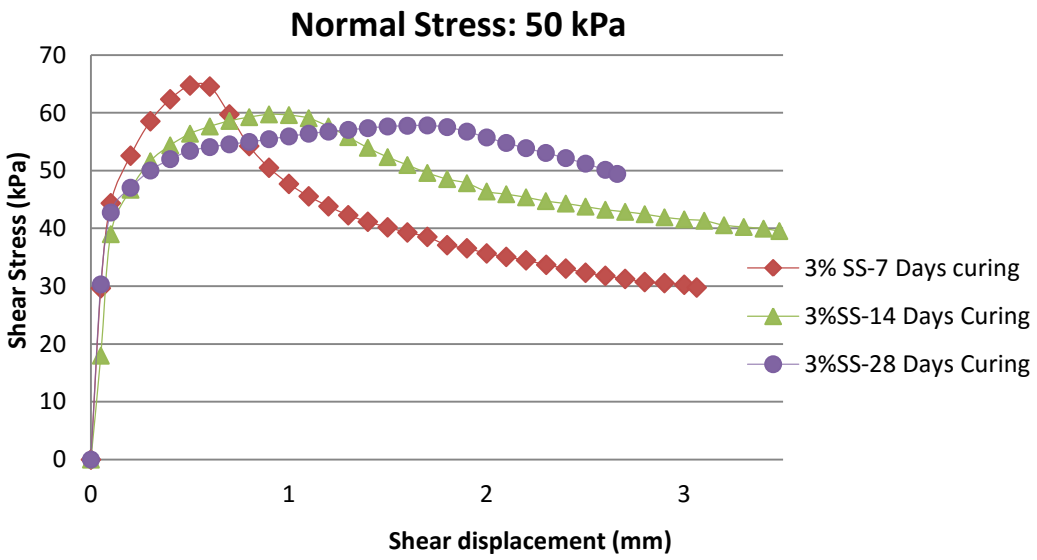

Figure 3.3 a

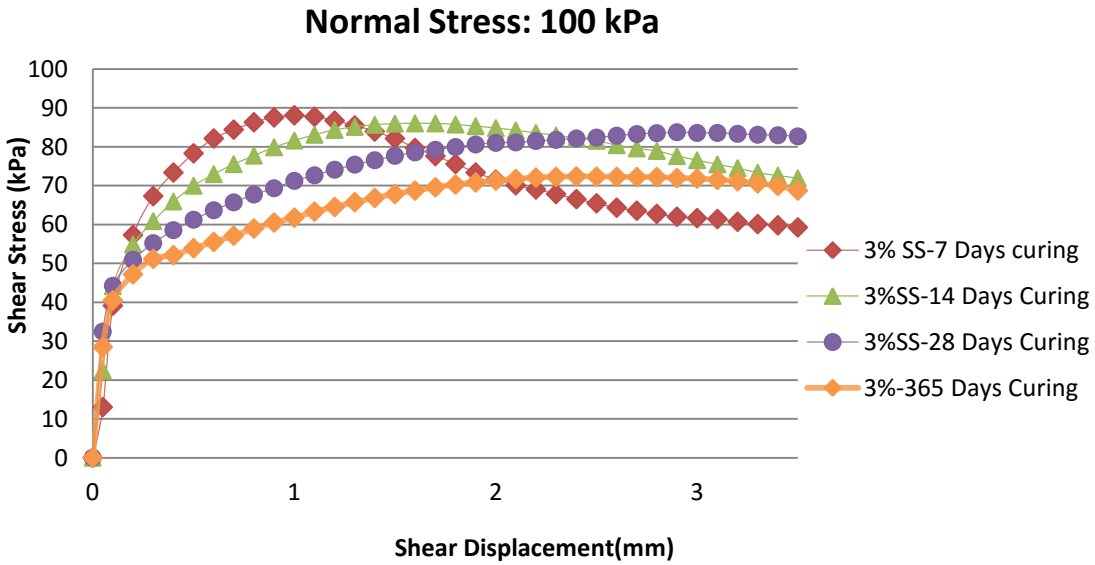

Figure 3.33 b

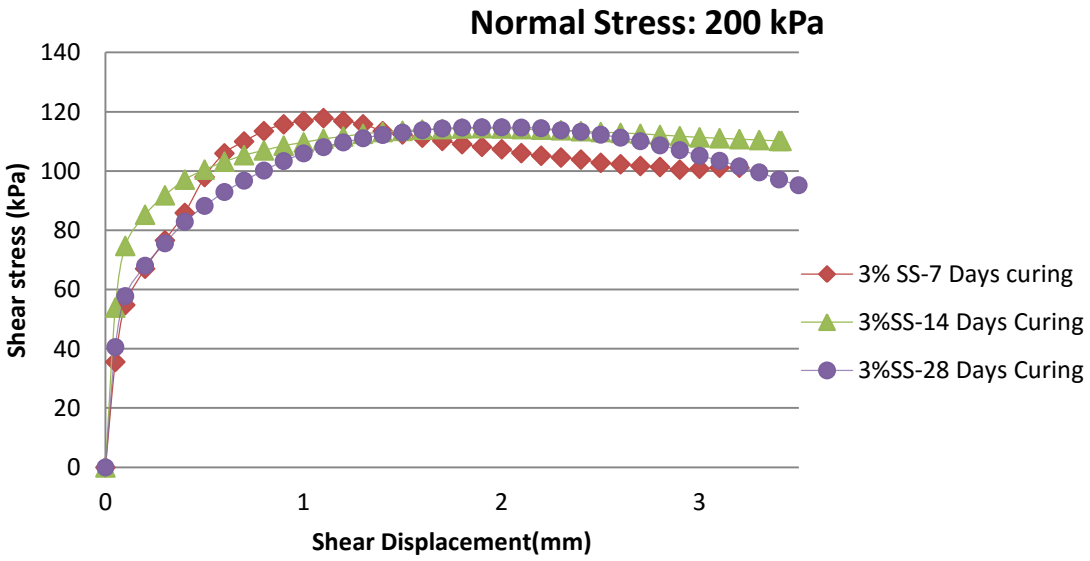

Figure 3.33 c

Figures 3.33 a- c: Shear stress-Sheardisplacement for pure bentonite after one day mellowing time and bentonite mixed with 3% sodium sulphate after various curing times under a normal stress of 50-200 kPa.

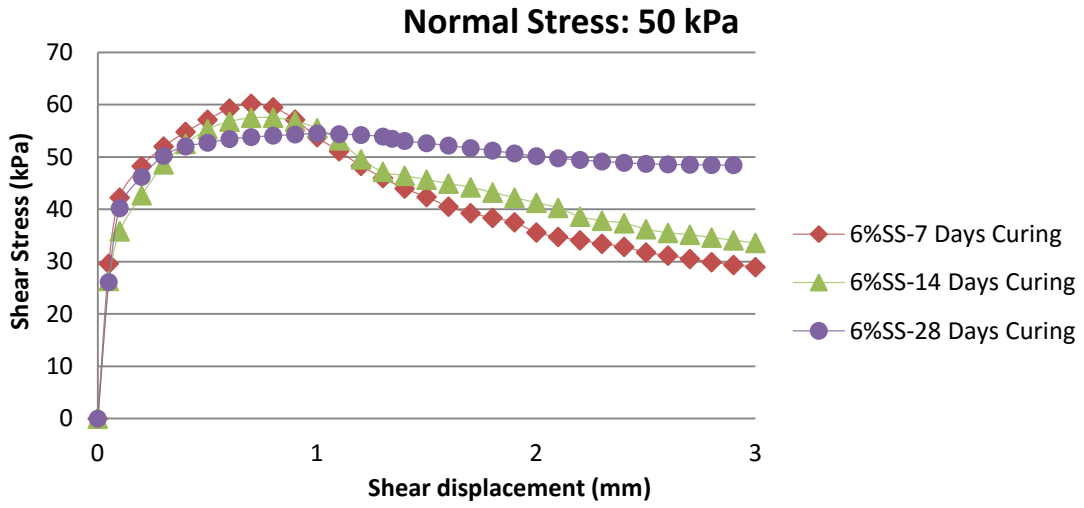

Figure 3.34 a

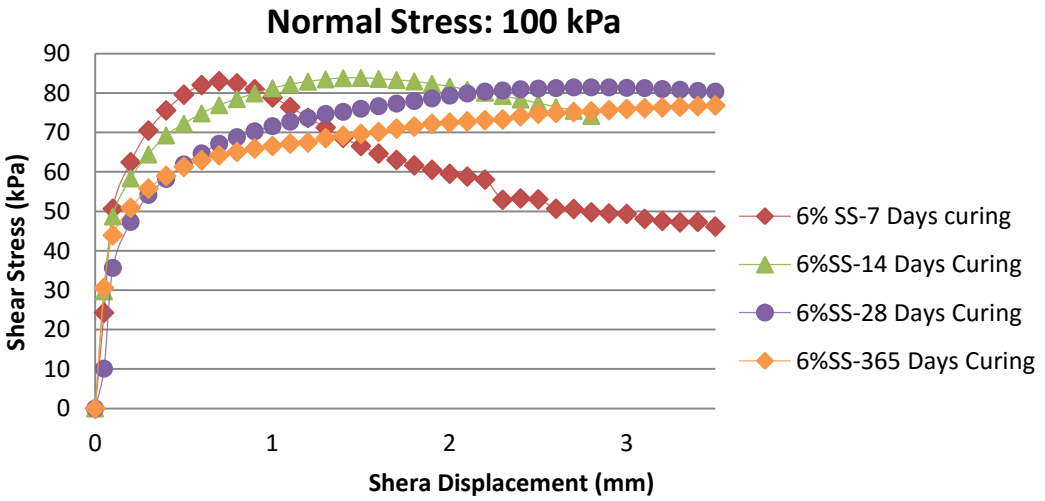

Figure 3.34 b

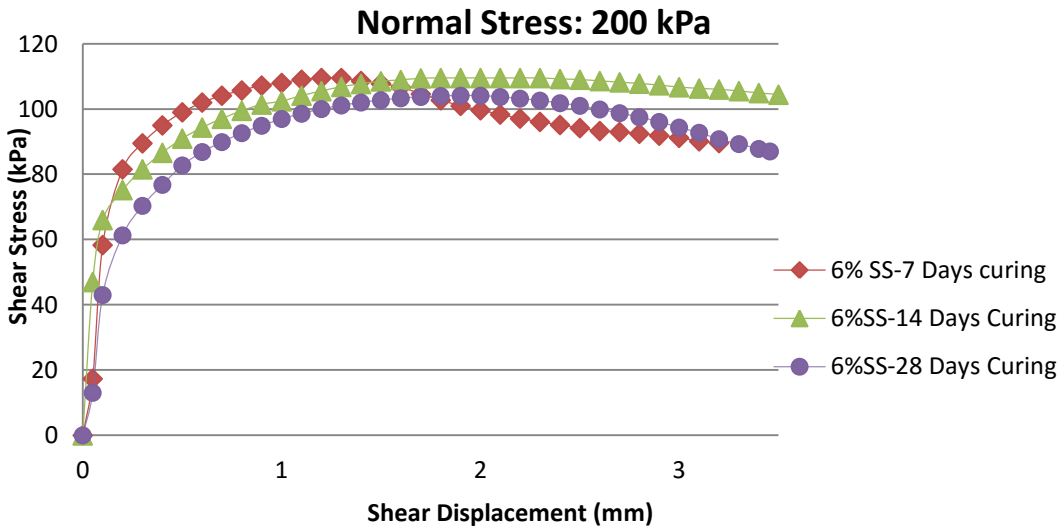

Figure 3.34 c

Figures 3.34 a- c: Shear stress-Shear displacement for pure bentonite after one day mellowing time and bentonite mixed with 6% sodium sulphate after various curing times under a normal stress of 50–200 kPa

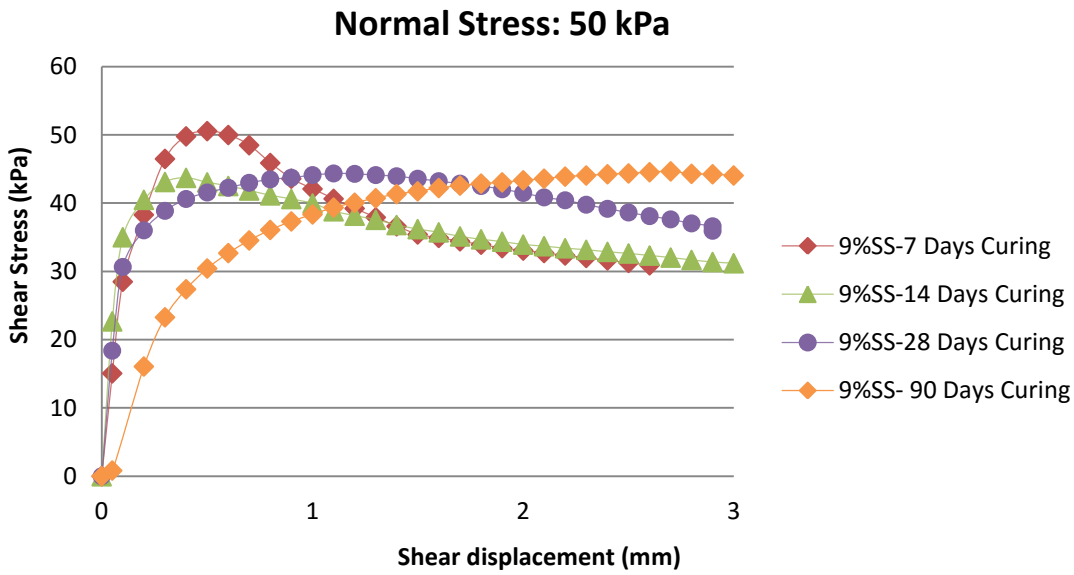

Figure 3.35 a

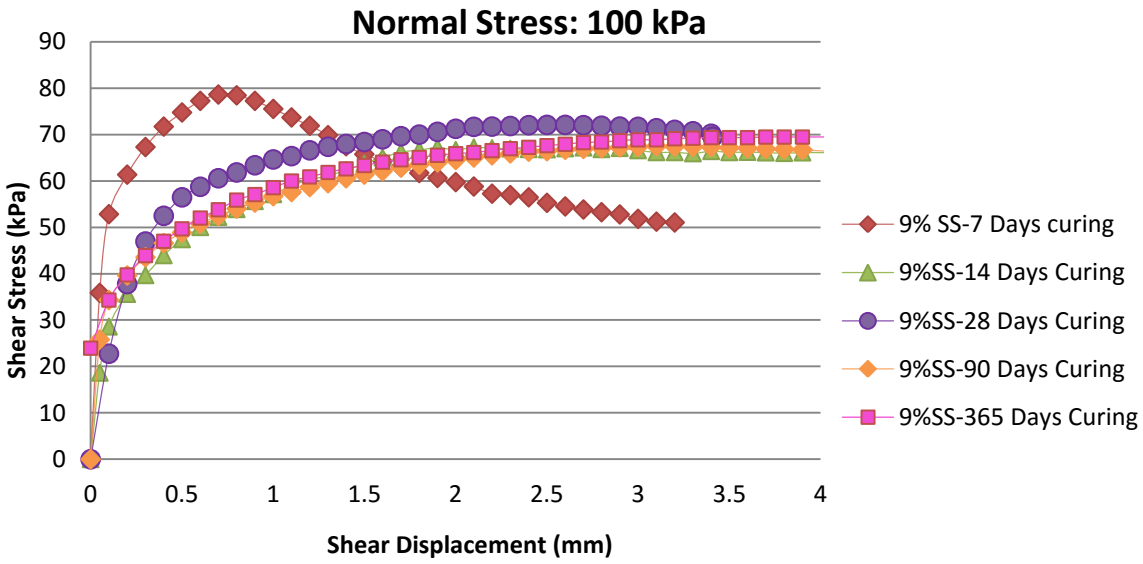

Figure 3.35 b

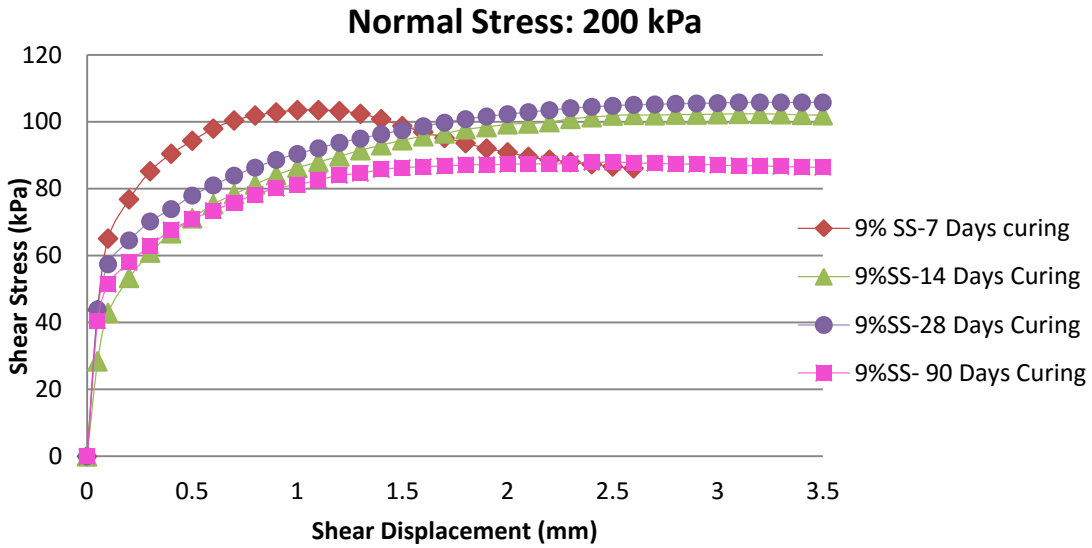

Figure 3.35 c

Figures 3.35 a- c: Shear stress-Shear displacement for pure bentonite after one day mellowing time and bentonite mixed with 9% sodium sulphate after various curing times under a normal stress of 50–200 kPa

To better understand the curves illustrated above and the effect of curing time along with sulphate content, the results are discussed in three different categories based on the curing time. These results are also presented in Tables 3.9 to 3.11.

- **Curing from seven days to 14 days**

An increase in curing period from seven days to 14 days led to a decrease in the peak shear values by 7%, 4% and 13% from their previous values for the samples mixed with 3%, 6% and 9% sodium sulphate respectively at a normal stress of 50 kPa. In the same manner, at normal stress of 100 kPa the peak shear dropped by 2% and 14% for the samples mixed with 3% and 9% Na_2SO_4, however it remained almost constant for the samples with 6% salt.

At a normal stress of 200 kPa, the peak shear remained almost the same for the samples with 6% and 9% and decreased by 2% for the samples with 3% sulphate.

- **Curing from 14 days to 28 days**

Extending the time of curing from 14 days to 28 days caused a slight decrease in the peak stress value by 3% and 5% for the samples with 3% and 6% sulphate repectively at normal stresses of 50 kPa. However, there was a 1.5 % increase in the peak stress value for those samples treated with 9% at the same stress level. In the same way, at a normal stress of 100 kPa, peak stress decreased by 3% in the samples with 3% and 6% sulphate, and increased by 7% for the specimens with 9% of this salt. A different trend was observed at a normal stress of 200 kPa, with the peak stress remaining at almost the same value in the samples with 3% salt, and decreasing by 5% for the samples with 6% salt. By contrast, for specimens with 9% Na_2SO_4, the peak stress level increased to 3% more than its 14 day value at this normal stress.

- **Curing from 28 days to 90 days**

Only the samples mixed with 9% Na_2SO_4 were cured for 90 days due to the large number of tests. As seen in Figures 3.5 a- c, for a curing period from 28 days to f 90 days, the peak stress remained almost the same at a normal stress of 50 kPa, decreased by 6% at a normal stress of 100 kPa, and suddenly dropped by 16% at a stress level of 200 kPa.

- **Curing up to 365 days**

This curing time was tested on specimens containing all percentages of sulphate, but only under a normal stress of 100 kPa. As shown in Figures 3.33 b, 3.34 b and 3.35 b, an incremental

increase in the curing time from 28 days to 365 days for samples mixed with 3% and 6% Na_2SO_4 led to a decrease in the peak stress value by 13% and 5% in the 28 day samples, while those mixed with 9% Na_2SO_4 exhibited a 3% increase.

Generally speaking, increasing the curing time mostly caused the peak shear stress of pure bentonite to decrease slightly or remarkably, and to remain almost constant in samples with any percentage of sulphate. However, the peak strength value increased slightly in samples mixed with 9% sulphate for curing times of 14 days to 28 days and 90 days to 365 days.

As seen from Figures 3.33 a - 3.35 c, increasing the curing time from seven days to 28 days in most of the samples mixed with sulphate caused flatter curves. The failure also occurred with the larger displacements. However, it seems that beyond 28 days, increasing the time of curing and the dosage of sulphate had less influence on the nature of the curves. Of all the specimens, the samples cured for seven days had the steepest curves and shortest displacements.

Nevertheless, samples with 9% sulphate exhibited more complicated behaviour. In these samples, curves appeared with a flatter shape when the time of curing was increased, at a normal stress of 50 kPa. Similarly, at a normal stress of 200 kPa, the curves exhibited a flatter shape from seven days to 14 days, almost the same shape from 14 to 28 days, and once again a flatter shape from 28 days to 90 days. The trend was more complicated at a normal stress of 100 kPa. At this stress level, curves repeatedly appeared smoother from seven days to 14 days, but showed the opposite trend from 14 days to 28 days. From 28 days to 90 days, the curves appeared more horizontal in shape, and after 90 days they had almost the same shape as for the

14 day curing period. The remarkable point is that, even though there was a change from 14 days to 28 days, the curves for the curing times of 90 and 365 days displayed almost the same behaviour as the curves for the 14 day curing period under a normal stress of 100 kPa.

- ***Effect of sodium sulphate along with normal stress on shear stress-horizontal displacement curves***

Tables 3.9 to 3.11 present the values of peak stress obtained from pure bentonite (PB) and samples mixed with different percentages of sodium sulphate (SS) under the same period of curing. Figures 3.36 a to 3.39 also illustrate the shear stress-horizontal displacement curves obtained from direct shear tests. These figures present the effect of different contents of sodium sulphate after the same curing times at the given vertical stresses.

Table 3.9: The values of peak stress for bentonite mixed with various percentages of sodium sulphate after seven days of curing at normal stresses of 50–200 kPa

Sulphate Percentage	**0%**	**3%**	**6%**	**9%**
Normal Stress (kPa)	**Curing (days)**			
	0	**7**		
	Peak Shear Stress (kPa)			
50	86.36	64.74	60.16	50.57
100	95.12	88.09	83.03	78.62
200	123.2	117.9	109.5	103.5

Table 3.10: The values of peak stress for bentonite mixed with various percentages of sodium sulphate after 14 days of curing at normal stresses of 50–200 kPa

Sulphate Percentage	**0%**	**3%**	**6%**	**9%**
Normal Stress (kPa)	**Curing (days)**			
	0	**14**		
	Peak Shear Stress (kPa)			

50	86.36	59.74	57.5	43.72
100	95.12	86.01	83.86	67.18
200	123.2	114.5	109.5	102.4

Table 3.11: The values of peak stress for bentonite mixed with various percentages of sodium sulphate after 28 days of curing at normal stresses of 50–200 kPa

Sulphate Percentage	**0%**	**3%**	**6%**	**9%**
Normal Stress (kPa)	**Curing (days)**			
	0	**28**		
	Peak Shear Stress (kPa)			
50	86.36	57.83	54.5	44.37
100	95.12	83.74	81.48	72.07
200	123.2	114.8	104.1	105.8

Table 3.12: The values of peak stress for bentonite mixed with various percentages of sodium sulphate after 365 days of curing at normal stresses of 100 kPa

Sulphate Percentage	**0%**	**3%**	**6%**	**9%**
Normal Stress (kPa)	**Curing (days)**			
	0	**365**		
	Peak Shear Stress (kPa)			
100	95.12	72.37	77.19	69.45

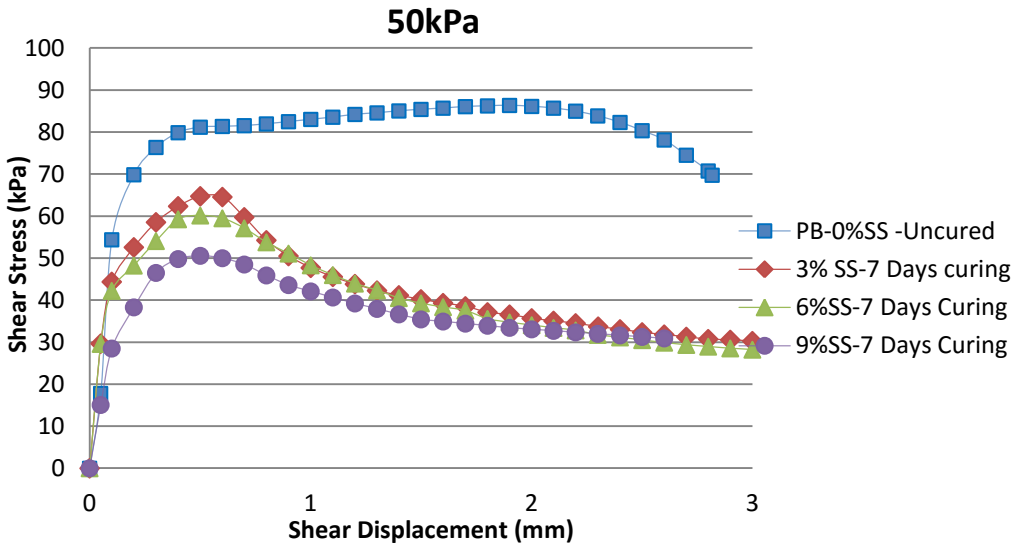

Figure 3.36 a

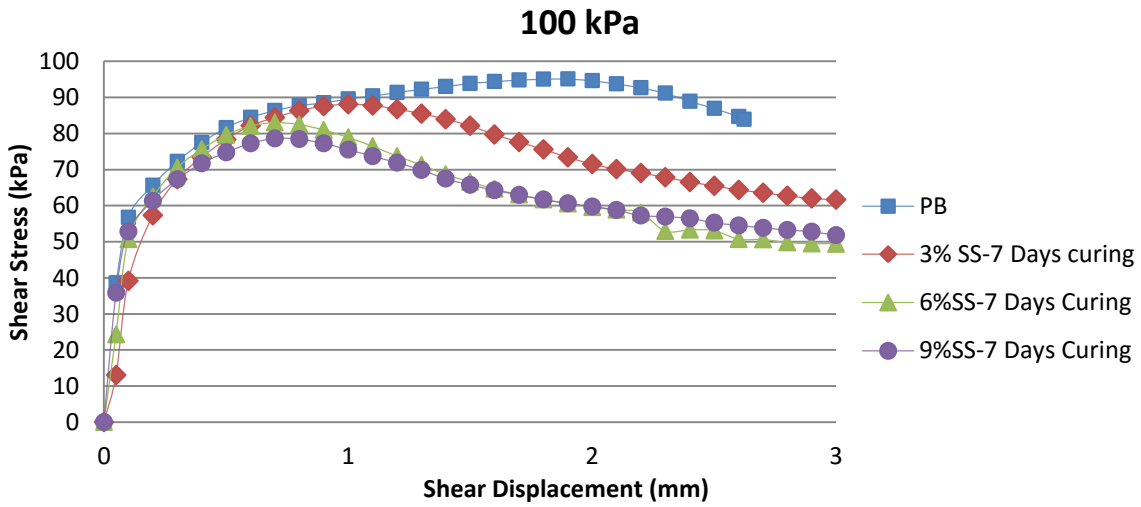

Figure 3.36 b

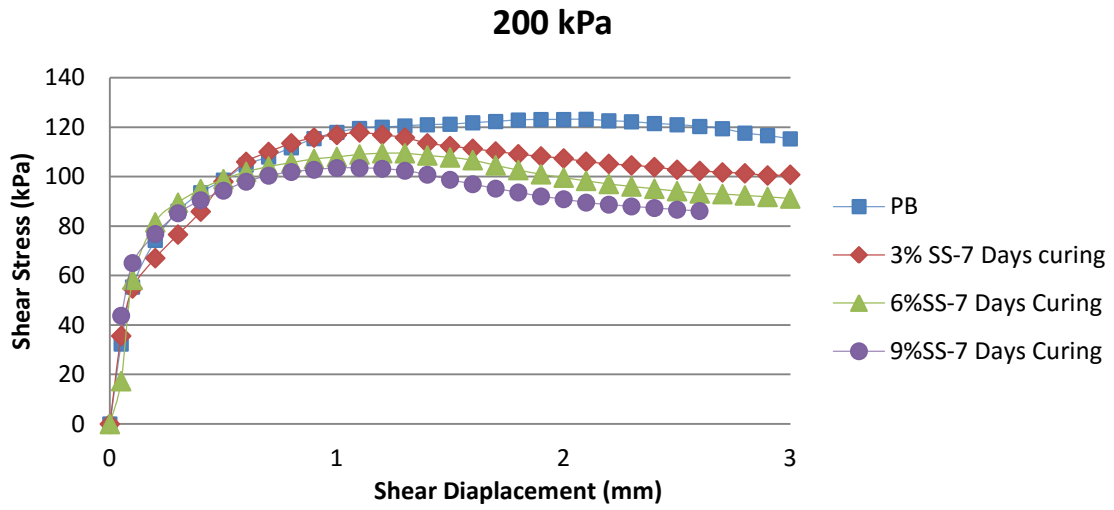

Figure 3.36 c

Figures 3.36 a- c: Shear stress-Shear displacement for pure bentonite after one day mellowing time and sodium sulphate mixed bentonite at normal stresses of 50–200 kPa at seven days' curing time

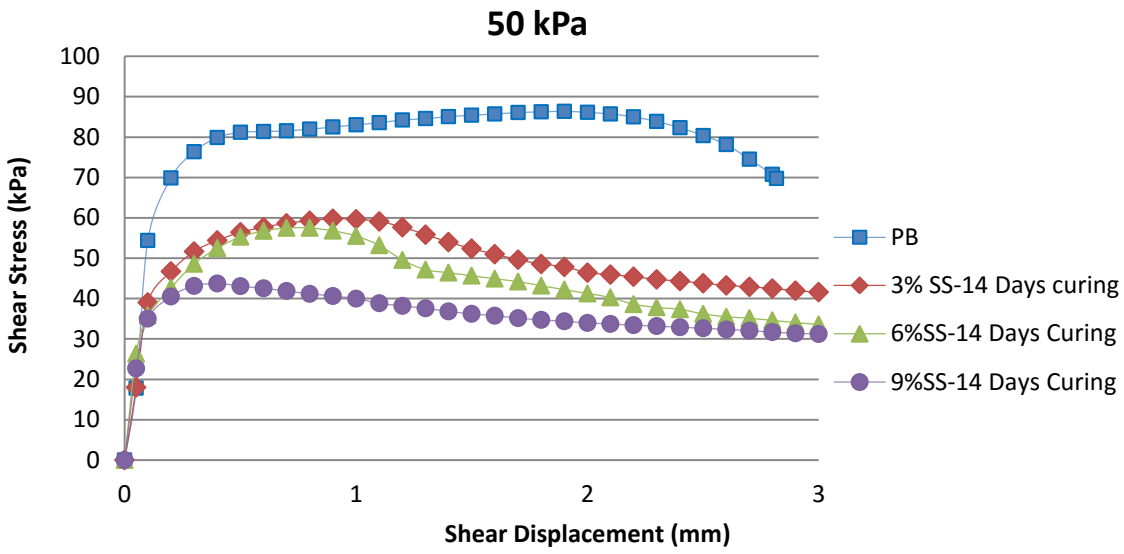

Figure 3.37 a

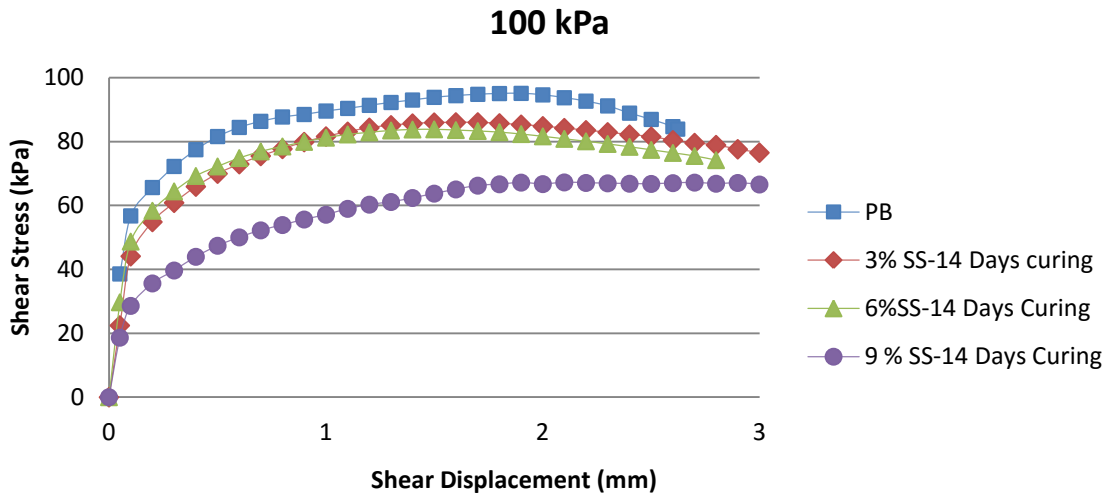

Figure 3.37 b

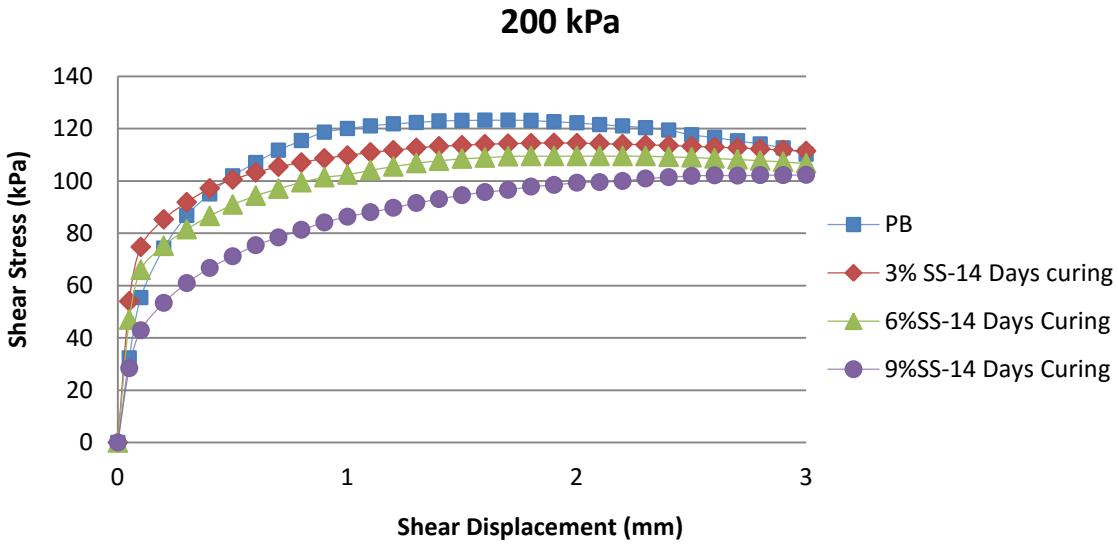

Figure 3.37 c

Figures 3.37 a- c: Shear stress-Shear displacement for pure bentonite after one day mellowing time and sodium sulphate mixed bentonite at normal stresses of 50–200 kPa at 14 days' curing time

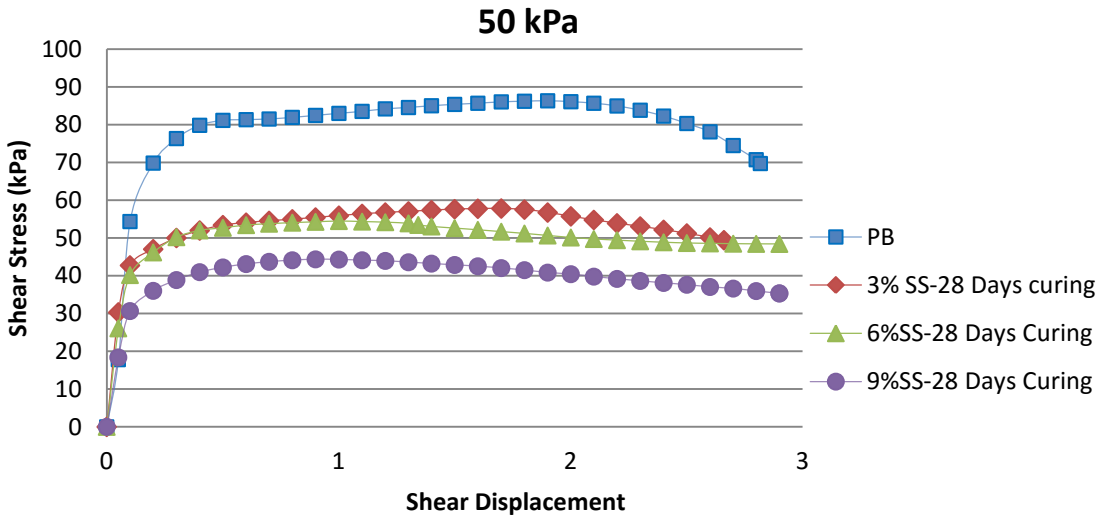

Figure 3.38 a

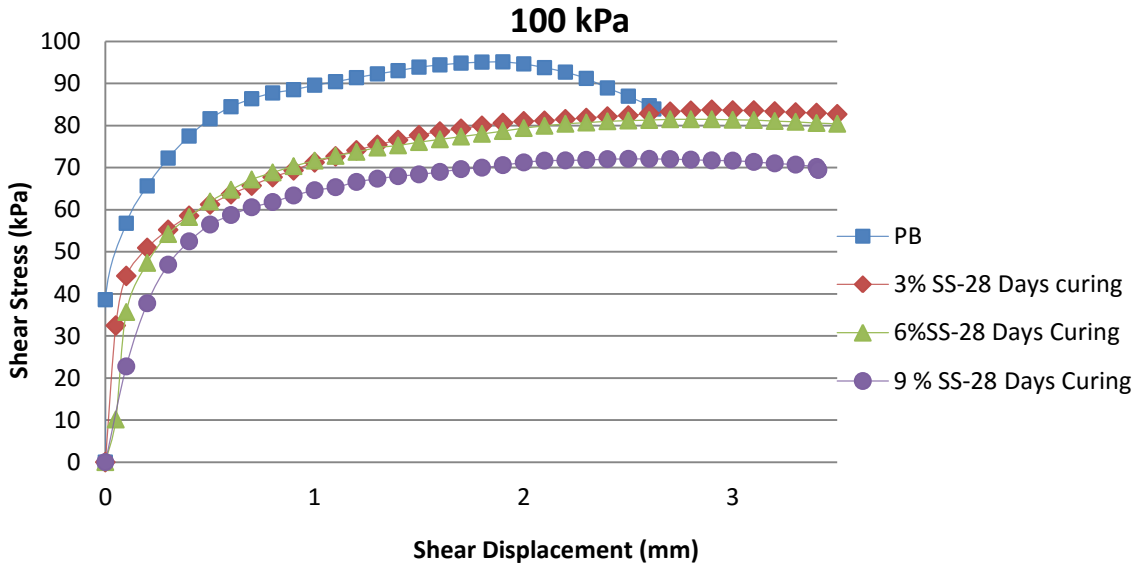

Figure 3.38 b

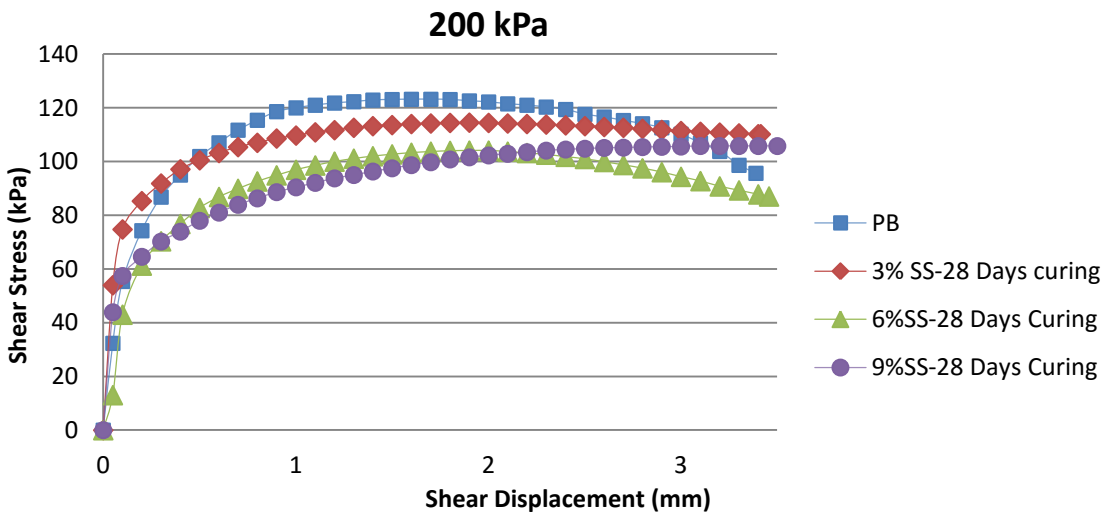

Figure 3.38 c

Figures 3.38 a- c: Shear stress-Shear displacement for pure bentonite after one day mellowing time and sodium sulphate mixed bentonite at normal stresses of 50–200 kPa at 28 days' curing time

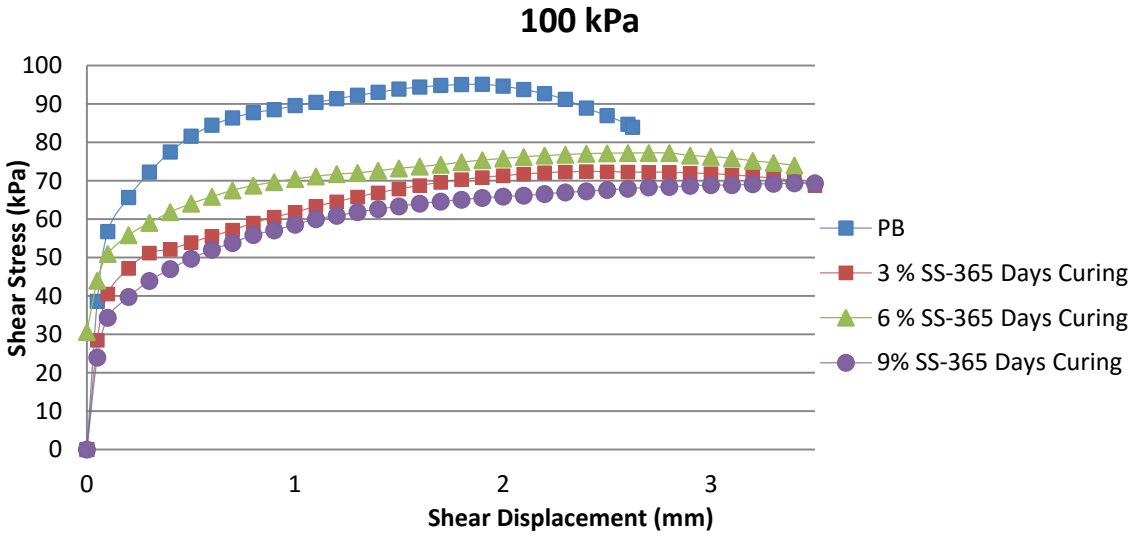

Figures 3.39: Shear stress-Shear displacement for pure bentonite after one day mellowing time and sodium sulphate mixed bentonite at normal stresses of 100 kPa at 365 days' curing time

As seen from the results presented in Tables 3.9 to 3.11, the addition of any level of sodium sulphate to bentonite led to a decrease in the peak shear stress of this soil at any given normal stress and curing time. However the rate of decrease varied with different sulphate

concentrations, normal stress levels and curing times. In almost all samples, an increment in sodium sulphate content caused the peak shear stress of bentonite clay to decrease at a given normal stress after all curing times up to 28 days. As shown in Table 3.12, there was a different trend for samples under a curing time of 365 days. For this curing period, the peak stress value for samples with 3% sulphate was 24% less than those of the bentonite samples with no curing time. With an incremental addition of salt to 6%, the peak value increased to 7% more than for the samples with 3% sulphate, and then with the addition of 9% salt the peak stress value dropped by 10%.

Overall, there was a remarkable decrease in the peak stress value with the addition of 3% salt to bentonite. At a vertical pressure of 50 kPa, the addition of 3% sodium sulphate to bentonite caused the peak shear stress value to drop by up to 33% after a curing time of 28 days. However, increasing the normal stress led to a smaller decrease in peak shear stress. At a normal stress of 100 kPa, the addition of 3% sodium sulphate to bentonite caused the peak shear stress value to drop by up to 12% after 28 days' curing time, and at normal stress of 200 kPa this decrease was up to 9.5% for samples under a seven day curing period. Increasing the dosage of sulphate from 3% to 6% had less effect on the difference between the peak stress values than increasing the dosage from 6% to 9%, and increasing the addition of sulphate from 6% to 9% was less effective than increasing the dosage from 0% to 3% at all curing times, particularly at lower normal stress levels (50 and 100 kPa). In other words, increasing the salt from 3% to 6%led to a decrease in peak value of up to 7% for the samples at a normal stress of 50 kPa under seven days' curing time, while the addition of another 3%, bringing it the

concentration to 9%, caused the peak value to drop by up to 20% for samples at a normal stress of 100 kPa under 14 days' curing time.

As seen in Figures 3.36 a to 3.39, increasing the normal stress led to the peak shear stress becoming less pronounced with shear happening in larger displacements for all of the samples mixed with any level of sulphate. Furthermore, the curves obtained from the samples tested under 50 kPa vertical stress exhibited sharper peaks compared with those tested under 100 kPa, and the curves at 100 kPa were steeper in shape compared with those at 200 kPa for each curing time.

For more details, the shear stress-displacement of all specimens tested under a vertical stress of 100kPa, and the related tables are presented in Appendices 10 to 23.

- ***Effect of sodium sulphate on cohesion and angle of friction***

The effects of sodium sulphate on the shear strength characteristics of bentonite, cohesion and friction angle are shown in Figures 3.40 to 3.45 and in Table 3.13. Figures 3.40 to 3.42 illustrate the shear stress-normal stress plots obtained from untreated samples and samples treated with various concentrations of sulphate after the same curing times.

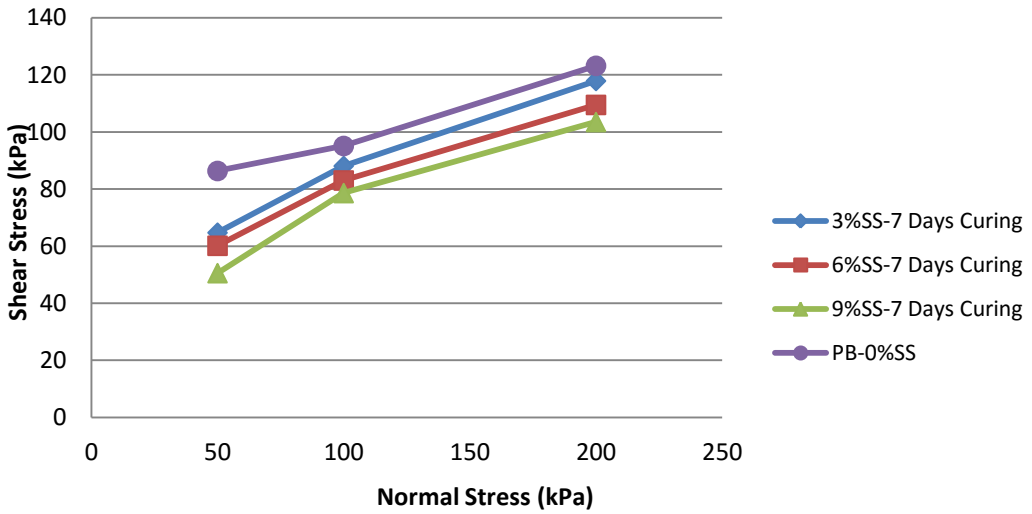

Figure 3.40: Shear stress vs normal stress for untreated samples and samples mixed with different quantities of sulphate after seven days' curing time.

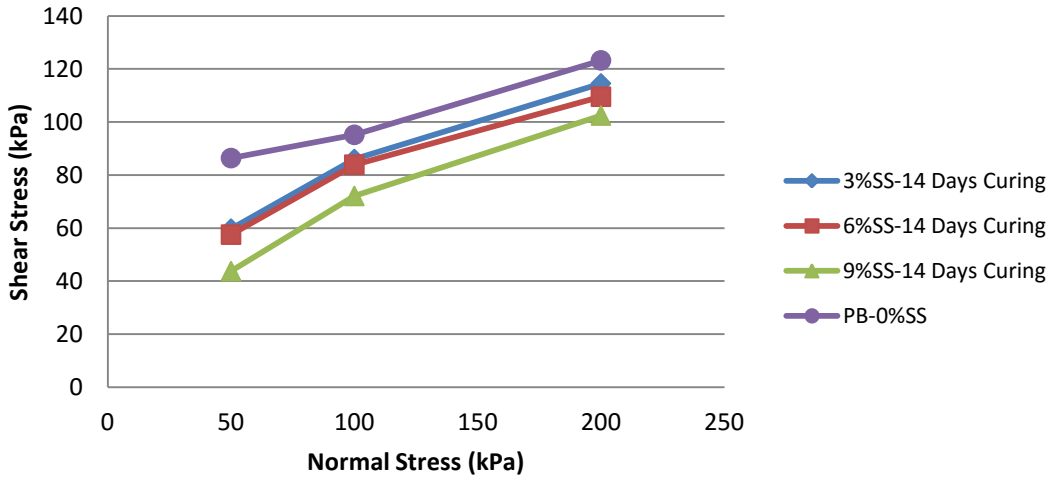

Figure 3.41: Shear stress vs normal stress for untreated samples and samples mixed with different quantities of sulphate after 14 days' curing time

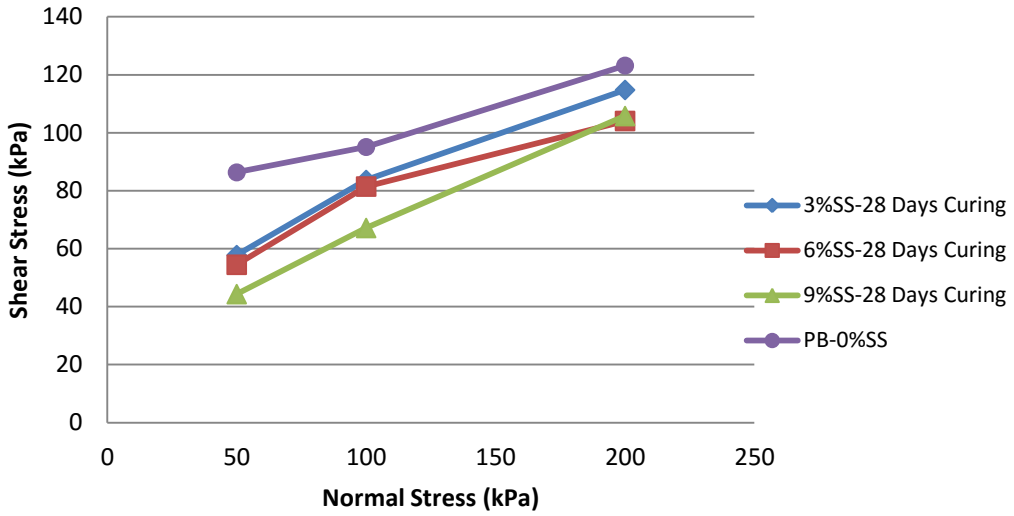

Figure 3.42: Shear stress vs normal stress for untreated samples and samples mixed with different quantities of sulphate after 28 days' curing time

Figures 3.43 to 3.45 show the shear stress-normal stress plots obtained from those samples with the same sulphate content after different curing times.

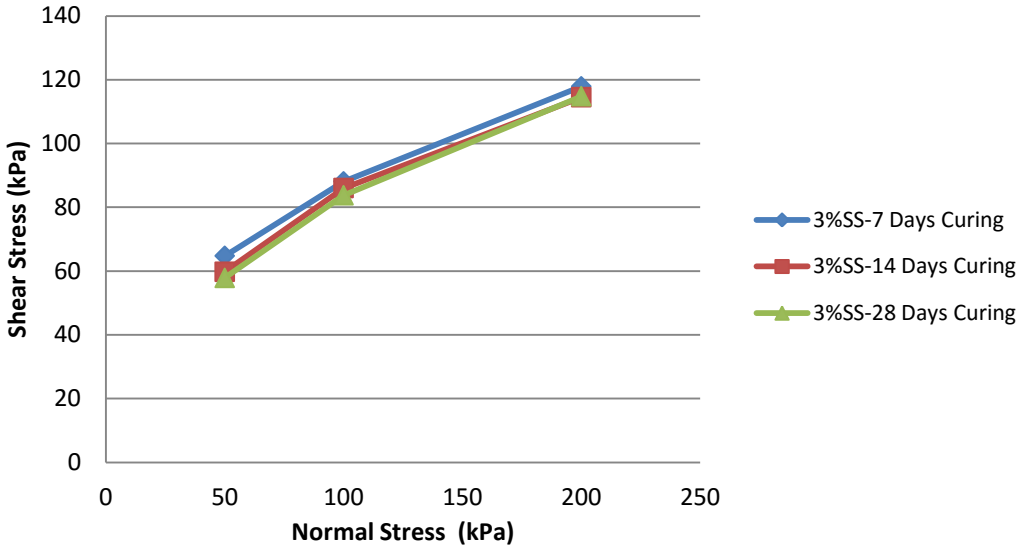

Figure 3.43: Shear stress vs normal stress for untreated samples and samples mixed with 3% of sulphate after seven to 28 days' curing time

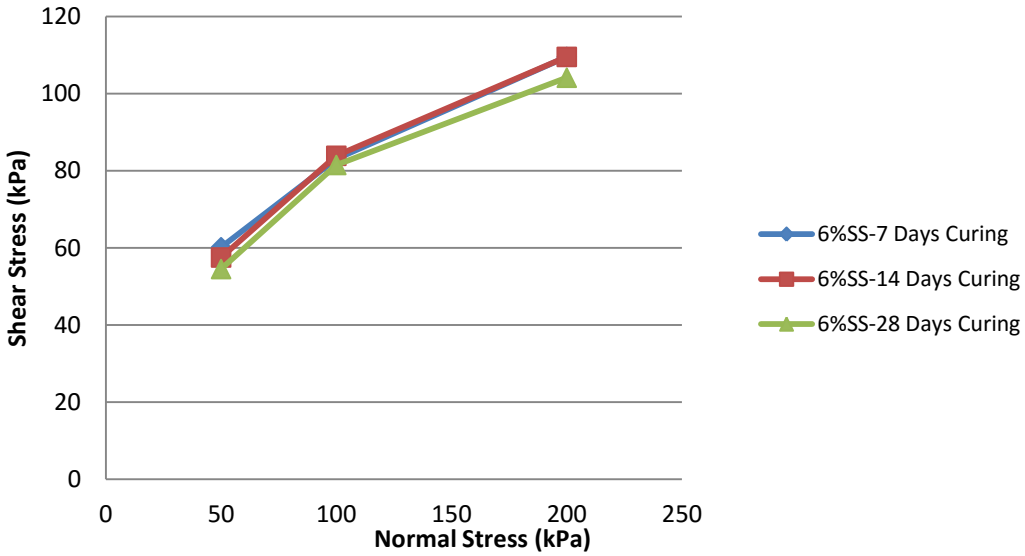

Figure 3.44: Shear stress vs normal stress for untreated samples and samples mixed with 6% of sulphate after seven to 28 days curing time

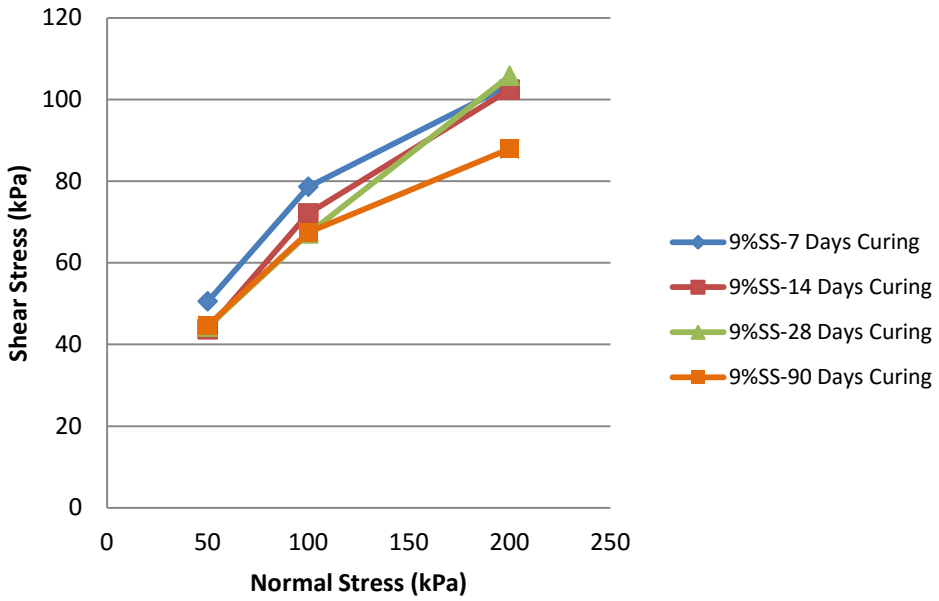

Figure 3.45: Shear stress vs normal stress for untreated samples and samples mixed with 9% of sulphate after seven to 90 days' curing time

Table 3.13 illustrates the cohesion and friction angle of Pure Bentonite and 20 Sulphate –mixed specimens. From the results, it can be seen that generally by the addition of Sodium Sulphate the friction angle decreased, in contrast, the cohesion of soil increased. However, the dosage of sulphate and the duration of curing will affect on the variation of friction angle and the cohesion.

The results show that the addition of 3% sulphate to bentonite led to an increase in the friction angle, followed by a slight decrease with the addition of another 3% sulphate, for all curing

times of up to 28 days. The addition of another 3% sulphate, to reach 9% sulphate, led to an increase of 5.5% in the friction angle for samples with a 28 day curing period.

Increasing the curing period to 28 days caused an increase in the friction angle value for most of the samples, especially those with 9% salt. However, extending the period of curing from 28 days to 90 days caused the friction angle to drop by 28% for these specimens. It was note that the samples mixed with 9% of sulphate after 28 days of curing had the highest friction angle value of other samples at curing times of seven to 28 days.

At the same time, increasing the sulphate content of bentonite to 3% led to a remarkable decrease in the cohesion value after all curing times up to 90 days, particularly for the samples under 28 days' curing time. In these samples, the cohesion value dropped by 41%. The addition of another 3% sulphate, bringing the concentration to 6%, did not much alter the level of cohesion, however, the addition of the last dosage of sulphate, bringing the concentration to 9%, caused a considerable reduction in the cohesion value, especially in the samples cured for 28 days. The cohesion value for these specimens dropped to 62% less than its value for pure bentonite.

Increasing the period of curing to 28 days caused a decrease in the cohesion value for all of the samples, especially for those with 9% salt after 28 days' curing time. However, extending the curing period from 28 days to 90 days caused the cohesion value to increase by 25%.

Generally speaking, there is approximately an inverse relationship between the cohesion value and the amount of sulphate dosage and curing time. Once again, it can be said that the samples mixed with 9% sulphate have the most impact on the value of cohesion. These specimens have the lowest value of cohesion among other samples at curing times of 7 to 28 days.

Table 3.13: Variation in cohesion (c') and internal friction angle (φ') with the addition of various quantities of sodium sulphate and different curing times for bentonite

Sulphate Percentage	φ′ (°)					c' (kPa)				
	Curing Period (Days)									
	0	7	14	28	90	0	7	14	28	90
0%	14	-	-	-	-	72	-	-	-	-
3%	-	19 7'	19 30'	20 18'	-	-	50	45	42	-
6%	-	17 44'	18 28'	17 31'	-	-	47	45	43	-
9%	-	18 41'	20 44'	21 46'	15 27'	-	38	29	27	34

To gain a better understanding and compare the results presented in Table 3.13, these findings are illustrated in column charts in Figures 3.46 and 3.47.

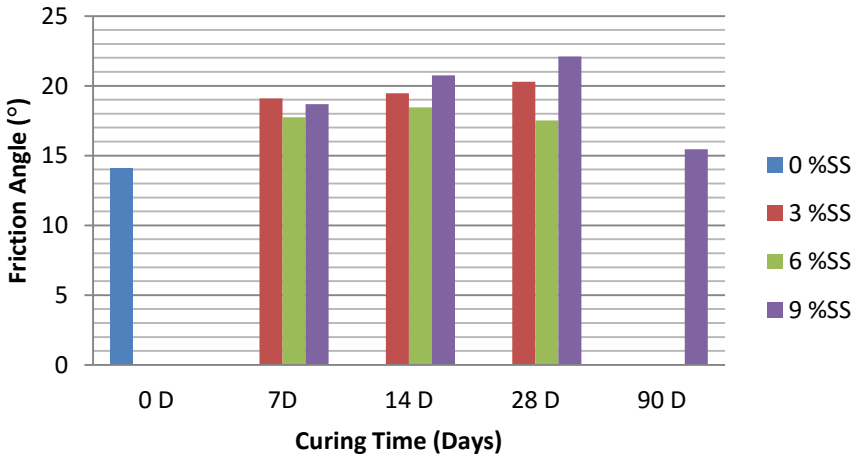

Figure 3.46: Variations in internal friction angle (φ') with various contents of sodium sulphate after different curing times for bentonite

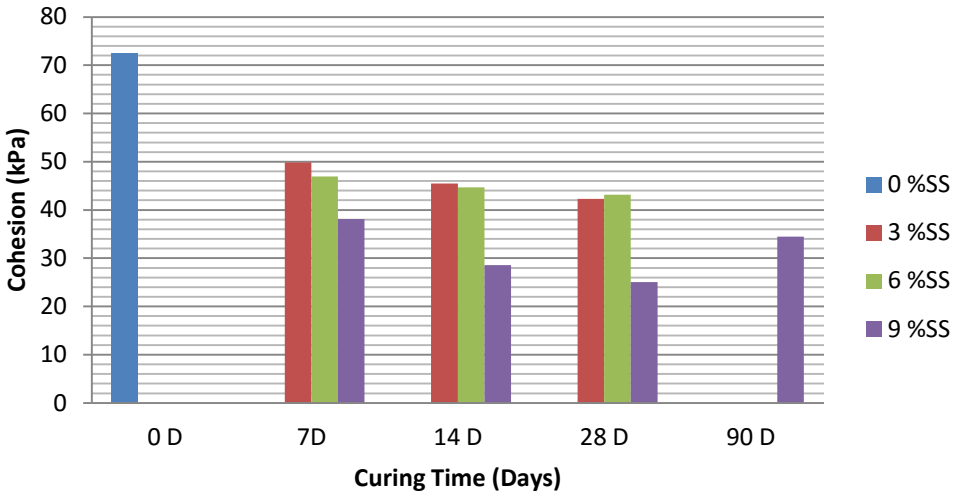

Figure 3.47: Variations in cohesion (c') with various contents of sodium sulphate after different curing times for bentonite

3.4 Micro-analytical Observation (SEM) / (EDS)

3.4.1 SEM

Scanning electron microscopy (SEM) is a commonly used method of gathering information from the surface of a sample, such as the external texture, particle orientation and the construction of crystals in the sample. In this context, Secondary electron (SE) signals were used mostly which are valuable for observing the topographic data from the surface of the sample and generating high resolution images.

SEM was performed on platinum coated samples using Zeiss Evo 40XVP apparatus to investigate the external morphology (texture), microstructure and orientation of materials making up the soil combination. The specimens were scanned, secondary electrons were collected by a secondary detector or a backscatter detector and a magnified picture of the samples was obtained. The instruments are displayed in Figure 3.48.

Figure 3.48: SEM & EDS apparatus

3.4.2 EDS

Energy dispersive spectroscopy (EDS) is carried out to break the characteristic of chemical elements of the samples into an energy spectrum. The energy spectrum is sketched as a plot of x-ray counts versus energy (in eKv). Each element is characterised by the energy peaks matching to its unique atom properties. Also, the amount of availability of atoms is specified by each particular line in spectrum in the collected area of the samples (Goodge, 2011, Tarrant, 2011).

In this study, the chemical composition and the fundamental compositional information of the specimens were provided by EDS. The elements were illustrated as an energy spectrum by using a SiLi X-ray detector mounted in the sample chamber and EDS system software, as shown in Figure 3.48.

3.4.3 Sample preparation

In order to carry out SEM investigations, after the completion of the direct shear tests, a series of samples were collected to observe the microstructure of the shear surface of those samples mixed with different percentages of sulphate. For this purpose, nine bentonite samples were selected with three different dosages of sulphate, 3%,6% and 9%, and three different curing times for each, being seven days, 14 days and 28 days. A pure bentonite sample with no curing time was also examined to observe the surface structure in the absence of salt. The following steps were taken to prepare all specimens for SEM imaging.

1. Samples were fractured carefully to the desired size with a razor blade and then transferred to the oven with forceps.
2. Samples were oven dried since it is only possible to scan dried samples in the regular SEM method used in this study.
3. Samples were sputter coated with a conductive metal such as platinum in a vacuum environment to remove any remaining water, solvent and other materials that could vaporise.

4. Samples were put in the specimen chamber located under the secondary electron detector and EDS detector.
5. The SEM imaging was followed by EDS by switching over to the EDS detector.

3.4.4 SEM/EDS results and discussion

The micrograph investigation was performed to investigate the interaction between bentonite and sodium sulphate particles on a micron scale through SEM analysis using a voltage of 15kV at a working distance of 8.5 mm. The specimens were collected from the direct shear device after completion of the shear phase to observe the surface structures in the presence and the absence of salt. Figures 3.49(a) and 3.49(b) illustrate the shear surface of pure bentonite in the absence of sulphate with no curing time, at two foci of 100 μm and 2 μm.

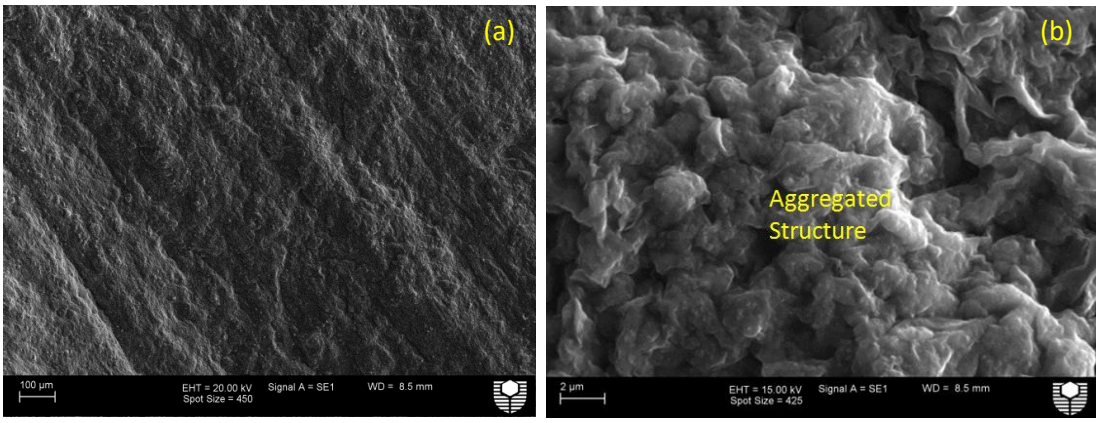

Figure 3.49: Scanning electron micrographs showing the shear surface of a bentonite sample with no curing time (a) at a focus of 100 μm; (b) at a focus of 2 μm

These micrographs revealed the aggregated, dense and continuous structure of the surface of bentonite soil. This structure is associated with the characteristics of a clay soil system in which

dipolar water molecules are attracted to charged clay particles. This attraction causes the clay particles to move towards each other and become attached and accumulated.

After completion of the SEM imaging, energy dispersive spectroscopy (EDS) was carried out on a selected area of the shear surface of the bentonite sample. To obtain more accurate results, five points were selected in this area, and the line spectrum of each point was plotted in a different colour (see Figure 3.50).

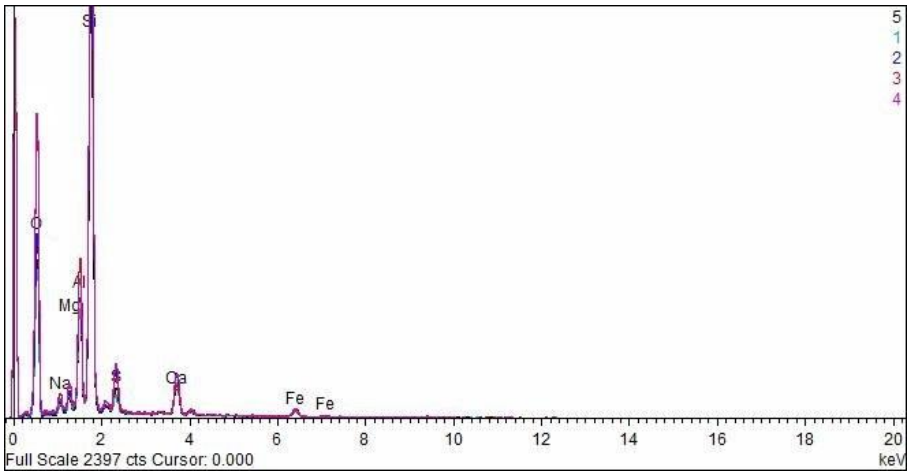

Figure 3.50: Energy dispersive spectroscopy (EDS) of five points of the bentonite sample

In the graph illustrated in Figure 3.50, each of the peaks indicates the availability and amount of the bentonite components. This graph showed the high proportions of the three basic components (Si, O and Al) of bentonite clay. The high level of these elements was associated with the presence of silicon dioxide (SiO_2) and aluminium oxide (Al_2O_3) at 63.2% and 13.3% respectively in the bentonite clay (refer to Table 3.1 in Section 3.1.1 of this chapter). The other components (i.e., Ti, Fe, Ca, Mg, K and Na) were present in lower proportions in bentonite.

In addition to the pure bentonite sample with no curing time, SEM analysis was carried out on nine bentonite samples with three different dosages of sulphate, 3%, 6% and 9%, and three different curing times for each, being seven days, 14 days and 28 days. To better understand the SEM images obtained from these samples, the effect of curing time is discussed for each sulphate content individually as follows:

3.4.4.1 SEM/EDS examination on specimens mixed with 3% sodium sulphate:

The micrograph investigation was performed on samples with 3% sulphate after curing times of seven days, 14 days and 28 days. A voltage of 15kV at a working distance of 8.5 mm was used for all samples. Figures 3.51 to 3.53 illustrate these specimens at two foci of 100 μm and 2 μm. The smaller magnification (100 μm) of the shear surface shows that the soil particles are oriented in the direction of shear.

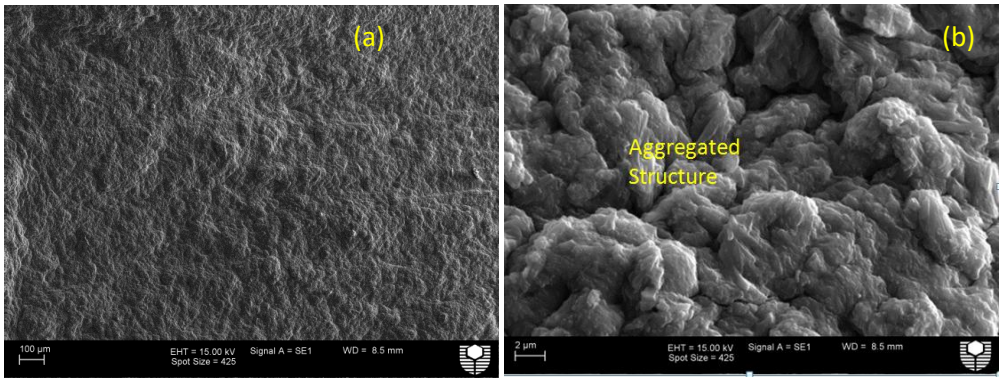

Figure 3.51: Scanning electron micrographs showing the shear surface of a bentonite sample with 3% SS under seven days' curing (a) at a focus of 100 μm; (b) at a focus of 2 μm

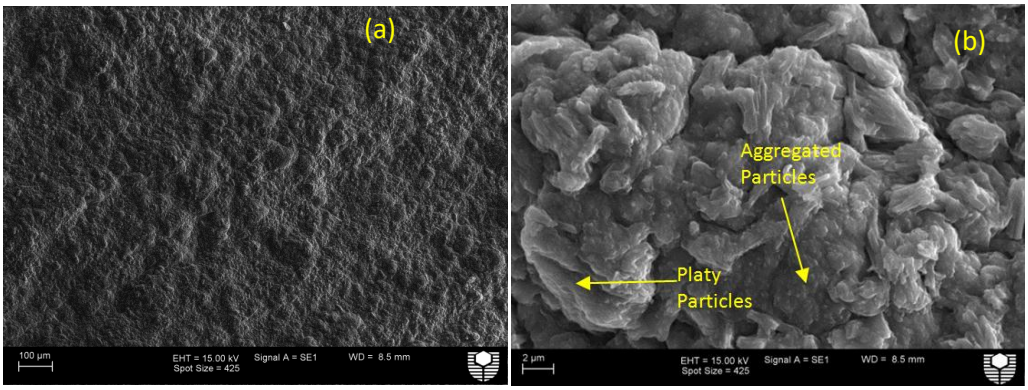

Figure 3.52: Scanning electron micrographs showing the shear surface of a bentonite sample with 3% SS under 14 days' curing (a) at a focus of 100 µm; (b) at a focus of 2 µm

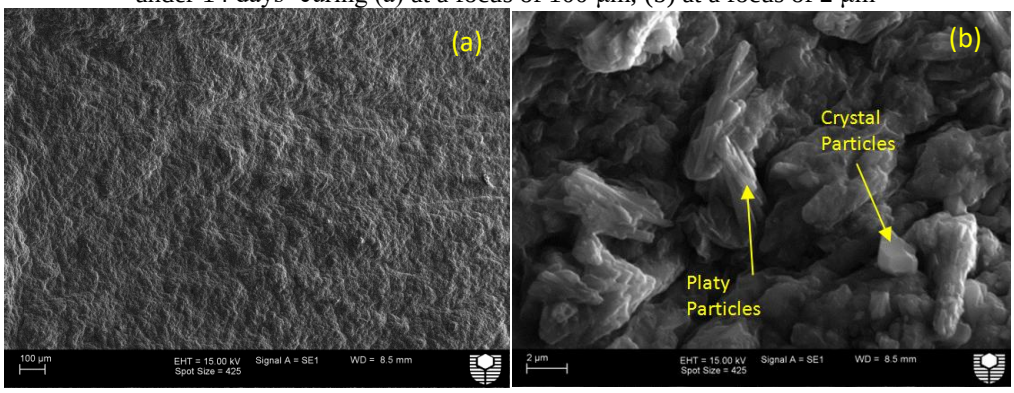

Figure 3.53: Scanning electron micrographs showing the shear surface of a bentonite sample with 3% SS under 28 days' curing (a) at a focus of 100 µm; (b) at a focus of 2 µm

It can be seen from these micrographs that in the samples with seven days' curing (Figure 3.51(b)), the shear surface was very similar to that of the untreated sample (Figure 3.51(b)). In the sample with 14 days' curing (Figure 3.53(b)), in addition to the aggregated particles, some platy particles were occasionally observed. These were apparently sulphate crystals which appeared on the surface of the soil. Figure 3.53(b) revealed that in addition to the platy particles, some crystal particles were observed occasionally on the surface of the sample cured for 28 days.

After completion of the SEM imaging, energy dispersive spectroscopy (EDS) was carried out on a selected area on the shear surface of the samples with 3% sodium sulphate under three different curing times of seven days, 14 days and 28 days. To achieve more accurate results, five points were selected in this area for each sample, and the line spectrum of each point was plotted in a different colour in Figures 3.54(a) to 3.54(c).

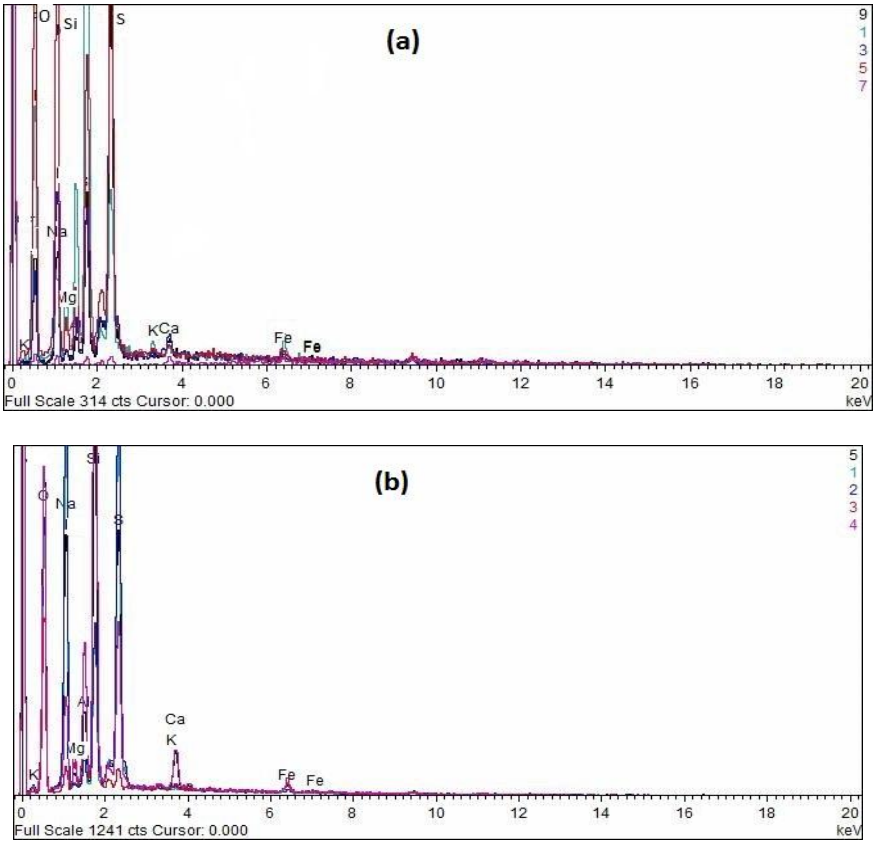

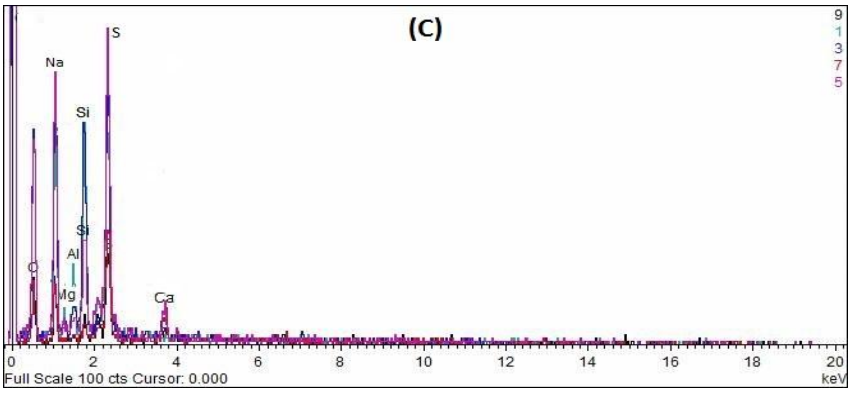

Figure 3.54: Energy dispersive spectroscopy (EDS) of five points of the smples mixed with 3% SS (a) under seven days' curing; (b) under 14 days' curing; (c) under 28 days' curing

These figures showed the high proportion of O, Na, Si and S in the samples treated with 3% sodium sulphate for all curing times. Similar to the pure bentonite sample, the high levels of of Si and O were associated with the presence of silicon dioxide (SiO_2) and aluminium oxide (Al_2O_3) with 63.2% and 13.3% respectively in the bentonite clay (refer to Table 3.1 in Section 3.2.1 of this chapter). The other chemical components (i.e., Ti, Fe, Ca, Mg and K) were present at lower concentrations, as detected by EDS examination.

Comparisons between these graphs and the pure bentonite line spectrum showed increments in the dosage of sodium (Na), and the presence of sulphur (S) as a new element due to the addition of sodium sulphate to the bentonite clay. See Table 3.14 for more information. Hence, the EDS analysis confirmed the presence of the sodium sulphate (Na_2SO_4) seen in the SEM images, with the high concentration of Na and S in the spectrum line results.

Table 3.14 shows the average proportion of all elements at five points on the shear surface of a pure bentonite sample and bentonite specimens mixed with 3% sulphate under three different curing times.

Table 3.14: The average proportion of elements on the shear surface

Added Sulphate content (%)	Curing time (days)	Elements proportion (%)							
		O	Na	Mg	Al	Si	S	Ca	Fe
0	0	64.32	1.1	1.24	5.2	23.59	1.97	1.87	0.72
3	7	52.61	13.07	1.38	2.09	11.03	15.6	1.94	2.27
	14	58.19	13.21	0.72	2.89	14.93	14.68	0.61	0.56
	28	57.3	18.27	0.88	1.23	6.11	14.07	1.71	0.44

3.4.4.2 SEM/EDS examination on specimens mixed with 6% sodium sulphate:

Investigations into the morphology of the samples with 6% sulphate after curing times of seven days, 14 days and 28 days are presented in Figures 3.55 to 3.57 at two foci of 100 μm and 2μm. The smaller magnification (100 μm) of the shear surface shows that the soil particles are oriented in the direction of shear. A voltage of 15kV at a working distance of 8.5 mm was used for all samples.

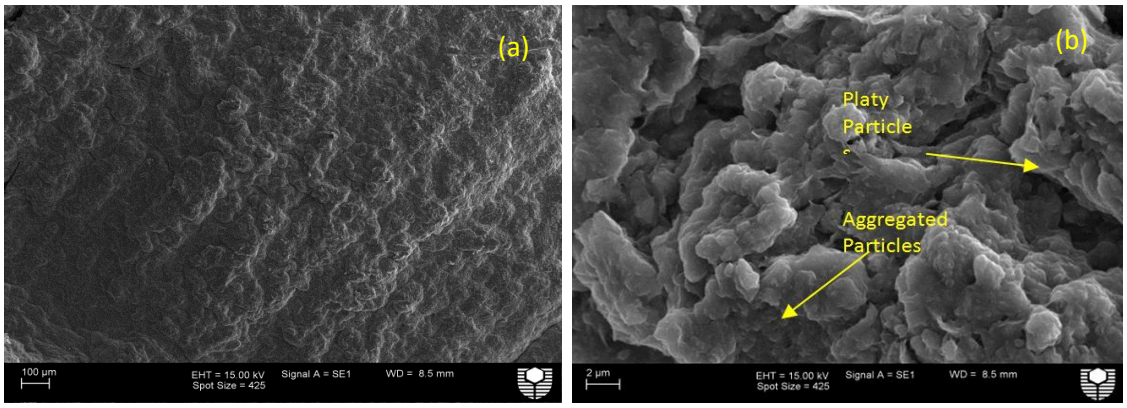

Figure 3.55: Scanning electron micrographs showing the shear surface of a bentonite sample with 6% SS under seven days' curing (a) at a focus of 100 µm; (b) at a focus of 2 µm

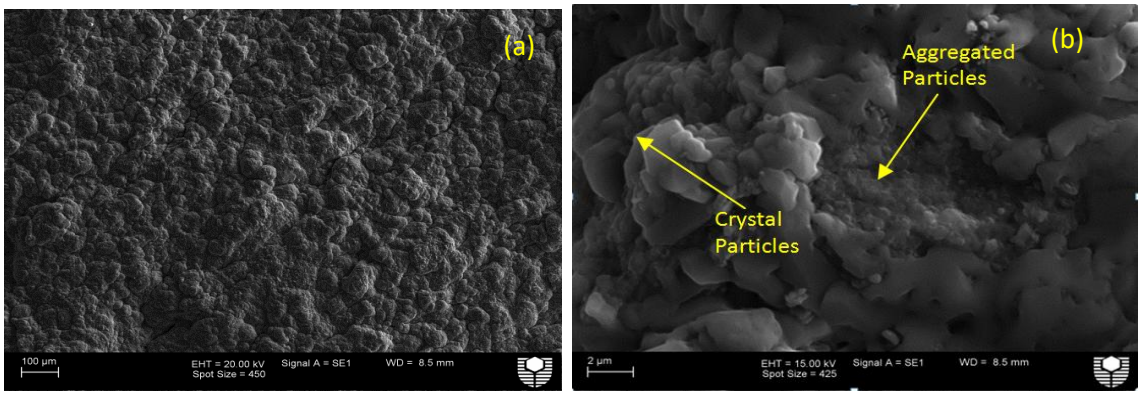

Figure 3.68: Scanning electron micrographs showing the shear surface of a bentonite sample with 6% SS under 14 days' curing (a) at a focus of 100 µm; (b) at a focus of 2 µm

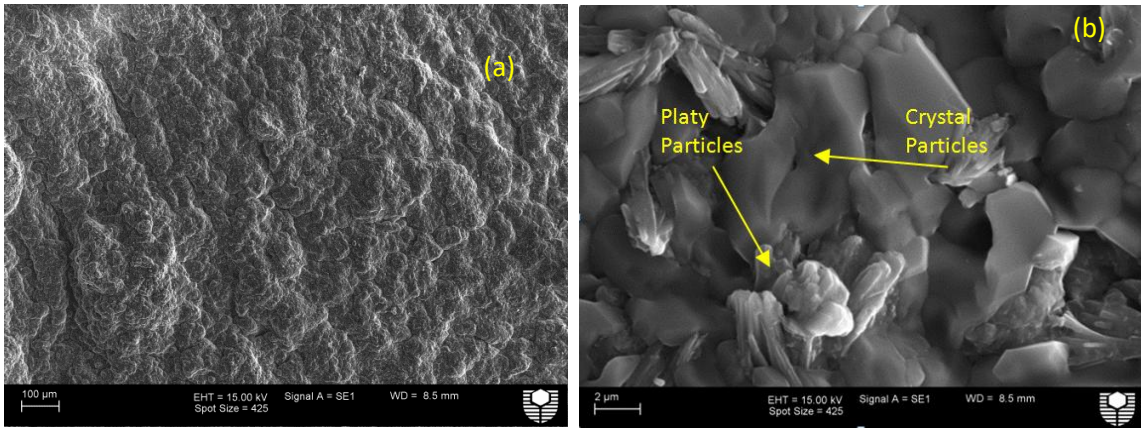

Figure 3.56: Scanning electron micrographs showing the shear surface of a bentonite sample with 6% SS under 28 days' curing (a) at a focus of 100 µm; (b) at a focus of 2 µm

As seen from these micrographs, in the samples with seven days' curing time (Figure 3.55(b)), the surface of shear was similar to that of the untreated sample (Figure 3.49(b)). However, in addition to aggregated particles, some platy particles appeared randomly on the surface of this specimen. Figures 3.56(b) and 3.57(b) revealed the presence of significant quantities of sulphate crystals on the surface of shear in samples with a longer curing time (14 days and 28 days), and that they surrounded the clay particles. These particles are apparently sulphate crystals which continued to grow in the presence of water in samples with a longer curing time (14 days and 28 days).

EDS was also carried out on a selected area on the shear surface of samples with 6% sodium sulphate, under three different curing times of seven days, 14 days and 28 days. To gain more accurate results, five points were selected in this area for each sample, and the line spectrum of each point was plotted in a different colour in Figures 3.58(a) to 3.58(c).

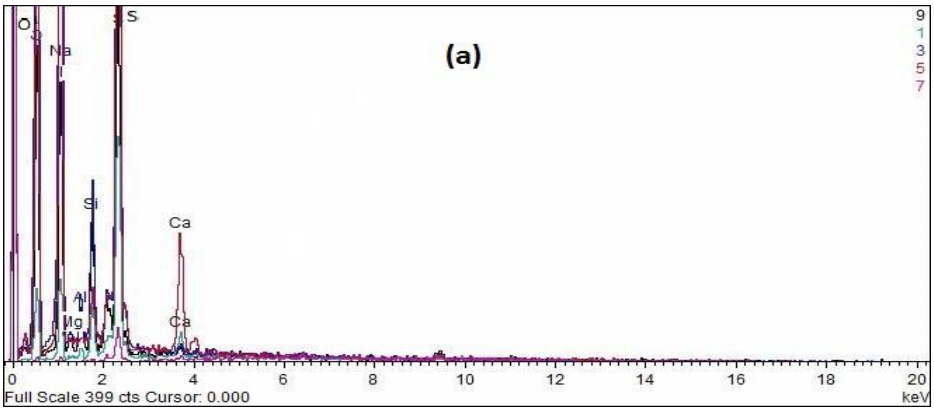

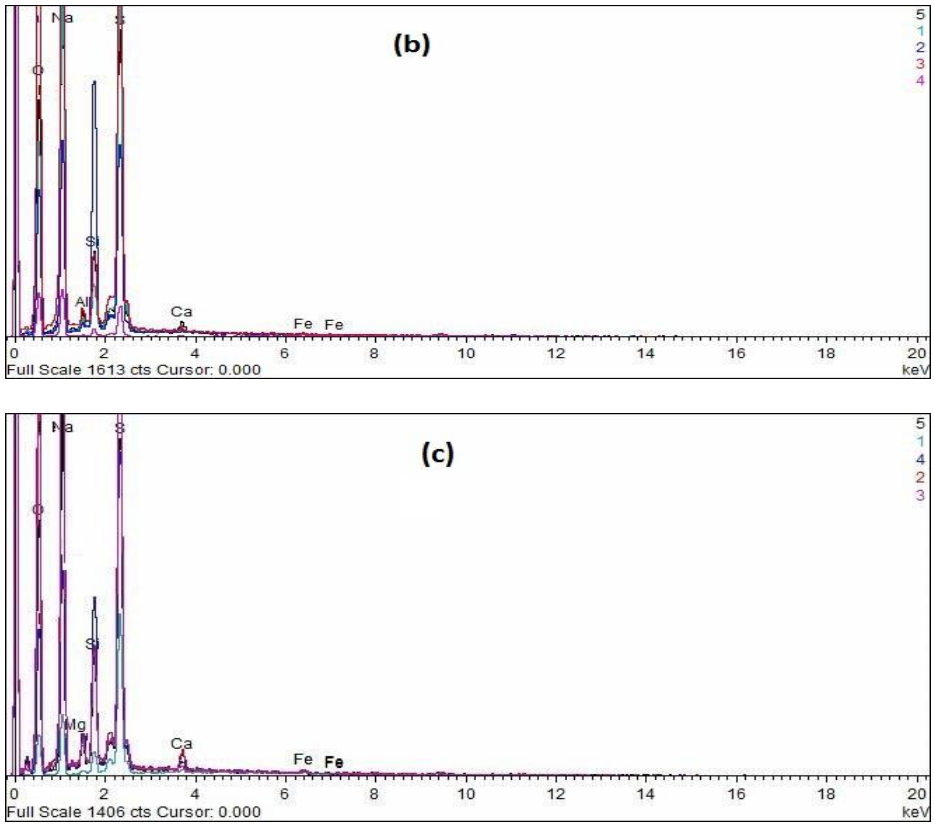

Figure 3.57: Energy dispersive spectroscopy (EDS) of five points of the smples mixed with 6% SS (a) under seven days' curing; (b) under 14 days' curing; (c) under 28 days' curing

Similar to the samples with 3% sulphate, the spectra of the samples with 6% sulphate highlight the high proportion of sodium (Na), sulphur (S), silicon (Si) and oxygen (O), and a lower porportion of other components (i.e., Fe, Ca, Mg and K).

The EDS analysis confirmed the presence of sodium sulphate (Na_2SO_4) components in the SEM images, showing the higher concentration of sodium (Na) and sulphur (S) elements in the spectrum line results. These results also confirmed that the proportions of these elements on the

shear surface of the samples with 6% sodium sulphate are slightly higher compared to those of samples with 3% Na_2SO_4. See Table 3.14 and 3.15 for more information.

Table 3.15 shows the average proportion of all elements at five points on the shear surface of a pure bentonite sample and bentonite specimens mixed with 6% sulphate under three different curing times.

Table 3.15: The average proportion of elements on the shear surface of samples with 6% SS

Added Sulphate content (%)	Curing time (days)	Elements proportion (%)							
		O	Na	Mg	Al	Si	S	Ca	Fe
0	0	64.32	1.1	1.24	5.2	23.59	1.97	1.87	0.72
6	7	57.76	17.63	0.36	0.73	2.73	16.85	1.92	2.03
	14	56.18	23.21	0.34	0.51	5.05	13.41	0.13	0.17
	28	56.4	20.72	0.18	1	4.87	16.06	0.48	0.28

3.4.4.3 SEM/EDS examination on specimens mixed with 9% sodium sulphate:

Investigations into the morphology of the samples with 9% sulphate after curing times of seven days, 14 days and 28 days are presented in Figures 3.59 to 3.61 at two foci of 100 μm and 2μm. The smaller magnification (100 μm) of the shear surface shows that the soil particles are oriented in the direction of shear. A voltage of 15kV at a working distance of 8.5 mm was used for all samples.

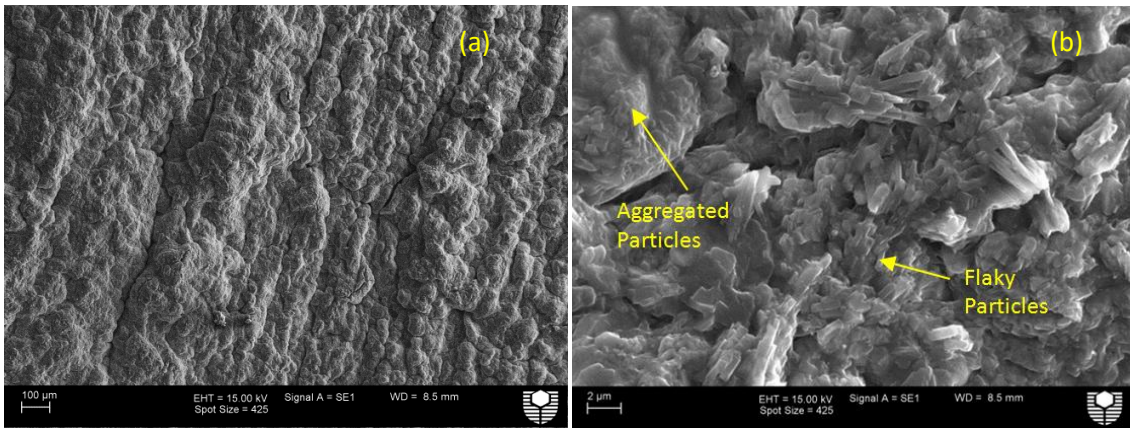

Figure 3.58: Scanning electron micrographs showing the shear surface of a bentonite sample with 9% SS under seven days' curing (a) at a focus of 100 µm; (b) at a focus of 2 µm

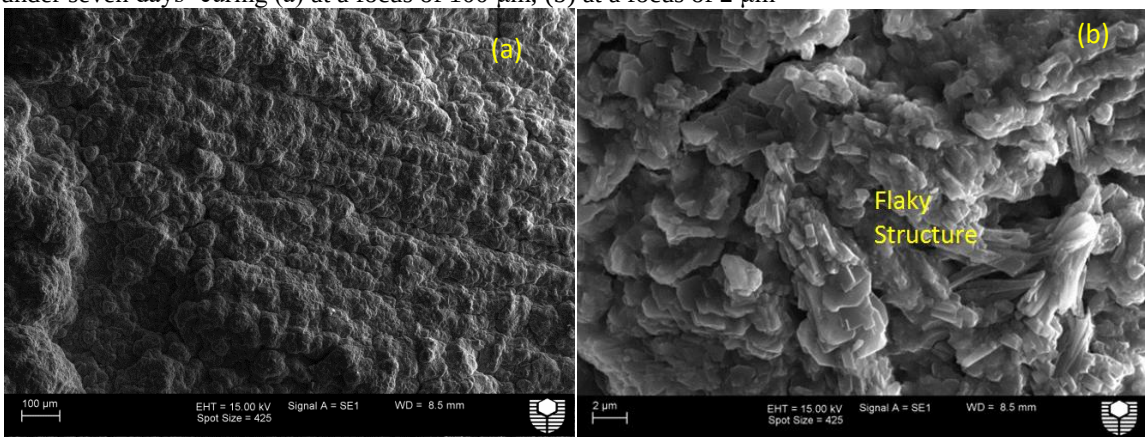

Figure 3.59: Scanning electron micrographs showing the shear surface of a bentonite sample with 9% SS under 14 days' curing (a) at a focus of 100 µm; (b) at a focus of 2 µm

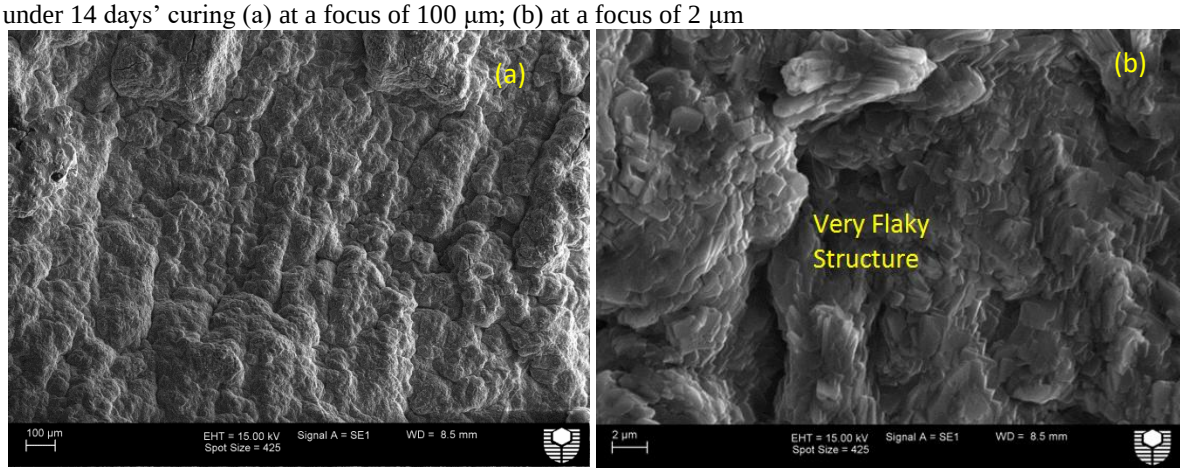

Figure 3.60: Scanning electron micrographs showing the shear surface of a bentonite sample with 9% SS under 28 days' curing (a) at a focus of 100 µm; (b) at a focus of 2 µm

As seen from these pictures, the surface structures in the samples with 9% sulphate at all curing times appeared very different to those of the untreated sample and the samples treated with 3% and 6% sulphate (see Figures 3.49, 3.51 to 3.53 and 3.55 to 3.57 respectively). As seen from Figures 3.59 (b), in the sample with 9% sulphate under a curing time of seven days, the clay particles looked very platy. Figures 3.60(b) and 3.61(b) revealed that the degree of flakiness increased in the specimens with 9% sulphate under a longer curing time (14 days and 28 days).

EDS was used to analyse the elemental components of the samples with 9% sodium sulphate. Figures 3.62(a) to 3.62(c) illustrate the spectrum data for the surface area of these samples after three different curing times of seven days, 14 days and 28 days. These results were obtained at five selected points on the shear surface, and the line spectrum of each point was plotted in a different colour .

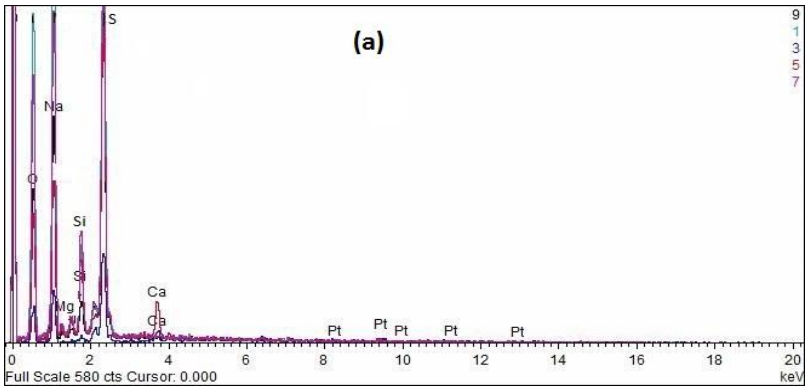

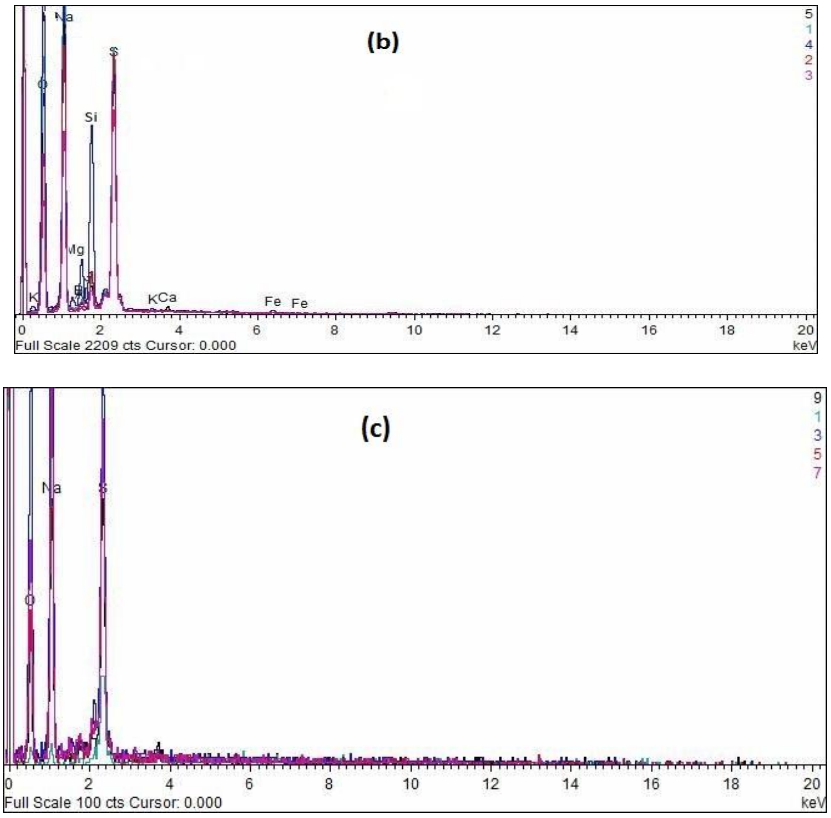

Figure 3.61: Energy dispersive spectroscopy (EDS) of five points of the smples mixed with 9% SS (a) under seven days' curing; (b) under 14 days' curing; (c) under 28 days' curing

Investigation into the line spectrum results for samples with 9% sulphate at all curing times shows that, in addition to the main common components of bentonite (O, Si and Al), sodium (Na) and sulphur (S) were present in high quantities due to the high availability of these components in sodium sulphate salt. The other components (i.e., Ti, Fe, Ca, Mg and K) were present in lower quantities.

This tendency is similar to that of the Na and S contents in the samples mixed with lower contents of Na_2SO_4, however the concentration is slightly higher in the samples mixed with 9%

sulphate due to the addition of higher quantities of this salt. Refer to Table 3.16 for more information.

Table 3.16 shows the average proportion of all elements at five points on the shear surface of a pure bentonite sample and bentonite specimens mixed with 9% sulphate under three different curing times.

Table 3.16: The average proportion of elements on the shear surface of samples with 9%SS

Added Sulphate content (%)	Curing time (days)	Elements proportion (%)							
		O	Na	Mg	Al	Si	S	Ca	Fe
0	0	64.32	1.1	1.24	5.2	23.59	1.97	1.87	0.72
9	7	54.76	20.96	0.53	0.68	2.95	18.92	1.02	0.18
	14	55.41	24.39	0.15	0.65	2.78	16.41	0.09	0.12
	28	55.06	23.56	0.03	0.24	0.85	19.15	0.67	0.44

3.5 Summary of the chapter

3.5.1 Summary of compaction tests

Based on the compaction tests conducted on the bentonite-sodium sulphate mixtures, the following outcomes were observed:

- The addition of sodium sulphate to bentonite led to a slight increase in the maximum dry density (MDD) of this soil. A maximum MDD was obtained of up to 3% more than its previous value in the bentonite sample for samples with 1% sodium sulphate.
- The addition of sodium sulphate salt to up to 1% increased the optimum moisture content (OMC) marginally by up to 1% more than its value in the bentonite sample, and then suddenly decreased by up to 32% less than its initial value with the continued addition of salt up to 3%.
- The addition of sodium sulphate to up to1% did not affect on the nature of compaction curves, and the degree of saturation at the points of (MDD and OMC) almost remained in the same range. Incremental addition of salt from 1% to up to 3% altered the nature of compaction curves. The curves appeared with flatter shapes , and the points of (MDD and OMC) were obtained at lower degrees of saturation. This shows that the a proper compation is less likely to be achieved with the presence of sodium sulphate beyond 1% by the dry weight of bentonite soil.
- Of the various sodium sulphate-bentonite clay mixtures, the sample with 1% sodium sulphate revealed the highest MDD up to 3% more than its previous value in the bentonite sample, and the sample with 3% of this salt showed the lowest OMC up to 32% less than its initial value . Therefore, it can be concluded that 3% sodium sulphate was the most effective of all the quantities, and this percentage of the salt was used as the initial value in the direct shear tests.

3. 5. 2 Summary of direct shear tests

- Adding any percentage of sodium sulphate additives to bentonite decreased the peak shear stress in all the samples at all curing times.
- Extending the curing time mainly caused a slight drop in the peak stress values. These values occasionally remained constant in samples mixed with any percentage of sulphate and sometimes increased in the samples mixed with 9% sulphate. The impact was more observable in samples with 3% sulphate for the extending the time of curing from 28 days to 365 days, and for the samples with 9% sulphate from 28 days to 90 days. The peak stress values decreased by 13% in the former and 16% in the latter.
- Even though increasing the curing time did not have a significant effect on the peak stress value in most of the cases, it did have a considerable impact on the nature of the shear stress-horizontal displacement curves at any percentage of sulphate, particularly under the lower normal stresses and with up to 28 days' curing. Increasing the curing time led to flatter curves with the failure in larger displacements in most of the cases.
- Incrementally increasing the normal stress value caused flatter curves with less pronounced peak stress in all samples mixed with any sulphate content, after any curing time.
- Addition of sodium sulphate to bentonite led to a decrease in cohesion and in contrast, an increase in the friction angle value. The most remarkable decrease and increase were obtained 62% 55% respectively for the samples with 9% sulphate and 28 days curing time.
- The results proved that there was practically an inverse relationship between the value of cohesion and the amount of sulphate and curing time. By contrast, there was almost a

positive correlation between the friction angle value and the amount of sulphate and curing time. Increasing the dosage of sulphate from 3% to 6% exceptionally led to a decreased friction angle value, which then increased at a dosage of 6% to 9%.

- Increasing the curing time was more efficient at a curing time of 28 days to 90 days in specimens mixed with 9% sulphate than those samples cured from seven days to 28 days at any percentage of sulphate.
- Increasing the period of curing to 28 days caused a decrease in the cohesion value and an increase in the friction angle value for all samples, especially those with 9% salt after 28 days' curing time. Nevertheless, extending the period of curing from 28 days to 90 days caused the cohesion value to increase by 25% and the friction angle to drop by 28% compared to their previous values.

3.5.3 Summary of SEM/EDS analysis

The scanning electron micrographs showed that the surface structure of bentonite clay was changed by the presence of sodium sulphate. The SEM images of the pure bentonite sample with no curing time showed that the surface structure of the bentonite was aggregated and flocculated. This structure is associated with the characteristics of a clay soil system in which the charged clay particles tend to clump together and create a flocculated and cemented structure.

The SEM images of specimens with 3% sodium sulphate at all curing times were similar to those of a bentonite sample. However the clay particles appeared platy occasionally on the shear surface of theses specimens (Refer to Figure 3.51 to 3.53).

The changes in the surface structure were more noticeable for the samples with a higher sodium sulphate content (6% and 9%), and a longer curing time (14 days and 28 days). The SEM investigation revealed that in the specimens with 6% sodium sulphate with longer curing time (14 days and 28 days), the clay particles were surrounded by crystal-shaped particles (Refer to Figure 3.56 and 3.57). These crystals were expected to be the white crystalline mineral of sodium sulphate known as thenardite (Na_2SO_4) which usually forms at the top of the soil profile as it dries during the evaporation process.

There was a marked difference in the shear surface of the samples mixed with 9% sulphate compared to samples with 3% and 6% of this salt. SEM images of the samples with 9% sulphate illustrated a flaky structure, and the degree of flakiness was higher for samples under a longer curing time (14 days and 28 days), (Refer to Figure 3.59 and 3.60).

Generaly speaking, the shear surface of bentonite and samples mixed with 3% sodium sulphate looked flocculated and rough, and flaky with thin and very smooth plates in the samples with a higher salt content (9%). This flaky structure was due to an increase in the amount of Na^+ cations. The increased concentration of Na^+ in the pore water influences the interparticle forces between clay particles. These changes in the environment of deposition alters the way the clay particles are arranged, and causes the clay particles to become arranged in a parallel orientation with a platy appearance.

The EDS analysis also confirmed the presence of the sodium sulphate (Na_2SO_4) components seen in the SEM images, with a higher concentration of sodium (Na) and sulphur (S) elements appearing in the spectrum line results.

Chapter 4

Numerical Modelling

4. Numerical Modelling

4.1 Introduction

This chapter was separated in different phases as outlined in Figure 4.0:

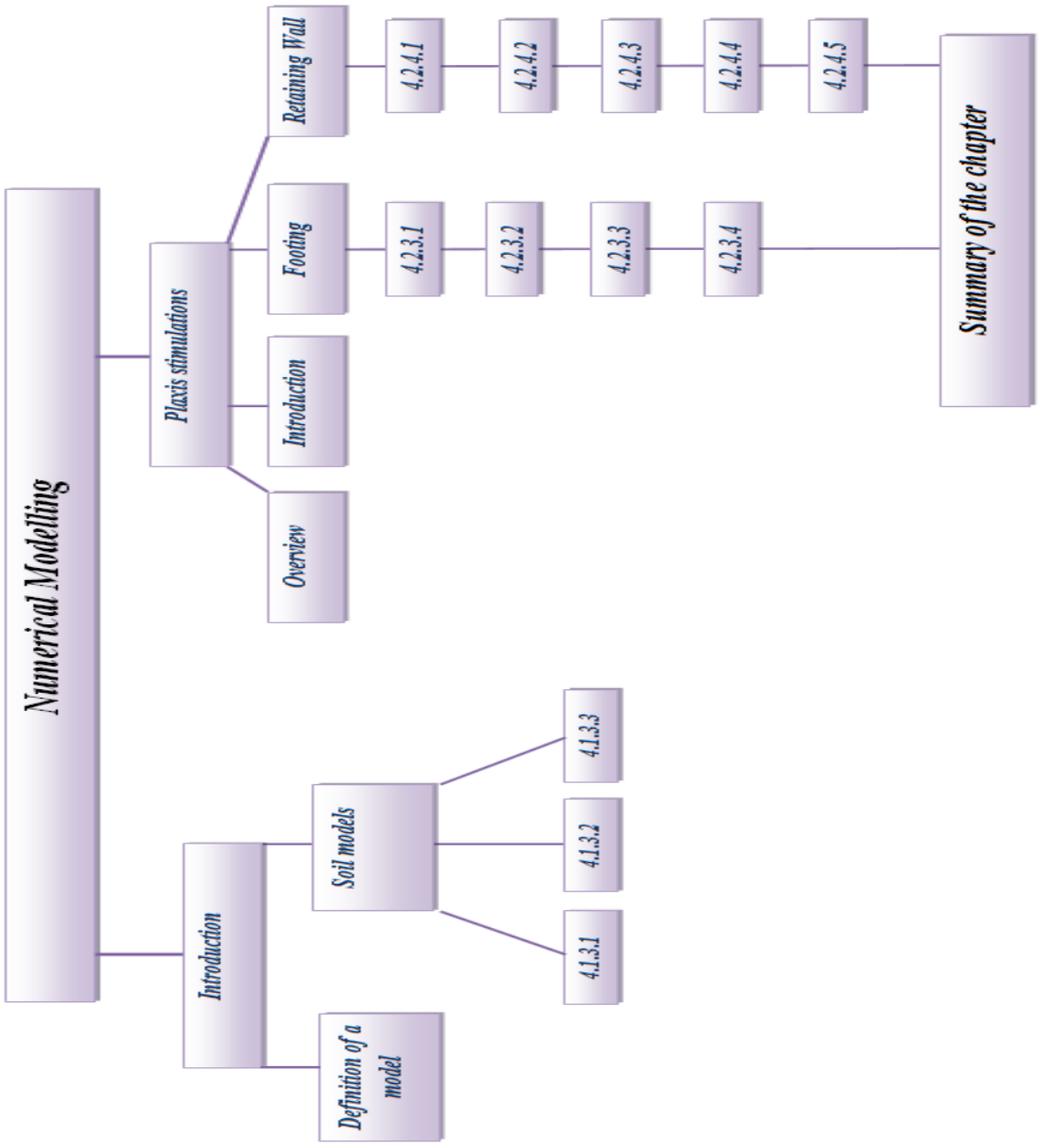

Figure 4.0: The outline of Numerical Modelling chapter

4.1.1 Background

Soil is a complicated material to study due to its nonlinear and irreversible behaviour. It exhibits a distinct behaviour from that of other materials that have been investigated in solid and fluid mechanics. Soil is a multi-phase material composed of solid particles that are in contact with each other with interparticle forces. These forces cause individual particle deformation and relative sliding between particles. The total strain of a soil mass is particularly due to the interparticle sliding that leads to the nonlinear and irreversible behaviour of soil (Lambe and Whitman, 1969).

Geotechnical engineers deal with complex geotechnical design related to soil properties, deformation, stability, seepage or groundwater that sometimes leads to solving extremely complex mathematical problems. Hence, using powerful numerical tools for analysing complex soil issues is becoming more popular among geotechnical engineers.

The finite element method (FEM) is the fundamental method of numerical modelling. This method is based on using two-dimensional or three-dimensional elements associated with nodes. Many researchers have conducted a vast variety of studies into using FEM in structural analysis, aircraft engineering, etc, including Adini& Clough, 1960; Raphael& Clough, 1965; Taylor& Brown, 1967; Turner& Clough, 1956; Wilson, 1960. This method was also used in geotechnical engineering at Berkeley (University of California) during the period 1957 to 1970. However, it was only first presented formally outside Berkeley in a published paper by Clough in 1960 (Clough & Wilson, 1999).

4.1.2 Definition of a soil model

In 1987, John Burland defined a triangle which was linked to three aspects of geotechnical engineering practice (Barbour & Krahn, 2004). He described four distinct but interconnected elements to tackle the difficulty of geotechnical problems. These three elements which form his triangle are:

- The ground profile, which is an essential outcome of site investigation;
- The ground behaviour, which includes laboratory testing and measurement;

Appropriate modelling, which is a prediction of soil response by idealising or simplifying our observations about the real condition of soil and bringing them together into a responsive soil model (Burland, 1987). Figure 4.1 illustrates the Burland Triangle.

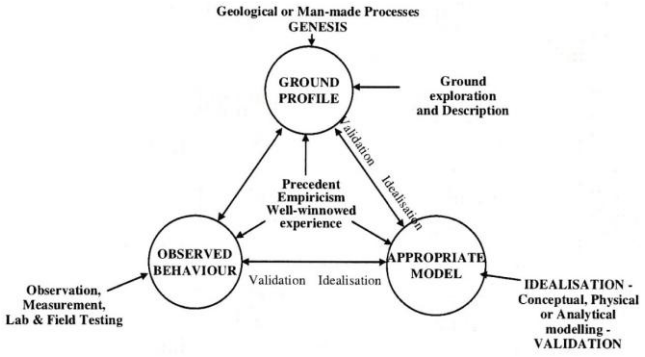

Figure 4.1: Burland Triangle (Anonymous, 1999 as cited in Barbour & Krahn, 2004)

As seen from Figure 4.1, all three aspects are linked together by experience. The process of modelling has a significant role in all geotechnical engineering projects and requires a good understanding of site investigations, soil behaviour and an appropriate conceptual model. These elements can be combined using physical or analytical models to help with prediction and

design. Burland's triangle can be defined as the process by which an appropriate numerical model can be extracted from a sophisticated physical soil condition to simplify developing an applicable mathematical abstraction. Burland's triangle is the simplest definition of modelling which is illustrated in Figure 4.2.

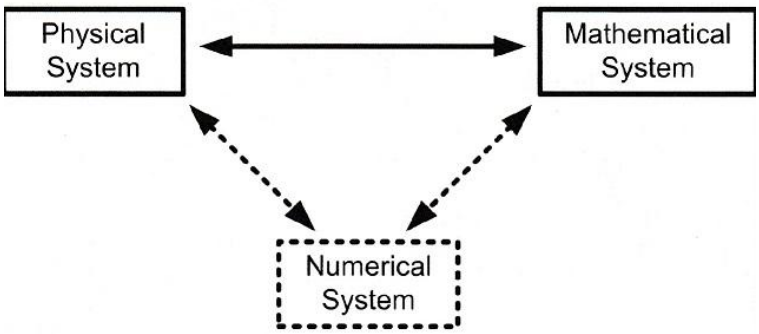

Figure 4.2: Simple definition of modelling (Barbour & Krahn, 2004)

Even though numerical software has been recognised as a tool to deal with the complexity of geotechnical problems, there are some concerns in relation to the dissimilarity between predictions and the reality, and possibly even between varied predictions. One reason is the difficulties in the proper modelling of a soil cluster in three dimensions. Another reason is uncertainty about the accuracy of laboratory test results and measured soil properties used to describe a suitable theoretical model of soil behaviour (Barbour & Krahn, 2004).

4.1.3 Soil models

Interpretation of laboratory data has become more important as a result of substantial attention to numerical modelling in recent years. Many researchers are faced with a lack of previous experience in modelling many complicated projects. Hence, the first step is defining a conceptual model of soil behaviour which gives appropriate attention to the laboratory results and gaining enough confidence to prepare accurate input data for the numerical software. Then we can move forward to the next step which is the definition of an appropriate constitutive model for using FEM in computing codes (Graham, 2006). In recent years, many constitutive soil models have been developed by geotechnical scientists to tackle the complexity of soil characteristics. These models are developed based on the relationship between stress and strain expressed by corresponding matrixes as presented in Equation 4.1.

$$\begin{Bmatrix} \sigma_x \\ \sigma_y \\ \sigma_z \\ \tau_{xz} \\ \tau_{yz} \\ \tau_{xy} \end{Bmatrix} = \begin{bmatrix} D_{11} & D_{12} & D_{13} & D_{14} & D_{15} & D_{16} \\ D_{21} & D_{22} & D_{23} & D_{24} & D_{25} & D_{26} \\ D_{31} & D_{32} & D_{33} & D_{34} & D_{35} & D_{36} \\ D_{41} & D_{42} & D_{43} & D_{44} & D_{45} & D_{46} \\ D_{51} & D_{52} & D_{53} & D_{54} & D_{55} & D_{56} \\ D_{61} & D_{62} & D_{63} & D_{64} & D_{65} & D_{66} \end{bmatrix} \begin{Bmatrix} \varepsilon_x \\ \varepsilon_y \\ \varepsilon_z \\ \gamma_{xz} \\ \gamma_{yz} \\ \gamma_{xy} \end{Bmatrix}$$

Eq. 4.1

Where:

D = the constitutive matrix of material

σ = the vector of stress state

ε = the vector of strain state

In non-linear elastic models, the material's constitutive matrix may vary by increments of stress and strain and it is not a constant value such as in linear analysis.

Using constitutive soil models in numerical software allows engineers to solve different complex geotechnical problems that traditional analysis is not capable of doing. However, the precise prediction of soil mass behaviour at a given loading system is still not possible due to the complex behaviour of soil particles and the interaction among particles. Hence, the use of an appropriate constitutive soil model plays a significant role in predicting soil behaviour in numerical modelling of soil.

In recent years, the use of advanced soil models has grown rapidly. These models are more capable to express the stress and strain relationship of soil media rather than the conventional linear elastic model. These models include, but are not limited to Drucker-Prager model, Mohr-Coulomb (MC) model, (HS) model, (HS small) model, (SSC) model, (JR) model and (MCC) model. All of these models have their advantages and drawbacks depending on the typicality of the soil application. The most serious limitation associated with more sophisticated soil models is the large number of parameters involved which cannot be collected from ordinary standard tests. Another issue is the difference between the responses of the different applied soil models. Therefore, the choice of model is related to many circumstances such as the type of analysis, the required accuracy of responses and the available soil data.

Among these models, the Mohr-Coulomb model is widely used in an extensive range of geotechnical practices due to its simplicity. This method, which was employed in this study,

and other three commonly used models are presented comprehensively in the following sections.

4.1.3.1 Linear Elastic model

This is the simplest model, and is based on Hooke's assumption that the soil stress-strain relationship is isotropic linear elasticity. Potts and Zdravkovic (1999) described this model using the following features:

- Soil behaviour is assumed to be linear, i.e. its stiffness does not change by increments of stress and strain, and it is a constant value.
- Soil behaviour is isotropic, i.e. every plane acts in a symmetric manner.
- Soil has an elastic behaviour; i.e. incremental strains are fully recovered on unloading the principal incremental stress.

The linear elastic model is an idealised behaviour which only relies on two independent parameters to represent soil behaviour. These parameters are Young's modulus (E) and Poisson's ratio (ν). Therefore, the symmetrically constitutive matrix becomes Equation 4.2.

$$[D] = [D^e] = \frac{E}{(1+\nu)(1-2\nu)} \begin{bmatrix} 1-\nu & \nu & \nu & 0 & 0 & 0 \\ & 1-\nu & \nu & 0 & 0 & 0 \\ & & 1-\nu & 0 & 0 & 0 \\ & & & \frac{1-2\nu}{2} & 0 & 0 \\ & \text{sym} & & & \frac{1-2\nu}{2} & 0 \\ & & & & & \frac{1-2\nu}{2} \end{bmatrix}$$

Eq. 4.2

In geotechnical studies, the matrix above is commonly indicated by the shear modulus (G) and bulk modulus (K) for more convenience, as shown in Equation 4.3.

$$[D^e] = \begin{bmatrix} K+\frac{4}{3}G & K-\frac{2}{3}G & K-\frac{2}{3}G & 0 & 0 & 0 \\ & K+\frac{4}{3}G & K-\frac{2}{3}G & 0 & 0 & 0 \\ & & K+\frac{4}{3}G & 0 & 0 & 0 \\ & & & G & 0 & 0 \\ & \text{sym} & & & G & 0 \\ & & & & & G \end{bmatrix}$$

Eq. 4.3

Where:

$$K=\frac{E}{3(1-2\nu)} \; ; \; G=\frac{E}{2(1+\nu)}$$ Eq. 4.4

The linear elastic model is not appropriate for soils because soils are neither linear elastic nor isotropic. However, it is a simple model which is used to obtain a good approximation to a limited scale in very specific structural conditions. These conditions may include the simulation of the bedrock layer's behaviour, or an interpretation of the behaviour of some structural elements in interaction with soil. This approximation is only valid for estimating the elastic strains associated with applied stresses within a lightly strained soil mass. The formulation of elastic behaviour based on this model is also used in some other soil models including the Mohr-Coulomb model. In this model, the soil behaviour inside the linear elastic zone is considered with additional nonlinear behaviour outside of this zone

4.1.3.2 Mohr-Coulomb model

The Mohr-Coulomb model represents a linear elastic, perfectly plastic behaviour of soil. This model is widely used for a first analysis of the soil problem. Kok et al. (2009) described Mohr-Coulomb's stress-strain behaviour in two parts. The first part shows the linear behaviour of soil and is defined by two well-known parameters from Hooke's law, Poisson's ratio (ν) and Young's modulus (E). The second part represents the failure criteria of the Mohr-Coulomb theory which is defined by two significant strength characteristics of soil. Theses parameters are the friction angle (ϕ) and cohesion (c) along with an additional parameter, the dilatancy angle (ψ). The dilatancy angle is obtained by applying the non-associated flow rule considering a permanent volume change in soil under shearing due to the plastic behaviour of soil. Figure 4.3 demonstrates the plastic perfectly elastic assumption of this model.

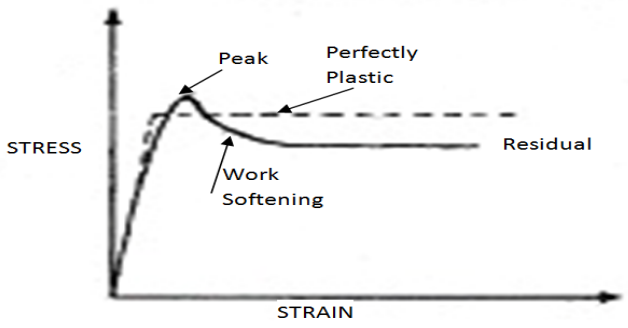

Figure 4.3: The assumed elastic-perfectly plastic behaviour of (MC) model (Kok et al., 2009)

One of the advantages of using the Mohr-Coulomb model is that it is extensible into a three-dimensional space model using only two essential characteristics of soil strength which are

generally obtained from standard laboratory tests. Figure 4.4 shows the Mohr-Coulomb model in the three-dimensional space.

Mohr's circles of stress at failure can be plotted using laboratory test results in terms of effective stresses as illustrated in Figure 4.5. The Coulomb failure criterion is ideally assumed to be a straight line which is tangent to the failure circles from several tests. This line is expressed as below (Pott & Zdravkonic, 1999):

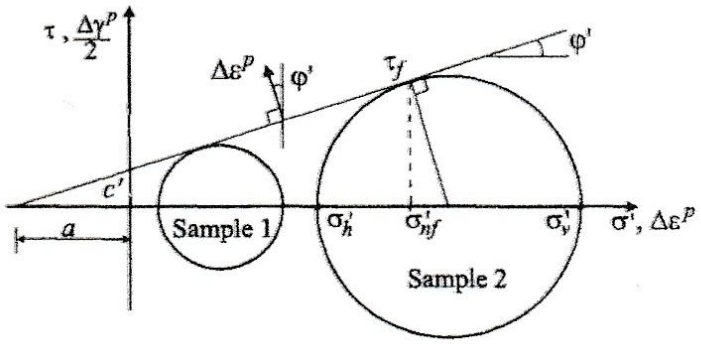

Figure 4.5: Mohr's circles of effective stress (Pott & Zdravkonic, 1999)

$$\tau_f' = c' + \sigma'_{nf} \tan \varphi' \qquad \text{Eq. 4.5}$$

Where:

τ_f' = shear stress on the plane of failure in the form of effective

σ_{nf}' = normal stress on the plane of failure in the form of effective

c' = cohesion written in the form of effective

φ' = Internal friction angle in the form of effective

Equation 4.6 can be rewritten using Mohr's circle of stress, shown in Figure 4.5, and considering that $\sigma'_1 = \sigma'_v$ and $\sigma'_3 = \sigma'_h$ (Pott and Zdravkonic, 1999).

$$\sigma'_1 - \sigma'_3 = 2\, c'\cos\varphi' + (\sigma'_1 + \sigma'_3)\sin\varphi' \qquad \text{Eq. 4.6}$$

Where σ'_1 and σ'_3 are correspondingly the major and minor principal stresses. The Mohr-Coulomb failure criterion presented in Equation 4.5 is adopted as the yield function below:

$$F(\{\sigma\}, \{k\}) = (\sigma'_1 - \sigma'_3) - 2\, c'\cos\varphi' + (\sigma'_1 + \sigma'_3)\sin\varphi' \qquad \text{Eq. 4.7}$$

The yield function of Equation 4.6 in principal stress space forms an irregular hexagonal cone as shown in Figure 4.6 with the yield surface. This cone is open in the direction of the hydrostatic compressive axis.

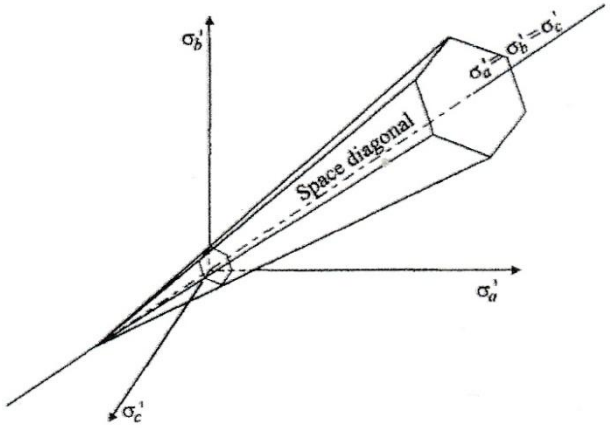

Figure 4.6: The yield surface of (MC) model in principal stress space (Pott and Zdravkonic, 1999)

Since the Mohr-Coulomb model is based on the assumption of the perfect plasticity behaviour of soil, the state parameter of yield function {k}, is required to be constant, and is not affected by the plastic strain. Furthermore, a plastic potential function is used to complete the plastic potential of the model. This feature which is defined by another additional parameter, dilatancy angle (ψ'), is expressed as below (Brinkgreve et al., 2006):

$$P(\{\sigma\}, \{m\}) = (\sigma'_1 - \sigma'_3) - (\sigma'_1 + \sigma'_3) \sin \psi' = 0 \quad \text{Eq. 4.8}$$

Where:

ψ' = the angle of dilatancy

If ψ'=ϕ', then P ({σ}, {m}) = F ({σ}, {k}) and the material has an associated flow rule.

If ψ'< ϕ' the non-associated conditions happens.

If ψ' = 0, zero plastic dilation happens (Particularly when the plastic volume strain is zero).

If ϕ' =0 and c'>0, the model becomes identical to the Tresca model in which the yield function is described as below:

$$P(\{\sigma\}, \{k\}) = (\sigma'_1 - \sigma'_3) - 2S_u = 0 \quad \text{Eq. 4.9}$$

Where:

Su is the undrained strength

The Tresca model is very similar to the (MC) model while disregarding the effect of internal friction. Therefore, the plastic volumetric strain can be predicted by defining the angle of dilation in this function (Brinkgreve et al., 2006).

In general, the use of Mohr-Coulomb model requires five parameters, of which three define the plastic behaviour of the model (c',ϕ', and ψ'). The other two parameters which control the elastic zone are the commonly used Young's modulus (E) and Poisson ratio(ν'). However, the number of parameters can be reduced to four by assuming the associated conditions ψ'=ϕ' (Pott and Zdravkonic, 1999).

The Mohr-Coulomb model is the most used model because the computations can be rapidly compared to other models, and a primary analysis of the soil behaviour can be obtained. The model only needs a maximum of five parameters which can be obtained easily from in-situ or standard laboratory tests. Also, it is appropriate enough for simulating the yielding of soil which is sometimes all that is required for an initial estimate. However, this model is not advanced enough to predict strain hardening or softening effects of the plastic behaviour of soil.

4.1.3.3 The (HS-small) model

The hardening soil model (HS-standard) was designed by Potts and Puzrin (1997) and Schanz Vermeer and Bonier (1999), in order to define a new model to decrease the void volume in soil due to plastic deformation. A stress-dependent stiffness was used to consider the dilatancy during shearing, and to develop irreversible strains while reaching a yield surface criterion. This stiffness is a significant advantage of this model compared to more simple models such as Mohr-Coulomb, the Cap model and Modified Cam Clay. The benefit is the capability of this model to predict the magnitude of soil deformation more precisely by considering three different input stiffness parameters. These parameters are secant stiffness (E50), tangent

stiffness for primary odometer loading (E_{oed}) and unloading/reloading stiffness (E_{ur}) at engineering strains ($\varepsilon \sim 10^{-3}$ to10^{-2}).They are commonly obtained from the triaxial test as shown in Figure 4.7.

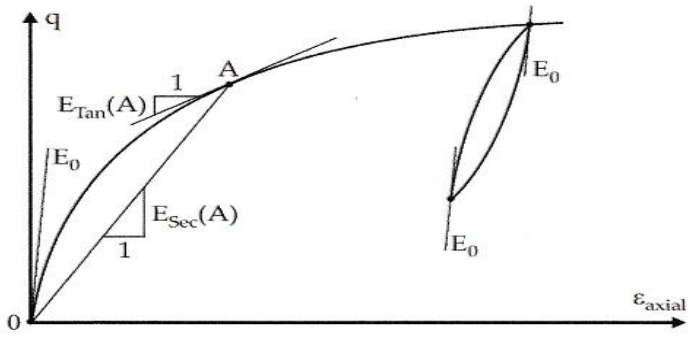

Figure 4.7: Definition of secant and tangent moduli in triaxial stress-stain space (Benz &Vermeer, 2007)

In 2006, Thomas Benz introduced a new hardening soil model with small strain based on the Hardin-Drnevich model by modification of the previous HS model. Benz's model has solved a vast range of geotechnical problems which dealt with soil behaviour under small strains (Benz and Vermeer, 2007). This new computational model overcomes the difficulty of the previous soil models in dynamic applications. The soil stiffness at very small strains is higher than engineering strains. The stiffness exhibits a non-linear behaviour by increasing the level of strains, and varies depending on the magnitude of load/stress occurring during the construction stage. Figure 4.8 shows the soil's stiffness versus log (strain) which demonstrates the stiffness reduction in a S-shaped curve. This behaviour of stiffness expresses the real nature of the soil, and its irreversible plastic deformation which depends on the history of loading. Hence, this

model can be considered to be one of the most advanced models for predicting settlement in deep excavation, or at the bottom of retaining walls and for accurate tunnelling.

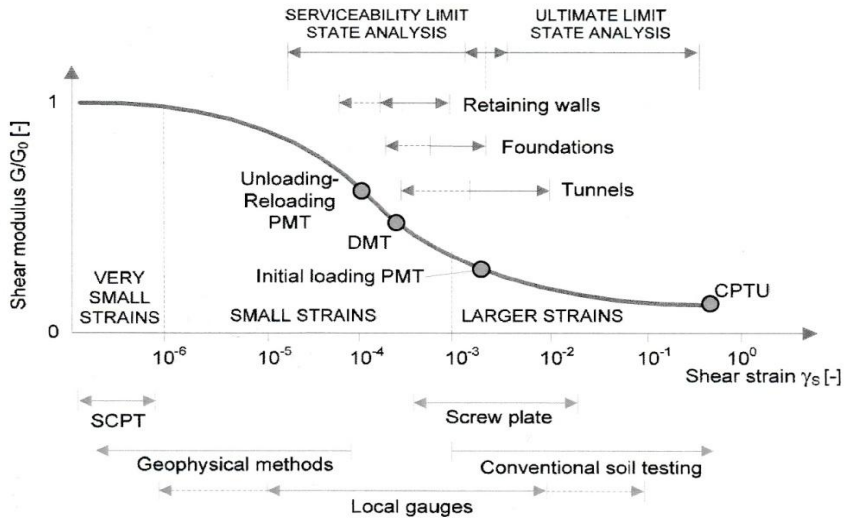

Figure 4.8: The representative definition of the variation in soil stiffness against the shear strain rates; comparison with the scale of common geotechnical problems and various soil tests according to Atkinson and Sallfors (1991), updated by Obrzud (2010), cited in Zimmermann et al. (2010)

In this model, the stiffness at very small strains and its nonlinear reliance on strain value should be used instead of the stiffness related to the strain range at the end of stage construction. The HS-small model has all the features of the HS model with two additional features which are defined as initial shear modulus (G_0) at very small strains and the shear stress amount ($\gamma_{0.7}$) at which the secant shear modulus G_s is approximatley 70% of $G_{0.}$

All other parameters including different stiffness parameters $E_{50,}$ E_{oed} and E_{ur} are the same as in the HS model as explained above. Assuming a constant Poisson ratio (ν), the small-strain Young's modulus can be determined from G_0 as follows:

$$E_0=2\ G_0\ (1+\nu) \qquad \text{Eq. 4.10}$$

Based on Hardin and Drnevich (1972), the stress-strain curves for small strains can be expressed by a simple hyperbolic law:

$$\frac{G_s}{G_0}=\frac{1}{1+\left|\frac{\gamma}{\gamma_r}\right|} \qquad \text{Eq. 4.11}$$

Where the threshold shear strain γ_r is determined as below:

$$\gamma_r=\frac{\tau_{max}}{G_0} \qquad \text{Eq. 4.12}$$

Based on Santos and Correia (2001), Equation 4.11 can be written in a different way by considering: $\gamma_r=\gamma_{0.7}$:

$$\frac{G_s}{G_0} = \frac{1}{1 + a\left|\frac{\gamma}{\gamma_{0.7}}\right|} \quad \text{where } a = 0.385$$

Eq. 4.13

When considering the simple formulation of stress-strain as:

$\tau = G_s.\gamma$

Equation 4.12 can be written as follows:

$$\tau = G_s\gamma = \frac{G_0\gamma}{1 + 0.385\frac{\gamma}{\gamma_{0.7}}}$$

Eq. 4.14

The tangent shear modulus (G_t) can be calculated from taking the derivative of equation above with respect to γ as below:

$$G_t = \frac{G_0}{\left(1 + 0.385\frac{\gamma}{\gamma_{0.7}}\right)^2}$$

Eq. 4.15

The HS-small model produces a good approximation in dynamic and reloading calculations in geotechnical problems; it shows hysteresis in cycling loading, and it tends to damp in dynamic analysis. However, it cannot assemble the strains with multiple cycling loads, nor initiate pore water pressure under undrained conditions. Also, like the HS model, it has the

limitation of lacking the void ratio dependency and kinematic hardening (Plaxis 2D manual; Benz and Vermeer, 2007).

4.2 Plaxis simulation

4.2.1 Overview

Plaxis 2D, which is a two-dimensional finite element program, was first released in 1998. It has been developed significantly in recent years to analyse deformation and stability in most geotechnical engineering projects. This program can model soil clusters using various consecutive soil models from the very simple linear-elastic model to the advanced HS-small model. The soil models can be simulated using either plane strain or axisymmetric systems. The triangular soil element can be defined as 6-node or 15-node with two degrees of freedom for each node as illustrated in Figure 4.9.

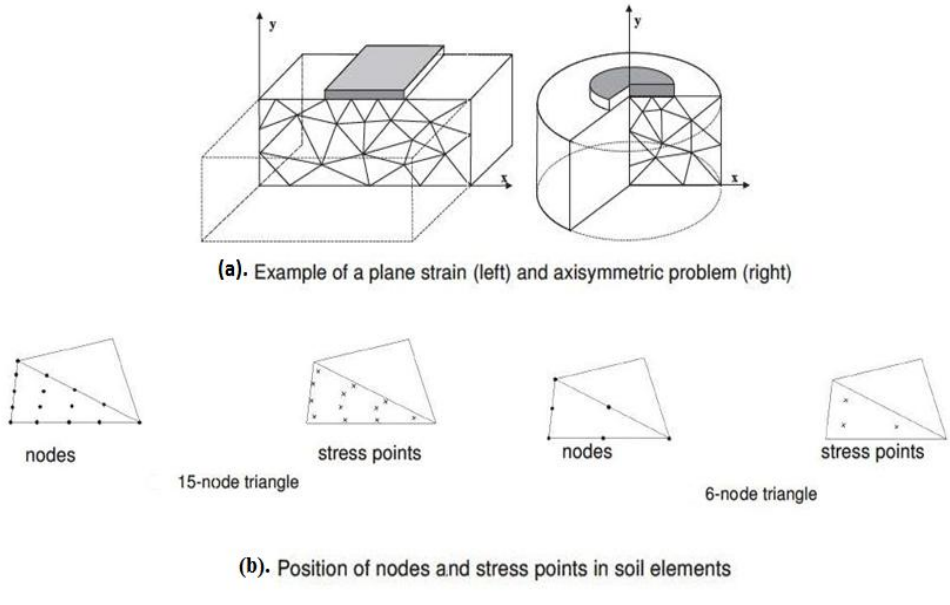

Figure 4.9: Example of a plane strain and axisymmetric system (a) 6-node and 15-node triangular elements (b) (Plaxis Reference Manual)

4.2.2 Introduction

The Plaxis 2D finite element package was employed in this study to analyse two typical geotechnical problems. One is the settlement of a footing under various loads, and the other is the seismic response of a retaining wall under earthquake loads.

These two geotechnical scenarios were modelled in this study, and the results of laboratory tests were used as the input data for some layers of conceptual geometry. The same framework was considered for both scenarios as below:

- ✓ To investigate the effect of sodium sulphate on the behaviour of soil in these models, the laboratory results obtained from the samples with and without sulphate were used. The results from the greatest changes in the friction angle value and cohesion were chosen, which were associated with the specimens with 9% sulphate after 28 days' curing time. See Table 3.13 in Chapter 3.
- ✓ Bentonite clay was considered as the top layer of the soil cluster in the Plaxis models. This soil is widely used as subgrade in Western Australia.
- ✓ The shear modulus was approximated using the average value of initial tangent of the stress-strain curves obtained from the tests on the sample under 100Kpa normal stress.
- ✓ The linear elastic-perfectly plastic Mohr-Coulomb model was used in both examples due to its simplicity, which reduces the time required for dynamic analysis, and also to avoid the need for large numbers of parameters which are necessary for using other advanced consecutive models.
- ✓ A proper boundary condition was applied at the bottom of the soil cluster to avoid any influence from the outer boundary.
- ✓ The phreatic level (water level) was considered in the lower part of both examples to prevent the need for any groundwater flow calculation in the results.
- ✓ Viscous conditions were considered for boundaries to avoid the reflection of waves on the boundaries.

4.2.3 Simulation of a footing

A concrete footing under a static load and a dynamic load was modelled. An axisymmetric analysis was employed using 15-node triangular elements due to the three-dimensional nature of the dynamic waves. The geometry of the model, the input data for the model and the comparison of the output results are presented step by step in this example.

4.2.3 .1 Geometry of the model

In this example, a footing with a length of 1 m in both directions and a height of 0.6 m was modelled. The footing is made of concrete and laid on a bentonite layer of 3 m thickness. Under the bentonite layer there is a sandy layer which continues to a significant depth. However, only 7 m of its thickness was modelled. The model was extended in a horizontal direction to a total length of 40 m to account for the fact that the soil is a semi-infinite medium in reality, as drawn in Figure 4.10.

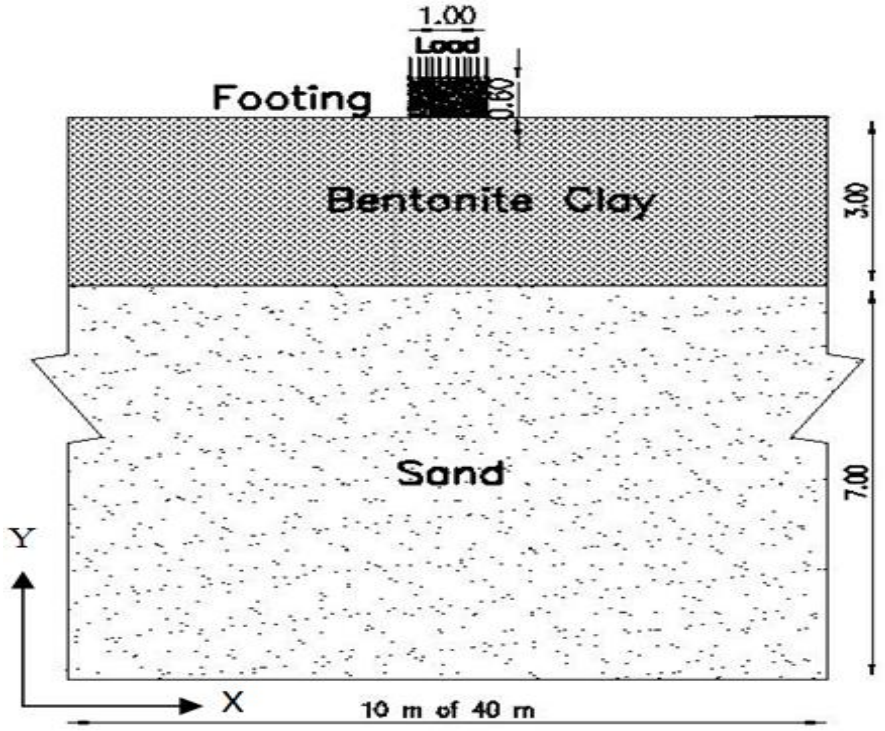

Figure 4.10: Geometry of the concrete footing on a bentonite layer

4.2.3.2 Loading input

A vibration source such as a generator was used to produce a uniform harmonic loading with a frequency of 20 Hz and amplitude of 25kN/m^2 to simulate oscillations which were transferred to the footing and to the soil layers. The vibration time was assumed to be 1.5 s and another 1.5 s was considered for the free vibration to account for physical damping due to the viscous effects. This oscillation is plotted against time in Figure 4.11.

The weight of the generator, 10kN/m^2, was applied as a distributed static load on the footing.

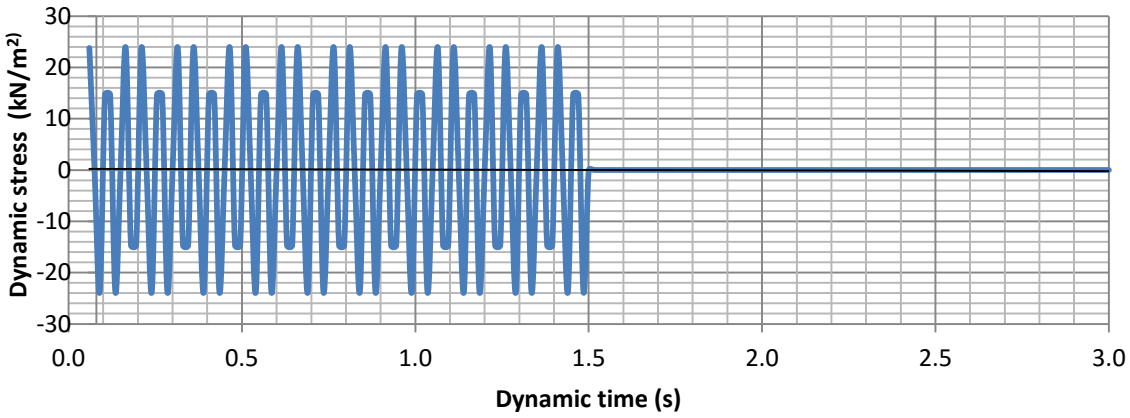

Figure 4.11: Harmonic dynamic stress versus time

4.2.3 .3 Material properties of the model

The material of footing was considered concrete with high elasticity modulus which represented a rigid structure. The behaviour of footing was assumed linear-elastic with Poisson ratio of 0.2. The material properties of the footing are presented in Table 4.1. Two separate material parameters were assigned to the geometry considering two different layers of soil, the bentonite clay layer and sand layer as seen in Tables 4.2 and 4.3. To investigate the effect of sodium sulphate in the first layer of the soil model (bentonite layer), the experimental results obtained from the untreated samples and samples with 9% sulphate after 28 days of curing were used in two separate models(for more informtion see Table 3.13 in chapter three). For the sand layer, the material properties of sand in the Plaxis manual were used for both models, and the Mohr-Coulomb model and drained conditions were used for both layers of the soil cluster.

Table 4.1 The material properties of the footing

Parameters	Term	Unit	Value
Distributed weight	W	Kn/m^2	14.11
Elasticity modulus	E	Kn/m^2	$21*10^6$
Poisson ratio	ν	_	0.2
Flexural rigidity	EI	$kN.m^2/m$	$37.8*10^4$
Normal stiffness	EA	kN/m	$12.6*10^6$

Table 4.2: The material properties of bentonite layer

Soil Sample			PB Soil	PB+9%SS Soil
Term	Parameters	Unit	Value	
Specific weight of soil under phreatic level	γ_{sat}	kN/m^3	19	19
Specific weight of soil over phreatic level	γ_{unsat}	kN/m^3	16	16
Shear modulus	G'	kN/m^2	$2.44*10^4$	$1.44*10^4$
Poisson ratio	ν'	_	0.3	0.3
Cohesion	C'_{ref}	kN/m^2	72	27.5
Angle of friction	φ'	°	14	21.76
Angle of dilatancy	ψ'	°	0	0

Table 4.3: The material properties of sand layer (Plaxis manual)

Term	Parameters	Unit	Value
Specific weight of soil under phreatic level	γ_{sat}	kN/m^3	17
Specific weight of soil over phreatic level	γ_{unsat}	kN/m^3	20
Shear modulus	G'	kN/m^2	$1.3*10^4$
Poisson ratio	ν'	_	0.3
Cohesion	C'_{ref}	kN/m^2	1
Angle of friction	φ'	°	30
Angle of dilatancy	ψ'	°	0

4.2.3.4 Results and discussion

The footing problem was modelled in three phases in Plaxis and calculations were performed under different conditions of loading in each phase. Initial stresses were calculated for all elements by considering the effect of gravity to take into account the loading history of the soil before applying any other load. The plastic calculation involved in the first phase was conducted with a fully drained behaviour to assess the long-term settlement and predict the final situation accurately. After plastic analysis in the static loading phase, both nodal displacements and strains were set to zero to avoid any impact on later calculations. To compare the results obtained from both models and analyse the effect of sulphate on the conceptual model, the results were tabulated against each other for each phase.

Lateral displacements, as well as total displacements, are presented at 20 selected nodes in the bentonite layer. All of these nodes were chosen in elements under or very close to the footing with a maximum horizontal distance of 1 m. These nodes with their vertical distance from the footing, as well as their displacements, are presented in Tables 4.4 to 4.6. Each table shows the displacements under different conditions of loading.

Table 4.4: Displacements obtained from the model with pure bentonite soil and the model with 9% sulphate-mixed bentonite under distributed static load at selected nodes

Point's coordinates	Deformation in PB soil (mm)	Deformation in PB+9% SS soil(mm)	Difference of deformations (mm)

NO	X distance from the centre of footing(cm)	Y distance from the ground (cm)	U_{X1}	U_{Y1}	U_1	U_{X2}	U_{Y2}	U_2	$\Delta u_X=\|U_{X2}\|-\|U_{X1}\|$	$\Delta u_Y=\|U_{Y2}\|-\|U_{Y1}\|$	$\Delta u=\|U_2\|-\|U_1\|$
1	-162.23	0	0.14	-1.08	1.09	0.19	-1.19	1.20	0.05	0.11	0.11
2	162.23	0	-0.15	-1.00	1.01	-0.19	-1.10	1.12	0.04	0.10	0.10
3	-78.06	0	0.08	-1.29	1.30	0.12	-1.53	1.53	0.04	0.23	0.23
4	78.06	0	-0.10	-1.25	1.25	-0.13	-1.47	1.48	0.03	0.22	0.23
5	-50.00	0	-0.01	-1.49	1.49	-0.01	-1.85	1.85	0.00	0.37	0.37
6	50.00	0	-0.01	-1.46	1.46	-0.01	-1.82	1.82	0.00	0.36	0.36
7	0	0	-0.01	-1.47	1.47	-0.01	-1.84	1.84	0.00	0.36	0.36
8	-121.60	28	0.06	-1.18	1.18	0.07	-1.34	1.34	0.01	0.16	0.16
9	149.66	28	-0.09	-1.04	1.04	-0.10	-1.15	1.15	0.01	0.11	0.11
10	-37.50	29	0.00	-1.42	1.42	0.00	-1.74	1.74	0.00	0.32	0.32
11	37.50	29	-0.01	-1.40	1.40	0.00	-1.71	1.71	-0.01	0.31	0.31
12	0.00	29	0.00	-1.43	1.43	0.00	-1.75	1.75	0.00	0.33	0.33
13	-80.97	55	0.00	-1.28	1.28	-0.01	-1.50	1.50	0.01	0.22	0.22
14	80.97	55	0.01	-1.24	1.24	0.03	-1.45	1.45	0.02	0.21	0.21
15	-25.00	59	0.00	-1.38	1.38	0.00	-1.66	1.66	0.00	0.29	0.29
16	25.00	59	0.01	-1.36	1.36	0.02	-1.64	1.64	0.01	0.28	0.28
17	0.00	59	0.00	-1.38	1.38	0.01	-1.67	1.67	0.01	0.29	0.29
18	-55.97	114	-0.01	-1.28	1.28	-0.02	-1.48	1.48	0.01	0.21	0.21
19	55.97	114	0.04	-1.24	1.24	0.07	-1.44	1.45	0.03	0.20	0.20
20	0.00	117	0.02	-1.30	1.30	0.02	-1.52	1.52	0.01	0.22	0.22

Table 4.5: Displacements obtained from the model with pure bentonite soil and the model with 9% sulphate-mixed bentonite under dynamic vibration at selected nodes

Point's coordinates			**Deformation in PB soil (mm)**			**Deformation in PB+9% SS soil(mm)**			**Difference of Deformations (mm)**		
NO	X distance from the centre of footing(cm)	Y distance from the ground (cm)	U_{X1}	U_{Y1}	U_1	U_{X2}	U_{Y2}	U_2	$\Delta u_X=\|U_{X2}\|-\|U_{X1}\|$	$\Delta u_Y=\|U_{Y2}\|-\|U_{Y1}\|$	$\Delta u=\|U_2\|-\|U_1\|$
1	-162.23	0	0.25	0.27	0.37	-0.13	0.14	0.19	-0.12	-0.13	-0.18
2	162.23	0	0.26	0.20	0.33	-0.07	0.18	0.19	-0.20	-0.02	-0.14
3	-78.06	0	-0.55	2.85	2.90	-0.12	2.36	2.36	-0.42	-0.49	-0.54
4	78.06	0	0.61	2.77	2.84	0.25	2.02	2.03	-0.37	-0.76	-0.81
5	-50.00	0	-0.03	7.52	7.52	0.03	4.75	4.75	0.01	-2.78	-2.78
6	50.00	0	-0.03	7.46	7.46	0.03	4.49	4.49	0.01	-2.98	-2.98
7	0	0	-0.03	7.49	7.49	0.03	4.62	4.62	0.01	-2.88	-2.88

8	-121.60	28	0.27	0.37	0.46	0.01	0.32	0.32	-0.25	-0.05	-0.14
9	149.66	28	0.16	0.22	0.27	-0.10	0.18	0.20	-0.06	-0.04	-0.07
10	-37.50	29	0.13	1.59	1.60	0.17	1.16	1.17	0.04	-0.44	-0.43
11	37.50	29	0.02	1.59	1.59	-0.06	1.09	1.10	0.04	-0.50	-0.50
12	0.00	29	0.07	1.51	1.51	0.05	1.04	1.04	-0.02	-0.47	-0.47
13	-80.97	55	0.25	0.39	0.46	0.11	0.3	0.33	-0.13	-0.08	-0.13
14	80.97	55	-0.14	0.30	0.34	0.06	0.32	0.32	-0.08	0.02	-0.02
15	-25.00	59	0.11	0.49	0.51	0.11	0.47	0.48	0.00	-0.02	-0.02
16	25.00	59	0.07	0.48	0.48	-0.04	0.46	0.47	-0.03	-0.01	-0.02
17	0.00	59	0.03	0.50	0.50	0.09	0.49	0.49	0.05	-0.01	-0.01
18	-55.97	114	0.14	0.33	0.35	0.15	0.25	0.29	0.01	-0.08	-0.07
19	55.97	114	0.08	0.33	0.34	-0.07	0.20	0.21	-0.01	-0.13	-0.13
20	0.00	117	0.11	0.36	0.38	0.03	0.25	0.25	-0.08	-0.11	-0.13

Table 4.6 Displacements obtained from the model with pure bentonite soil and the model with 9% sulphate-mixed bentonite under the free vibration condition at selected nodes

Point's coordinates			**Deformation in PB soil (mm)**			**Deformation in PB+9% SS soil(mm)**			**Difference of Deformations (mm)**		
NO	X distance from the centre of footing(cm)	Y distance from the ground (cm)	U_{X1}	U_{Y1}	U_1	U_{X2}	U_{Y2}	U_2	$\Delta u_X=\|U_{X2}\|-\|U_{X1}\|$	$\Delta u_Y=\|U_{Y2}\|-\|U_{Y1}\|$	$\Delta u=\|U_2\|-\|U_1\|$
1	-162.23	0	-0.02	0.36	0.36	0.19	0.32	0.37	0.16	-0.04	0.01
2	162.23	0	0.28	0.34	0.43	0.03	0.33	0.34	-0.24	-0.01	-0.10
3	-78.06	0	-0.44	2.84	2.87	-0.08	2.12	2.12	-0.36	-0.72	-0.75
4	78.06	0	0.62	2.72	2.79	0.24	1.90	1.91	-0.37	-0.82	-0.87
5	-50.00	0	0.02	7.34	7.34	0.04	4.19	4.20	0.02	-3.14	-3.14
6	50.00	0	0.62	2.72	2.79	0.62	2.72	2.79	0.58	-1.32	-1.25
7	0	0	0.02	7.30	7.30	0.04	4.12	4.12	0.02	-3.18	-3.18
8	-121.60	28	0.06	0.42	0.43	0.18	0.32	0.37	0.12	-0.10	-0.06
9	149.66	28	0.21	0.34	0.40	0.04	0.32	0.33	-0.18	-0.01	-0.07
10	-37.50	29	0.17	1.44	1.45	0.15	0.73	0.75	-0.02	-0.71	-0.71
11	37.50	29	0.08	1.43	1.43	0.04	0.74	0.74	-0.04	-0.69	-0.69
12	0.00	29	0.12	1.34	1.34	0.09	0.61	0.62	-0.03	-0.73	-0.72
13	-80.97	55	0.12	0.30	0.32	0.14	0.22	0.26	0.03	-0.08	-0.06
14	80.97	55	0.14	0.28	0.31	0.05	0.25	0.25	-0.09	-0.04	-0.06
15	-25.00	59	0.13	0.35	0.38	0.11	0.18	0.22	-0.02	-0.17	-0.16
16	25.00	59	0.13	0.35	0.37	0.08	0.20	0.21	-0.05	-0.15	-0.15
17	0.00	59	0.13	0.35	0.37	0.09	0.19	0.21	-0.04	-0.16	-0.16
18	-55.97	114	0.11	0.33	0.35	0.10	0.23	0.25	-0.01	-0.10	-0.10

19	55.97	114	0.13	0.32	0.34	0.11	0.24	0.27	-0.02	-0.08	-0.08
20	0.00	117	0.12	0.33	0.35	0.10	0.21	0.24	-0.02	-0.11	-0.11

As seen in Tables 4.4 to 4.6, the vertical displacements and consequently the total displacements at all nodes in phase one (under static loads) were slightly higher in the model with 9% sodium sulphate than those of the untreated model. Replacing the PB soil with the PB+9% SS soil increased the total displacements at selected nodes by up to 0.37 mm in the first phase. This value was obtained at a node located at the surface of the soil under the edge of the ooting (see node 5 in Table 4.4). In the first phase, the soil was only under the weight of the footing and the generator.

On the other hand, the vertical displacements and the total displacements at all nodes are slightly lower in other two phases (under dynamic loads) in the model with 9% sodium sulphate . The maximum difference between the total displacements in dynamic phases was obtained 3.18 mm at a node located at the surface of the soil and the center of footing (see node 7 in Table 4.6).

Moreover, replacing the PB soil with the PB+9% SS soil did not change the horizontal displacements significantly in the first phase to take into account, and they marginaly increased at some points and decreased at other points in dynamic phases.

The total displacements in the models with untreated bentonite and bentonite treated with 9% (SS) under various loading conditions are also illustrated in Figures 4.12 to 4.14.

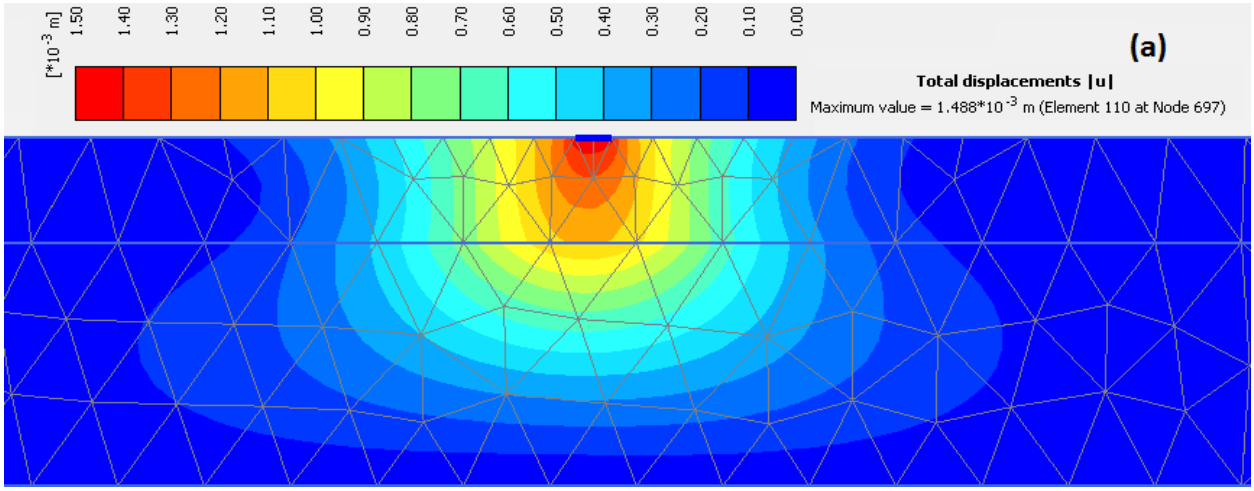

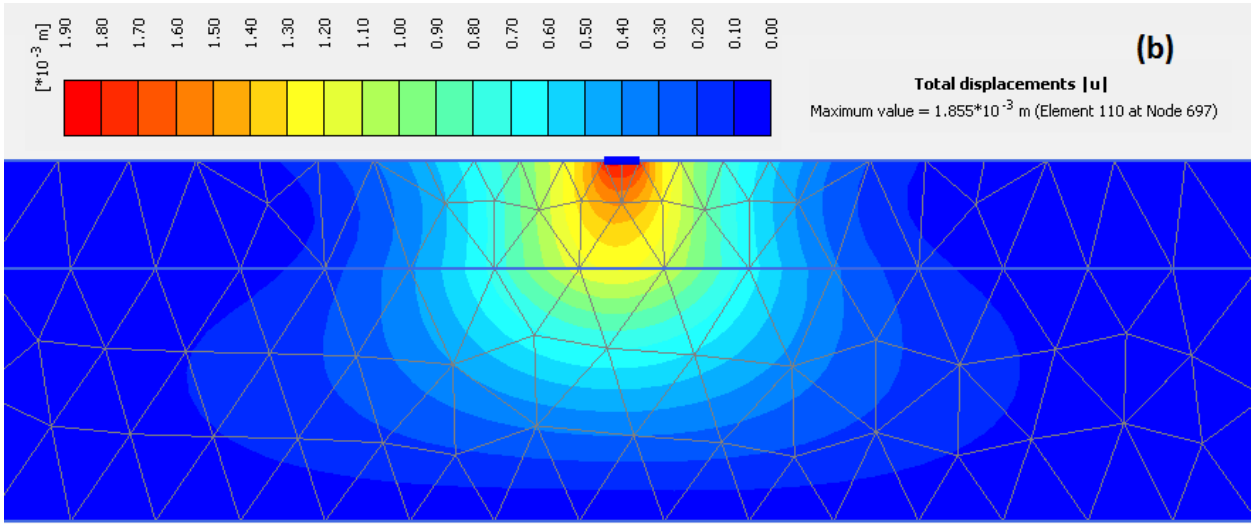

Figure 4.12: Total displacement in (a) PB soil and in (b) PB soil with 9% SS (b) in the first phase, static loading

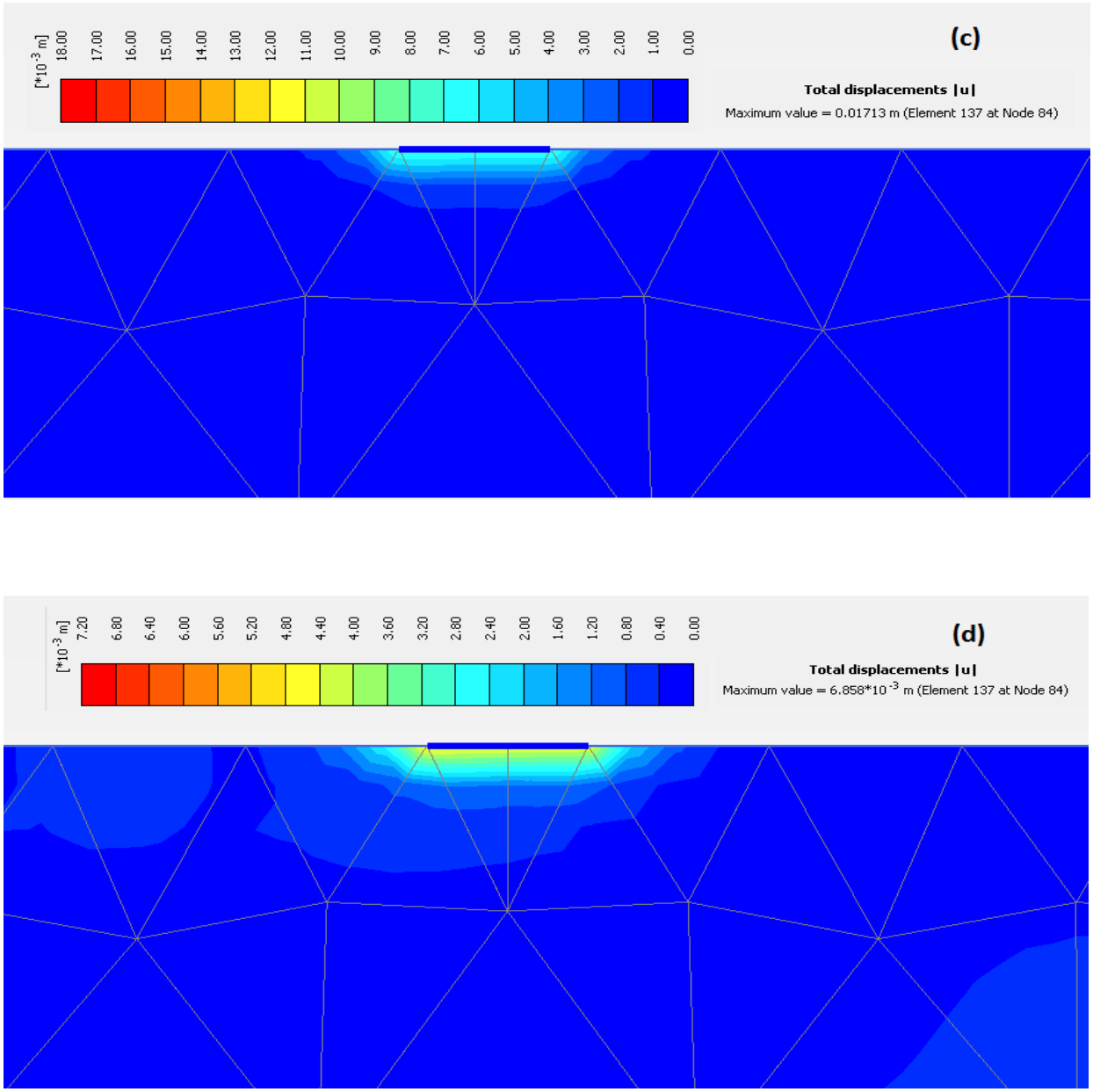

Figure 4.13: Total displacement in (c) PB soil, in (d) PB soil mixed with 9% SS in the second phase, dynamic loading

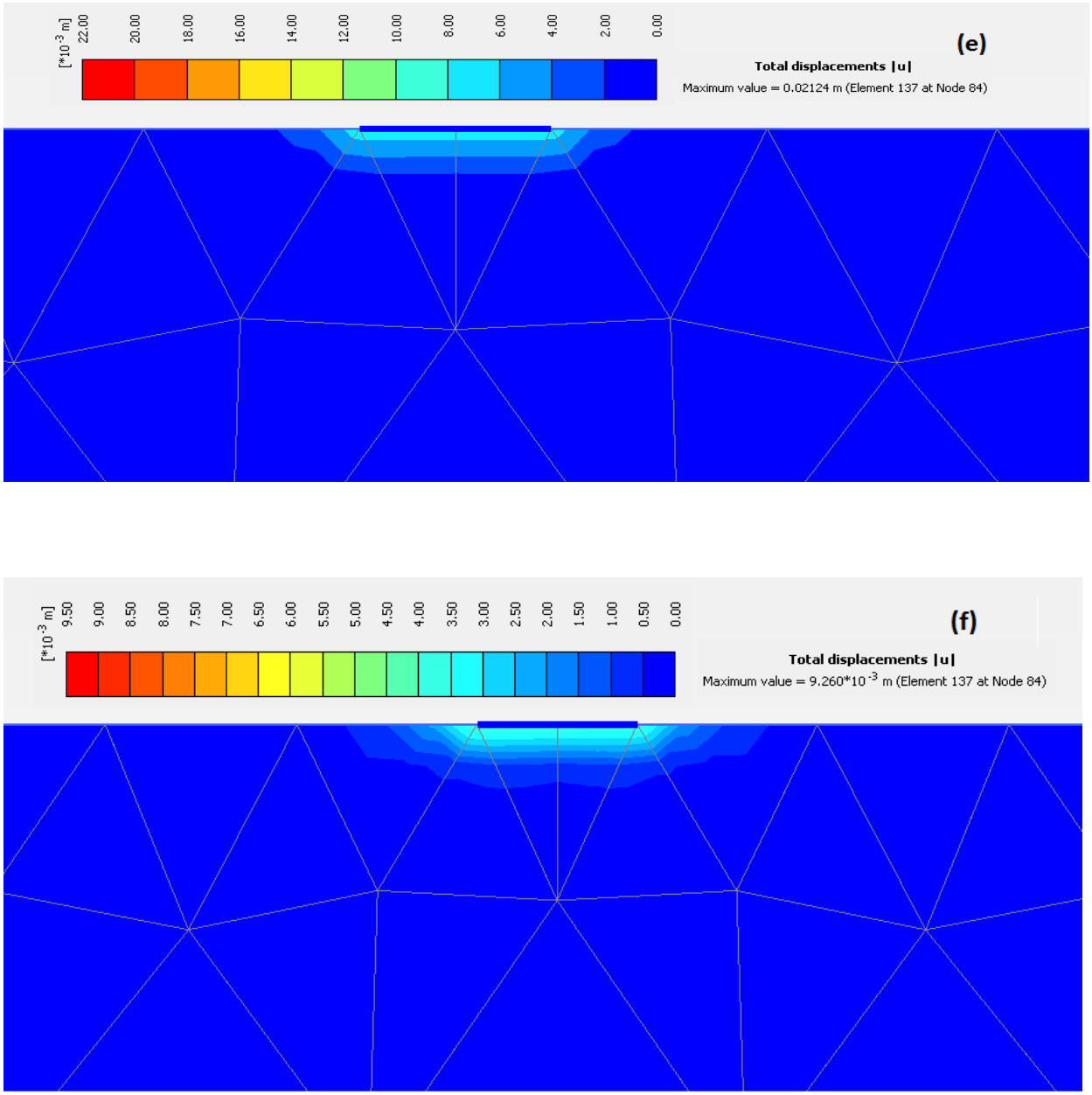

Figure 4.14: Total displacement in (e) PB soil and (f) PB soil mixed with 9% SS (d) in the third phase, free vibration

To gain a better understanding of the effect of sulphate on the soil under a vertical dynamic load, the vertical displacements of some nodes close to the footing for both models are plotted versus dynamic time in Figures 4.15 to 4.18. These figures show the vertical displacements of

these nodes under the vertical dynamic load versus the total time considered for dynamic load application and free vibration. The values of vertical displacement at some peaks are written to compare the difference of these values in both models.

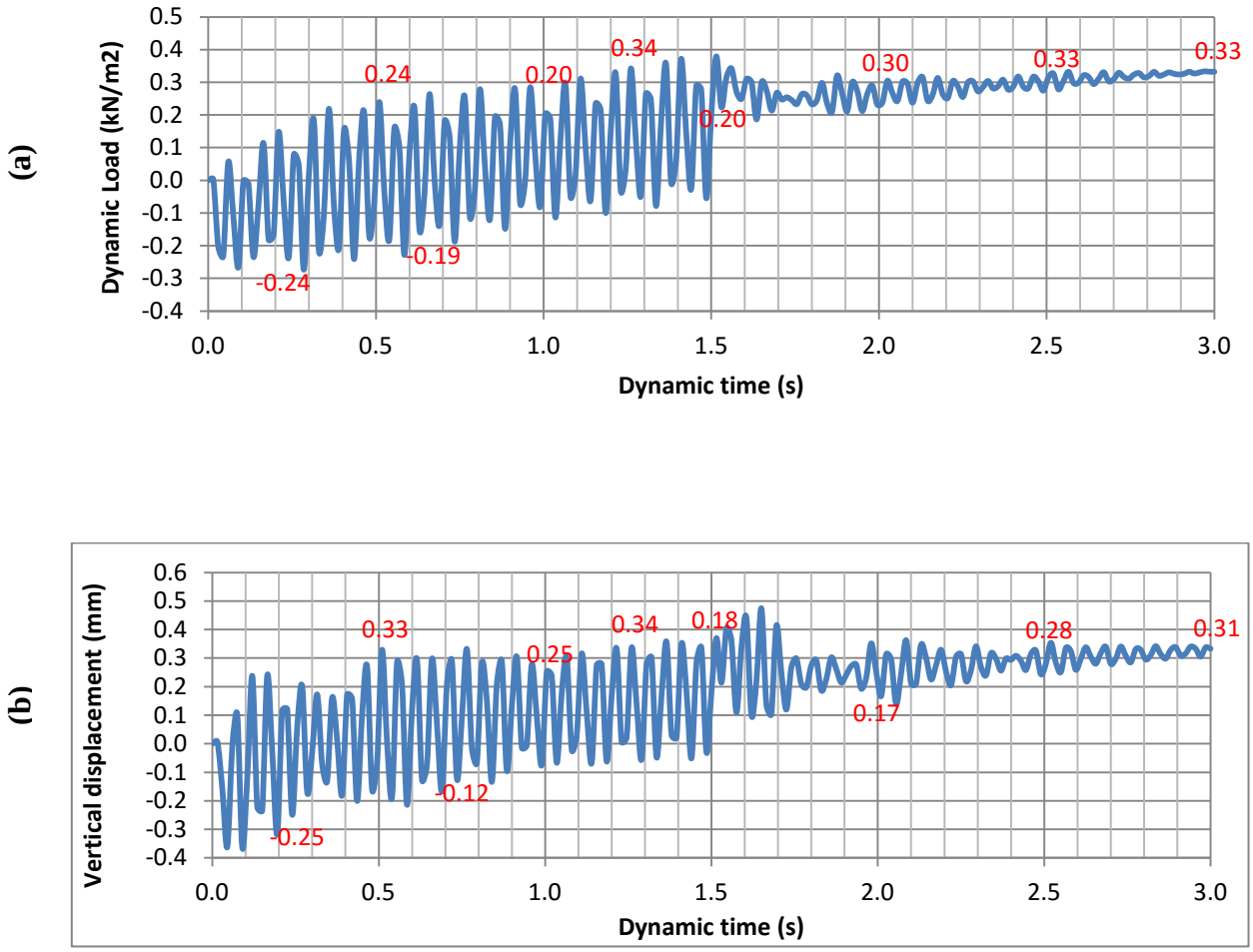

Figure 4.15: Vertical displacement at the point (X=21.62 m; Y=10 m) in (a) BP soil and (b) PB soil mixed with 9% sulphate

(c)

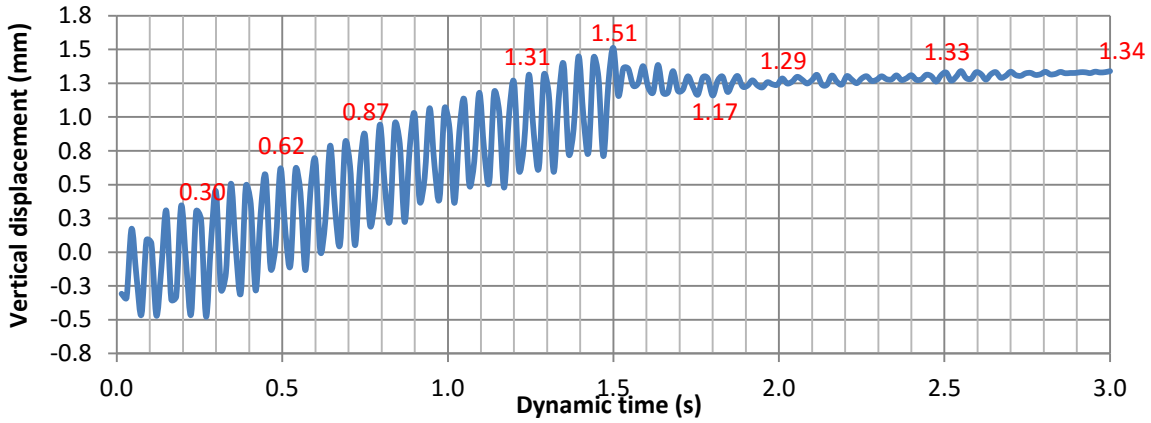

(d)

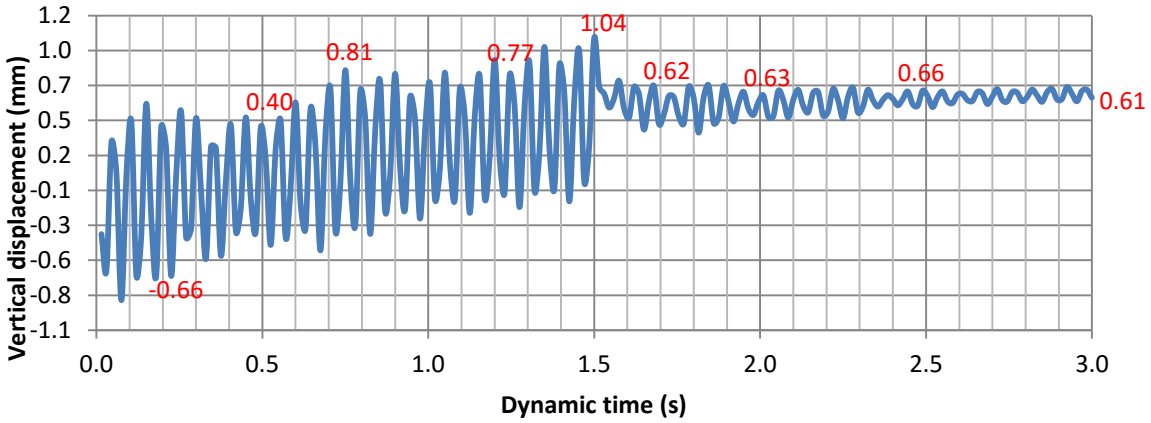

Figure 4.16: Vertical displacement at the point (X=20 m; Y=9.71 m) in (c) BP soil and (d) PB soil mixed with 9% sulphate

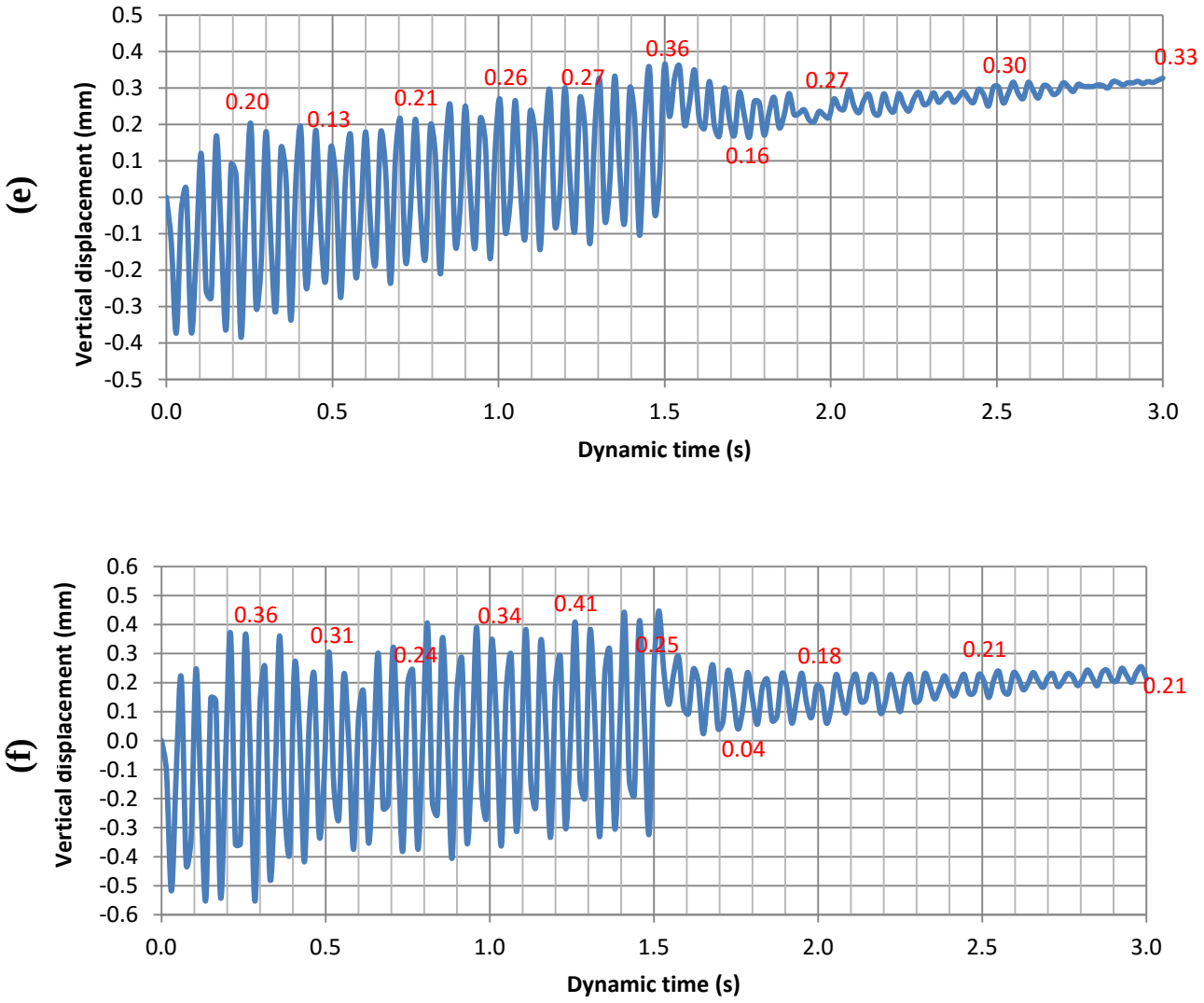

Figure 4.17: Vertical displacement at point A(X=20; Y=8.83) in (e) BP soil and (f) PB soil mixed with 9% sulphate

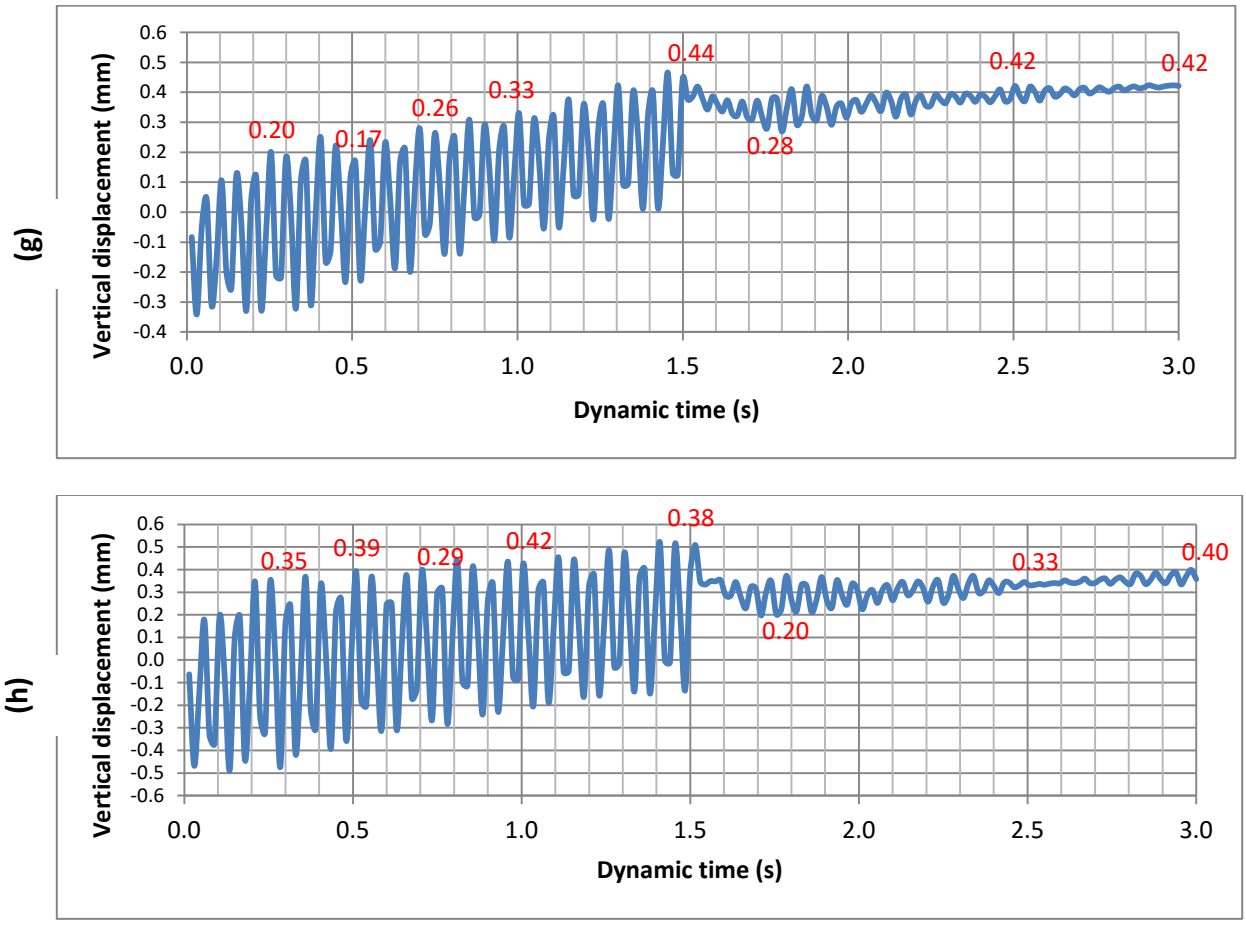

Figure 4.18: Vertical displacement at point A (X=20.94; Y=9.72) in (g) BP soil and (h) PB soil mixed with 9% sulphate

The friction and the growth of irreversible deformation in the soil create the viscosity in the soil body which causes damping in dynamic calculations. The Mohr-Coulomb model generated irreversible (plastic) strains and consequently caused damping in the footing model. The presence of geometric damping in Figures 4.15 to 4.18 is entirely clear, the waves causing oscillated displacements started to dissipate at t=1.5s (after turning the generator off). After this time, the displacement amplitude becomes much lower and the displacement curve appears with very small peak amplitudes close to zero. However, the vertical displacement still has a

non-zero value indicating the plastic behaviour of the Mohr-Coulomb model which is associated with the expansion of irreversible deformation in the soil body.

As shown in Figures 4.15 to 4.18, the values of the peak amplitudes of vertical displacement curves are written next to them at the same selected times for all curves. A thorough look at these curves shows that the amplitude of vertical displacement increased at some points and decreased at other points in the first half of dynamic time (t=0s to t=1.5s) in the model with bentonite mixed with 9% sodium sulphate compared to the model with pure bentonite. Nonetheless, they decreased slighlty in the second half (t=1.5s to t=3s), and the lower permanent vertical deformation was obtained for each point at the end of dynamic times (t=3s) in the model with 9% sulphate. These values of vertical deformation at theses plots also confirm the results presented in Tables 4.5 and 4.6, showing the lower vertical deformations for the soil with 9% Na_2SO_4 at the end of second and third pahses (under dynamic loads).

4.2.4 Simulation of a gravity retaining wall

Tiznado et al. (2011) modelled a retaining wall under seismic loads and investigated the displacement at the bottom of the wall while considering the effect of these loads on the deformable soil behind the wall. They observed that the acceleration generated by the strong seismic motions of the Chile earthquake (Ms=7.8) in March 1985 in the soil behind the wall was larger significantly than the acceleration at the wall base. Their finding was different from the typical wall movements obtained from the traditional methods. In this part of the chapter, the complicated wall problem was exemplified by modelling a similar gravity retaining wall under seismic loads on normally consolidated bentonite clay. However, instead of comparing

the acceleration values at the wall base and behind the wall, the results of the model with untreated bentonite were compared to the results for the model with bentonite mixed with 9% sodium sulphate. The same points in the base and behind the wall were chosen for both models. Due to the large size of the soil cluster and the complexity of the calculations, a two-dimensional plane-strain analysis was applied using six node triangular elements to reduce the time of calculation. To obtain more accurate results, the discretization of the continua was done before allowing Plaxis to automatically mesh the model, assigning more refined elements under and next to the wall as shown in Figure 4.19.

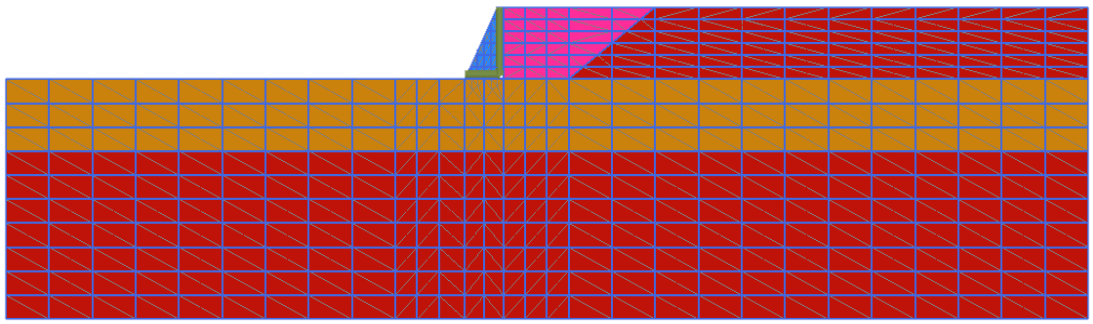

Figure 4.19: The discretization of the continua

4.2.4 .1 Geometry of the model

In this example, a gravity retaining wall was modelled with a height of 3 m, a bottom width of 1.8 m and a top width of 0.3m as illustrated in Figure 4.20(a).

Similarly to the previous example, two layers of soil were considered. The first layer was a bentonite layer of 3 m thickness underlaid by a deep sand layer, of which only 7 m of its thickness was modelled in Plaxis. This soil was simulated as the soil behind the wall as well

(backfill). A particular construction progression of the wall and backfill was simulated to obtain the initial stresses along with the weight of the cluster prior to the seismic application. After completion of the construction process, the nodal displacements were reset to zero to evaluate the effect of seismic loads independently. Standard fixities were also assigned to restrain the nodes against horizontal displacements at the lateral boundaries and both horizontal and vertical displacements at the bottom of the boundary. The model was extended in a horizontal direction to a total length of 50 m to account for the fact that the soil is a semi-infinite medium in reality, as in the previous model. Figure 4.20(b) illustrates the geometry of this model.

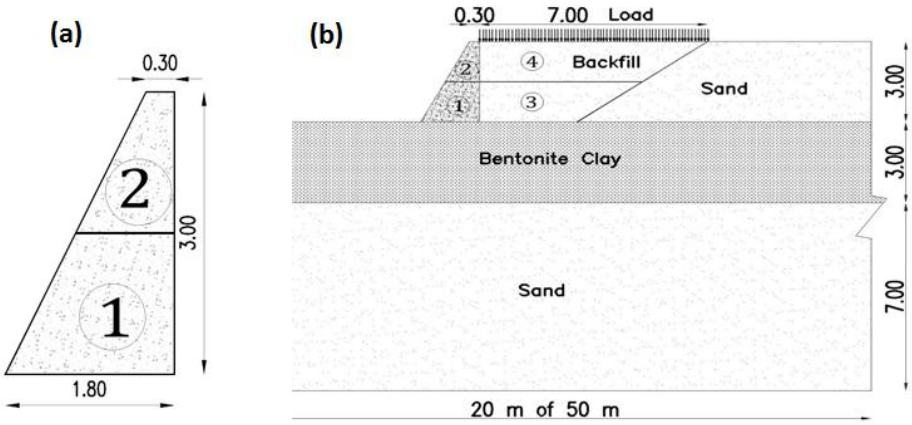

Figure 4.20: The gravity retaining wall (a); wall geometry modelled (b)

4.2.4.2 Loading input

The ongoing subduction of the Nazca Plate in the eastern Pacific Ocean under the South American Plate is mainly responsible for gigantic earthquakes occurring along the Chilean coast. One of these large earthquakes with a moment magnitude of 8.8 (Ms=8.8) took place off the coast of central Chile on February 27, 2010.The data recorded from this earthquake was

input into Plaxis for earthquake analysis of the wall model. This information was recorded at San Pedro station at 109.10 km epicentral distance. It was accessed from the United States Geological Survey (USGS) website provided by the Centre for Engineering Strong Motion Data (CESMD) by Ruben Boroschek et al. (2011) at the University of Chile. The corrected accelerogram of this earthquake is illustrated in Figure 4.21.

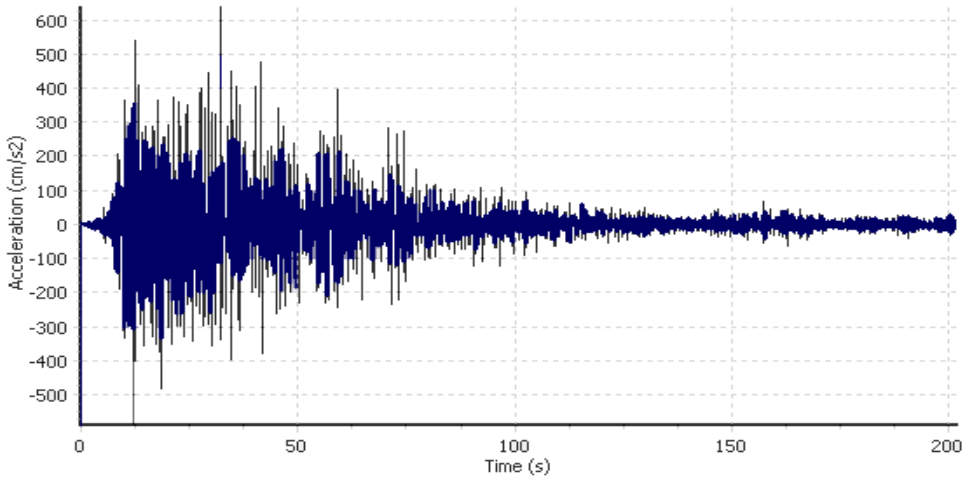

Figure 4.21: Recorded acceleration, Maule Chile (27/02/201 6:34:00 AM)

A distributed static load of 15kN/m2 was assigned on the surface of the backfill soil after completion of the construction stage.

4.2.4.3 Dynamic analysis

As mentioned above, the recorded data from the Chile earthquake was used in this study. This data was applied in the form of acceleration at the bottom boundary of the model, at the bedrock level. Viscous conditions were considered for the boundaries to avoid the reflection of bedrock motion on the boundaries. As mentioned before, the model was discretized to restrain

the height of the elements to the maximum value of the formula suggested by Kuhlemeyer and Lysmer (1973) for obtaining accuracy of the wave propagation dilemma as follows:

$$h_{max} = \frac{\lambda min}{5} = \frac{Vs}{5fmax} \qquad \text{Eq. 4.15}$$

Although material damping can be developed by all plastic models in Plaxis 2D due to irreversible plastic deformations, this damping is still not adequate to simulate the damping components of soil in reality. Hence, damping was considered in this example in the form of matrix [C]. This matrix is constituted of an allocation of mass matrix [M] and an allocation of stiffness matrix [K] as follows (Plaxis reference manual):

$$[C]=\alpha [M] +\beta [K] \qquad \text{Eq. 4.16}$$

The parameters α and β are the Rayleigh coefficients which can be obtained from the equation below:

$$\alpha+\beta\omega^2=2\omega \xi \quad \text{and} \quad \omega=2\pi f \qquad \text{Eq. 4.17}$$

Where:

ξ = the damping ratio which is a commonly used parameter for damping in engineering, known as damping ratio

ω = the angular frequency in rad/s

f = the frequency in Hz

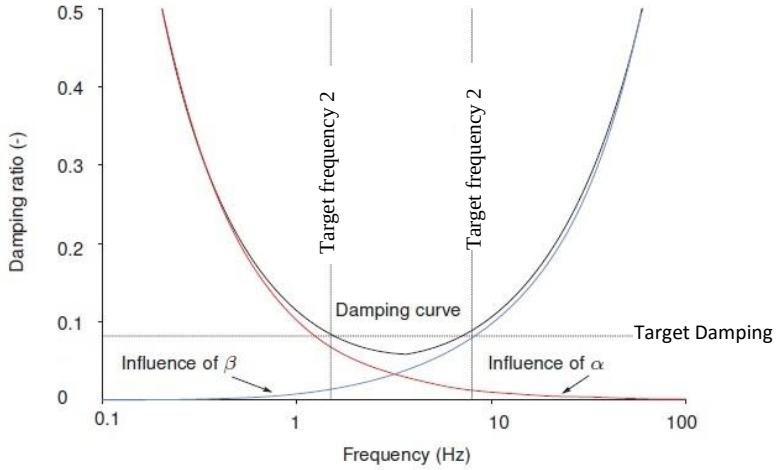

Figure 4.22: The impact of Rayleigh damping (Plaxis manual)

The parameters α and β can be obtained by solving Equation 4.17 for two distinct target frequencies and the associated target damping ratio. The effect of Rayleigh damping parameters can be seen in Figure 4.22, where the damping is less than the target damping within the range of target frequencies.

A constant viscous damping ratio of 1.5–4% is advised by Matasovic and Lanzo and Vucetic (as cited in Tiznado et al., 2011). Thus, a value of ξ=4% was taken into account in the present research.

4.2.4.4 Material properties of the model

Similar to the footing, the behaviour of wall was assumed linear-elastic with Poisson ratio of 0.2, and the wall's material was considered concrete with high elasticity modulus which

represented a rigid structure as presented in Table 4.1. Once again, two separate material parameters were assigned to the geometry considering two different layers of soil, the bentonite clay layer and sand layer as outlined in Tables 4.2 and 4.3. To investigate the effect of sodium sulphate along with the seismic loading, two bentonite clays were modelled with different percentages of sulphate for the first layer. The direct shear test results for pure bentonite Clay (PB) with no curing time and the bentonite mixed with 9% sodium sulphate (PB+9% SS) after 28 days' curing were used. The material properties for sand in the Plaxis manual were used for the sand layer and drained conditions were used for both layers to ignore the impact of pore water pressure.

Most of the literature including: Brinkgreve (1999) and Zimmermann., et. al (2010) suggested using the constitutive HS-small model to obtain more accurate results. However, the Mohr-Coulomb model was utilised in this example as well as in the previous model to ease the process of calculation. Also, the choice of soil model does not affect the conclusion where the main purpose of this thesis is to compare the results of the same model with two different percentages of sulphate.

4.2.4.5 Results and discussion

The wall problem was modelled in seven phases, after which the Plaxis calculations were performed under three different loading conditions: initial stresses (K_0 procedure), staged construction (plastic calculation) and seismic loading (dynamic calculation). After completion of the last step, the results were drawn out and compared together to investigate the difference between the results in the models with untreated bentonite and bentonite mixed with 9%

sodium sulphate. These findings are presented in two categories, under static loading and under seismic loading, which are presented in the following sections.

Figures 4.23 to 4.26 show the total displacement of the soil model in both horizontal and vertical directions under static and seismic stresses individually for bentonite model. These pictures are presented in a colour shading pattern to gain a better understanding of the displacement variation in the model. The values of displacement vary from the lowest absolute value indicated by the blue colour to the highest absolute value indicated by the red colour. These values can be positive (in the direction of the local axis) or negative (in the opposite direction of the local axis). The lateral total displacements (Ux and Uy) for both models (bentonite and bentonite with sulphate) exhibit similar colour shading. However, their values differ in almost all of the nodes in the soil cluster.

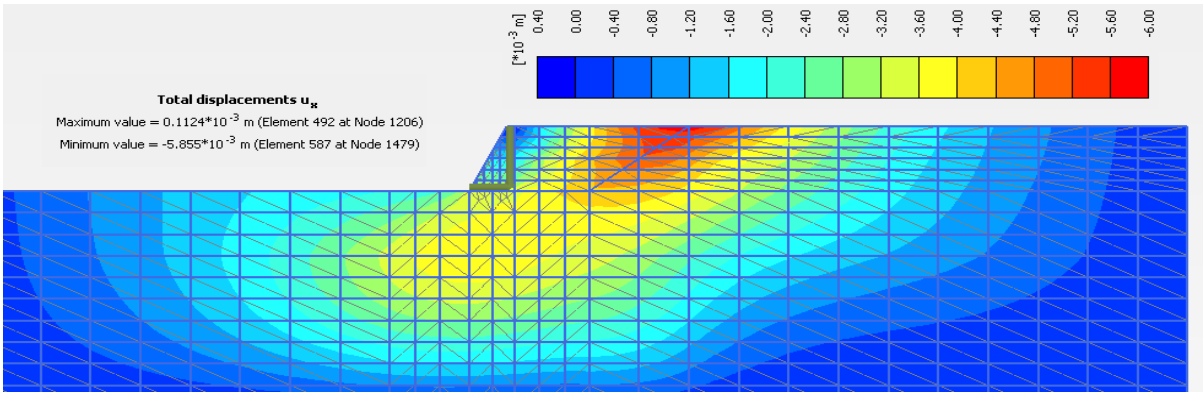

Figure 4.23: Colour shading of horizontal displacement (Ux) under the static loads in pure bentonite model

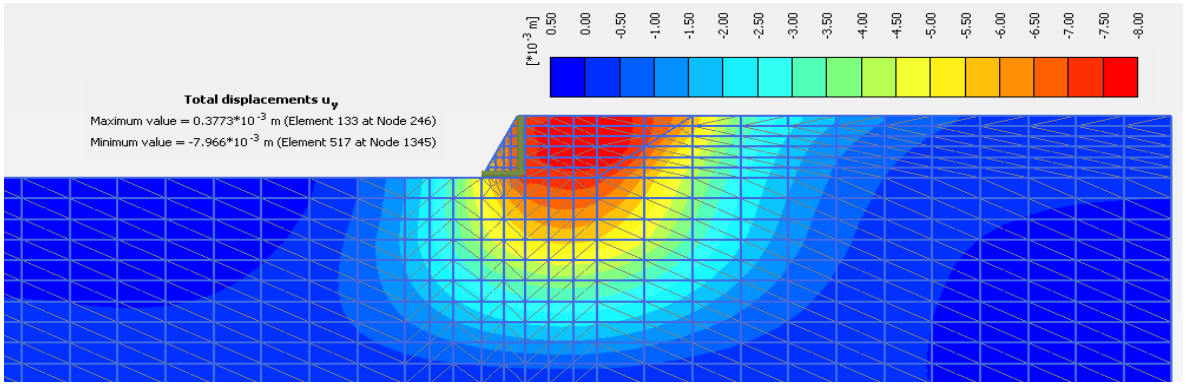

Figure 4.24: Colour shading of vertical displacement (Uy) under the static loads in pure bentonite model

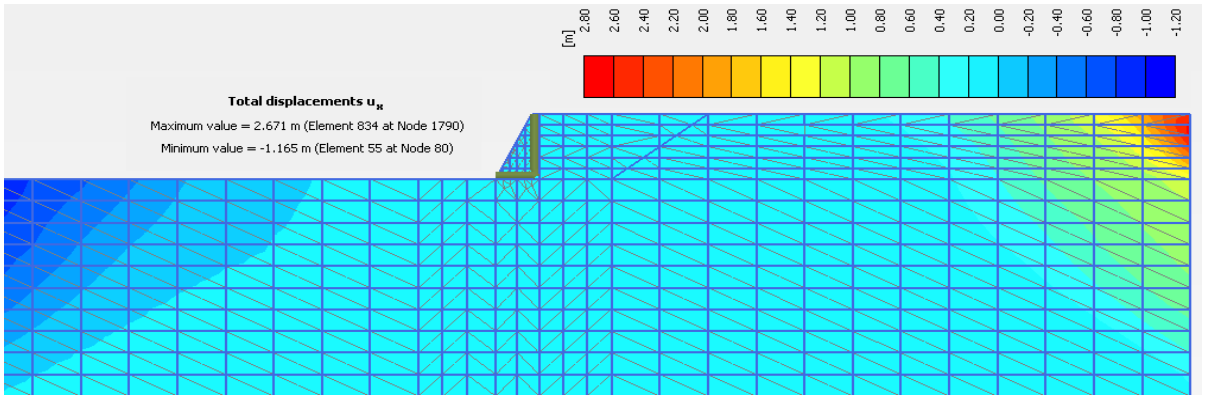

Figure 4.25: Colour shading of horizontal displacements (Ux) under seismic loads in pure bentonite model

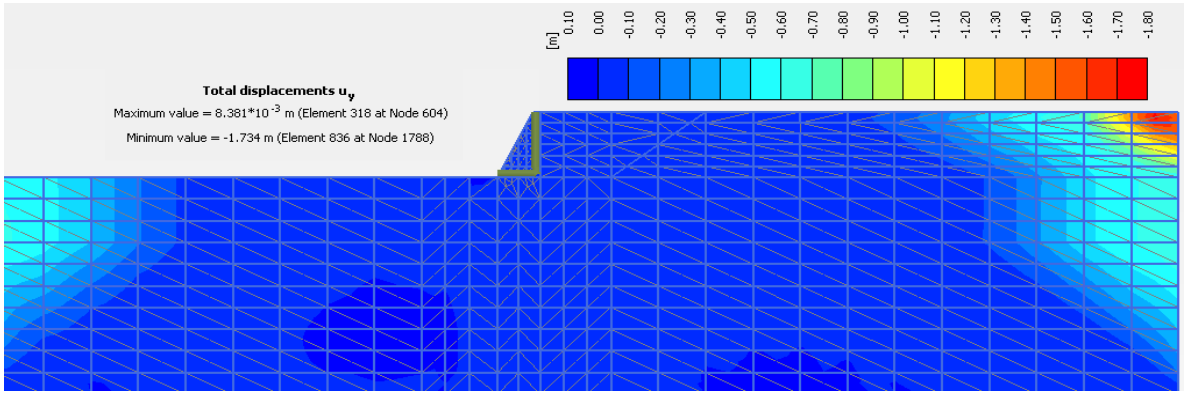

Figure 4.26: Colour shading of vertical displacements (Uy) under seismic loads in pure bentonite model

To gain a better understanding of the effect of sulphate on the deformation of bentonite, some points were selected in two critical areas: behind the wall (backfill) and at the base of the wall (subsoil).The horizontal displacements (Ux), vertical displacements (Uy) and total displacements (U) of these nodes for both models under static and seismic loads are presented in Tables 4.7 and 4.8.

With a close look at Table 4.7, it can be seen that the horizontal and vertical displacements (u_{X2} and u_{Y2}) are slightly higher in the model with 9% sulphate at all points located behind the wall (backfill) and at the bottom of the wall (subsoil) under static loads. Also, the total displacement (u) in both zones increased marginally in the model with 9% sulphate under static loads. The maximum difference between the total displacements in two models was 2.54 mm which was obtained at the surface of the soil at a horizontal distance of 1m from the back of the wall (see point 3 in Table 4.7).

Table 4.7 Total displacements at selected points in both models under static loads

Point's coordinates(backfill)			**Pure Bentonite (PB)'s deformation (mm)**			**Pure Bentonite(PB)+6%(SS) ' Deformation (mm)**			**Difference in deformations (mm)**		
No	**X distance from the back of the wall (cm)**	**Y distance from the base of the wall (cm)**	**U_{X1}**	**U_{Y1}**	**U_1**	**U_{X2}**	**U_{Y2}**	**U_2**	**$\Delta u_X=\|U_{X2}\|-\|U_{X1}\|$**	**$\Delta u_Y=\|U_{Y2}\|-\|U_{Y1}\|$**	**$\Delta u=\|U_2\|-\|U_1\|$**
1	0	300	0.11	-7.37	7.37	1.20	-9.19	9.27	1.09	1.82	1.90
2	0	200	-0.54	-7.37	7.39	-1.06	-9.19	9.25	0.51	1.82	1.86
3	100	300	-1.09	-7.42	7.50	-1.48	-9.39	10.04	0.39	1.97	2.54
4	0	125	-1.85	-7.37	7.59	-1.93	-9.19	9.39	0.08	1.82	1.80
5	0	75	-2.51	-7.37	7.78	-2.72	-9.19	9.58	0.20	1.82	1.79
6	0	-100	-3.69	-6.49	7.46	-4.23	-7.60	8.69	0.54	1.10	1.23
7	0	25	-3.09	-7.36	7.99	-3.58	-9.18	9.86	0.48	1.82	1.87
8	50	150	-2.47	-7.46	7.86	-2.63	-9.35	9.71	0.16	1.89	1.85

Point's coordinates(subsoil)			Pure Bentonite (PB)'s deformation (cm)			Pure Bentonite(PB)+6%(SS) ' Deformation (cm)			Difference in deformations		
11	-30	0	-3.38	-7.01	7.79	-4.02	-8.66	9.55	0.63	1.64	1.76
12	-105	0	-3.38	-6.14	7.01	-4.02	-7.36	8.39	0.63	1.21	1.37
13	-180	0	-3.37	-5.27	6.26	-4.01	-6.06	7.27	0.63	0.79	1.00
14	-180	-50	-3.38	-5.06	6.08	-4.00	-5.73	6.99	0.62	0.67	0.90
15	-104	-15	-3.43	-6.07	6.97	-4.07	-7.24	8.31	0.65	1.16	1.33

Table 4.8 shows the values of horizontal displacements (Ux), vertical displacements (Uy) and total displacements (U) of the selected nodes for both models under seismic loads.

Table 4.8 Total displacements at selected points in both models under seismic loads

Point's coordinates(backfill)			Pure Bentonite (PB)			Pure Bentonite(PB)+6%(SS)			Difference		
No	X distance from the back of the wall (cm)	Y distance from the base of the wall (cm)	U_{X1}	U_{Y1}	U_1	U_{X2}	U_{Y2}	U_2	$\Delta u_X=\|U_{X2}\|-\|U_{X1}\|$	$\Delta u_Y=\|U_{Y2}\|-\|U_{Y1}\|$	$\Delta u=\|U_2\|-\|U_1\|$
1	0	300	18.35	-6.88	19.60	12.13	-8.20	14.64	-6.215	1.320	-4.952
2	0	200	17.47	-6.88	18.78	10.78	-8.21	13.54	-6.694	1.321	-5.233
3	100	300	18.86	-8.01	20.49	13.03	-9.69	16.24	-5.831	1.686	-4.249
4	0	125	16.80	-6.89	18.16	9.75	-8.21	12.74	-7.054	1.321	-5.415
5	0	75	16.36	-6.89	17.75	9.06	-8.21	12.23	-7.294	1.321	-5.520
6	0	-100	14.82	-6.85	16.33	7.85	-8.22	11.36	-6.973	1.367	-4.965
7	0	25	15.91	-6.89	17.34	8.38	-8.21	11.73	-7.534	1.321	-5.609
8	50	150	17.31	-7.52	18.87	10.70	-9.03	14.00	-6.611	1.510	-4.873
Point's coordinates(subsoil)			Pure Bentonite (PB)			Pure Bentonite(PB)+6%(SS)			Difference		
9	-30	0	15.69	-6.62	17.03	8.03	-7.80	11.20	-7.654	1.178	-5.831
10	-105	0	15.69	-5.95	16.78	8.03	-6.77	10.50	-7.656	0.817	-6.275
11	-180	0	15.68	-5.28	16.54	8.01	-5.73	9.85	-7.665	0.450	-6.694
12	-180	-50	15.30	-5.61	16.30	8.32	-7.81	11.41	-6.984	2.197	-4.889
13	-104	-15	15.58	-6.00	16.70	8.49	-7.10	11.07	-7.094	1.105	-5.628

These values are recorded at the end of the assumed time for the earthquake in the dynamic phase. According to this table, the vertical displacements (u_{Y2}) in the model with 9% sulphate increased marginally in the both backfill and subsoil zones compared to the model with pure bentonite. In this model the values of (u_{Y2}) increased by up to 2.2 mm in the subsoil area at a point located under the wall (see point 12 in Table 4.8).

Nevertheless, the horizontal displacements and consequently the total displacements in this model (u_{X2} and u) in both areas exhibited lower values at the end of the seismic calculation. The maximum difference between the horizontal and total displacements in two models were obtained 7.6 mm and 6.7mm at a point located under the wall (see point 11 in Table 4.8).

The results presented in Table 4.8 do not give definite information about the displacement variations in the dynamic calculation since they only show the displacement at the end of the dynamic phase. The seismic acceleration plays the most important role in the earthquake calculations. So, to better understand the problem some points were selected randomly behind and under the wall as shown in Figure 4.27. The horizontal acceleration of these points, as well as the horizontal displacements were plotted versus dynamic time only for the model with pure bentonite in Figures 4.28 and 4.29, due to the similarity of these plots in both models.

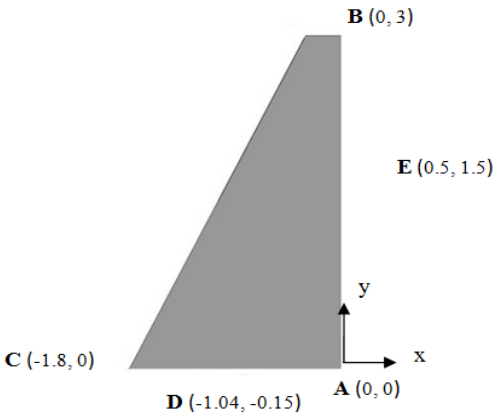

Figure 4.27: Selected point behind and under the wall

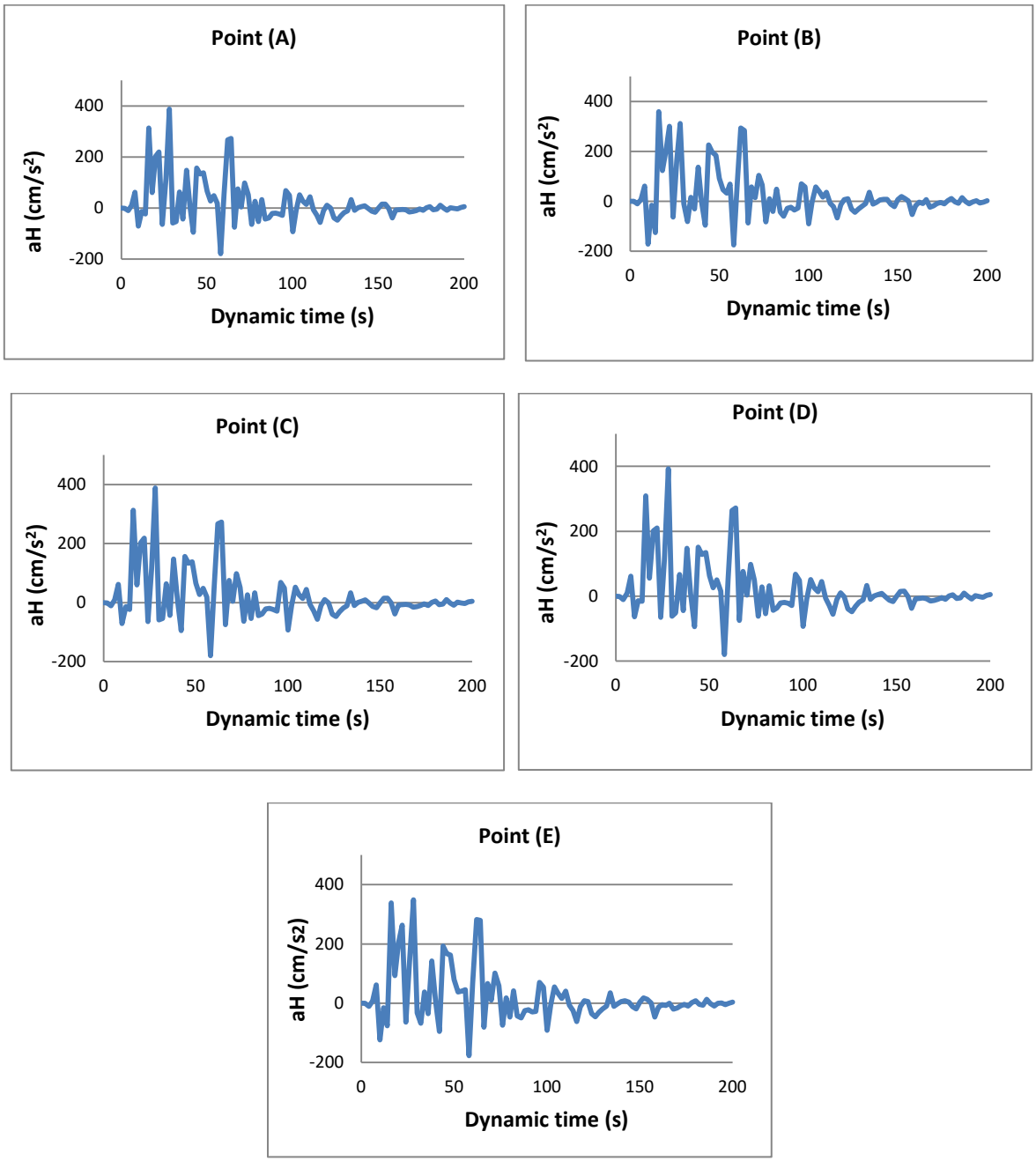

Figure 4.28: The horizontal acceleration versus dynamic time in the model with pure bentonite at points: A, B, C, D and E

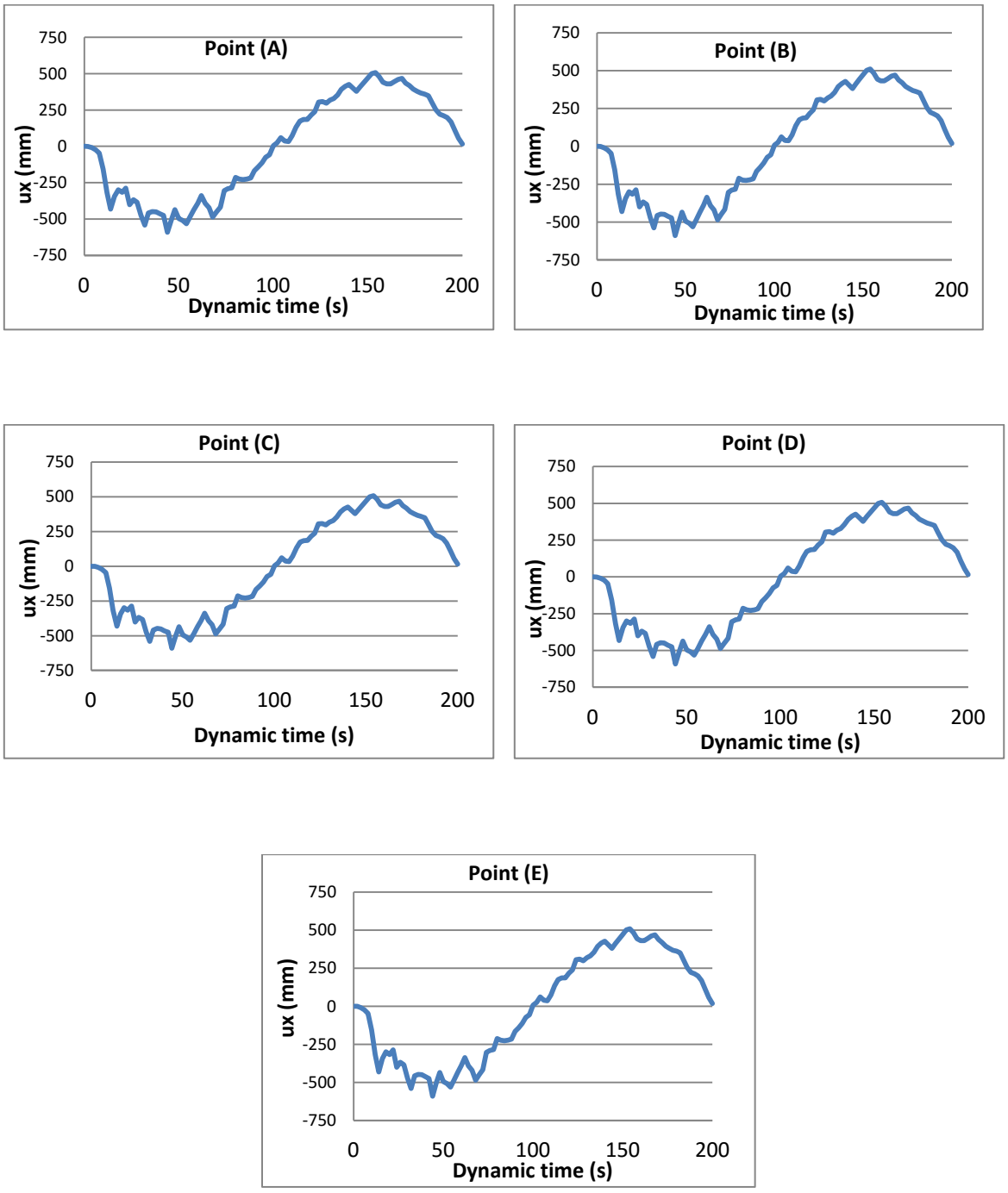

Figure 4.29: The horizontal displacement versus dynamic time in the model with pure bentonite at points: A, B, C, D and E

As seen in Figures 4.28 and 4.29, in all of the plots there is a vigorous oscillation of horizontal seismic acceleration in the first half of the dynamic loading which will be seized gradually after 100s of time. Figures 4.28 and 4.29 also reveal that, even though the bigger peaks of acceleration occurred mostly toward the positive direction of X axis in the first half of the seismic loading, the soil was deformed incrementally in the negative direction of X axis. This occurred in the second half of dynamic time as well but in the opposite direction. This incremental deformation of soil in both halves can be interpreted as the result of the irreversible strains of Mohr-Coulomb model. As mentioned above, all of the plots exhibited similar shapes in both models. However, they differ in the values of horizontal acceleration and displacement. Therefore, to compare the results of both models these values at selected peak times are presented for points A to E in Tables 4.9 to 4.13.

Table 4.9.The horizontal acceleration and displacements at point (A) in both models under seismic loads

Point (A)		**Pure Bentonite (PB)**		**Pure Bentonite(PB)+6%(SS)**		**Difference**	
No	**Dynamic Time(s)**	**a_{x1}(cm/s^2)**	**U_{x1}**	**a_{x2}(cm/s^2)**	**U_{x2}**	**$\Delta a_x=\|a_{X2}\|-\|a_{X1}\|$**	**$\Delta u_x=\|U_{X2}\|-\|U_{X1}\|$**
1	10	-71.13	-156.53	-139.89	-157.00	68.76	0.46
2	16	313.97	-344.18	350.67	-347.47	36.70	3.29
3	28	289.08	-384.16	388.13	-384.84	99.06	0.68
4	38	147.72	-450.34	175.19	-459.27	27.47	8.93
5	48	138.23	-436.03	164.28	-444.03	26.05	8.00
6	58	273.09	-392.02	293.41	-402.88	20.32	10.86
7	64	-179.47	-436.27	-190.23	-441.41	10.76	5.13
8	80	-53.35	-213.29	-63.52	-221.18	10.17	7.89
9	100	-92.48	-2.16	-103.12	4.34	10.64	2.18
10	110	44.60	73.21	39.39	65.88	-5.21	-7.33
11	126	-48.50	307.67	-47.34	300.53	-1.16	-7.14
12	134	38.06	354.31	33.25	346.72	-4.81	-7.59
13	154	14.98	507.57	14.84	499.88	-0.13	-7.69
14	166	-7.25	461.13	1.60	453.56	-5.65	-7.57
15	200	4.99	15.69	3.75	8.03	-1.24	-7.65

Table 4.10.The horizontal acceleration and displacements at point (B) in both models under seismic loads

Point (B)		Pure Bentonite (PB)		Pure Bentonite(PB)+6%(SS)		Difference	
No	**Dynamic Time(s)**	**a_{x1}(cm/s^2)**	**U_{x1}**	**a_{x2}(cm/s^2)**	**U_{x2}**	**$\Delta a_x=\|a_{X2}\|-\|a_{X1}\|$**	**$\Delta u_x=\|U_{X2}\|-\|U_{X1}\|$**
1	10	-171.55	-153.93	-300.68	-154.40	129.13	0.48
2	16	359.51	-345.07	397.37	-348.88	37.86	3.81
3	28	149.59	-382.74	311.63	-383.14	162.03	0.39
4	38	136.83	-449.11	161.75	-457.21	24.92	8.11
5	48	184.68	-435.15	230.30	-442.48	45.62	7.33
6	58	-174.34	-433.73	-185.83	-437.19	11.50	3.46
7	64	283.54	-391.08	306.44	-401.29	22.90	10.21
8	80	-40.10	-211.15	-52.60	-218.10	12.50	6.95
9	100	-90.30	7.36	-97.54	2.48	7.24	-4.89
10	110	36.71	75.83	22.72	70.03	-13.99	-5.80
11	126	-44.05	310.41	-38.97	304.72	-5.09	-5.69
12	134	43.57	356.66	36.80	350.36	-6.77	-6.30
13	154	11.53	510.22	8.00	503.98	-3.53	-6.24
14	166	6.72	463.56	4.34	457.26	-2.38	-6.29
15	200	2.71	18.35	-0.24	12.13	-2.47	-6.22

Table 4.11.The horizontal acceleration and displacements at point (C) in both models under seismic loads

Point (C)		Pure Bentonite (PB)		Pure Bentonite(PB)+6%(SS)		Difference	
No	**Dynamic Time(s)**	**a_{x1}(cm/s^2)**	**U_{x1}**	**a_{x2}(cm/s^2)**	**U_{x2}**	**$\Delta a_x=\|a_{X2}\|-\|a_{X1}\|$**	**$\Delta u_x=\|U_{X2}\|-\|U_{X1}\|$**
1	10	-70.45	-156.54	-139.15	-157.01	68.70	0.47
2	16	313.52	-344.17	350.29	-347.47	36.77	3.31
3	28	289.60	-384.16	388.52	-384.86	98.93	0.70
4	38	147.73	-450.33	175.21	-459.27	27.48	8.94
5	48	138.07	-436.02	164.10	-444.04	26.03	8.02
6	58	-179.48	-436.28	-190.23	-441.43	10.75	5.15
7	64	272.92	-392.01	293.30	-402.89	20.39	10.87
8	80	-53.37	-213.30	-64.52	-221.20	11.15	7.90
9	100	-92.48	4.33	-103.13	-2.19	10.66	-2.15
10	110	44.63	73.20	39.45	65.86	-5.17	-7.35
11	126	-48.53	307.66	-47.35	300.51	-1.19	-7.15
12	134	38.03	354.30	33.21	346.70	-4.81	-7.61
13	154	15.00	507.56	14.87	499.86	-0.13	-7.70
14	166	-7.32	461.13	1.50	453.55	-5.82	-7.58
15	200	5.00	15.68	3.76	8.01	-1.24	-7.67

Table 4.12.The horizontal acceleration and displacements at point (D) in both models under seismic loads

Point (D)		Pure Bentonite (PB)		Pure Bentonite(PB)+6%(SS)		Difference	
No	**Dynamic Time(s)**	**a_{x1}(cm/s^2)**	**U_{x1}**	**a_{x2}(cm/s^2)**	**U_{x2}**	**$\Delta a_x=\lvert a_{X2}\rvert-\lvert a_{X1}\rvert$**	**$\Delta u_x=\lvert U_{X2}\rvert-\lvert U_{X1}\rvert$**
1	10	-63.51	-156.70	-124.19	-157.10	60.67	0.40
2	16	309.19	-344.05	346.15	-346.89	36.96	2.84
3	28	299.09	-384.09	392.47	-384.30	93.37	0.21
4	38	148.03	-450.31	175.71	-458.60	27.68	8.28
5	48	134.75	-435.97	157.86	-443.33	23.11	7.36
6	58	-179.73	-436.38	-190.46	-440.99	10.73	4.60
7	64	271.55	-391.95	291.21	-402.16	19.67	10.21
8	80	-53.90	-213.36	-64.30	-220.65	10.40	7.29
9	100	-92.47	4.20	-103.43	-1.77	10.96	-2.42
10	110	45.09	73.11	40.65	66.33	-4.44	-6.78
11	126	-49.07	307.55	-47.43	300.96	-1.64	-6.58
12	134	37.50	354.23	32.88	347.21	-4.62	-7.02
13	154	15.40	507.46	15.24	500.33	-0.16	-7.13
14	166	-8.12	461.04	-0.44	454.05	-7.68	-7.00
15	200	5.15	15.58	4.05	8.49	-1.10	-7.09

Table 4.13.The horizontal acceleration and displacements at point (E) in both models under seismic loads

Point (E)		Pure Bentonite (PB)		Pure Bentonite(PB)+6%(SS)		Difference	
No	**Dynamic Time(s)**	**a_{x1}(cm/s^2)**	**U_{x1}**	**a_{x2}(cm/s^2)**	**Ux_2(cm)**	**$\Delta a_x=\lvert a_{X2}\rvert-\lvert a_{X1}\rvert$**	**$\Delta u_x=\lvert U_{X2}\rvert-\lvert U_{X1}\rvert$**
1	10	-124.13	-155.20	-224.72	-155.34	100.58	0.14
2	16	338.48	-344.60	376.36	-348.05	37.88	3.46
3	28	215.13	-383.48	348.97	-383.53	133.84	0.05
4	38	142.73	-449.50	168.94	-457.75	26.22	8.25
5	48	162.48	-435.36	198.97	-442.75	36.49	7.39
6	58	-176.76	-434.72	-187.80	-438.70	11.05	3.98
7	64	279.10	-391.33	300.77	-401.59	21.67	10.25
8	80	-46.49	-211.95	-60.09	-219.07	13.60	7.12
9	100	-91.41	6.16	-100.11	0.80	8.71	-5.37
10	110	40.42	74.81	30.45	68.57	-9.97	-6.24
11	126	-45.70	309.34	-43.55	303.25	-2.15	-6.09
12	134	40.95	355.77	35.15	349.13	-5.80	-6.63
13	154	13.18	509.19	11.25	502.55	-1.92	-6.64
14	166	10.01	462.63	15.57	456.02	-5.56	-6.61
15	200	3.79	17.31	1.67	10.70	-2.11	-6.61

As seen from Tables 4.9 to 4.13, the horizontal acceleration increased in the model with 9% sulphate at selected points at the times selected in the first half of seismic time (t=0s to t=100s),

yet it decreased slightly in the second half (t=100s to t= 200s). The increase was considerably higher at all points at earlier times (t=0s to t=28s), which relates to the larger acceleration peaks at the beginnsing of the Chilean rock motion records. The highest increase in the horizontal acceleration was 162 cm/s^2, being for point B (Figure 4.27), which was located at the top of the wall on the surface of the soil.

These tables also demonstrate that the horizontal displacement increased slightly at select points in the in the model with 9% sodium sulphate in the first half of seismic time (t=0s to t=100s), then decreased in the second half. The largest increase and decrease in the horizontal displacement was 10.8 mm and 7.7 mm more than its previous value respectively, being for point A and C, which were located at the bottom of the wall (see Figure 4.27).

It seems that the presence of sulphate had an adverse effect on the horizontal deformation of the bentonite under more violent oscillations.This effect dissipated with the dissipation of the seismic waves in the second half, and turned into a positive impact and slightly decreased the soil's horizontal deformation. These values also approve the results presented in Table 4.8, showing the lower horizontal displacements at the end of dynamic phase (under seismic loads) for the points in the model with 9% Na_2SO_4.

Figure 4.30 shows the colour shading of horizontal acceleration at the end of seismic loading for both models.

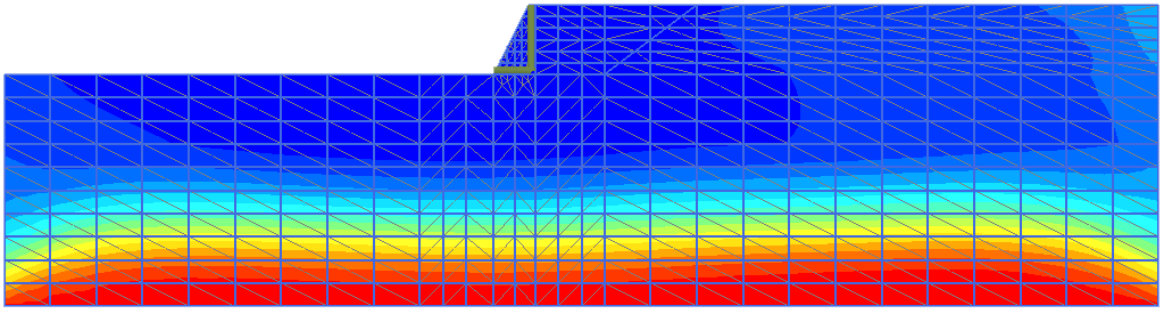

Figure 4.30: Colour shading of horizontal acceleration t the end of seismic loading phase

4.3 Summary of the chapter

4.3.1 Effect of sodium sulphate on the footing model

- Bentonite soil mixed with 9% sodium sulphate and cured for 28 days exhibited slightly higher values of vertical displacement and total displacement compared to pure bentonite soil under static loading. However, the value of theses displacements decreased marginally at end of dynamic loading (generator's oscillation) in the presence of sulphate. The difference between the total displacements in two models was up to 0.37 mm and 3.18 mm under static loading and dynamic loading respectively.

- Replacing the PB soil with the PB+9% SS soil did not change the horizontal displacements significantly under static loads to take into account. However, the horizontal displacements marginaly increased at some points and decreased at other points in dynamic phases.

4.3.2 Effect of sodium sulphate on the wall model

- In the static phase (under static loading), the horizontal and vertical displacements increased slightly in the zone behind (backfill) and under the wall (subsoil) in the model with 9% sulphate compared to those of pure bentonite model. Overall, the total displacement in the model with 9% sulphate increased by up to 2.54 mm more than its previous value in pure bentonite model. This value was obtained at a point located at the surface of the soil and behind the wall.
- In the dynamic phase (under seismic loading), the vertical displacements increased marginally in the both backfill and subsoil zones in the model with 9% sulphate compared to those of pure bentonite model. Nevertheless, the horizontal displacements and consequently the total displacements in this model in both areas exhibited lower values. In this model the values of vertical displacement increased by up to 2.2 mm in the subsoil area at a point located under the wall, and the horizontal and total displacements decreased by up to 7.6 mm and 6.7 mm respectively at a point located under the wall.
- The horizontal acceleration increased in the model with 9% sulphate in the first half of seismic time (t=0s to t=100s), while it decreased slightly in the second half (t=100s to t= 200s). The increase was considerably higher under the seismic oscillation with higher amplitudes in the first half of dynamic time (t=0s to t=28s) which relates to the larger acceleration peaks at the beginnsing of the Chilean rock motion records. The highest acceleration was recorded at the top of the wall with the amplitude being 162

cm/s^2 greater than in the pure bentonite model. This variation in the horizontal acceleration also caused a slight decrease in the values of horizontal displacements in the first half, and a following decrease in the second half in the model with 9% sulphate.

- Over all, it seems that the effect of sulphate on bentonite under seismic loading dissipated with the dissipation of the seismic waves in the second half, and turned into a positive impact and slightly decreased the soil's horizontal deformation.

Chapter 5

Summary and Conclusion

5. Summary & Conclusion

5.1 Introduction

This section contains a summary of the earlier chapters, presented in five separate subsections:

- Summary of the results of standard compaction ;
- Summary of the results of direct shear;
- Summary of the results of SEM/EDS;
- Summary of the results of numerical simulation;
- Recommendations.

5.2 Summary of the results of standard compaction

The results indicated a slight increase in the maximum dry density (MDD) of all bentonite specimens mixed with various percentages of sodium sulphate (Na_2SO_4). This increase was obtained to up to 3% for the samples mixed with 1% of this salt.

There was a slight increase in the optimum moisture content (OMC) with the addition of sodium sulphate to up to 1%. However, beyond this content (at 1.5 % and 3%), the OMC decreased considerably to up to 32% less than its initial value for the samples with 3% sulphate.

The addition of sodium sulphate in low percentages to up to 1% did not change the nature of compaction curves, and the degree of saturation at the points of MDD and OMC almost

remained at the same range as untreated samples. On the other hand, Incremental addition of salt from 1% to up to 3% not only caused flatter curves, but also the points of MDD and OMC were obtained at lower degrees of saturation compare to those of untreated specimens. Therefore, it can be concluded that the presence of this salt can lessen the quality of compaction , and a proper compation curve is less likely to be achieved with the presence of sodium sulphate beyond 1% by the dry weight of bentonite soil.

Application of 1% sodium sulphate had the greatest influence on MDD value by 3% more than its value in untreated samples, and the sample with 3% of this salt showed the lowest OMC by less than 32% than its initial value in pure bentonite specimens. Therefore, the application of 3% sodium sulphate was considered the most effective of all other quantities (0.5, 1%, 1.5% and 3%), and this percentage of the salt was used as the initial value in the direct shear tests.

5.3 Summary of the results of direct shear

The direct shear test results revealed the effect of two common factors on the value of peak stress, angle of friction and cohesion of bentonite treated with sodium sulphate. These factors were the salt content and the curing time as described below:

5.3.1 Effect of Sodium sulphate content on the peak stress of bentonite

The results revealed that the addition of any amount of sodium sulphate to bentonite led to a decrease in the peak shear stress of this soil at any given normal stress and curing time. However the rate of decrease varied with different sulphate concentrations, normal stress levels

and curing times. At a vertical pressure of 50 kPa, the addition of 3% sodium sulphate to bentonite caused the peak stress value for this soil to drop considerably. The peak stress value decreased by up to 33% after a curing time of 28 days.

Increasing the dosage of sulphate from 3% to 6% had less effect on the difference between the peak stress values than increasing the dosage from 6% to 9%. Also, the incremental addition of Na_2SO_4 from 6% to 9% was less effective than increasing the dosage from 0% to 3% at all curing times, particularly at lower normal stress levels (50 and 100 kPa). In other words, the addition of salt from 3% to 6% led to a decrease in the peak value of up to 7% at a normal stress of 50 kPa under seven days' curing time, while the addition of another 3%, bringing it from 6% to 9%, caused the peak value to drop by up to 20% in samples at a normal stress of 100 kPa after 14 days' curing time.

The addition of sodium sulphate to bentonite also had an impact on the nature of the shear stress-horizontal displacement curves. These curves exhibited a less pronounced peak stress and more gradual shape with any increment in the levels of this salt after any curing time.

5.3.2 Effect of curing time along with sodium sulphate on peak stress of bentonite

By extending the curing time from seven days to 14 days, the peak stress value mainly decreased slightly at all sulphate contents, and rarely remained constant in samples mixed with

either 6% or 9% sodium sulphate. The highest decrease was 14% for the samples with 9% sulphate under a normal stress of 100 kPa.

An increase in curing period from 14 days to 28 days caused a slight decrease in the peak stress value in most samples, which rarely remained constant in samples mixed with 3% salt. However, it sometimes increased in samples with 9% sulphate. The highest decrease of up to 5% was obtained for the samples with 6% sulphate at normal stresses of 50 and 100 kPa, and the greatest increase of peak stress was obtained up to 7% which to the samples with 9% salt at a normal stress of 200 kPa.

Extending the time of curing to 90 days for specimens with 9% sulphate caused the peak stress to retain almost the same value at normal stresses of 50 kPa, decrease by 6% at a normal stress of 100 kPa, and suddenly drop by 16% at a stress level of 200 kPa.

Increasing the curing time from 28 days to 365 days led to a decrease in the peak stress value by 13% and 5% in those specimens mixed with 3% and 6% Na_2SO_4, while those mixed with 9% Na_2SO_4 exhibited a 3% increase. This means that increasing the time of curing for longer periods such as 365 days improved the shear strength of soil mixed with higher amounts of sodium sulphate, while it had an inverse impact on the shear strength of soil mixed with less percentages of this salt.

Generally speaking, increasing the curing time mostly caused the peak shear stress of bentonite to decrease slightly or remarkably, and rarely to remain almost constant in samples with any

percentage of sulphate. Exceptionally, the peak strength value increased slightly in samples mixed with 9% sulphate for curing times from 14 days to 28 days and from 90 days to 365 days.

Also, increasing the curing time from seven days to up to 28 days in most of the samples mixed with sulphate caused flatter curves. The failure also occurred in the larger displacements. However, it appeared that beyond 28 days, increasing the time of curing and dosage of sulphate had less influence on the nature of the curves. Of all the specimens, samples cured for seven days had the steepest curves and shortest displacements.

5.3.3 Effect of sodium sulphate content along with curing time on cohesion and angle of friction of bentonite

The results showed that the addition of sodium sulphate to bentonite led to a remarkable decrease in cohesion and, by contrast, an increase in the friction angle value with any content of this salt. The addition of 3% sulphate to bentonite caused an increase the friction angle in all samples by up to 44% with a curing period of 28 days. It decreased slightly with an incremental addition of salt from 3% to 6%. With the addition of another 3% sulphate to reach a concentration of 9%, the friction angle value increased in all samples by up to 55.5% at samples with 28 days curing time.

At the same time, adding 3% sulphate to bentonite decreased the cohesion value remarkably after all curing times up to 90 days, particularly for the samples cured for 28 days. In these

samples, the cohesion value dropped by 41%. The addition of another extra 3% sulphate, bringing it to 6%, did not much alter the cohesion, but adding the final dosage of sulphate to reach a concentration of 9% caused the cohesion value to reduce considerably, especially in the samples cured for 28 days. The cohesion value for these specimens dropped to 62% less than that of bentonite.

Increasing the period of curing to 28 days caused a decrease in the cohesion value and an increase in the friction angle value for all of the samples, especially those with 9% salt after 28 days' curing time. However, extending the period of curing from 28 days to 90 days in the samples with 9% salt caused the cohesion value to increase by 25% and the friction angle to drop by 28% compared to their previous values.

Overall, the results proved that there was practically an inverse relationship between the cohesion value and the amount of sulphate and length of curing time. By contrast, there was almost a positive correlation between the friction angle value and the amount of sulphate and curing time. As an exception, increasing the dosage of sulphate additive from 3% to 6% led to a decreased friction angle value, which then increased at a dosage of 6% to 9%.

Among all of the samples, the sample mixed with 9% sulphate under a curing time of 28 days showed the lowest cohesion value and the highest friction angle value.

5.4 Summary of the results of SEM/EDS

The main factor in the shear strength of cohesive soils such as bentonite is the structure of the soil and the way that clay particles are arranged. In order to investigate the influence of sodium sulphate on the mineral structure of bentonite, SEM and EDS examinations were carried out on the shear surface of specimens to explore the changes in the surface texture of bentonite samples due to the addition of sodium sulphate. The SEM images of bentonite sample with no curing time showed a more compacted structure and flocculated particles of the surface of bentonite in the absence of salt. This structure is associated with the characteristics of a clay soil system in which the charged clay particles tend to clump together and create a flocculated and cemented structure.

The SEM images of specimens with 3% sodium sulphate at all curing times were similar to those of a bentonite sample, however the clay particles appeared platy occasionally on the shear surface of these specimens. The presence of platy particles on the shear surface was much more noticeable in the samples treated with 9% sulphate. There was a marked difference between the shear surfaces of the samples mixed with 9% sulphate and the pure bentonite sample. The scanning electron images of these samples illustrated a platy and flaky nature. The degree of flakiness was higher in those samples that had undergone a longer curing time (14 days and 28 days). This flaky structure was due to increments in the Na_2SO_4 content, resulting in an increase in the amount of Na+ cations. The increase in the Na^+ concentration in the pore water influences the interparticle forces between clay particles. These changes in the environment of deposition alters the way the clay particles are arranged, and causes the clay particles to become arranged in a parallel orientation and look platy.

The formation of some crystals was also observed occasionally on the surfaces of all specimens. The distribution of these crystals was more noticeable on the surface of specimens with 6% salt

with a longer curing time (14 days and 28 days). These crystals were expected to be the white crystalline mineral of sodium sulphate known as thenardite (Na_2SO_4) which usually forms at the top of the soil profile as it dries during the evaporation process. Longer curing times can lead to greater growth of these crystals.

EDS analysis also confirmed the presence of sodium sulphate (Na_2SO_4) components in the shear surface of all specimens treated with sodium sulphate, showing a higher concentration of sodium (Na) and sulphur (S) in the spectrum line results. A slight increase in the concentration of these elements was observed with the incremental addition of this salt.

Based on the SEM and EDS results and the results presented in Chapter 3 of this dissertation, and in the previously reviewed literature including Gratchev and Sassa (2009), Ruhl and Daniel (1997), D'Appolonia (1980) and Kashir and Yanf (2001), one hypothesis is that increasing the concentration of Na_2SO_4 results in an increase in the amount of Na^+ cations. These cations participate in cation exchange with clay particles leading to a reduction in the thickness of the diffuse double layer in bentonite clay. This results in the aggregation of clay particles and consequently a more open clay structure, decreasing the adhesion between the clay atoms and leading to a reduction in cohesion, and consequently the shear strength of the soil. The results obtained from the direct shear tests also confirmed this conclusion by showing a reduction in the cohesion and shear strength of all bentonite samples treated with this salt for curing times of up to 28 days The behaviour of the soil was more complicated for the longer periods of curing times such as 90 days and 365 days with the addition of sulphate salt. This can be due to developing more reactions between the clay particles and sulphate anions by time. The better

explanation will be obtained by the use of better method of observing rather than SEM such as XRD.

Another hypothesis is that the growth of sulphate crystals between clay particles leads to weakening of the interparticle bonds between clay particles, and consequently decreasing the shear strength of bentonite.

Overall, further studies are required into the microstructure in order to gain a better understanding of the cation and anion exchange mechanism, and the effect of curing time as well as other factors which can influence these reactions.

5.5 Summary of the results of numerical simulation

The numerical simulation presented in Chapter 4 was subdivided into two main models, a footing model and a retaining wall model. Within each model, two soil clusters were also modelled: one with pure bentonite and the other with bentonite mixed with 9% sodium sulphate after a curing time of 28 days. The laboratory results obtained from these soil samples were assigned to each corresponding model. The results are summarised below.

5.5.1 Effect of sodium sulphate on the footing model

The presence of 9% sodium sulphate in bentonite led to slightly larger values for vertical and consequently the total deformations under static loading. However, the values of these displacements were lower in this model under dynamic loading (generator vibration). The latter

out come was also observed in the vertical displacement versus dynamic time plots. As discussed in section 4.2.3.4 of chapter 4, the amplitude of vertical displacement increased at some points and decreased at other points in the first half of dynamic loadin (t=0s to t=1.5s) in the model with 9% sulphate. However, they decreased at the second half (t=1.5s to t= 3s), and the lower permanent vertical deformation was obtained at the end of dynamic times (t=3s) for each point in the model with 9% sulphate.

In other words, replacing PB soil with PB+9% SS soil had an adverse impact on the vertical and total displacements of soil under static loads, and postive effect under dynamic loads. The results showed that the maximum difference between the total displacements in the two models under the dynamic loads was 3.18 mm and under static loading was 0.37 mm at the surface of the soil. The largest difference between the displacements in the two models occurred at the points under the footing and closer to its centre or edges in both static and dynamic loading.

Moreover, addition of 9% Na_2SO_4 to pure bentonite did not have a significan impact on the horizontal displacements under static loads to take into account, and it marginaly increased the horizontal displacements at some points and decreased at other points in dynamic phases.

5.5.2 Effect of sodium sulphate on the wall model

The results illustrated that in the static loading phase, with the addition of 9% sodium sulphate to bentonite, the horizontal and vertical displacements increased slightly in the zones behind (backfill) and under (subsoil) the wall. Overall, the total displacement increased by up to 2.54 mm more than its value in pure bentonite model at a point located at the surface of the soil and behind the wall.

The dynamic displacements were obtained at the end of dynamic time (the assumed time for seismic loading). These results illustrated that the vertical displacements in the model with 9% sulphate increased in both zones by up to 2.2 mm at a point located in the subsoil area. The horizontal displacements and consequently the total displacements in this model exhibited rather lower values in both areas. The maximum differences between the values of horizontal and total displacements for both models were obtained 7.6 mm and 6.7 mm respectively at a point located under the wall.

Moreover, the results obtained from the horizontal acceleration of some selected points under and behind the wall versus dynamic time proved that the horizontal acceleration increased in the first half of seismic time (t=0s to t=100s) in the model with 9% sulphate, while it decreased slightly in the second half (t=100s to t= 200s). The higher values were observed at the times from 0s to 28s which relates to the larger acceleration peaks at the beginnsing of the Chilean rock motion records. The highest acceleration was recorded at the top of the wall with the amplitude being 162 cm/s^2 greater than in the pure bentonite model. This variation in the horizontal acceleration also caused a slight decrease in the values of horizontal displacements in the first half, and a following decrease in the second half in the model with 9% sulphate.

Consequently, the model with 9% sulphate exhibited the lower values for horizontal displacements at the end of time considered for seismic loading. It seemed that the presence of sulphate had an adverse effect on the horizontal deformation of the bentonite under more violent oscillations.This effect dissipated with the dissipation of the seismic waves in the second half, and turned into a positive impact and slightly decreased the soil's horizontal deformation.

Generaly speaking, it seems that replacing PB soil with PB+9% SS soil caused changes in the values of deformations under both static and dynamic loading in both footing and wall model. In both models, the presence of sulphate mostly had an adverse impact on the displacements of bentonite when the soil was under static loads or under dynamic loads with large peak amplitudes such as the beginning of an earthquake or when a generator is working. By contrast, it had a positive influence on the soil's deformation when the soil was under dynamic oscillation with small peak amplitudes such as dissipating the seismic osclillation by time or when a generator turns off and causes free vibration.

Over all, the maximum difference between displacements in footing model with and without sulphate was less than 4 mm, and for the wall model was less than 8 mm . These values seem very minor comared to the large sclae of both models. Therfore, it can be concluded that the presence of sodium sulphate in bentonite clay in both models did not have a significant impact on the values of soil's deformations under various conditions of loading (under static , dynamic and seismic loads).

5.6 Recommendations

In this study, an attempt was made to shed light on the effect of sodium sulphate on a clay soil covering three main areas: experimental, microanalytical and numerical. However, further comprehensive investigations into the effect of chemicals on soil in each of these areas are required due to the complexity of clay behaviour. The following list addresses the work still to be done in these three categories:

- ***Experimental approach***

This research recommends consideration the effect of some other aspects on the strength characteristics of bentonite clay including the temperatures and the applied effort in compaction test, in further studies. The earlier plays a main role in chemical interactions between salt and clay particles, and the latter has a crucial impact on the mechanical peroperties of soil. Also, the mixture of this salt with some other salts such as chlorides and carbonates can be considered in the furthure research.

- ***Microanalytical approach***

It is important to note that the SEM and EDS processes, the samples with the smooth surfaces were not used in this study. The specimens were collected from the direct shear device, and the SEM and EDS analysis were performed on the shear surfaces of the samples. Therefore, the EDS results (the line spectra) were just used for a qualitative measurement of the element of the surface of shear of the samples. In addition, although SEM imaging revealed the changes of the structure of the surface of the soil samples, further microanalytical observation such as x-ray diffraction (XRD) is required to explore interactions between sodium sulphate salt and the clay particles. This method is a powerfull tool to identify the changes in the crystalline soil minerals based on their unique atomic and molecular structure.

- ***Numerical approach***

  There is a lack of information in relation to determining the effect of chemicals on soils by computer modelling. Although, many experimental studies have been conducted on the impact of some chemicals on soil properties, or on the numerical modelling of complex geotechnical problems, there is yet to be a combined approach using both methods.

  In this research, the simple Mohr-Coulomb model was used in both footing and wall models for an initial estimate of the soil's behaviour under the influence of salt. Therefore, this research suggests consideration a more advanced constitutive model for the stimulation of soil behaviour in order to obtain more accurate results particularly for the application of dynamic loads in the further studies. Also, the use of triaxial tests is recommended rather than simple direct shear tests to obtain the most of the soil parameters which are involved in the use of more advanced soil models in numerical modelling.

References

219 References

References

Abood, T. T., Kasa, A. B., Chik, Z. B. (2007). Stabilisation of silty clay soil using chloride compounds. *Journal of Engineering Science and Technolog y, Vol. 2, No 1(2007) 102-110*

Adini, A., & Clough R. W. (1960). Analysis of Plate Bending by the Finite Element Method. *NSF Report, Grant G7337.*

Ajalloeian, R., Mansouri, H., Sadeghpour, A. H. (2013). Effect of Saline Water on GeotechnicalProperties of Fine-grained Soil. *EJGE, Vol. 18 [2013], Bund. G*

Alamgir, M. (1996). Analysis of soft ground reinforced by columnar in collusions. (*Ph.D Thesis), Department of Civil Engineering, Saga University, Saga, Japan*

Aldaood, A., Bouasker, M., Al-Mukhtar, M. (2014). Geotechnical properties of lime-treated gypseous soils. *Applied Clay Science, 88–89 (2014) 39–48*

Al-Mukhtar, M., Khattab, S., & Alcover, J. F. (2012). Microstructure and geotechnical properties of lime-treated expansive clayey soil. *Engineering Geology, 139-140 (2012) 17–27*

Anandarajah, A., Lu, N. (1991). Numerical study of the electrical double-layer repulsion between non-parallel clay particles of finite length. *Int J Numer Anal Method Geomech 1991,15(10):683–703.*

Anandarajah, A. (1994). Discrete element method for simulating behaviour of cohesive soil. *J Geotech Eng ASCE, 1994;120(9):1593–613.*

220 References

Anandarajah, A. (2003). Discrete element modeling of leaching-induced apparent overconsolidation in Kaolinite. *Soils Found, 2003; 43(6):1–12.*

Anonymous. (1999). Definition of Geotechnical Engineering. *Ground Engineering Magazine, Vol. 32, No. 11, p. 39.*

Arroyo, M., Ciantia, M., Castellanza, R., Gens, A., & Nova, R. (2012). Simulation of cement-improved clay structures with a bonded elasto-plastic model: A practical approach. *Computers and Geotechnics 45 (2012) 140–150*

AS1289. 2.1.1-2005. Methods of testing soils for engineering purposes: Soil moisture content tests-Determination of the moisture content of a soil –Oven drying method (standard method). *Australian: Australian standard.*

AS1289. 5. 1. 1- 2003. Methods of testing soils for engineering purposes: Soil compaction and density tests- Determination of the dry density/moisture content relation of soil using standard compactive effort. *Australian: Australian standard.*

AS1289. 6. 2. 2- 1998. Methods of testing soils for engineering purposes: Soil strength and consolidation tests- Determination of the shear strength of a soil- Direct shear test using a shear box. *Australian: Australian standard.*

AS1289. 6. 6. 1- 1998. Methods of testing soils for engineering purposes: Soil strength and consolidation tests- Determination of the one- dimensional consolidation properties of a soil – Standard method. *Australian: Australian standard.*

Athanasopoulos- Zekkos, A., Lamote, K., & Athanasopoulos, G. A. (2012). Use of EPS geofoam compressible inclusions for reducing the earthquake effects on yielding earth retaining structures. *Soil Dynamics and Earthquake Engineering, 41 (2012) 59–71*.

Atkinson, J., & Sallfors, G. (1991). Experimental determination of soil properties. In *Proc. 10th ECSMFE (Vol. 3, pp. 915-956).* Florence, Italy

Ayininuola, G. M., Agbede, O. A., & Franklin, S. O. (2009). Influence of Calcium Sulphate on Subsoil Cohesion and Angle of Friction. *Journal of Applied Sciences Research, 5(3): 297-304, 2009*

Azadegan, O., Yaghoubi, E., & Li, J. (2013). Evaluation of the Performance of Lime and Cement Treated Base Layers in Unpaved Roads. *EJGEVol. 18 [2013], Bund. D*

221 References

Baille, W., Tripathy, S., & Schanz, T. (2010). Swelling pressures and one-dimensional compressibility behaviour of bentonite at large pressures. *Appl Clay Sci, 2010;48:324–33.*

Barbour, S. L., & Krahn, J. (2004). The 2003 R.M. Hardy Lecture: Soil parameters for numerical analysis in clay. *GEOSPEC Geotechnical News.*

Basma, A. A., Tuncer, E. R. (1991). Effect of lime on volume change and compressibility of expansive clays. *Transportation Research Record, 1295, 52–61.*

Bayesteh, H., & Mirghasemi, A. A. (2012). Numerical simulation of pore fluid characteristic effect on the volume change behavior of montmorillonite clays. *Computers and Geotechnics 48 (2013) 146–155*

Benz T. (2007). Small-strain stiffness of soils and its numerical consequences. (Doctoral dissertation). Universitat Sttutgart, 2007, Munich, Germany.

Bergado, D. T., Taechakumthorn, C., Lorenzo, G. A., Abuel-Naga, H. M. (2006). Stress deformation behaviour under anisotropic drained triaxial consolidation of cement treated soft Bankok clay. *Soils Found 2006;46(5):629–37.*

Bjerrum., & Simons, N. E. (1960). Compression of Shear Strength Characteristics of Normally Consolidated Clay. Processings, Research Conference on Shear Strength of Cohesive Soils, ASCE, 711-726.

Bolt, G. H. (1956). Physico-chemical analysis of the compressibility of pure clays. *Geotechnique, 1956;6:86–93.*

Braga Reis, M. O. (1981). Formation of expansive calcium sulphate aluminate, the action of sulphate ion on weathered granites in a calcium hydroxide saturated medium. *Cement and Concrete Research,11: 541–547.*

Brinkgreve, R. B. (1999). Beyond 2000 in Computational Geotechnics/The netherlands/ 18-20 March.1999

Brinkgreve, R. B. J., Bakker, K. J., & Bonnier, P. G. (2006). The relevance of small-strain stiffness in excavation and tunnelling projects. In: H. F. Schweiger (ed.) Numerical Methods in Geotechnical Engineering (pp. 133–139). Taylor & Francis

222 References

Bulbul Ahmed, M. D., Abdul Alim, M. D., & Abu Sayeed. (2013). Improvement of soil strength using cement and limeAdmixtures. *Earth Science, 2013; 2(6): 139-144*

Burland, J. B. (1987). Nash Lecture: The Teaching of Soil Mechanics – a Personal View. *Proceedings, 9th ECSMFE, Dublin, Vol. 3, pp 1427-1447.*

Calvello, M., Lasco, M.,Vassallo, R., & Di Maio, C.(2005). Compressibility and residual shear strength of smectite clays: influence of pore aqueous solutions and organic solvents. *Rivista Italiana Di Geotecnica, 1/2005*

Clough, R. W. (1960). The Finite Element Method in Plane Stress Analysis. *Proc. 2nd ASCE Conf. On Electronic Computation, Pittsburg, Pa.*

Clough, R. W., & Wilson, E. L. (1999). Early Finite Element research at Berkeley. Fifth U.S National Conference on Computational Mechanics, Aug.4-6,1999

Costas, A., & Maria, C. (2008). Compressive strength of cement stabilized soils: A New Statistical Model. *EJGE, Vol. 13.*

Coulomb, C. A. (1776). Essai sur une application des regles de Maximums et Minimis á quelques Problèmes de Statique, relatifs á l'Architecture. *Memories de Mathematique et de Physique, Prèsentès, á l'Academie Royale des Science, Paris, Vol. 3, 38.*

Cuisinier, O., Javadi, A. A., Ahangar-Asr, A., Masrouri, F. (2012). Identification of coupling parameters between shear strength behaviour of compacted soils and chemical's effects with an evolutionary-based data mining technique. *Computers and Geotechnics, 48 (2013) 107–116*

D'Appolonia, D. (1980). Soil-bentonite slurry trench cutoffs. *Journal of the Geotechnical Engineering Division, Vol. 106, No. 4, April 1980, pp. 399-417*

Das, B. M. (1990). Principles of foundation Engineering (4th ed). PWS-Kent Publishing Co. Boston, Mass.

Das, B. (2008). Introduction to Geotechnical engineering: soil Compaction. *Thomson Learning*

Das, B. (2012). Fundamental of Geotechnical engineering: Ground Improvement (4^{th} edt). Stamfort, CT: Cengage learning

223 References

Delage, P. (2007). Microstructure features in the behaviour of engineered barriers for nuclear waste disposal. In Proc, experimental unsaturated soil mechanics. New York: Springer; 2007. p. 11–32.

Di Maio, C., & Fenelli, G. B. (1994). Residual strength of kaolin and bentonite: the influence of their constituent pore fluid. *Geotechnique 44, No. 4,217- 226*

Di Maio, C. (1996). Exposure of bentonite to the salt solution: osmotic and mechanical effects. *Geotechnique 46, No. 4,695-707*

Di Maio, C., Santoli, L., & Schiavone, P. (2004). Volume change behaviour of clays : the influence of mineral composition, pore fluid composition and stress state. *Mechanics of Materials 36 (2004) 435-451*

Dyson, G. M. (1961). Sodium Sulfate: Mellor's Comprehensive Treatise of Inorganic and Theoretical Chemistry, Vol. 2, Suppl. 2, Pt. 1, PP. 994-1053. New York: John Wiley & Sons.

El-Zein, A., & Balaam, N. (2006). Saturated-Unsaturated flow and solute transport in engineering liner systems: A new special-purpose finite element analysis softwareA. *Australian Geomechanics Vol 47 No 3*

Fell, R. (1994). Landslide risk assessment and acceptable risk. *Canadian Geotechnical Journal, 31, pp.261-272*

Gajo, A., & Maines, M. (2007) .Mechanical effects of aqueous solutions of inorganic acids and bases on anatural active clay. *Géotechnique, 57(8), 687–699.*

Garrett, D. E. (2001). Sodium Sulphate: Sodium Sulfate: Handbook of Deposits, Processing, Properties, and Use. *California: Academic Press*

Gens, A., Alonso, E. E. A. (1992). framework for the behaviour of unsaturated expansive Clays. *Can Geotech J, 1992;29:1013–32.*

Gens, A., Nova, R. (1993). Conceptual bases for constitutive model for bonded soil and weak rocks. *Geotechnical engineering of hard soil–soft rocks. Balkema.*

Goodge, J. 2011. Geochemical Instrumentation and Analysis. Geological Sciences University of Minnesota-Duluth.

224 References

Graham, J. (2006). The 2003 R.M. Hardy Lecture: Soil parameters for numerical analysis in clay. *Can. Geotech. J. 43: 187–209 (2006)*

Gratchev, I. B., & Sassa, K. (2009). Cyclic Behavior of Fine-Grained Soils at Different pH Values. *Journal of Geotechnical and Geoenvironmental Engineering, Vol. 135, No. 2*

Gratchev, I., & Towhata, I. (2013). Stress–strain characteristics of two natural soil subjected to long-term acidic contamination. *Soils and Foundations, 2013;53(3):469–476*

Grim, R. E. (1962). *Applied clay mineralogy. McGraw-Hill, New York*

Gueddouda, M. K., Goual, I., Lamara, M., Smaida, A., & Mekarta, B. (2011). Chemical Stabilization of Expansive Clays from Algeria. *Global Journal of researches in engineering: J General Engineering, Volume 11 Issue 5 Version 1.0, ISSN: 0975-5861*

Horpibulsuk, S. (2001). Analysis and assessment of the engineering behaviour of cement stabilized clays. (Doctoral dissertation). Saga University, Saga, Japan

Horpibulsuk, S., Miura, N., Koga, H., Nagaraj, T. S. (2004). Analysis of strength development in deep mixing – a field study. *Ground Improv J 2004;8(2):59–68.*

Horpibulsuk, S., Liu, M. D., Liyanapathirana, D. S., & Suebsuk, J. (2009). Behaviour of cemented clay simulated via the theoretical framework of the Structured Cam Clay model. *Computers and Geotechnics 37 (2010) 1–9*

Huang, J. T. (1994). The effects of density and cementation of cemented sands. (Doctoral dissertation). Sydney University. N.S.W

Hunter, D. (1988). Lime-Induced Heave in Sulphate- Bearing Soils. *Journal of GeotechnialEngineering, Vol. 114, N.* http://ascelibrary.org/doi/abs/10.1061/(ASCE)0733-9410(1988)114:2(150)

Iordanoff, I., Fillot, N., Berthier, Y. (2005). Numerical study of a thin layer of cohesive particles under plane shearing. *Powder Technol, 2005;159:46–54.*

Islam, M. Rafizul, M. D., Assaduzzaman, M. A. (2012). The effect of chemical admixtures on the geotechnical parameters of organic soil: a new statistical model. *Int. Journal of Applied Sciences and Engineering Research, Vol. 1, Issue 4*

225 References

Kabata-Pendias, A. (2010). Soil Constituents: Trace Elements in Soils and Plants, Fourth Edition, *CRC Press*

Kasama, K., Ochiai, H., Yasufuku, N. (2000). On the stress–strain behaviour of lightly cemented clay based on an extended critical state concept. *Soils Found 2000, 40(5):37–47.*

Kashir, M., & Yanful, E. (2001). Hydraulic conductivity of bentonite permeated with acid mine drainage. *Can. Geotech. J, 38, 1034–1048.*

Katti, D. R., Matar M. I., Katti, K. S., Amarasinghe, P. M. (2009). Multiscale modeling of swelling clays: a computational and experimental approach. *KSCE Journal of Civil Engineering, 2009;13(4):243–55.*

Kazemian, S., Huat, B. B. K., Prasad, A., Barghchi, M. (2010). A Review of Stabilization of Soft Soils by Injection of Chemical Grouting. *Australian Journal of Basic and Applied Sciences, 4(12): 5862-5868, 2010*

Khattab, S. A. A. (2002). Etude multi-échelles d'un sol argileux plastique traité à la chaux. (Doctoral dissertation). University of Orléans, France.

Khemissa, M., & Mahamedi, A. (2014). Cement and lime mixture stabilization of an expensive over-consolidated clay. *Applied Clay Science, 95 (2014) 104–110*

Kimoto, S., Oka, F., Fushita, T., & Fujiwaki, M. (2007). A chemo-thermo mechanically coupled numerical simulation of the subsurface ground deformations due to methane hydrate dissociation. *Computers and Geotechnics, 34 (2007) 216–228*

Kinuthia, J. M., Wild, S., & Jones, G.I. (1999). Effects of monovalent and divalent metal sulphates on consistency and compaction of lime-stabilised kaolinite.*Applied Clay Science,14 _1999. 27–45*

Kok Sien Ti, Bujang, B. K. Huat., Jamaloddin Noorzaei., Moh'd Saleh Jaafar. (2009). A Review of Basic Soil Constitutive Models for Geotechnical Application. *EJGE journal, Vol. 14, Bund. J*

Komine, H. (2008).Theoretical equations on hydraulic conductivities of bentonitebased buffer and backfill for underground disposal of radioactive wastes. *Journal of Geotechnical and Geoenvironment Engineering,* 134 *(4),* 497–508,

226 References

Kuhlemeyer, R. L., Lysmer, J. (1973). Finite element method accuracy for wave propagation problems. *J Soil Mech Found Div ASCE 1973;99(5):421–7.*

Lambe, T. W., & Whitman, R. V. (1969). Soil Mechanics. *John Wiley and Sons. Inc*

Lee, K. H., Lee, S. (2002). Mechanical properties of weakly bonded cement stabilized Kaolin. *KSCE J Civil Eng, 2002;6(4):389–98.*

Little, D., & Nair, S. (2009). Validation of Sensitivity of Sulphate-Bearing Soils to Ettringite Growth by Differential Scanning Calorimetry. Transportation Research Record. *Journal of the Transportation Research Board, No. 2104, Transportation Research Board of the National Academies (pp. 63–70). Washington, D.C*

Liu, M. D., & Carter, J. P. (2000). Modelling the destructuring of soils during virgin compression. *Géotechnique 2000; 50(4):479–83.*

Liu, M. D., & Carter, J. P. (2002). Structured cam clay model. *Can Geotech J 2002;39(6):1313–32.*

Liu, M. D., & Carter, J. P. (2003). The volumetric deformation of natural clays. *Int J Geomech, ASCE 2003;3(3/4):236–52.*

Lorenzo, G. A., Bergado, D. T. (2004). Fundamental parameters of cement-admixed clay the – new approach. *J Geotech Geoenviron Eng ASCE, 2004:1042–50.*

Lorenzo, G. A., Bergado, D. T. (2006). Fundamental characteristics of cement-admixed clay in deep mixing. *J Mater Civ Eng ASCE, 2006:161–74.*

Lu, N., Anandarajah, A. (1992). Emperical estimation of double layer repulsive force between two inclined clay particles of finite length. *J Geotech Geoenviron Eng 1992;118(4):628–34.*

Meegoda, N., & Ratnaweera, P. (1994). Compressibility of contaminated fine-grained soils. *Geotechnical Testing Journal1, 7(1),101–112.*

Mesri, G., Olson, R. E .(1971). Consolidation characteristic of montmorillonite. *Geotecnique, 1971;21:341–52.*

227 References

Mitchell, J. K., & Dermatas, D. (1992). Clay soil heave caused by lime-sulfate reactions. *ASTM STP 1135, Innovations and Uses forLime, Philadelphia.*

Mitchell, J. K. (1993). Fundamentals of soil behaviour. *John Wiley and Sons. Inc, 1993. p.422.*

Miura, N., Taesiri, Y., Koga, Y., & Nishida, K. (1988). Practical of improvement of Ariake clay by mixing admixtures. *Proceedings of the International Symposium on Shallow Sea and Lowland, Saga, pp. 159–168.*

Moayedi, H., Huat, B. B. K., Kazemian, S., & Daneshmand, S. (2012). Stabilization of organic soil using sodium silicate system grout. *International Journal of Physical Sciences, Vol. 7(9), pp. 1395 - 1402, 23*

Mohd Yunus, N. Z., Wanatowski, D., & Stace, L. R. (2011). Effect of Humic Acid on Physical and Engineering Properties of Lime-Treated Organic Clay. *World Academy of Science, Engineering and Technology, Vol:5 2011-11-22*

Mohr, O. (1990). Welche Umstände Bedingen die Elastizitätsgrenze und den Bruch eines Materials?. *Zeitschrift des Vereines Deutscher Ingenieure, Vol. 44, 1524-1530, 1572-1577.*

Mun, B., Kim, T., Moon, T., & Oh, J. (2012).SCM wall in the sand: Numerical simulation and design implications. *Engineering Geology, 151 (2012) 15–23*

Nagaraj, T. S., Pandian, N. S., & Narasimha Raju, P. S. R. (1998). Compressibility behavior of soft cemented soils. *Geotechnique 1998;48(2):281–7.*

Nalbantog˘ lu, Z. (2004). Effectiveness of Class C fly ash as an expansive soil stabilizer. *Construction and Building Materials, 18 (2004) 377–381*

Nor, Z. B. M.Y. (2007). Stabilisation of Organic Clay Using Lime-added Salt. *(Master Thesis) Universiti Teknologi Malaysia, Skudai.*

NSW department of Primary Industries. Bentonite. Retrieved from *http://www.dpi.nsw.gov.au/minerals/geological/industrial-mineral-opportunities*

Obrzud, R. F. (2010). The Hardening Soil model – a practical guidebook. Technical report Z_ Soil. PC 100701, Zace Services Ltd. Lausanne: Switzerland

Onitsuka, K., Modmoltin, M., Kouno, M., Negami, T. (2004). Effect of organic matter on lime and cement stabilized Ariake clay. *J. Geotech. Eng. ASCE (729/III-62), 1–13.*

228 References

Porbaha, A. (2000). State-of-the-art in deep mixing technology: Design considerations. *Ground Improvement, Vol.4, pp 111-125.*

Potts, D. M., & Zdravkovic, L. (1999). Finite Element Analysis in Geotechnical Engineering. Thomas Telford Ltd

Prabakar, J., Nitin Dendorkar., & Morchhale, R. K. (2004). Influence of fly ash on strength behavior of typical soils. *Construction and Building Materials 18 (2004) 263–267*

Proctor, R. R. (1933). Design and Construction of Rolled Earth Dams. *Engineering News Record, Vol. 3, 245-248, 286-289, 348-351, 372-376.*

Puppala, A. J., Napat Intharasombat, P. E., & Vempati, R. K. (2005). Experimental Studies on Ettringite-Induced Heaving in Soils. *Journal of Geotechnical and Geoenvironmental Engineering, Vol. 131, No. 3*

Ramesh, H. N., Nanda, H. S., & Manoj Krishna, K. V. (2013). Effect of Sodium Sulphate on the Index Properties and Compaction Behaviour of Neyveli Fly Ash- Shedi Soil Mixtures. *IOSR Journal of Mechanical and Civil Engineering (IOSR-JMCE) e-ISSN: 2278-1684,p-ISSN: 2320-334X, Volume 6, Issue 3 , PP 56-62*

Raphael, J. M., & Clough, R. W. (1965). Construction Stresses in Dworshak Dam. UCB/SESM Report No. 65/3, University of California, Berkeley

Ruhl, J., & Daniel, D. (1997). Geosynthetic clay liners permeated with chemical solutions and leachates. *Journal of Geotechnical and Geoenvironmental Engineering, 123(4) 369–381*.

Santos, J. A., Correia, A. G. (2001). Reference threshold shear strain of soil, its application to obtain a unique strain-dependent shear modulus curve for soil. In: Proceedings of the 15th International Conference on Soil Mechanics and Geotechnical Engineering (vol. 1, A. A. pp. 267–270) Balkema, Istanbul

Sariosseiri, F., Muhunthan, B. (2009). Effect of cement treatment on geotechnical properties of some Washington State soils. *Eng Geol 2009; 104:119–25*.

Schanz, T., Vermeer, P., & Bonier, P. (1999). Formulation and verification of the Hardening Soil model In Beyond 2000 in Computational Geotechnics. *Balkema, Rotterdam*

229 References

Seetharam, S. C., Cleall, P. J., Thomas, H. R. (2006). Modelling some aspects of ion migration in a compacted bentonitic clay. *Engineering Geology, 85 (2006) 221–228*

Seidell, A. (1965). In: Solubilities (Linke, W. F., ed), 4th ed., Vol. 2. *American Chemical Society, Washington, D. C.*

Shariatmadari, N., Salami, M., & Karimpour Fard, M. (2011). Effect of inorganic salt solutions on some geotechnical properties of soil-bentonite mixtures as barriers. *International Journal of Civil Engineering, Vol. 9, No. 2*

Sharma, M. S., Baxter, C. D. P., Huffman, W., Moran, K., & Vaziri, H. (2011). Characterization of weakly cemented sands using nonlinear failure envelopes. *International Journal of Rock Mechanics and Mining Science, 48(1), pp 146-151.*

Shear Strength of Soils. (2011). *Copyright © 2011 John Wiley & Sons Retrieved from www.knovel.com.*

Sherwood, P.T. (1962). Effect of sulphates on cement- and lime-stabilised soils. *Building and Highway Research Board, 353, 98–107.*

Sibelco Australia. Retrieved from *http://www.sibelco.com.au*

Sinat, K. (2006). Influence of Storage Conditions on Geotechnical Properties of Ariake Clay and on its Chemical Stabilization. (Doctoral dissertation). Saga University, Saga.

Sivapullaiah, P.V., Sridharan, A., & Ramesh, H.N. (2000). Strength behaviour of lime-treated soils in the presence of sulphate. *Can. Geotech, J. 37: 1358–1367*

Slaty, F., Khoury, H., Wastiels, J., & Rahier, H. (2013). Characterization of alkali activated kaolinitic clay. *Applied Clay Science, 75–76 (2013) 120–125*

Sposito, G. (2008). Soil Minerals: The Chemistry of Soils, Second Edition, *Oxford University Press*

Sridharan, A., Sivapullaiah, P. V., & Ramesh, H. N. (1995). Consolidation behaviour of lime treated sulphate soils. In Proceedings of the International Symposium on Compression and Consolidation of Clayey Soils. *Hiroshima, Japan, Vol. 1, pp. 183–188.*

230 References

Sridharan, A., & Prakash, K. (1999). Mechanisms are controlling the undrained shear strength behaviour of clays. *Canadian Geotechnical Journal 36, 1030–1038.*

Strakhov, N. M. (1970). Principles of Lithogenesis (Review of USSR Sodium Sulfate Deposits). *New York: Plenum Publishing.*

Studds, P. G., Stewart, D. I., & Cousens, T.W. (1998). The effects of salt solutions on the properties of bentonite-sand mixtures. *Clay Minerals, (1998) 33,651-660*

Tarrant, R. 2011. EXPERIMENT 31 —The Scanning Electron. Microscope. Australia: School of Physics - The University of Sydney.

Taylor, R. L., & Brown, C. B. (1967). Darcy Flow Solution with a Free Surface. *J. Hyd. Div., ASCE, Vol. 93.*

Tiznado, J. C., & Rodrı´guez-Roa, F. (2010). Seismic lateral movement prediction for gravity retaining walls on granular soils. *Soil Dynamics and Earthquake Engineering 31 (2011) 391–400*

Turkoz, M., Savas, H., Acaz, A., & Tosun, H. (2014). The effect of magnesium chloride solution on the engineering properties of clay soil with expansive and dispersive characteristics. *Applied Clay Science, 101 (2014) 1–9*

Turner, M., Clough, R. W., Martin, H. C., & Topp, L. J. (1956). Stiffness and Deflection Analysis of Complex Structures. *J. Aeronautical Science 23 (9), pp. 805-823*

Umesha, T. S., Dinesh, S. V., & Sivapullaiah, P. V. (2012). Effects of acids on geotechnical properties of black cotton soil. *International Journal of Geology, Issue 3, Volume 6*

Van Olphen, H. (1991). An introduction to clay colloid chemistry. *2nd ed. New York: Wiley Interscience; 1991. p. 301.*

Villar, M. V., Sánchez, M., & Gens, A. (2008). Behaviour of a bentonite barrier in the laboratory: Experimental results up to 8 years and numerical simulation. *Physics and Chemistry of the Earth, 33 (2008) S476–S485*

Wilson, E. L. (1960). Matrix Analysis of Nonlinear Structures. *Proc. 2nd ASCE Conf.On Electronic Computation, Pittsburg, Pa.*

231 References

Xing, H., Yang, X., Xu, C., & Ye, G. (2008). Strength characteristics and mechanism of salt-rich-soil –cement. *Engineering Geology, 103 (2009) 33-38*

Yao, M. (2001). Three-dimensional discrete element method analysis of cohesive soil. (Doctoral dissertation). Johns Hopkins University, Baltimore, United State

Yin, J. H., Lai, C. K. (1998). Strength and stiffness of Hong Kong marine deposit mixed with cement. *Geotech Eng J, 1998;29(1):29–44.*

Yu, H. S. (1998). CASM: a unified state parameter model for clay and sand. *Int J Numer Anal Method Geomech, 1998;22:621–53.*

Zhang, D., Cao, Z., Fan, L., Liu, S., & Liu, W. (2014). Evaluation of the influence of salt concentration on cement stabilized clay by electrical resistivity measurement method. *Engineering Geology, 170 (2014) 80–88*

Zhang, H. Y., Cui, S. L., Zhang M., & Jia, L. Y. (2011). Swelling behaviors of GMZ bentonite–sand mixtures inundated in NaCl–Na_2SO_4 solutions. *Nuclear Engineering and Design, 242 (2012) 115– 123*

Zhang, R., & Li, J. (2006). Simulation on mechanical behaviour of cohesive soil by Distinct Element Method. *J Terramech, 2006; 43(3):303–16.*

Zimmermann, TH., Truty. A., Podles, K. Numerics in Geotechnics and Structures. *Elmepress International(2010).*

Appendices

Chapter 3

Appendix .1

Temp.(°C)	Na2SO4	Temp.(°C)	Na2SO4
-1.25	4.15	110	29.58
0	4.31	120	29.48
5	5.84	130	29.53
10	8.26	140	29.58
15	11.66	150	29.68
20	15.97	160	29.82
25	21.88	170	30.07
27.5	25.15	180	30.26
30	29.18	190	30.46
32.38	33.2	200	30.60
		210	30.65
-3.55	12.8	220	30.94
-1.25	4.15	230	31.32
0	15.11	233	31.7
5	18.9	241	31.88
10	23.02	250	30.56
15	27.11	260	29.48
20	31.13	270	27.95
23.7	34.38	280	26.04
24.25	34.3	290	23.55
		300	19.87
35	32.93	3005	20.3
40	32.48	310	15.61
45	32.07	320	11.58
50	31.69	324.5	10.0
60	31.13	330	6.80
70	30.65	340	4.03
80	30.17	350	2.34
90	29.87	3545	1.62
100	29.68	360	0.89
101.9	29.68	382	0.38

Solubility and Density of Sodium Sulphate in Water (wt. %)(Donald E.Garret, Seidell,Strakhov &Dyson)

Compaction results

Appendix 2

Pure bentonite		
Added moisture %	***Accurate moisture content %***	***Dry density of soil (γd) gr/cm3***
18	29.44	1.034
22	33.22	1.039
30	43.18	1.103
45	55.55	1.023
50	65.05	0.929

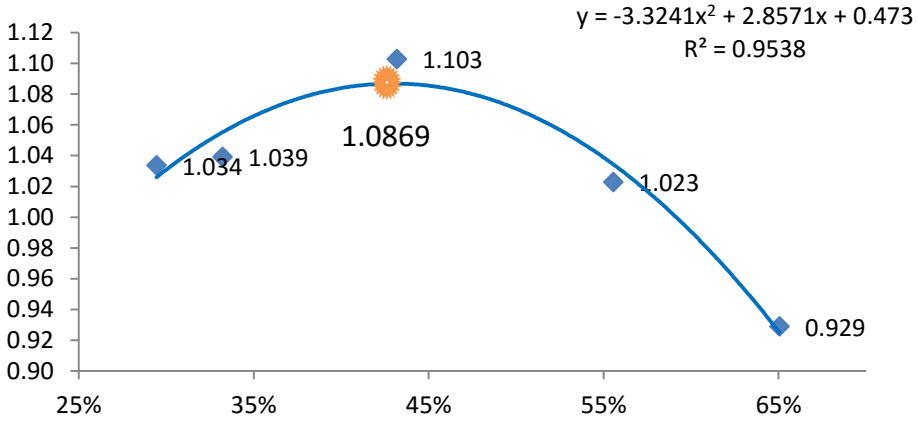

Appendix 3

Pure bentonite+0.5 % Sulphate		
Added moisture %	*Accurate moisture content %*	*Dry density of soil (γd) gr/cm3*
18	32.63	1.025
22	33.09	1.04
30	43.27	1.081
45	50.52	1.076
50	58.87	0.982

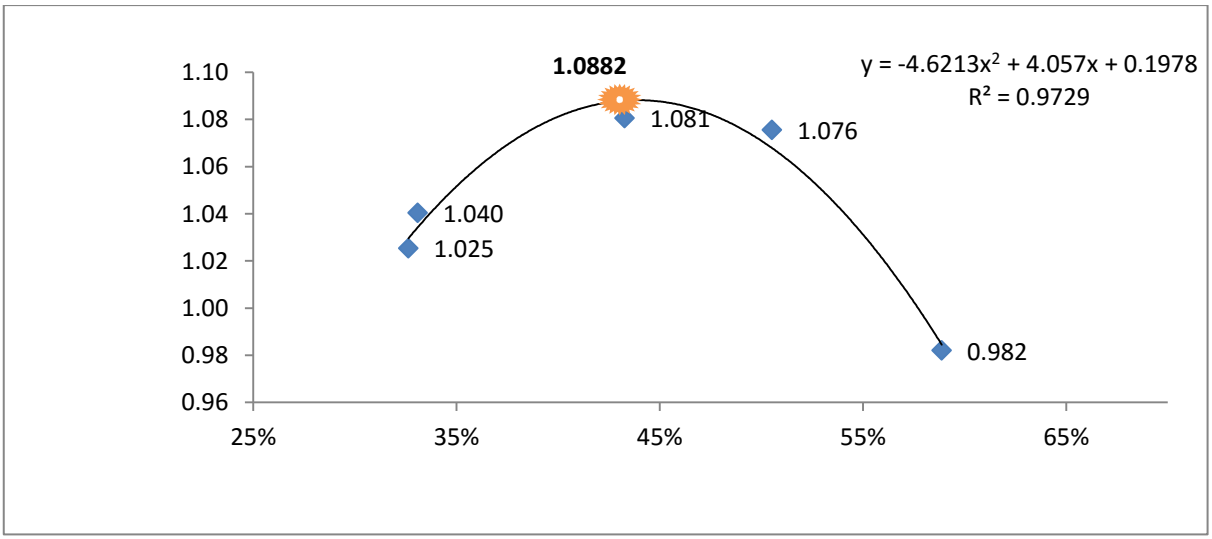

Appendix 4

Pure bentonite+1 % Sulphate		
Added moisture %	*Accurate moisture content %*	*Dry density of soil (γd) gr/cm3*
18	30.41	1.037
22	34.78	1.098
30	41.40	1.112
40	51.18	1.092
45	58.06	1.024

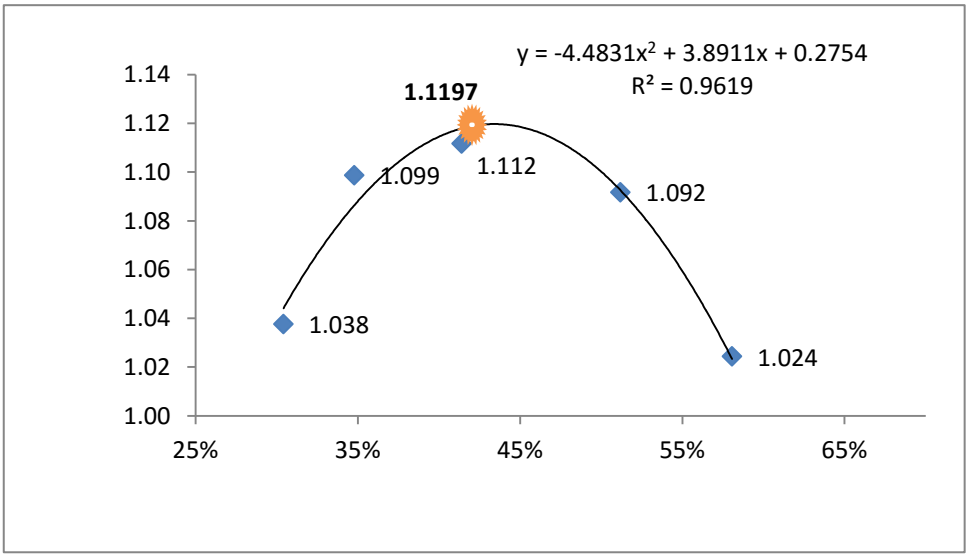

Appendix 5

Pure bentonite+1.5 % Sulphate		
Added moisture %	*Accurate moisture content %*	*Dry density of soil (γd) gr/cm3*
18	30.66	1.094
22	32.39	1.105
30	42.20	1.104
45	56.90	1.029

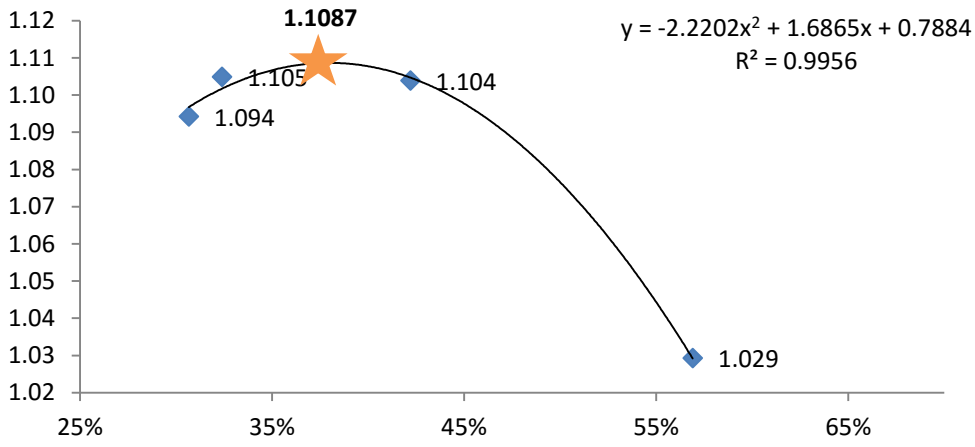

Appendix 6

Pure bentonite+3 % Sulphate		
Added moisture %	*Accurate moisture content %*	*Dry density of soil (γd) gr/cm3*
18	29.75	1.087
22	32.55	1.092
40	52.33	1.078
45	55.33	1.00
50	58.24	0.924

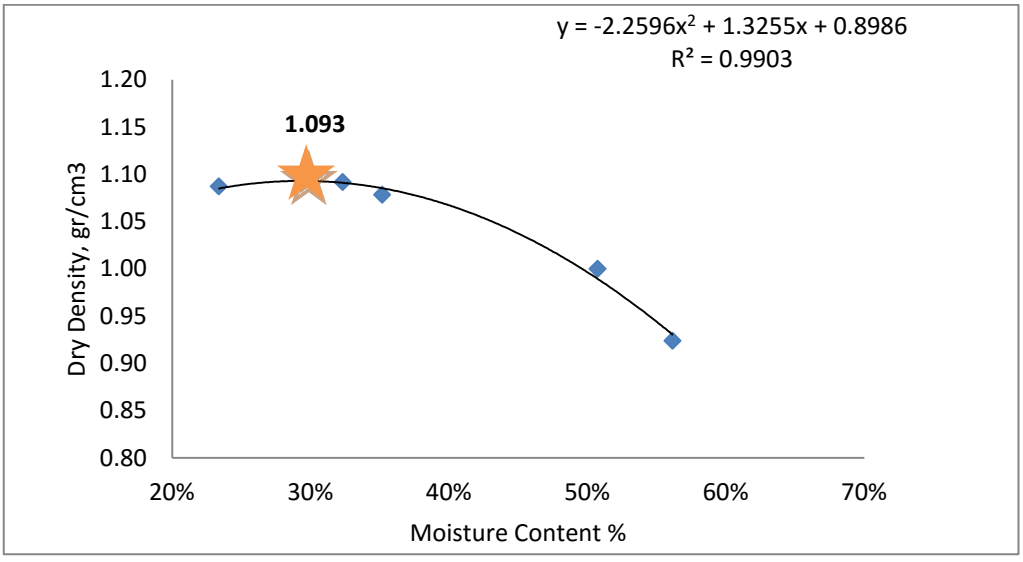

Consolidation

Appendix 7

Pure bentonite (Normal stress 50kPa)

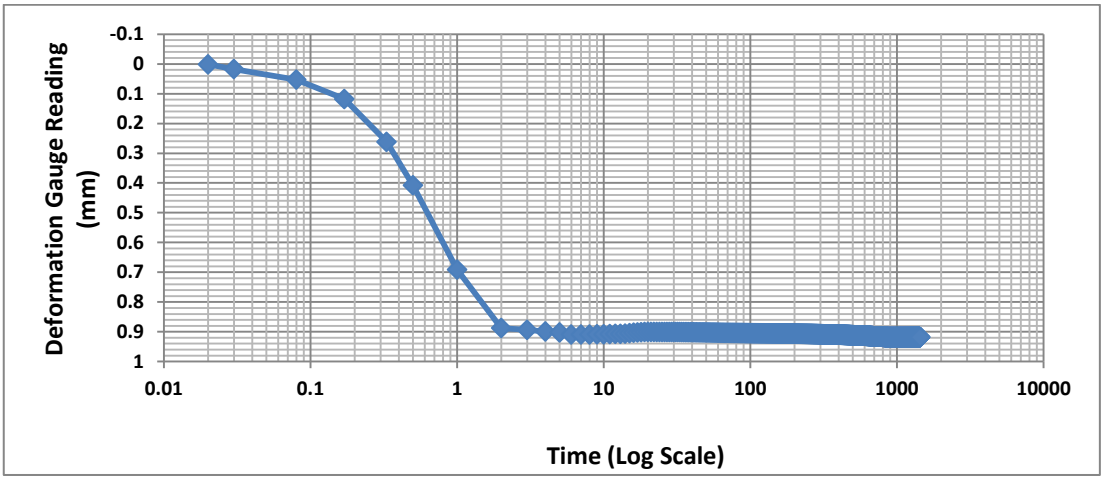

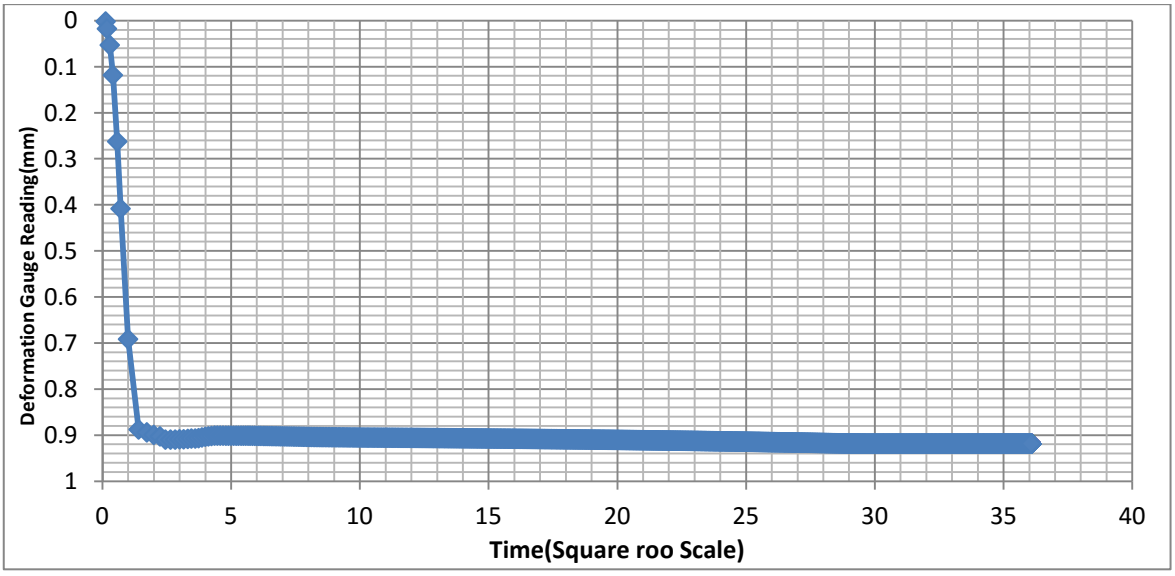

Appendix 8

Pure bentonite (Normal stress 100kPa)

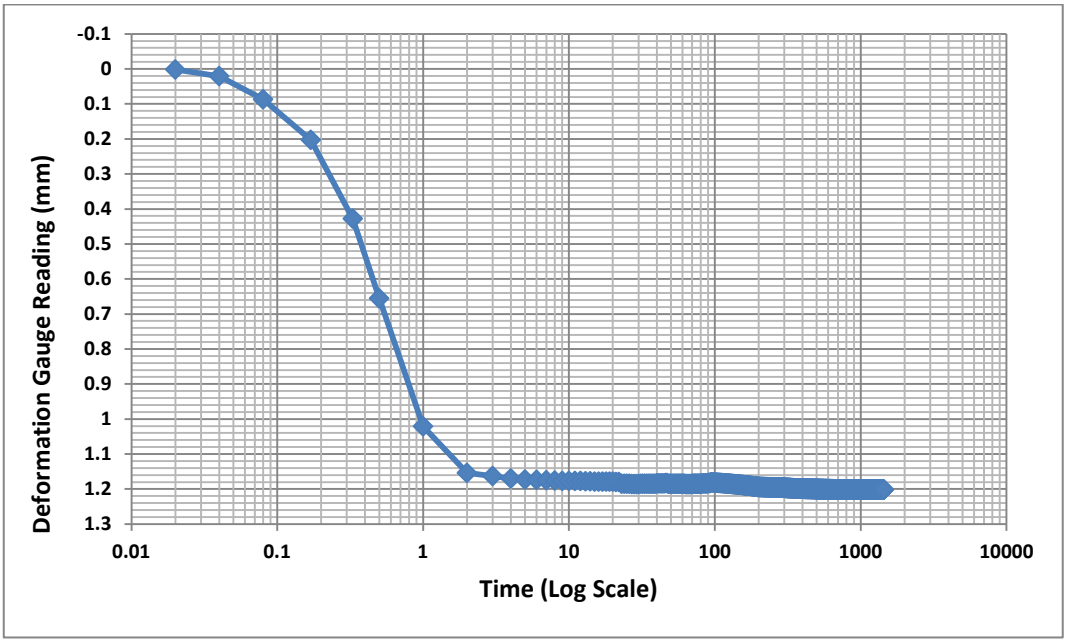

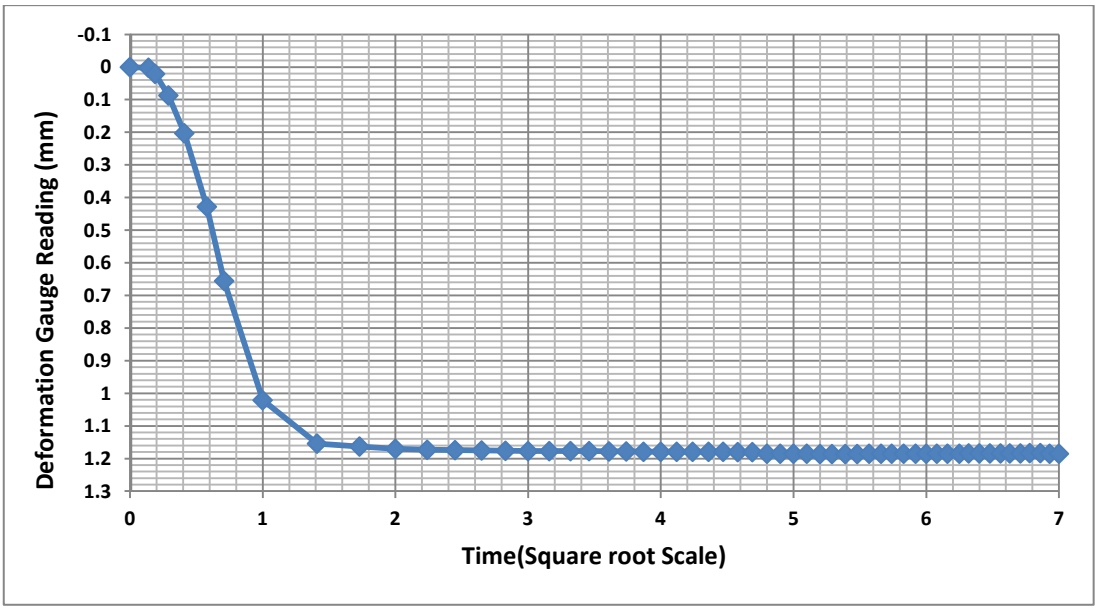

Appendix 9

Pure bentonite (Normal stress 200kPa)

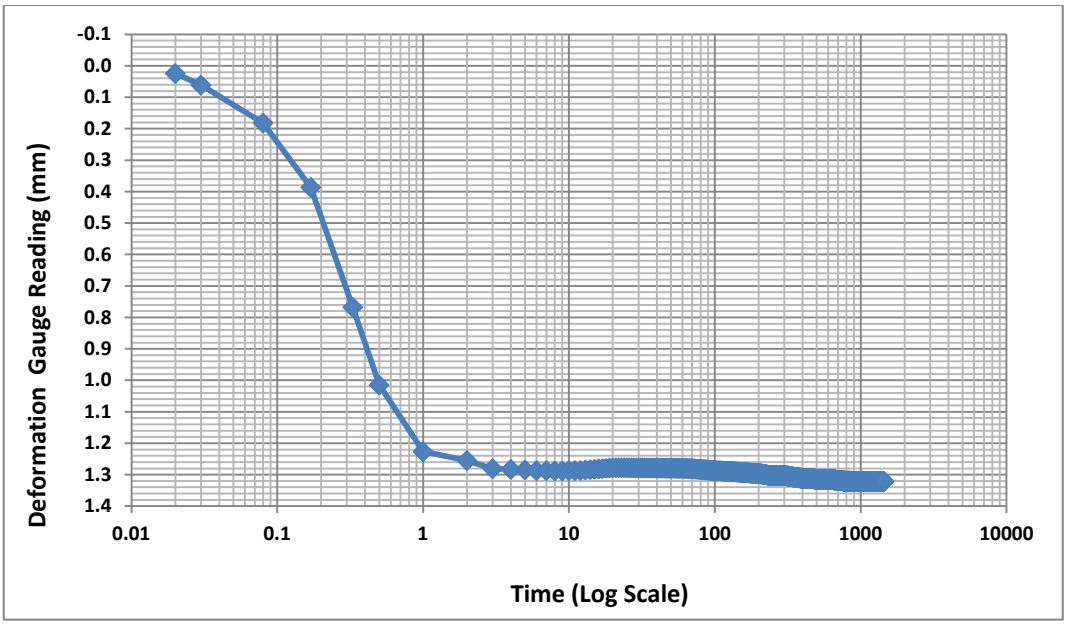

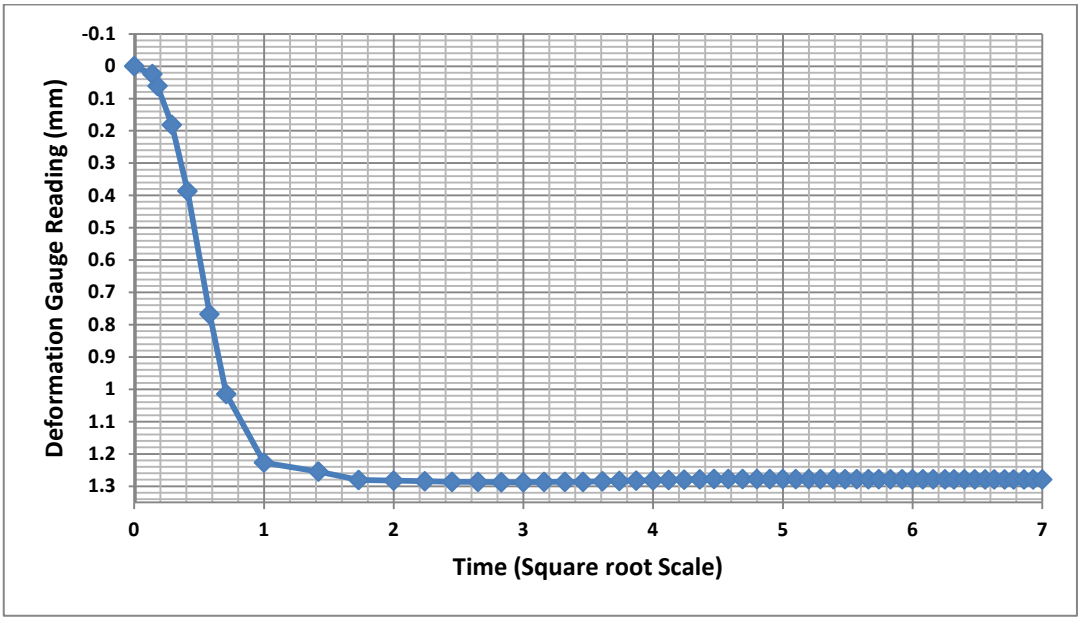

Appendix 10

Pure bentonite (Normal stress 100kPa) **No curing**

Elapsed Time min	Vertical Stress kPa	Vertical Displacement mm	Horizontal Stress kPa	Horizontal Displacement mm
0.00	99.76	-0.0053	0.0031	0.0000
1.6	100	-0.05591	38.6	0.1002
2.16	99.74	-0.05827	56.76	0.2003
4.05	99.74	-0.05118	65.64	0.3005
6.07	99.74	-0.03937	72.25	0.4007
8.07	99.59	-0.02362	77.49	0.5009
10.05	99.74	-0.01811	81.6	0.601
11.97	99.74	-0.01181	84.46	0.7
13.8	99.59	-0.006299	86.36	0.8002
15.78	99.74	-0.004724	87.73	0.9003
17.73	100	0.0007874	88.51	1.001
19.61	99.89	0.0007874	89.58	1.101
21.55	100	-0.0007874	90.41	1.201
23.44	100	-0.005512	91.37	1.301
25.23	100	-0.01024	92.26	1.4
27.15	100	-0.01417	93.03	1.5
29.13	100	-0.01811	93.87	1.6
31.1	99.89	-0.02126	94.4	1.701
33.06	100	-0.02677	94.82	1.801
35.03	100	-0.02992	95.06	1.901
36.88	100	-0.0315	95.12	2.001
38.91	99.89	-0.03307	94.64	2.1
40.66	99.89	-0.03307	93.75	2.2
42.53	100	-0.03465	92.68	2.3
44.56	99.89	-0.03937	91.19	2.401
46.63	99.89	-0.04173	88.92	2.501
48.34	100	-0.04409	86.96	2.601
50.22	100	-0.04646	84.7	2.623
50.84	100	-0.04724	83.92	2.623

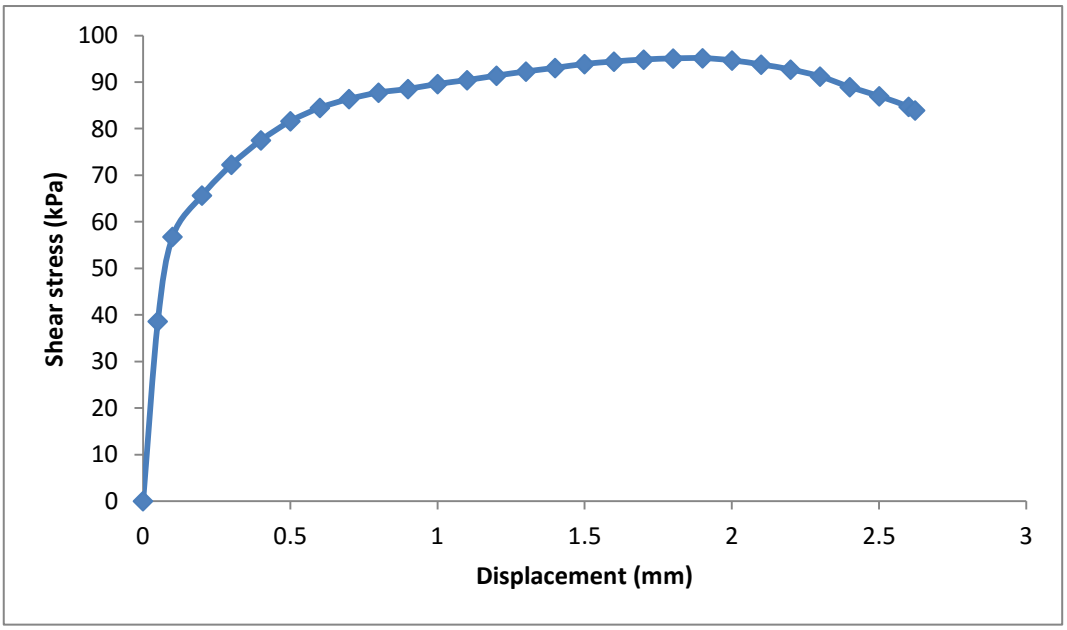

Appendix 11

Pure bentonite+3% SS (Normal stress 100kPa) **7 days curing**

Elapsed Time min	Vertical Stress kPa	Vertical Displacement mm	Horizontal Stress kPa	Horizontal Displacement mm
0.00	99.94	0.0036	0.005	0.00
1.61	99.89	0.001575	13.04	0.1002
2.35	100	-0.004724	39.13	0.2003
4.43	100	-0.01969	57.3	0.3005
6.48	100	-0.02835	67.3	0.4007
8.3	100	-0.02913	73.38	0.5009
10.32	100	-0.03071	78.32	0.601
12.4	100	-0.03701	82.13	0.7002
14.19	100	-0.04016	84.4	0.8002
16.14	100	-0.04488	86.3	0.9003
18.05	100	-0.04961	87.55	1.001
20.03	99.89	-0.05276	88.09	1.101
21.93	100	-0.05433	87.73	1.201
23.84	99.89	-0.05591	86.72	1.301
25.8	100	-0.05748	85.47	1.423
27.63	100	-0.05827	83.92	1.511
29.44	100	-0.05906	82.13	1.612
31.65	100	-0.06063	79.69	1.701
33.53	100	-0.06299	77.61	1.801
35.36	100	-0.06378	75.58	1.901
37.32	100	-0.06457	73.38	2.001
39.23	100	-0.06535	71.53	2.105
41.11	100	-0.06535	70.1	2.232
42.97	100	-0.06614	69.03	2.311
45	100	-0.06693	67.84	2.401
47.1	99.89	-0.06772	66.53	2.501
48.85	100	-0.07008	65.46	2.601
50.76	99.89	-0.07165	64.33	2.701
52.73	100	-0.07559	63.55	2.852
54.61	100	-0.07874	62.72	2.902
56.61	100	-0.08268	62	3.030
58.66	100	-0.08425	61.65	3.101
60.56	100	-0.08661	61.41	3.201
62.43	100	-0.09213	60.69	3.301
64.49	99.89	-0.0937	60.1	3.401
66.24	100.2	-0.1024	59.8	3.505
68.16	100	-0.1039	59.26	3.603
70.09	100	-0.1087	58.85	3.712
72.13	100	-0.111	58.43	3.796
73.92	99.89	-0.1165	58.07	3.796

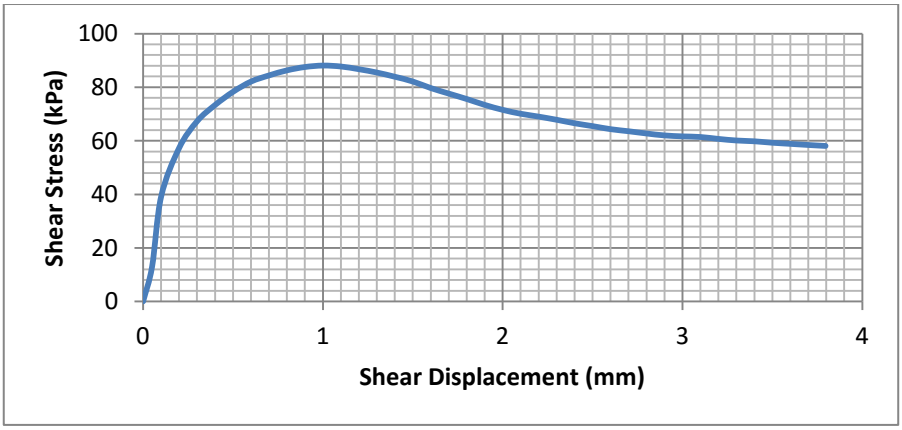

Appendix 12

Pure bentonite+3% SS (Normal stress 100kPa) **14days curing**

Elapsed Time min	Vertical Stress kPa	Vertical Displacement mm	Horizontal Stress kPa	Horizontal Displacement mm
0.00	100	0.062	0.00	0.00
1.75	100	0.7055	22.45	0.1002
2.15	100	0.7024	44.13	0.2003
4.21	99.89	0.7016	54.86	0.3005
6.00	99.74	0.7024	60.87	0.4007
8.05	99.74	0.7032	65.93	0.5009
10.01	99.89	0.7055	69.98	0.601
11.93	99.89	0.7047	72.96	0.700
13.81	99.89	0.7047	75.52	0.8002
15.73	99.89	0.7039	77.73	0.9003
17.64	99.89	0.7032	79.87	1.001
19.53	99.89	0.7032	81.6	1.101
21.45	99.89	0.7024	83.09	1.201
23.49	99.89	0.7032	84.34	1.301
25.36	99.89	0.7032	85.11	1.432
27.22	99.89	0.7032	85.65	1.521
29.16	99.89	0.7032	85.95	1.636
31.06	99.89	0.7032	86.01	1.701
32.91	99.89	0.7039	86.01	1.801
34.76	100	0.7039	85.71	1.901
36.77	99.89	0.7047	85.29	2.001
38.88	99.89	0.7047	84.81	2.119
40.62	100	0.7047	84.22	2.207
42.56	100	0.7055	83.56	2.302
44.47	99.89	0.7039	82.91	2.401
46.35	100	0.7024	82.19	2.501
48.35	99.89	0.6992	81.54	2.601
50.33	100	0.6969	80.41	2.701
52.19	100	0.6929	79.57	2.825
54.08	100	0.6898	78.92	2.901
56.15	100	0.6882	77.61	3.102
57.89	100	0.6843	76.54	3.101
59.8	100	0.6795	75.46	3.201
61.72	100	0.6764	74.51	3.301
63.71	100	0.6701	73.32	3.401
65.59	100	0.6646	72.6	3.536
67.43	100	0.6606	71.89	3.605
69.44	100	0.6583	71.23	3.703
71.32	100	0.6567	70.52	3.801
73.15	100	0.6559	69.92	3.901
75.19	100	0.6543	69.27	4.001
77.13	100	0.6512	68.79	4.012
77.37	100	0.6512	68.73	4.015

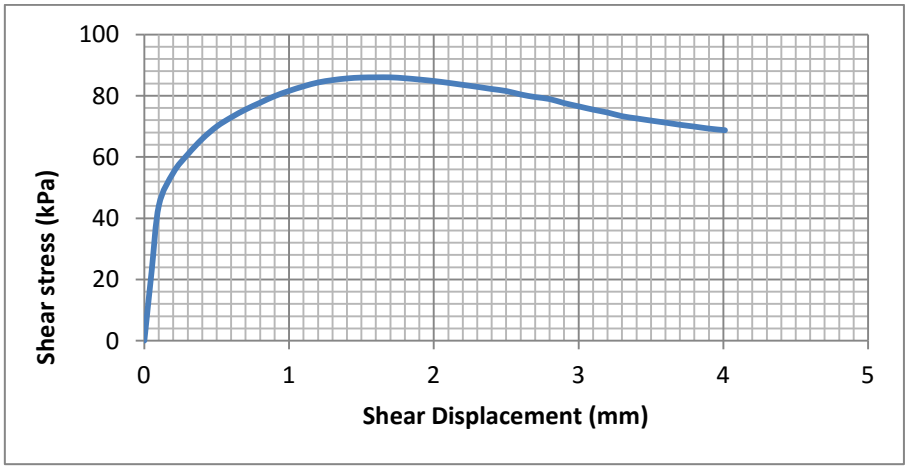

Appendix 13

Pure bentonite+3% SS (Normal stress 100kPa) **28 days curing**

Elapsed Time min	Vertical Stress kPa	Vertical Displacement mm	Horizontal Stress kPa	Horizontal Displacement mm
0.00	99.89	0.0039	0.001	0.006
1.85	99.74	0.03071	32.46	0.1002
2.06	99.74	0.03386	44.25	0.2003
4.22	99.59	0.04173	50.92	0.3005
6.12	99.74	0.05354	55.21	0.4007
8.1	99.59	0.06299	58.55	0.5009
9.98	99.59	0.07638	61.23	0.601
11.97	99.74	0.08504	63.67	0.7008
13.96	99.74	0.09528	65.7	0.8002
15.88	99.74	0.1047	67.72	0.9003
17.81	99.74	0.1173	69.33	1.001
19.91	99.74	0.1189	71.23	1.101
21.65	99.74	0.1244	72.66	1.201
23.64	99.74	0.1339	74.09	1.301
25.63	99.74	0.1402	75.4	1.444
27.57	99.74	0.148	76.54	1.508
29.48	99.59	0.1559	77.67	1.603
31.44	99.74	0.1614	78.56	1.701
33.34	99.74	0.1661	79.22	1.801
35.28	99.59	0.1709	79.93	1.901
37.17	99.74	0.1756	80.59	2.001
39.19	99.74	0.1819	81	2.111
41.07	99.74	0.1874	81.12	2.232
43.01	99.74	0.1953	81.48	2.312
44.83	99.74	0.2008	81.78	2.401
46.82	99.74	0.2047	82.13	2.501
48.74	99.89	0.2079	82.37	2.601
50.66	99.74	0.2094	82.85	2.701
52.63	99.74	0.2102	83.27	2.812
54.36	99.89	0.2118	83.5	2.905
56.46	99.89	0.2134	83.74	3.005
58.4	99.74	0.2142	83.56	3.101
60.38	99.89	0.215	83.56	3.201
62.2	99.74	0.215	83.33	3.301
64.06	99.89	0.2157	83.09	3.401
66.11	99.89	0.2157	82.97	3.503
68.01	99.89	0.2173	82.67	3.608
69.96	99.89	0.2173	82.25	3.730
71.89	99.89	0.2173	81.9	3.801
73.79	99.89	0.2173	81.48	3.901
75.65	99.89	0.2173	80.94	4.001
77.6	100	0.2173	80.11	4.101
79.55	100	0.2173	79.39	4.238
81.44	99.89	0.2157	78.5	4.319
83.31	100	0.215	77.73	4.403
85.38	100	0.2126	76.54	4.520

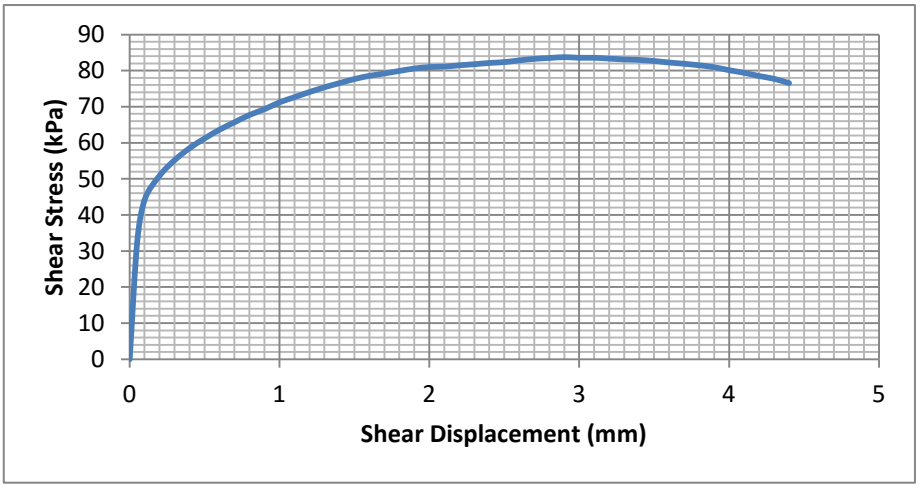

Appendix 14

Pure bentonite+3% SS (Normal stress 100kPa) **365 days curing**

Elapsed Time min	Vertical Stress kPa	Vertical Displacement mm	Horizontal Stress kPa	Horizontal Displacement mm
0.00	100	0.23	0.003	0.0011
1.91	99.74	0.5929	28.47	0.1002
2.06	99.59	0.5969	40.5	0.2003
4.02	99.74	0.6039	47.17	0.3005
5.93	99.74	0.6087	51.16	0.4007
7.9	99.74	0.615	52.12	0.5009
9.88	99.89	0.6205	53.9	0.601
11.75	99.74	0.6228	55.51	0.7032
13.54	99.89	0.6236	57.12	0.8002
15.75	99.89	0.6236	58.97	0.9003
17.74	99.89	0.6244	60.51	1.001
19.49	99.89	0.6244	61.76	1.101
21.57	99.74	0.6236	63.31	1.201
23.41	99.89	0.6228	64.5	1.301
25.42	100	0.6236	65.75	1.417
27.34	99.89	0.6236	66.83	1.523
29.31	100	0.6236	67.84	1.604
31.29	99.89	0.622	68.73	1.701
33.21	99.89	0.6228	69.57	1.801
35.08	99.89	0.622	70.28	1.901
37.07	99.89	0.622	70.82	2.001
38.91	99.74	0.622	71.29	2.123
40.92	99.74	0.622	71.71	2.211
42.85	99.89	0.6213	72.07	2.303
44.79	99.89	0.6213	72.25	2.401
46.72	99.89	0.622	72.37	2.501
48.77	99.89	0.6268	72.31	2.601
50.59	99.74	0.6276	72.25	2.701
52.49	99.89	0.6291	72.19	2.807
54.41	99.89	0.6307	72.19	2.903
56.32	99.74	0.6307	71.95	3.006
58.27	99.89	0.6323	71.83	3.101
60.17	99.89	0.6331	71.47	3.201
62.03	99.89	0.6331	71.12	3.301
64.13	100	0.6346	70.58	3.401
65.95	99.89	0.6472	69.92	3.505
67.99	99.89	0.6472	68.73	3.607

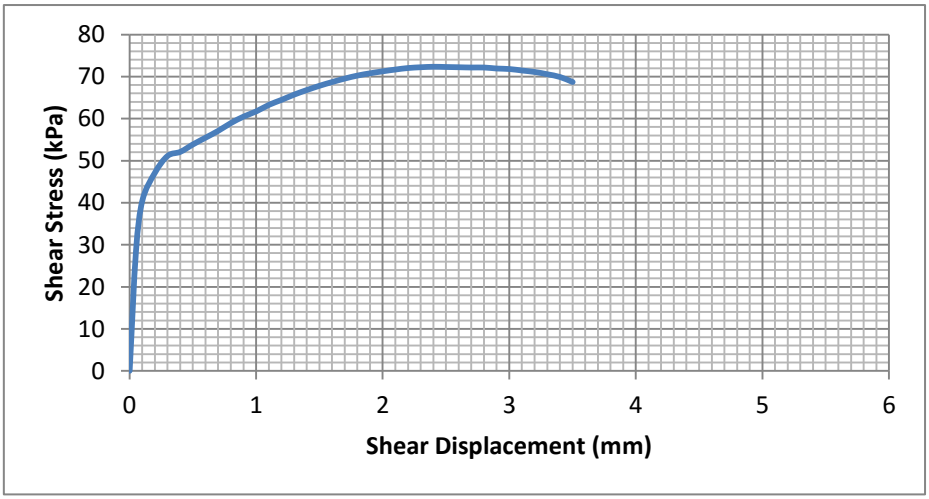

Appendix 15

Pure bentonite+6% SS (Normal stress 100kPa) **7 days curing**

Elapsed Time min	Vertical Stress kPa	Vertical Displacement mm	Horizontal Stress kPa	Horizontal Displacement mm
0.00	100	0.00012	0.0014	0.003
1.72	100	0.001575	24.3	0.1002
2.14	99.89	-0.0007874	50.69	0.20030
4.09	99.89	-0.001575	62.48	0.3005
6.19	99.89	-0.0007874	70.52	0.4007
8.01	99.89	-0.0007874	75.64	0.5009
9.87	99.89	-0.0007874	79.63	0.601
11.85	99.89	0.001575	82.07	0.713
13.84	99.74	0.00315	83.03	0.8002
15.79	99.74	0.003937	82.49	0.9003
17.63	99.89	0.003937	81	1.001
19.56	99.89	0.003937	78.92	1.101
21.49	100.2	0.005512	76.48	1.201
23.45	100	0.004724	73.74	1.301
25.32	99.89	0.004724	71.29	1.411
27.27	100	0.004724	68.67	1.531
29.17	100	0.003937	66.59	1.608
31.02	100	0.002362	64.68	1.701
32.98	100	0.000236	63.07	1.801
34.94	100	-0.002362	61.7	1.901
36.85	99.89	-0.004724	60.57	2.001
38.78	99.89	-0.007087	59.56	2.112
40.7	100	-0.01024	58.85	2.207
42.65	100	-0.01181	58.07	2.303
44.45	100	-0.01732	52.95	2.401
46.41	100	-0.01969	53.31	2.501
48.26	100	-0.02126	53.07	2.601
50.22	100	-0.02441	50.69	2.701
52.29	99.89	-0.02756	50.63	2.812
54.17	100	-0.0315	49.79	2.908
56.27	100	-0.03386	49.49	3.003
58.08	100	-0.03543	49.38	3.101
60.06	100	-0.03701	48.12	3.201
61.98	100	-0.03858	47.59	3.301
63.86	100	-0.04094	47.23	3.401
65.74	100	-0.04331	47.35	3.502
67.74	100	-0.04409	46.16	3.510
67.89	100	-0.04488	46.1	3.523

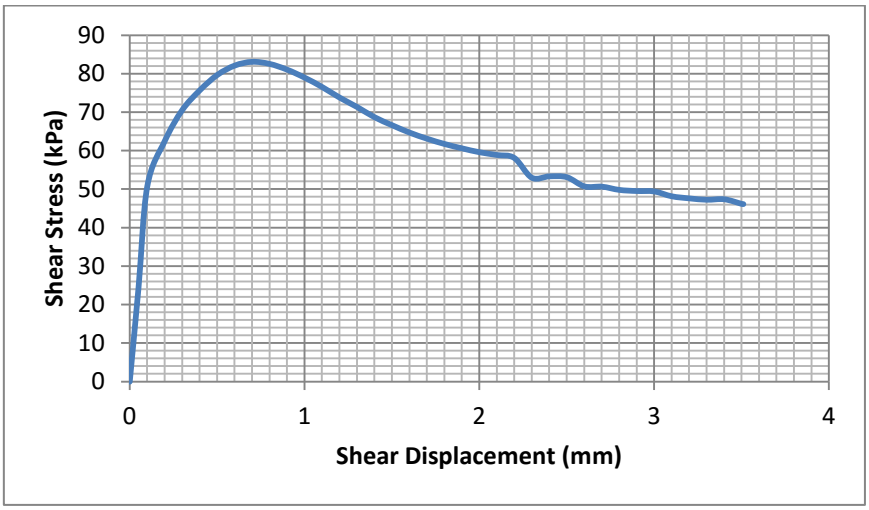

Appendix 16

Pure bentonite+6% SS (Normal stress 100kPa) **14 days curing**

Elapsed Time min	Vertical Stress kPa	Vertical Displacement mm	Horizontal Stress kPa	Horizontal Displacement mm
0.00	100	0.01136	0.003	0.006
1.66	100	0.2386	29.72	0.1002
2.16	99.89	0.237	48.72	0.2003
4.14	100	0.2339	58.37	0.3005
5.96	99.89	0.2283	64.44	0.4007
8.02	100	0.2252	69.27	0.5009
9.84	99.89	0.2197	72.25	0.601
11.73	100	0.211	74.87	0.732
13.66	100	0.2055	76.95	0.8002
15.64	100	0.1992	78.5	0.9003
17.63	100	0.1945	79.93	1.001
19.52	100	0.1882	81.24	1.101
21.58	100	0.1827	82.25	1.201
23.46	100	0.1811	82.91	1.301
25.5	99.89	0.1787	83.5	1.403
27.22	99.89	0.1795	83.8	1.510
29.12	99.89	0.1795	83.86	1.606
31.2	100	0.1756	83.62	1.701
33.21	100	0.1756	83.33	1.801
35	100	0.1756	82.97	1.901
36.85	100	0.1764	82.37	2.001
38.88	99.89	0.1732	81.66	2.110
40.88	99.89	0.1732	80.88	2.212
42.62	100	0.1724	80.11	2.308
44.6	99.89	0.1724	79.28	2.401
46.48	99.89	0.1724	78.38	2.501
48.52	100	0.1724	77.43	2.601
50.43	100	0.1717	76.48	2.701
52.35	100	0.1693	75.52	2.803
54.31	100	0.1677	74.21	2.905

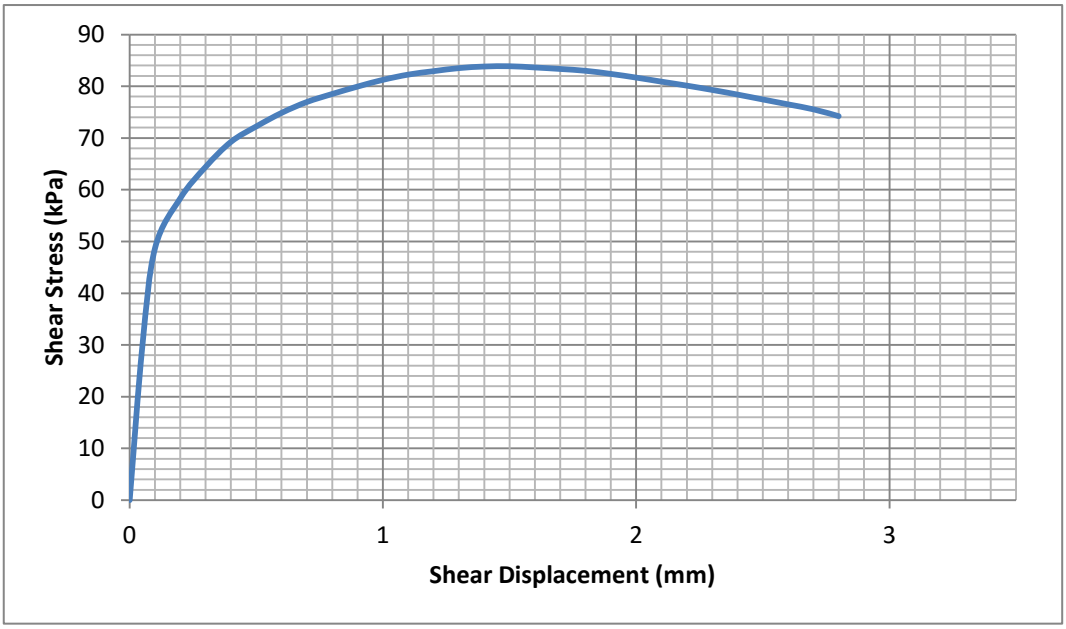

Appendix 17

Pure bentonite+6% SS (Normal stress 100kPa) **28 days curing**

Elapsed Time min	Vertical Stress kPa	Vertical Displacement mm	Horizontal Stress kPa	Horizontal Displacement mm
0.00	100	0.1605	0.006	0.0011
1.45	99.89	0.6205	10.13	0.1002
3.25	99.89	0.6189	35.68	0.2003
5.38	99.74	0.6205	47.35	0.3005
7.48	99.59	0.6252	54.2	0.4007
9.26	99.74	0.6307	58.25	0.5009
11.27	99.74	0.6386	61.94	0.601
13.19	99.59	0.6433	64.74	0.7102
15.24	99.74	0.6465	67.18	0.8002
17.13	99.74	0.6535	68.85	0.9003
19.04	99.59	0.6575	70.34	1.001
20.98	99.59	0.6598	71.65	1.101
22.88	99.74	0.6622	72.78	1.201
24.69	99.74	0.663	73.74	1.301
26.82	99.74	0.6661	74.75	1.402
28.68	99.89	0.6677	75.28	1.503
30.56	99.74	0.6709	76.06	1.610
32.51	99.89	0.6717	76.71	1.701
34.47	99.89	0.6724	77.37	1.801
36.34	99.89	0.6724	78.02	1.901
38.24	99.74	0.674	78.68	2.001
40.27	99.89	0.6764	79.39	2.103
42.28	99.74	0.678	79.93	2.235
44.12	99.89	0.6795	80.41	2.311
46.04	99.74	0.6803	80.7	2.401
48	99.89	0.6819	81	2.501
49.9	99.74	0.6843	81.18	2.601
51.95	99.74	0.6858	81.3	2.701
53.89	99.89	0.6866	81.48	2.812
55.75	99.74	0.6866	81.48	2.903
57.62	99.74	0.6882	81.48	3.005
59.65	99.89	0.689	81.36	3.101
61.44	99.74	0.6906	81.3	3.201

63.34	99.89	0.6913	81.06	3.301
65.27	99.89	0.6921	80.88	3.401
67.22	99.89	0.6921	80.59	3.556
69.15	100	0.6929	80.41	3.623
71.04	100	0.6929	79.93	3.711
72.92	99.89	0.6937	79.33	3.801
74.93	99.89	0.6945	78.74	3.901
76.75	99.89	0.6953	77.91	4.001
78.8	99.89	0.6961	76.77	4.101
80.7	99.89	0.6961	75.76	4.204
82.7	99.89	0.6961	74.63	4.303
84.46	99.89	0.6961	73.44	4.402
86.35	100	0.6961	72.25	4.501
88.28	100	0.6961	71.06	4.601
90.26	99.89	0.6961	69.75	4.701
92.14	99.89	0.6945	68.49	4.801
94.1	99.89	0.6937	67.07	4.932
95.97	100	0.6913	65.87	4.928
96.53	100	0.6906	65.58	4.928

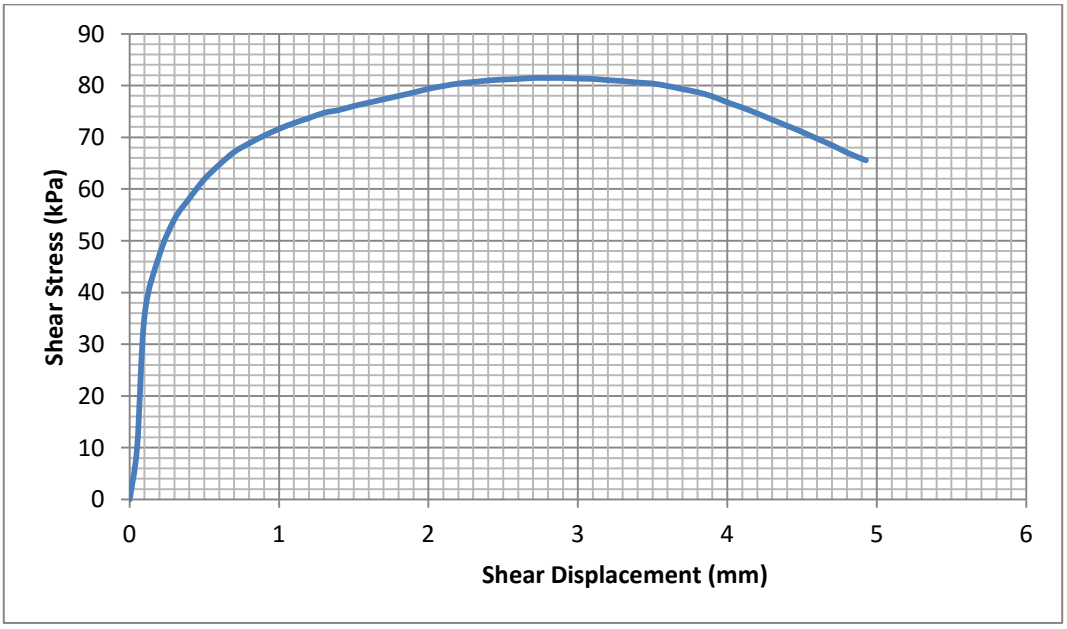

Appendix 18

Pure bentonite+6% SS (Normal stress 100kPa) **365 days curing**

Elapsed Time min	Vertical Stress kPa	Vertical Displacement mm	Horizontal Stress kPa	Horizontal Displacement mm
0.0	99.89	0.8063	0.007	0.00
1.90	99.89	1.045	30.61	0.1002
2.02	99.74	1.046	43.96	0.2003
4.05	99.74	1.051	50.92	0.3005
6.23	99.74	1.056	55.81	0.4007
8	99.74	1.06	59.02	0.5009
10.01	99.59	1.062	61.31	0.601
11.91	99.74	1.065	62.98	0.736
13.84	99.74	1.068	64.23	0.8002
15.95	99.74	1.069	65.13	0.9003
18.01	99.74	1.072	65.96	1.001
19.8	99.89	1.076	66.62	1.101
21.76	99.74	1.077	67.21	1.201
23.78	99.89	1.08	67.51	1.301
25.65	99.89	1.08	68.6	1.403
27.57	100	1.08	69.2	1.507
29.53	99.89	1.08	69.68	1.609
31.43	100	1.08	70.15	1.701
33.3	100	1.081	71.01	1.801
35.24	100	1.08	71.54	1.901
37.29	100	1.08	72.24	2.001
39.12	99.89	1.078	72.54	2.100
40.91	99.89	1.076	72.84	2.205
43.05	99.89	1.073	73.14	2.303
45.02	100	1.072	73.34	2.401
46.79	99.89	1.072	74.15	2.501
48.85	99.89	1.071	74.8	2.601
50.66	99.89	1.071	75	2.701
52.72	100	1.07	75.2	2.802
54.6	99.89	1.069	75.4	2.903
56.5	99.89	1.069	75.7	3.00
58.4	100	1.066	76	3.101
60.38	99.89	1.066	76.2	3.201
62.33	99.89	1.065	76.4	3.301
64.32	100	1.069	76.55	3.401
66.15	100	1.069	76.7	3.503
68.01	99.89	1.069	76.9	3.602
69.91	99.89	1.068	77.1	3.730
71.83	99.89	1.066	77.19	3.801
73.85	99.89	1.066	76.54	3.901
75.78	99.89	1.066	76.24	4.001
77.67	99.89	1.066	75.82	4.101
79.54	100	1.065	75.17	4.203
81.54	99.89	1.065	74.63	4.274
82.88	99.89	1.064	73.97	4.312

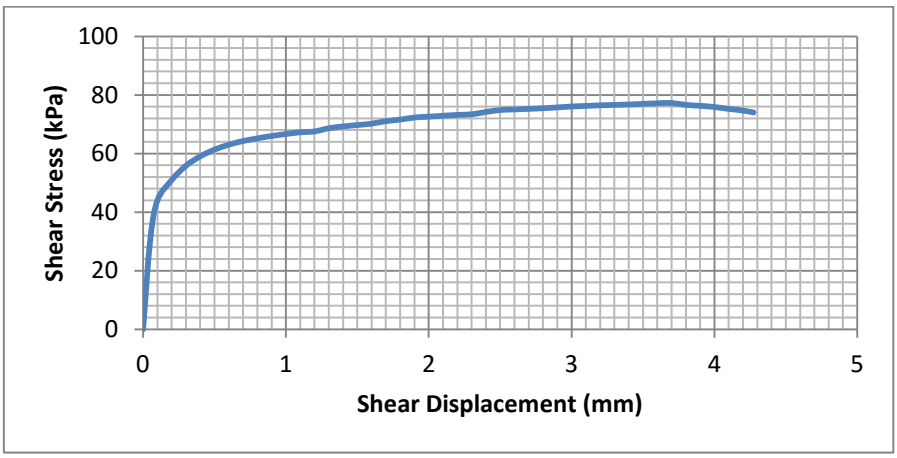

Appendix 19

Pure bentonite+9% SS (Normal stress 100kPa) **7 days curing**

Elapsed Time min	Vertical Stress kPa	Vertical Displacement mm	Horizontal Stress kPa	Horizontal Displacement mm
0.00	100	0.0063	0.003	0.006
4.49	100	0.01417	35.86	0.1002
6.7	99.89	0.01417	52.83	0.2003
8.67	99.89	0.01417	61.35	0.3005
10.66	99.89	0.01417	67.3	0.4007
12.73	99.89	0.01496	71.71	0.5009
14.53	99.89	0.01496	74.75	0.601
16.49	99.89	0.01575	77.25	0.7036
18.41	99.89	0.01575	78.62	0.8002
20.45	99.74	0.01654	78.44	0.9003
22.34	99.89	0.01654	77.25	1.001
24.27	99.89	0.01811	75.52	1.101
26.16	99.89	0.01811	73.68	1.201
28.04	100	0.01811	71.89	1.301
29.77	100	0.01811	69.86	1.425
31.95	100	0.01732	67.48	1.501
33.81	99.89	0.01575	65.75	1.608
35.76	100	0.01417	64.27	1.701
37.65	100	0.01102	62.96	1.801
39.61	100	0.009449	61.7	1.901
41.47	100	0.007874	60.63	2.001
43.33	100	0.003937	59.74	2.103
45.38	100	0.001575	58.79	2.205
47.39	100	-0.001575	57.24	2.308
49.25	100	-0.003937	56.94	2.401
51.19	100	-0.007874	56.46	2.501
53.09	100	-0.01496	55.27	2.601
54.96	100	-0.02047	54.5	2.701
57.01	100	-0.0252	53.84	2.8065
58.99	100	-0.0315	53.25	2.910
60.85	100	-0.03386	52.77	3.003
62.73	100	-0.03622	51.82	3.101
64.82	100	-0.03937	51.22	3.201
65.79	100	-0.04094	51.04	3.210

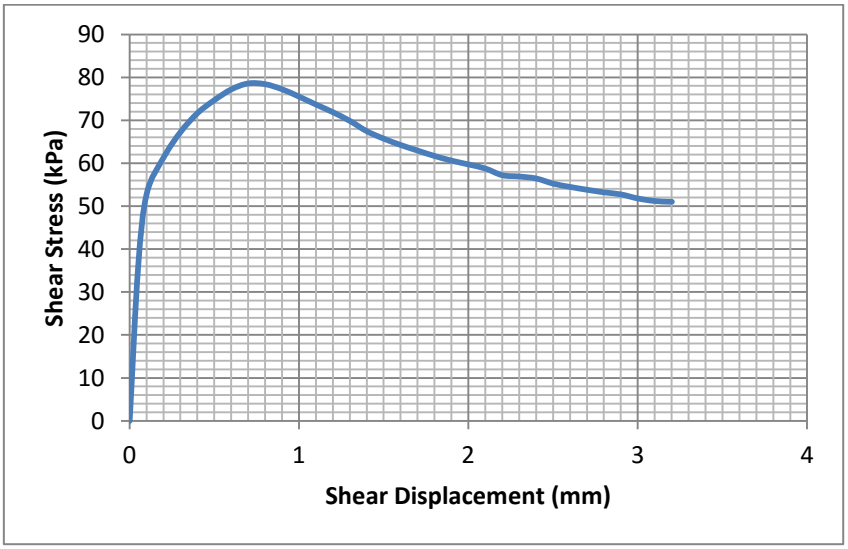

Appendix 20

Pure bentonite+9% SS (Normal stress 100kPa) **14 days curing**

Elapsed Time min	Vertical Stress kPa	Vertical Displacement mm	Horizontal Stress kPa	Horizontal Displacement mm
0.00	100	0.0256	0.002	0.00
1.46	99.74	0.8055	18.64	0.1002
2.06	99.44	0.8165	28.59	0.2003
4.21	99.59	0.8228	35.62	0.3005
6.04	99.74	0.8283	39.67	0.4007
8.03	99.59	0.837	43.96	0.5009
9.97	99.59	0.8457	47.41	0.601
11.97	99.74	0.8535	50.03	0.706
13.87	99.59	0.8583	52.23	0.8002
15.68	99.74	0.8646	53.9	0.9003
17.57	99.59	0.8677	55.63	1.001
19.59	99.59	0.8717	57.12	1.101
21.43	99.74	0.874	58.97	1.201
23.43	99.74	0.8764	60.28	1.301
25.29	99.74	0.878	61.11	1.432
27.14	99.74	0.8795	62.36	1.503
29.03	99.74	0.8827	63.73	1.6165
30.96	99.74	0.885	65.04	1.701
32.86	99.74	0.8866	66.23	1.801
34.71	99.74	0.8898	66.65	1.901
36.72	99.59	0.8913	67.18	2.001
38.59	99.59	0.8929	66.71	2.108
40.43	99.74	0.8953	67.24	2.213
42.47	99.74	0.8976	67.07	2.332
44.4	99.74	0.9008	66.95	2.401
46.36	99.74	0.9016	66.83	2.501
48.48	99.74	0.9063	66.77	2.601
50.23	99.74	0.9063	67.01	2.701
52.16	99.74	0.9071	67.18	2.8.05
54.18	99.74	0.9079	66.83	2.9.03
56.15	99.74	0.9079	67.07	3.063
57.97	99.74	0.9087	66.59	3.101
59.95	99.74	0.9102	66.17	3.201
61.86	99.74	0.9118	66.17	3.301
63.82	99.74	0.9126	65.93	3.401
65.78	99.74	0.915	66.41	3.505
67.72	99.89	0.9157	66.17	3.6036
69.74	99.74	0.9165	66.23	3.710
71.59	99.89	0.9173	66.11	3.801
73.5	99.89	0.9181	65.99	3.901
75.35	99.74	0.9189	66.11	4.001
77.36	99.74	0.9189	66.11	4.101
79.31	99.74	0.9197	66.05	4.2004
81.18	99.74	0.9189	65.7	4.3102
83.14	99.74	0.9189	65.75	4.403
85.09	99.89	0.9189	65.81	4.447
86	99.74	0.9197	65.58	4.456

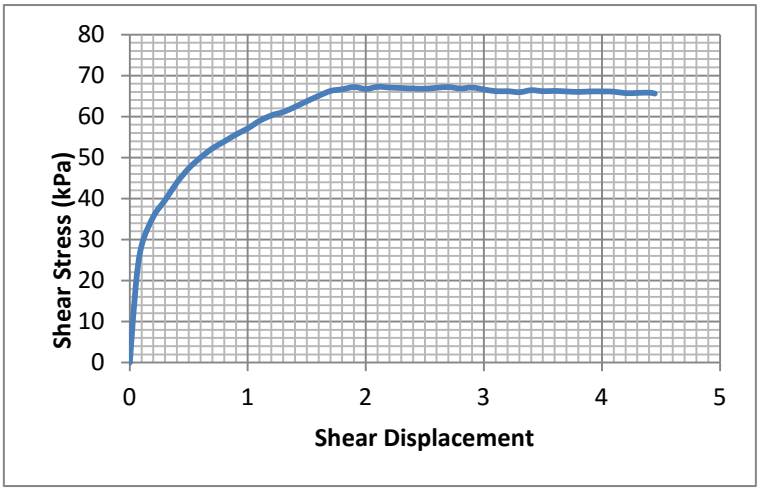

Appendix 21

Pure bentonite+9% SS (Normal stress 100kPa) 28 **days curing**

Elapsed Time min	Vertical Stress kPa	Vertical Displacement mm	Horizontal Stress kPa	Horizontal Displacement mm
0.00	99.89	0.0045	0.00	0.0000
1.89	99.74	0.9976	22.75	0.1002
2.22	99.74	1.005	37.76	0.2003
4.26	99.74	1.012	46.93	0.3005
6.19	99.74	1.017	52.47	0.4007
8.21	99.74	1.021	56.46	0.5009
10.04	99.74	1.027	58.73	0.601
12.05	99.74	1.035	60.57	0.7163
13.89	99.59	1.046	61.82	0.8002
15.85	99.74	1.059	63.37	0.9003
17.89	99.74	1.075	64.62	1.001
19.88	99.74	1.077	65.34	1.101
21.8	99.74	1.083	66.59	1.201
23.73	99.74	1.083	67.36	1.301
25.71	99.59	1.084	67.96	1.407
27.7	99.74	1.087	68.38	1.503
29.64	99.74	1.091	68.97	1.600
31.46	99.74	1.094	69.63	1.701
33.38	99.74	1.096	69.98	1.801
35.39	99.74	1.099	70.58	1.901
37.26	99.74	1.103	71.23	2.001
39.15	99.74	1.107	71.65	2.113
41.19	99.74	1.109	71.71	2.220
43.02	99.74	1.109	71.83	2.3136
44.9	99.74	1.112	72.01	2.401
46.89	99.89	1.116	72.07	2.501
48.7	99.89	1.117	72.07	2.601
50.67	99.74	1.119	72.01	2.701
52.65	99.74	1.12	71.89	2.802
54.56	99.74	1.12	71.71	2.9032
56.55	99.89	1.12	71.65	3.015
58.48	99.89	1.12	71.35	3.101
60.42	99.89	1.12	71	3.201
62.31	99.89	1.12	70.7	3.301
64.34	100	1.12	70.16	3.401
66.2	99.89	1.119	69.51	3.409
66.32	99.89	1.119	69.45	3.409

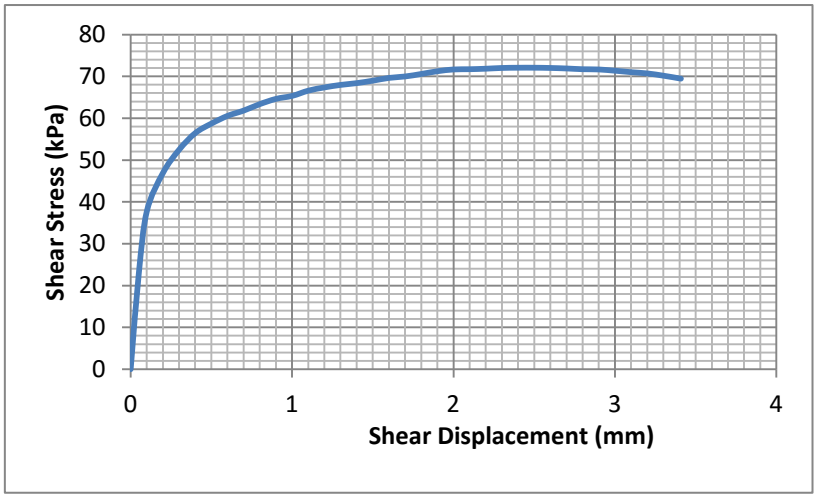

Appendix 22

Pure bentonite+9% SS (Normal stress 100kPa) **90 days curing**

Elapsed Time min	Vertical Stress kPa	Vertical Displacement mm	Horizontal Stress kPa	Horizontal Displacement mm
0.00	99.85	0.012	0.00	0.00
1.63	99.74	0.8213	25.79	0.1002
2.05	99.74	0.8339	34.31	0.2003
4.18	99.59	0.8488	39.61	0.3005
6.25	99.74	0.8591	43.54	0.4007
8.26	99.59	0.8693	46.58	0.5009
10.26	99.59	0.8827	48.84	0.601
12.23	99.74	0.889	50.81	0.703
14.09	99.59	0.8976	52.47	0.8002
16.09	99.74	0.9032	54.02	0.9003
17.99	99.74	0.9126	55.33	1.001
20.09	99.74	0.9165	56.7	1.101
21.92	99.74	0.9189	57.6	1.201
23.81	99.74	0.9228	58.67	1.301
25.75	99.74	0.9283	59.5	1.410
27.77	99.74	0.9331	60.57	1.5206
29.68	99.74	0.9378	61.35	1.6105
31.49	99.74	0.9402	62.12	1.701
33.42	99.74	0.9433	62.9	1.801
35.37	99.74	0.9457	63.49	1.901
37.32	99.74	0.948	63.97	2.001
39.19	99.74	0.9496	64.5	2.110
41.16	99.74	0.9504	65.04	2.214
43.01	99.74	0.952	65.52	2.302
44.91	99.74	0.9528	65.93	2.401
46.95	99.74	0.9528	66.29	2.501
48.95	99.74	0.9535	66.41	2.601
50.8	99.89	0.9543	66.71	2.701
52.76	99.89	0.9543	66.89	2.8032
54.71	99.89	0.9551	67.07	2.912
56.68	99.74	0.9551	67.24	3.005
58.58	99.89	0.9559	67.36	3.101
60.42	99.89	0.9567	67.48	3.201
62.35	99.74	0.9567	67.42	3.301
64.36	99.74	0.9567	67.36	3.401
66.23	99.89	0.9575	67.3	3.5085
68.13	99.89	0.9575	67.12	3.6133
70.19	99.89	0.9748	67.07	3.7106
72.01	99.89	0.9756	66.89	3.801

73.89	99.74	0.9756	66.83	3.901
75.83	99.74	0.9756	66.71	4.001
77.67	100	0.9764	66.47	4.101
79.53	99.89	0.9764	66.35	4.2036
81.51	99.89	0.9756	66.17	4.3103
83.29	99.89	0.9756	66.05	4.403
85.3	99.89	0.9756	65.81	4.501
87.28	99.89	0.9756	65.58	4.601
89.22	99.89	0.9756	65.4	4.701
91.08	99.89	0.9764	65.16	4.741
91.94	99.89	0.9764	65.04	4.753

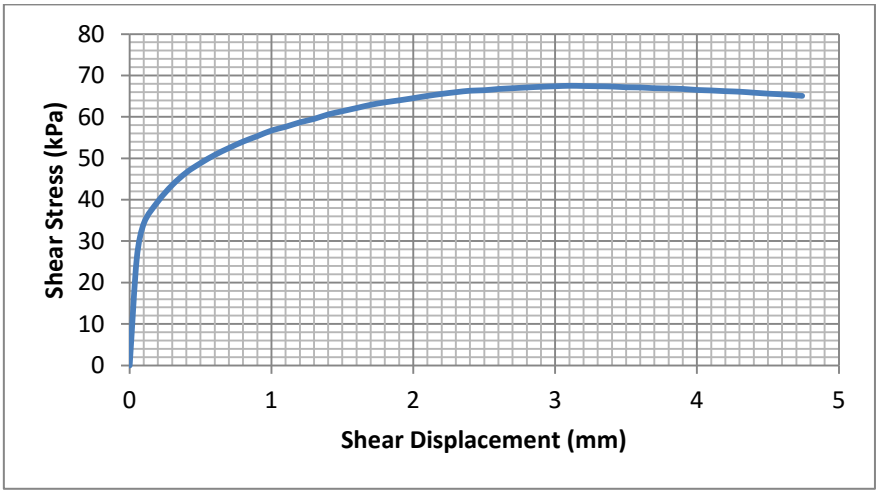

Appendix 23

Pure bentonite+9% SS (Normal stress 100kPa) 365 **days curing**

Elapsed Time(min)	Vertical Stress(kPa)	Vertical Displacement(mm)	Horizontal Stress(kPa)	Horizontal Displacement (mm)
0.00	100.00	0.036	0.001	0.000
1.93	99.74	1.256	23.94	0.1002
2.25	99.74	1.263	34.31	0.2003
4.23	99.59	1.269	39.73	0.3005
6.26	99.74	1.284	43.9	0.4007
8.25	99.59	1.294	46.99	0.5009
10.21	99.74	1.299	49.67	0.601
12.15	99.59	1.304	52	0.7003
13.99	99.74	1.309	53.78	0.8002
15.9	99.59	1.311	55.87	0.9003
17.82	99.74	1.316	57.06	1.001
19.8	99.74	1.32	58.55	1.101
21.84	99.74	1.32	59.98	1.201
23.6	99.74	1.323	60.87	1.301
25.52	99.74	1.324	61.82	1.433
27.46	99.74	1.324	62.6	1.5125
29.5	99.74	1.328	63.31	1.6023
31.43	99.74	1.328	64.03	1.701
33.26	99.89	1.327	64.56	1.801
35.11	99.74	1.327	65.04	1.901
37.05	99.74	1.326	65.52	2.001
39.03	99.89	1.325	65.87	2.1003
40.87	99.89	1.324	66.11	2.2023
42.9	99.74	1.324	66.53	2.3054
44.76	99.74	1.323	66.95	2.401
46.66	99.89	1.323	67.24	2.501
48.68	99.89	1.323	67.6	2.601
50.65	99.89	1.322	67.9	2.701
52.46	99.74	1.322	68.26	2.8040
54.39	99.89	1.32	68.38	2.900
56.4	99.89	1.317	68.67	3.004
58.37	99.89	1.313	68.85	3.101
60.2	99.74	1.311	68.85	3.201
62.13	99.89	1.31	69.09	3.301
64.04	99.89	1.31	69.21	3.401
66.04	99.74	1.306	69.33	3.5442
67.9	99.89	1.305	69.33	3.6132
69.82	99.74	1.302	69.33	3.715
71.87	99.74	1.301	69.45	3.801
73.69	99.74	1.298	69.45	3.901
75.68	99.89	1.295	69.45	4.001
77.59	99.89	1.295	69.45	4.101
79.42	99.74	1.294	69.45	4.2442
81.34	99.74	1.292	69.33	4.344
83.3	99.89	1.291	69.33	4.435
85.3	99.74	1.291	69.39	4.501
87.24	99.89	1.291	69.33	4.601
89.12	99.89	1.291	69.27	4.701
91.13	99.89	1.291	69.27	4.801
92.99	99.74	1.287	69.15	4.9156
94.96	99.74	1.287	69.09	5.023
96.78	99.89	1.287	69.03	5.1002
98.7	99.74	1.287	69.03	5.2013
100.62	99.74	1.287	69.03	5.301
102.55	99.89	1.287	68.97	5.401
104.53	99.89	1.286	68.85	5.501
106.49	99.74	1.286	68.73	5.6236
108.37	99.74	1.286	68.61	5.7123
110.16	99.74	1.286	68.49	5.8365
112.25	99.74	1.286	68.44	5.901
114.09	99.89	1.286	68.26	6.001
115.97	99.74	1.286	68.14	6.101
117.93	99.74	1.285	67.96	6.201
119.87	99.74	1.285	67.96	6.365
121.76	99.74	1.285	67.78	6.425
123.66	99.89	1.286	67.66	6.5325
125.64	99.74	1.286	67.48	6.601
127.57	99.74	1.287	67.36	6.701
129.52	99.89	1.287	67.36	6.805

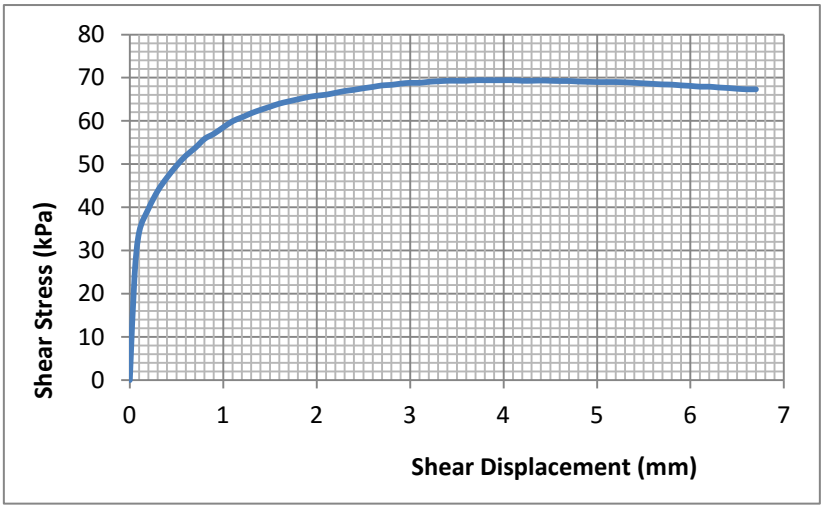
80
70
60
50
40
30
20
10
0
Shear Stress (kPa)
0
1
2
3
4
5
6
7
Shear Displacement (mm)